



The
University
Of
Sheffield.

Adgrg6 drug discovery using the zebrafish model

By Anzar Asad

A thesis submitted in partial fulfilment of the requirements for the degree of
Doctor of Philosophy

The University of Sheffield Department of Biomedical Science

In partnership with Sosei Heptares

Supervisors: Prof. Tanya Whitfield, Dr. Sarah Baxendale and Dr. Giselle Wiggin

Advisors: Dr. Vincent Cunliffe and Dr. Anne-Gaelle Borycki

September 2021

Acknowledgements

I would first like to thank my supervisors Professor Tanya Whitfield, Dr Sarah Baxendale and Dr Giselle Wiggan for their continued encouragement, guidance and support throughout the course of my PhD study. They not only helped me develop my technical skills in the laboratory setting but have also had a positive impact on my growth as a scientist, for which I am truly grateful.

I extend my thanks to Dr Elvira Diamantopoulou and Dr Christopher Derrick from whom I learnt a great deal. They helped me settle into the lab and always took time to answer my stupid questions - mostly without being amused.

I am grateful to the Sosei Heptares Protein Engineering and Pharmacology teams for being extremely welcoming and helpful, which allowed me to make the most of my short three-month placement.

To my friends, thanks for all the laughs and good times that have made this experience not only tolerable but also memorable. Whether it was complaining about failed experiments and stupid mistakes at the pub on a Friday or going on trips away to unwind, it was always a pleasure. In particular, I want to thank Nabarun, Arka, Jonny and Joe for never failing to entertain me and providing nonstop sports commentary and transfer rumours, keeping me up-to-date. Thanks also to Dr Matty Wind, the countless victories against you at tennis never failed to raise my spirits after a tough day at work.

A huge thank you to my family, I could not imagine completing this without their love and support. To my sister, thanks for continuously checking in on my thesis progress and keeping me on track. Thanks to my brother for movie nights and snooker games that helped take my mind off work. To my Mum and Dad, I would not be where I am today without them both. They have always believed in me and encouraged me to overcome whatever challenge I may face. For this, I am forever grateful. A further thanks to my Mum for all the amazing food that kept me well fed whilst I was writing up. Finally to my grandparents, I am grateful for their love and prayers.

Abstract

Schwann cells are the principal myelinating glial cells of the Peripheral Nervous System (PNS) that insulate neuronal axons with a lipid-rich myelin sheath. Defects of the myelin sheath can impair nerve conduction and are associated with various developmental and demyelinating diseases, including those involving Schwann cell pathobiology that lead to weakness, paralysis and death in severe cases. Lethal Congenital Contracture Syndrome 9 (LCCS9) is an example in which myelination of the PNS is defective as a result of a missense mutation in *ADGRG6*, which encodes the adhesion G protein-coupled receptor G6 (ADGRG6, formerly GPR126) with conserved roles in Schwann cell maturation.

adgrg6 is expressed in zebrafish and has conserved regulatory roles in myelination of the PNS and additional roles in semicircular canal formation in the inner ear. As part of an ongoing drug-screening project, I set out to identify small molecules that are potent and specific modulators of the Adgrg6 signalling pathway, using zebrafish larvae as a whole-animal screening platform due to their amenability for high-throughput drug screening and gene expression analysis by whole-mount *in situ* hybridisation.

In the current work, I first characterised the peripheral myelination phenotype in hypomorphic *adgrg6*^{tb233c} mutant larvae, before optimising pharmacological conditions for a screening assay using *myelin basic protein (mbp)* mRNA expression in the PNS as a transcriptional readout of Adgrg6 pathway activity. We previously identified candidate pathway modulators from the Spectrum and Tocris compound libraries, using otic *versican b (vcanb)* mRNA expression in a primary screen for phenotypic rescue of *adgrg6* hypomorphic mutants, before testing hits on a counter-screening *mbp* assay. I have similarly screened the Sigma LOPAC library of 1280 pharmacologically active compounds. This collection contains 685 compounds not represented in our previous screens, of which 275 are structurally diverse from any compounds we have previously tested. The LOPAC screen has identified 42 hit compounds that can downregulate *vcanb* in otic tissue, 17 of which also restore *mbp* expression around the posterior lateral line ganglion of *adgrg6* hypomorphic mutant larvae. Hit compounds include classes of molecules identified previously, including dihydropyridines, together with some new candidate modulators of the Adgrg6 signalling pathway; those that are ineffective at rescuing the otic phenotype in a truncating mutant allele are likely to interact directly with the Adgrg6 receptor. Preliminary cAMP assays in HEK293 cells failed to illustrate potential agonistic effects of candidate compounds including, ivermectin and ebastine from the LOPAC library. However, testing ADGRG1 antagonists, including dihydromunduletone (DHM), revealed potential antagonism towards the zebrafish Adgrg6 receptor. Moreover, preliminary work in zebrafish revealed that wild-type larvae

could somewhat phenocopy *adgrg6* hypomorphic mutants following DHM injection into the larval ear. Further work is necessary to confirm observations in this study; however, the discovery of Adgrg6 compound modulators will provide useful tools to modulate the receptor's pathway activity, with the potential to give additional insights into its underlying mechanism of action. Compounds could also hold potential for therapeutic use against demyelinating or *ADGRG6*-linked human diseases.

Statement of contribution

I state that the work included in this thesis is my own; however, my joint-first and co-author contributions in the studies below may overlap.

Baxendale S*, **Asad A***, Shahidan NO, Wiggin GR and Whitfield TT (2021). The adhesion GPCR Adgrg6 (Gpr126): insights from the zebrafish model. *genesis, The Journal of Genetics and Development*, e23417. Special Issue: *Aquatic Models of Developmental Disorders*, ed. S. A. Moody. DOI: 10.1002/dvg.23417 [Invited review].

Diamantopoulou E*, Baxendale S*, de la Vega de León A, **Asad A**, Holdsworth CJ, Abbas L, Gillet VJ, Wiggin GR and Whitfield TT (2019). Identification of compounds that rescue otic and myelination defects in the zebrafish *adgrg6* (*gpr126*) mutant. *eLife* 8, e44889.

*denotes equal contribution

List of Abbreviations

+ss/-ss - presence/absence of *adgrg6* exon 6
Adgrg6 - Adhesion G protein-coupled receptor G6
ADMET - absorption, distribution, metabolism, excretion, toxicity
aGPCR - adhesion G protein-coupled receptor
ALL - anterior lateral line
ALLg - ALL ganglion
AMC - Arthrogyrosis Multiplex Congenita
ALLn -ALL nerve
AV - anteroventral
Ca²⁺ - calcium
cAMP - cyclic adenosine monophosphate
CIDP - Chronic Inflammatory Demyelinating Polyradiculoneuropathy
CMT - Charcot Marie Tooth
CNS - central nervous system
Col4 - collagen IV
CREB - cAMP-responsive-element-binding protein
CTF - C-terminal fragment
DHM - dihydromunduletone
CUB - Complement C1r/C1s, Uegf, Bmp1
DI - dendrogram index
DIC - differential interference contrast
DMEM - Dulbecco's modified eagle medium
DMSO - dimethyl-sulfoxide
ECM - extracellular matrix
DIG - digoxigenin
ECR - extracellular region
FBS - foetal bovine serum
EGFP - enhanced GFP
EGFR - epidermal growth factor receptor
FAK - focal adhesion kinase
FDA - Food and Drug Administration

FGF - fibroblast growth factor
GAIN - GPCR autoproteolysis-inducing domain
FP - forward primer
FSK - forskolin
Gab1 - GRB2 Associated Binding Protein 1
GBS - Guillain-Barre Syndrome
GPCR - G protein-coupled receptor
GPS - GPCR proteolytic site
HM - hybridisation mix
hpf - hours post fertilisation
IBMX - 3-isobutyl-1-methylxanthine
Ig - immunoglobulin
IL - interleukin
GFP - green fluorescent protein
HEK293 - human embryonic kidney 293 cells
Hh - Hedgehog
HM - hybridisation mix
HormR - Hormone Receptor
HTRF - homogeneous time-resolved fluorescence
IOLn - infraorbital line nerve
IP - inner primer
iSC - immature Schwann cells
ISH - *in situ* hybridisation
Krox20/Egr2 - early growth response protein 2
Lam211 - laminin-211
LCCS9 - Lethal Congenital Contracture Syndrome 9
MBP - myelin basic protein
LOPAC - library of pharmacologically active compounds
MI2 - middle line MI2 neuromast
MS - Multiple Sclerosis
MUND - mundulone
NRG - neuregulin
NTF - N-terminal fragment

Oct6/Pou3f1- POU class 3 homeobox 1
PBS - phosphate buffered saline
OP - outer primer
PBST - PBS Tween
PBSTr - PBS Triton
PKA - protein kinase A
PLL - posterior lateral line
PCR - polymerase chain reaction
PFA - paraformaldehyde
PLLg - PLL ganglion
PLLn - PLL nerve
PNS - peripheral nervous system
RNA - ribonucleic acid
PrP - prion protein
PTU - 1-phenyl 2-thiourea
PTX - Pentraxin
RP - reverse primer
RT - room temperature
SAG - statoacoustic ganglion
SCP - Schwann cell precursor
SEA - Sperm protein, Enterokinase and Agrin
SOLn - suprorbital line nerve
Sox10 - SRY-box transcription factor 10
SRE - serum response element
SRF - serum response factor
TM - transmembrane
Tm - melt temperature
TNF - tumour necrosis factor
tSCs - terminal Schwann cells
vcana - versican a
vcanb - versican b
WGA - wheat germ agglutinin
WISH - whole-mount *in situ* hybridisation
7TM - 7-pass transmembrane helix domain

Table of Contents

Acknowledgements.....	2
Abstract.....	3
Statement of contribution.....	5
Abbreviations.....	6
Chapter 1.....	16
Introduction	17
1.1 Schwann cells.....	17
1.1.1 Function of Schwann cells.....	17
1.1.2 Myelin diseases of the peripheral nervous system.....	17
1.1.3 Development of Schwann cells.....	18
1.1.4 The zebrafish model.....	19
1.1.4a Study of myelination in zebrafish.....	19
1.1.4b Drug screening in zebrafish larvae.....	20
1.2 Developmental roles of <i>Adgrg6</i> in zebrafish.....	21
1.2.1 <i>Adgrg6</i> in Schwann cells.....	21
1.2.1a Promyelinating Schwann cells.....	21
1.2.1b Radial sorting	23
1.2.1c Regeneration.....	23
1.2.2 The vertebrate inner ear.....	28
1.2.2a The zebrafish vestibular system.....	28
1.2.2b A role for <i>Adgrg6</i> in morphogenesis of the zebrafish semicircular canals system	29
1.3 Adhesion G protein-coupled receptor G6.....	32
1.3.1 G protein-coupled receptors (GPCRs).....	32
1.3.1a Classes of GPCRs	32
1.3.1b G protein signalling pathways.....	32
1.3.2 The <i>adgrg6</i> gene	33
1.3.3 aGPCR Structure, <i>Adgrg6</i>	33
1.3.3a Structural domains.....	33
1.3.3b Structural conformation of the <i>Adgrg6</i> ECR	34
1.3.4 <i>Adgrg6</i> activation mechanism and intracellular signalling pathway	38
1.3.4a Overview	38
1.3.4b <i>Adgrg6</i> coupling to G proteins	38
1.3.4c <i>Adgrg6</i> NTF binding partners and intracellular signalling	38

1.3.4d Adrg6: <i>stachel</i> mediated activation	39
1.4 Adrg6 and drug discovery	40
1.4.1 Identification of <i>ADGRG6</i> as disease gene.....	40
1.4.2 GPCRs as druggable targets: Adrg6.....	43
1.4.3 Small molecule ligands of GPCRs as biological tools.....	44
1.4.4 Small molecule zebrafish screens for Adrg6 modulators.....	44
1.5 Key Aims and Hypotheses	47
Chapter 2.....	49
Materials & Methods	49
2.1 Molecular work	49
2.1.1 RNA extraction	49
2.1.2 cDNA synthesis.....	49
2.1.3 Primers	50
2.1.4 Polymerase Chain Reaction	51
2.1.4a PCR overview.....	51
2.1.4b Nested PCR.....	51
2.1.4c Site-directed mutagenesis of human and zebrafish <i>ADGRG6</i>	52
2.1.5 Plasmid digestion	52
2.1.6 Ligation.....	52
2.1.7 Transformation of competent cells	53
2.1.8 Synthesis of DIG-labelled RNA probes	53
2.2 Zebrafish husbandry	54
2.2.1 Zebrafish wild types	54
2.2.2 Zebrafish transgenic and mutant lines.....	54
2.2.3 Zebrafish care.....	54
2.2.4 Zebrafish crosses and harvesting of embryos.....	54
2.3 <i>in vivo</i> drug screening	55
2.3.1 Sigma LOPAC library preparation.....	55
2.3.2 Compound plate preparation	55
2.3.3 Preparation of embryos	56
2.4 Testing of candidate Adrg6 antagonists.....	57
2.4.1 Compound administration in media	57
2.4.2 Compound microinjection	57
2.5 Whole-mount <i>in situ</i> hybridisation	58
2.5.1 Protocol.....	58
2.5.2 Drug treated embryos.....	59

2.5.3 Scoring of embryos in assay plates	60
2.5.4 Brightfield and DIC imaging	60
2.6 Immunohistochemistry	61
2.6.1 Zebrafish antibodies.....	61
2.6.2 Antibody Staining.....	61
2.6.3 Confocal A1 Microscope	62
2.7 Human cell culture	62
2.7.1 Cell lines and culture.....	62
2.7.2 Cell transfection	63
2.7.2a Transfection by BacMam	63
2.7.2b Transient transfection.....	63
2.7.3 Immunocytochemistry	63
2.7.3a Antibodies	63
2.7.3b Antibody staining	63
2.7.4 Compound treatment	64
2.7.4a Forskolin dose-response	64
2.7.4b Drug treatment of HEK293 cells.....	64
2.7.5 cAMP assay	65
Chapter 3.....	67
Characterisation of Schwann cell development in wild type and <i>adgrg6^{tb233c}</i> zebrafish mutants...	67
3.1 Introduction	67
3.2 Results.....	70
3.2.1 Expression pattern of <i>adgrg6</i>	70
3.2.1a Otic expression of <i>adgrg6</i>	70
3.2.1b Expression of <i>adgrg6</i> and <i>sox10</i> along the posterior lateral line nerve	73
3.2.2 Anterior expression of <i>sox10</i> and <i>adgrg6</i> in wild-type and <i>adgrg6^{tb233c}</i> mutant larvae..	76
3.2.3 Characterisation of <i>mbp mRNA</i> and transgenic <i>mbp</i> -driven EGFP expression in wild-type and <i>adgrg6^{tb233c}</i> mutant zebrafish larvae.....	79
3.2.3a Expression of <i>mbp mRNA</i> in zebrafish larvae	79
3.2.3b Transgenic <i>mbp</i> -driven EGFP expression along the lateral line and cranial nerves ..	82
3.2.4 Characterisation of additional Schwann cell myelination markers	86
3.2.4a Expression of <i>oct6</i> in wild-type and <i>adgrg6^{tb233c}</i> mutant zebrafish larvae	86
3.2.4b Expression of <i>krox20</i> in wild-type and <i>adgrg6^{tb233c}</i> mutant zebrafish larvae	88
3.2.4c Expression of <i>claudin k</i> in wild-type and <i>adgrg6^{tb233c}</i> mutant zebrafish larvae	90
3.3 Discussion.....	92
Chapter 4.....	95

Phenotypic screening in zebrafish larvae reveals candidate modulators of the adhesion GPCR	
Adrg6	95
4.1 Introduction	95
4.2 Results	98
4.2.1 Optimisation of the mbp counter-screening assay	98
4.2.2 Pharmacological screening	102
4.2.3 Primary screening assay	102
4.2.3a First round of screening	102
4.2.3b Retesting compounds of interest	106
4.2.3c Compounds overlapping across screened libraries	110
4.2.3d Structurally novel compounds in the LOPAC library	111
4.2.4 Counter-screen	114
4.2.4a Testing primary screen hits on the optimised mbp assay	114
4.2.4b Testing hit compounds in dose-response assays	122
4.2.5 Testing Adrg6 pathway hits on other alleles	126
4.2.5a Strong loss-of-function adrg6 mutant allele (<i>fr24</i>) in vcanb assay	126
4.2.5b Missense <i>tk256a</i> allelic mutants in optimised mbp assay	127
4.2.6 Retesting apomorphine in phenotypic screening assays	131
4.3 Discussion	133
Chapter 5	141
Gα _s pathway activity in human and zebrafish <i>ADGRG6</i> -expressing HEK293 cells	141
5.1 Introduction	141
5.2 Results	143
5.2.1 Effect of human and zebrafish <i>ADGRG6</i> mutations on Gα _s pathway activity	143
5.2.2 Expression of human and zebrafish <i>ADGRG6</i> constructs	149
5.2.3 Optimisation of HEK293 cell baculoviral transfection with human and zebrafish <i>ADGRG6</i> constructs for suitability with small molecule treatments	155
5.2.4 HEK293 cell responses to candidate Adrg6 modulators	158
5.2.5 HEK293 cell responses to known biological Adrg6 NTF ligands	162
5.2.6 Candidate Adrg6 antagonists in cAMP assays	164
5.2.7 Zebrafish treatment with dihydromunduletone	170
5.3 Discussion	174
Chapter 6	178
Synopsis	178
6.1 Summary of results	178
6.2 Combined zebrafish and cell approach	180

6.3 Relevance and future directions	181
6.4 Concluding remarks	182
Bibliography	184
Appendix	199

List of Figures

Figure 1.1 Peripheral myelination and inner ear phenotypes in <i>adgrg6</i> ^{tb233c} zebrafish mutants.	25
Figure 1.2 Schematic illustration of intracellular signalling pathways involved in the coordination of radial sorting and myelination of the PNS.	27
Figure 1.3 Otic expression of <i>adgrg6</i> in the developing embryo and proposed roles of its encoded protein, in semicircular canal morphogenesis.	31
Figure 1.4 Schematic models of zebrafish Adgrg6 protein structure and mechanism of activation.	36
Figure 2.1 Nested PCR primer setup.	52
Figure 2.2 Layout of compound screening assay plate.	56
Figure 2.3 Biolane HTV1 16V in situ robot (Intavis) for automated WISH.	59
Figure 2.4 Layout of compound source plate.	65
Figure 3.1 <i>adgrg6</i> mRNA expression pattern in the inner ear, at 48 and 72 hpf, of wild-type and <i>adgrg6</i> ^{tb233c} mutant zebrafish.	72
Figure 3.2 <i>adgrg6</i> mRNA expression along the lateral line, at 48 and 96 hpf, in wild-type and <i>adgrg6</i> ^{tb233c} mutant zebrafish.	74
Figure 3.3 <i>adgrg6</i> mRNA expression in <i>adgrg6</i> ^{tk256a} and <i>adgrg6</i> ^{fr24} mutant larvae.	75
Figure 3.4 <i>adgrg6</i> and <i>sox10</i> mRNA expression along PLL in wild-type and <i>adgrg6</i> ^{tb233c} mutant larvae.	75
Figure 3.5 <i>sox10</i> and <i>adgrg6</i> mRNA expression along anterior lateral line and cranial nerves in wild-type and <i>adgrg6</i> ^{tb233c} mutant larvae.	78
Figure 3.6 <i>mbp</i> mRNA expression in Schwann cells along the lateral line and cranial nerves, between 72 and 96 hpf, in wild-type and <i>adgrg6</i> ^{tb233c} mutant larvae.	81
Figure 3.7 Expression pattern of acetylated α -tubulin in 96 hpf <i>tg(mbp:EGFP-CAAX)</i> larvae in the wild type and <i>adgrg6</i> ^{tb233c} background.	84
Figure 3.8 Expression pattern of acetylated α -tubulin in 96 hpf <i>tg(mbp:EGFP-CAAX)</i> larvae in the wild type and <i>adgrg6</i> ^{tb233c} background.	85
Figure 3.9 <i>oct6</i> mRNA expression, at 48 and 96 hpf, in wild-type and <i>adgrg6</i> ^{tb233c} mutant larvae.	87
Figure 3.10 <i>krox20</i> mRNA expression, at 72 hpf, in wild-type and <i>adgrg6</i> ^{tb233c} mutant larvae.	89
Figure 3.11 <i>cldnk</i> mRNA expression, at 72 and 96 hpf, in wild-type and <i>adgrg6</i> ^{tb233c} mutant larvae.	91
Figure 4.1 Optimisation of a counter-screening <i>mbp</i> assay.	101
Figure 4.2 Overview of the screening assay protocol and scoring systems utilised to assess <i>vcanb</i> and <i>mbp</i> expression following compound treatment.	104
Figure 4.3 A primary drug screen reveals 48 hit compounds that consistently downregulate <i>vcanb</i> in <i>adgrg6</i> ^{tb233c} mutant larvae.	105

Figure 4.4 Network analysis of LOPAC, Spectrum and Tocris library compounds.....	108
Figure 4.5 Primary screen performance of compounds that were common between multiple libraries.	112
Figure 4.6 Screening 48 selected hits on an optimised <i>mbp</i> counter-screening assay reveals 24 <i>vcanb</i> specific hits and 17 hits that can also restore <i>mbp</i> expression in <i>adgrg6^{tb233c}</i> mutant larvae.....	117
Figure 4.6 (supplement) Comparison of hit compound assay scores (48).	118
Figure 4.7 Hits that are likely Adgrg6 pathway specific.....	119
Figure 4.8 Compounds identified as <i>vcanb</i> specific or transcriptional downregulators.	121
Figure 4.9 Testing Adgrg6 pathway hits in dose-response assays on <i>adgrg6^{tb233c}</i> mutants.....	124
Figure 4.10 Testing Adgrg6 pathway hits on <i>fr24</i> and <i>tk256a</i> allelic mutants	128
Figure 4.11 Testing Adgrg6 pathway hits in dose-response <i>vcanb</i> assay on <i>fr24</i> allelic mutants.....	130
Figure 4.12 Retesting apomorphine in phenotypic screening assays reveals it can mediate partial rescue of the <i>mbp</i> and <i>vcanb</i> phenotype in <i>adgrg6^{tb233c}</i> mutant larvae.	132
Figure 5.1 Cell baculoviral transduction	146
Figure 5.2 Fold-change in intracellular cAMP levels associated with expression of various human and zebrafish <i>ADGRG6</i> alleles.....	147
Figure 5.2 (supplement) cAMP levels detected in cells expressing various human and zebrafish <i>ADGRG6</i> alleles.	148
Figure 5.3 Expression of the GFP-tagged human <i>ADGRG6</i> gene in HEK293 cells.....	151
Figure 5.4 Expression of the GFP-tagged zebrafish <i>adgrg6</i> gene in HEK293 cells.....	152
Figure 5.4 (supplement) FuGENE-based transfection efficiency.	154
Figure 5.5 Optimisation of baculovirus dose for transduction of HEK293 cells.	157
Figure 5.6 HEK293 cell cAMP response curve to treatment with candidate Adgrgr6 agonists.....	160
Figure 5.7 HEK293 cell cAMP response curve to 30- or 120-minute treatment with candidate Adgrgr6 agonists.....	161
Figure 5.8 HEK293 cell cAMP response curve to known Adgrgr6 NTF ligands.....	163
Figure 5.9 HEK293 cell cAMP response curve to treatment with known ADGRG1 antagonists.	166
Figure 5.10 HEK293 cell cAMP response to treatment with low and high concentrations of known ADGRG1 antagonists.....	168
Figure 5.11 Preliminary comparison of cAMP levels in HEK293 cells transfected with various human and zebrafish <i>ADGRG6</i> alleles and wild-type-transfected cells treated with candidate receptor antagonists.....	169
Figure 5.12 Zebrafish phenotypes associated with dihydromunduletone treatment.....	172

List of Tables

Table 1.1 List of key zebrafish <i>adgrg6</i> mutants (Baxendale et al., 2021)	37
Table 1.2 List of key <i>ADGRG6</i> variants associated with human disease conditions (Baxendale et al., 2021)	42
Table 2.1 Primers for PCR and sequencing	50
Table 2.2 Zebrafish <i>adgrg6</i> primers for site-directed mutagenesis.....	50
Table 2.3 Human <i>ADGRG6</i> primers for site-directed mutagenesis	51
Table 2.4 PCR thermocycler protocol	51
Table 2.5 List DIG-labelled RNA probes	53
Table 2.6 Zebrafish transgenic line	54
Table 2.7 Zebrafish <i>adgrg6</i> mutant lines	54
Table 2.8 List of in situ hybridisation reagents	60
Table 2.9 List of primary antibodies.....	61
Table 2.10 List of secondary antibodies.....	61
Table 2.11 List of primary antibodies.....	63
Table 2.12 List of secondary antibodies.....	63
Table 3.1 Schwann cell gene markers.....	69
Table 4.1 Experimental conditions trialled with IBMX for optimisation of a counter-screening <i>mbp</i> assay.....	100
Table 4.2 Experimental conditions trialled with dihydropyridines for optimisation of a counter-screening <i>mbp</i> assay	100
Table 4.3 List of structurally novel hit compounds from the <i>vcanb</i> assay.....	113
Table 4.4 Novel <i>mbp</i> assay hits.....	120
Table 4.5 List of <i>Adgrg6</i> pathway hits tested on <i>fr24</i> allelic mutants.....	129

Chapter 1.

Introduction

1.1 Schwann cells

1.1.1 Function of Schwann cells

Schwann cells are the principal non-neuronal cells, known as glia, of the peripheral nervous system (PNS). They are known to provide trophic support for peripheral neurons but their main function is to insulate neuronal axons through the process of myelination. Schwann cells ensheath large diameter ($>1 \mu\text{m}$) (Gamble and Breathnach, 1965; Jessen and Mirsky, 1991, 2005) sensory and motor axons in the PNS with a lipid-rich myelin sheath that provides electrical insulation, similar to oligodendrocytes in the central nervous system (CNS). The myelin sheath reduces transverse capacitance and increasing transverse resistance of neuronal axons, which reduces charge loss as electrical impulses propagate along them (Nave and Werner, 2014). Furthermore, Schwann cells restrict clustering of axonal sodium channels to periodic gaps in the myelin sheath, the nodes of Ranvier, which drive saltatory nerve conduction (Voas *et al.*, 2009). Alternatively, small diameter ($\sim <1 \mu\text{m}$) axons are assembled together into Remak bundles that are enveloped by non-myelinating Schwann cells; such axons localise to troughs within these cells (Gamble and Breathnach, 1965; Jessen and Mirsky, 2005).

Although Schwann cells differentiate into myelinating or Remak cells, they have the ability to switch between the two subtypes in addition to a third type known as repair Schwann cells (Jessen and Mirsky, 2019a, 2019b). Upon nerve injury, extrinsic signals are known to activate reprogramming of Schwann cells to the repair cell lineage that coordinates remyelination. Repair Schwann cells secrete various molecules including cytokines such as $\text{IL-1}\beta$ and $\text{TNF-}\alpha$, to recruit macrophages, and trophic factors (Jessen and Mirsky, 2019a) to promote regeneration of axons, which in zebrafish has been observed towards their original trajectory (Rosenberg *et al.*, 2014). During this process, myelin is cleared and secretion of extracellular matrix components that form the basal lamina, including collagen and laminin, is increased to provide a support structure for regeneration.

1.1.2 Myelin diseases of the peripheral nervous system

Defects of the myelin sheath can impair nerve conduction, compromising function of the nervous system, and are associated with numerous human diseases that can lead to weakness, poor coordination, paralysis and death in severe cases (Margulis, Soloviev and Shubladze, 1946; Ravenscroft *et al.*, 2015; D'Rozario, Monk and Petersen, 2017; Kamil *et al.*, 2019). Diseases that affect

Schwann cells in particular include autoimmune and immune-mediated demyelinating diseases with comparable pathology to multiple sclerosis (MS) in the CNS. In cases of Guillain-Barre Syndrome (GBS) and Chronic Inflammatory Demyelinating Polyradiculoneuropathy (CIDP) the immune system attacks the myelin sheath in the PNS, leading to segmental demyelination (Kamil *et al.*, 2019). Similar pathology is also observed in diseases with genetic predisposition such as Charcot Marie Tooth (CMT) disease, which is associated with mutations in various genes, including those that encode myelin-related proteins (Kamil *et al.*, 2019). Alternatively, genetic predisposition is associated with disorders such as lethal congenital contracture syndromes (LCCS) that are characterised by the formation of joint contractures, known to result from inactivity of neuromuscular junctions (Hall, 1985; Ravenscroft *et al.*, 2015). LCCS9 is an example in which myelination of the PNS is defective as a result of a missense mutation in *ADGRG6*, which encodes an adhesion type G protein-coupled receptor (aGPCR) that regulates Schwann cell development (Ravenscroft *et al.*, 2015).

Demyelination can also be triggered by nerve injury, trauma and stress-inducing conditions that are damaging to Schwann cells, such as hyperglycemia in diabetes (Gonçalves *et al.*, 2017). Overall, damage to Schwann cells can compromise nerve homeostasis and glial-axon communication, which in turn can lead to neurodegeneration as neurons rely on Schwann cells for trophic support (Gonçalves *et al.*, 2017; Kamil *et al.*, 2019).

1.1.3 Development of Schwann cells

Schwann cells originate from neural crest cells following multiple intermediate stages of development including Schwann cell precursors (SCPs) and immature Schwann cells (iSCs), all marked by the expression of *SOX10*, which encodes a key transcription factor that regulates differentiation of neural crest-derived cell types (Jessen and Mirsky, 2005; Wahlbuhl *et al.*, 2012; D’Rozario, Monk and Petersen, 2017). Studies have revealed that Sox10 and its interaction with multiple other transcription factors, including Pax3, FoxD3 and Krox20 (EGR2), principally regulate Schwann cell development (Wahlbuhl *et al.*, 2012; reviewed in Jessen and Mirsky, 2019a). The initial transition of neural crest cells to SCPs appears to be coordinated by Sox10 and Pax3 (Jessen and Mirsky, 2019a); mutations in genes encoding these transcription factors are associated with disturbed neural crest development and depletion of SCPs has been observed in rodents (Franz, 1993; Doddrell *et al.*, 2012; Wahlbuhl *et al.*, 2012).

SCPs are highly proliferative cells that migrate along growing axons, providing trophic support for sensory and motor neurons (Riethmacher *et al.*, 1997; Jessen and Mirsky, 2005; Lyons *et al.*, 2005). During this developmental stage, axonal release of epidermal growth factor neuregulin-1 (NRG1), ligand of ErbB family tyrosine kinases expressed by Schwann cells, drives SCP migration and is important for their survival (Dong *et al.*, 1995; Riethmacher *et al.*, 1997). Zebrafish *erbb3* mutant

larvae exhibit down-regulated expression of *foxd3*, marking Schwann cells, and BrdU incorporation, marking dividing cells, highlighting a disruption to both migration and survival (Lyons *et al.*, 2005).

Following migration, signalling of key molecules including NRG1, Notch and FGF2 is thought to mediate SCP differentiation into iSCs (Jessen and Mirsky, 2005) that secrete extracellular matrix (ECM) components including collagen IV (Col4) and laminin-211 (Lam211). Both molecules have been identified as key regulators of peripheral axon sorting and myelination (Bunge and Bunge, 1986; Bunge, Bunge and Eldridge, 1986; Dong *et al.*, 1995; Detrait *et al.*, 1999; Monk *et al.*, 2011; Paavola *et al.*, 2014; Petersen *et al.*, 2015). Initially iSCs segregate axons through a process known as radial sorting, reaching a 1:1 ratio of axon:Schwann cell before myelination signalling pathways are initiated (Jessen and Mirsky, 2005; Raphael, Lyons and Talbot, 2011). ErbB signalling has a key role in the extension of Schwann cell processes into axon bundles during radial sorting that is disrupted in zebrafish larvae by treatment with ErbB inhibitor, AG1478 (Raphael, Lyons and Talbot, 2011). However, it is important to note that the extracellular N-terminal fragment (NTF) of adhesion G protein-coupled receptor G6 (*Adgrg6*) also has a key mechanosensing role in the radial sorting process (see section 1.2.1b) (Monk *et al.*, 2011; Petersen *et al.*, 2015).

Subsequent to axon sorting, activation of pro-myelinating markers such as Krox20 (*Egr2*), regulated by the ErbB and *Adgrg6* signalling pathways, facilitate the extension and wrapping process by which Schwann cells insulate individual axons (Svaren and Meijer, 2008; D’Rozario, Monk and Petersen, 2017; Ghidinelli *et al.*, 2017). Krox20 is a key transcription factor that regulates expression of various myelination genes including myelin basic protein (Mbp) that forms a key component of the myelin sheath (Svaren and Meijer, 2008; Monk *et al.*, 2009). It is important to note that studies on *Adgrg6* (Monk *et al.*, 2011), *Krox20* (reviewed in Svaren and Meijer, 2008) and *ErbB* (Riethmacher *et al.*, 1997) mutants have all revealed Schwann cell myelination defects.

1.1.4 The zebrafish model

1.1.4a Study of myelination in zebrafish

The majority of research that has contributed to our understanding of Schwann cell development and function has been elucidated from studies on rodents, *in vitro* models and examination of human tissue histology. However, morphogenetic changes and signalling pathways associated with myelination are conserved between mammals and zebrafish, and have led to the growing use of zebrafish as a model system to study myelination *in vivo* (D’Rozario, Monk and Petersen, 2017). Zebrafish embryos develop rapidly and are small and optically transparent, which makes them amenable with various analytical techniques including high-resolution imaging *in vivo*. Transgenic lines have been exploited to non-invasively track development of glial cells and the process of myelination

(Lyons *et al.*, 2005; Snaidero *et al.*, 2014; Almeida *et al.*, 2018; Preston *et al.*, 2019). In particular the Tg(*mbp*:EGFP-CAAX) line has been widely utilised to assess a range of myelin sheath features including its thickness, length and the number of myelin sheaths per oligodendrocyte (Almeida *et al.*, 2011, 2018; Snaidero *et al.*, 2014), which are known to myelinate multiple axons.

Alternatively, whole-mount *in situ* hybridisation can be utilised to illustrate mRNA expression pattern of various glial cell markers including Schwann cell myelination genes, such as *krox20* and *mbp*, in zebrafish mutants that display defects in myelination (Monk *et al.*, 2009). In particular, examination of such genes and others in *adgrg6* mutants that exhibit reduced Mbp expression (Monk *et al.*, 2009), resembling LCCS9 in humans (Ravenscroft *et al.*, 2015), have been exploited to illustrate the genetic mechanisms that may underlie mutant phenotypes (Monk *et al.*, 2009) (see section 1.2.1).

1.1.4b Drug screening in zebrafish larvae

Drug screening is currently dominated by target-based strategies due to the establishment of high throughput infrastructure for *in vitro* research and the recognition of numerous proteins as druggable targets (Swinney and Anthony, 2011; MacRae and Peterson, 2015). Despite these advantages, FDA-approved first-in-class drugs between 1999 and 2008 were not dominated by those uncovered through target-based approaches; in fact, a higher percentage of approved drugs were attributed to phenotypic approaches (Swinney and Anthony, 2011). Nevertheless, the majority of screening is performed *in vitro* with follow up work conducted in rodents as pharma appear reluctant to pilot alternative models due to uncertainties clouding the translation of discoveries to humans.

In recent years, interest in zebrafish has been growing following optimisation of zebrafish absorption, distribution, metabolism, excretion and toxicity (ADMET) assays (Parng *et al.*, 2002; Berghmans *et al.*, 2008; Bourrachot, Simon and Gilbin, 2008; Hill, 2011; Van den Bulck *et al.*, 2011; Diekmann and Hill, 2013). Over 70% of human genes have at least one orthologue in zebrafish (Howe *et al.*, 2013) and their small, externally-developing embryos present a whole animal drug screening model amenable to medium- and high-throughput approaches (Parng *et al.*, 2002). The availability of human disease-resembling zebrafish mutants, including those that resemble peripheral myelination diseases, has driven their use throughout the scientific community for drug screening (Baxendale *et al.*, 2012; MacRae and Peterson, 2015; Bremer, Skinner and Granato, 2017; Bradley *et al.*, 2019; Diamantopoulou *et al.*, 2019) (see also section 1.4). The establishment of CRISPR/Cas9 technology now offers a pathway to generate targeted mutant zebrafish lines, modelling human disease, for screening purposes (reviewed in Cornet, Di Donato and Terriente, 2018). Alternatively, wild-type larvae have also been utilised to screen for compounds that promote myelinating oligodendrocytes

without the added context of a specific disease phenotype (Early *et al.*, 2018). Multiple hits were identified that may have therapeutic potential in disease states, although this remains to be tested.

It is important to consider that phenotypic screens in zebrafish may not reveal compounds that hit a desired target and the mechanism of action of a therapeutic compound can be challenging to resolve. Therapeutic effects of FDA-approved compounds have been replicated in the zebrafish model (Baraban *et al.*, 2005; Berghmans *et al.*, 2008; Baxendale *et al.*, 2012). Groups are utilising this model to screen FDA-approved drugs for repurposing, in addition to screening other compounds with the aim of discovering new hits (Chiu *et al.*, 2008; Wang *et al.*, 2010; Baxendale *et al.*, 2012; Early *et al.*, 2018; Bradley *et al.*, 2019; Diamantopoulou *et al.*, 2019). Screening approved compounds for repurposing may not always be successful as compounds are likely to have higher selectivity for their known targets, which may not be favourable to the particular phenotype assessed in the screen. However, this strategy reduces the time frame and potential investment required to develop a therapeutic hit compound as their pharmacokinetic and safety profile is well documented following phase I testing. The bioavailability profile of compounds can also vary between zebrafish and mammals, thus hit compounds from zebrafish screens may not necessarily translate to humans (Long *et al.*, 2019). Nevertheless, prudent use of zebrafish is beginning to translate into compounds entering clinical trials and those approved for human use (North *et al.*, 2007; Baxendale, van Eeden and Wilkinson, 2017; Patton, Zon and Langenau, 2021).

1.2 Developmental roles of *Adgrg6* in zebrafish

1.2.1 *Adgrg6* in Schwann cells

1.2.1a *Promyelinating Schwann cells*

Studies have shown that *Adgrg6*, a member of the aGPCR subfamily, is an essential regulator that initiates myelination in Schwann cells (Monk *et al.*, 2009, 2011; Geng *et al.*, 2013). In the one-day-old zebrafish embryo, the expression of *adgrg6* is very similar to that of the transcription factor gene *sox10*, and *adgrg6* expression in the ear and neural crest is reduced in *sox10*^{-/-} mutants, suggesting that Sox10 may be an upstream regulator of *adgrg6* expression in these tissues (Geng *et al.*, 2013). However, SCPs are thought to develop independent of *adgrg6* expression as mutant *adgrg6* zebrafish larvae do not exhibit SCP migration defects and expression of *nrg1(III)* or *erbb3* is not disrupted (Monk *et al.*, 2009).

A range of mouse and zebrafish *Adgrg6* mutants exhibit reduced expression of pro-myelinating gene markers including *oct6*, *krox20* and *mbp* indicating that *Adgrg6* is involved in the regulation of these genes (Monk *et al.*, 2009, 2011; Geng *et al.*, 2013; Paavola *et al.*, 2014; Petersen *et al.*, 2015; Leon *et*

al., 2020). In the zebrafish larval PNS, *mbp* is robustly expressed in Schwann cells along the posterior lateral line nerves (PLLn) and ganglia (PLLg) (Brösamle and Halpern, 2002) whereas in *adgrg6* mutants this expression is significantly reduced (figure 1.1A) (Monk *et al.*, 2009; Geng *et al.*, 2013; Paavola *et al.*, 2014; Petersen *et al.*, 2015; Leon *et al.*, 2020). Treatment of zebrafish *adgrg6* mutant larvae with forskolin, an adenylyl cyclase agonist, mediates restoration of pro-myelinating genes (Monk *et al.*, 2009; Geng *et al.*, 2013), highlighting the role of intracellular cAMP signalling in myelinating Schwann cells (Raff, Hornby-Smith and Brockes, 1978; Monuki *et al.*, 1989). Contrastingly, reduced *mbp* expression in zebrafish *krox20* mutants cannot be rescued by forskolin, further supporting an upstream role for Adgrg6 (Monk *et al.*, 2009).

NRG1 released by neuronal axons has also been identified as a key trans-regulator of myelination as *Nrg1*ErbB2* compound heterozygote mutants exhibit significantly thinner myelin ensheathment of sciatic nerve axons (Michailov *et al.*, 2004). It appears therefore that a combination of Adgrg6 and NRG1 signalling is necessary for myelination; the former induces cAMP elevation, which has been shown to mediate switching of NRG1 signalling from proliferation to myelin differentiation (Arthur-Farraj *et al.*, 2011; Ghidinelli *et al.*, 2017). Treatment of zebrafish *adgrg6* hypomorphic mutants with the prion protein (PrP), an identified Adgrg6 ligand, has been shown to increase *Mbp* expression that is downregulated in DMSO controls (Küffer *et al.*, 2016). Current literature suggests that Adgrg6 is activated by biological ligands including Lam211 (Petersen *et al.*, 2015), Col4 (Paavola *et al.*, 2014) and PrP (Küffer *et al.*, 2016) leading to a signalling cascade resulting in expression of multiple transcription factors that drive expression of *mbp* and other lipid genes to facilitate myelination (Monk *et al.*, 2009; Schaefer and Brösamle, 2009; D’Rozario, Monk and Petersen, 2017).

There is evidence to suggest that protein kinase A (PKA), an identified component of the Adgrg6 signalling pathway, acts as an intermediate regulator of myelination (Mogha *et al.*, 2013; Ghidinelli *et al.*, 2017). Ghidinelli *et al.* (2017) have shown that PKA requires precise regulation by Lam211 as its overactivation can result in myelination prior to the completion of axonal sorting in sciatic nerves of *Lama2* – encoding the $\alpha 2$ subunit of Lam211 – null mice. Interestingly, active PKA levels are elevated in *Lama2* null mice whereas cAMP levels remain normal, and therefore Ghidinelli *et al.* (2017) propose a model in which Lam211 independently inhibits PKA activation, potentially through known binding with integrin or dystroglycan receptors (Feltri *et al.*, 2002; Berti *et al.*, 2011; Pellegatta *et al.*, 2013). Col4 may behave similarly as it has also been shown to bind with integrins and appears to perform similar functions to Lam211 (Detrait *et al.*, 1999; Paavola *et al.*, 2014; Labelle-Dumais *et al.*, 2019).

1.2.1b Radial sorting

Initial studies utilising *Adgrg6* knock-out mice uncovered a delay in radial sorting of peripheral axons by Schwann cells proposing an underlying role of *Adgrg6* in this process (Monk *et al.*, 2011). This hypothesis was met with initial uncertainty as zebrafish hypomorphic mutants, with a mutation in its C-terminal fragment (CTF), did not exhibit a similar phenotype (Monk *et al.*, 2009). However, axonal sorting deficiencies were observed in zebrafish *adgrg6^{stl47}* mutants that produce an early N-terminal truncated peptide (Petersen *et al.*, 2015). Moreover, this deficiency was unresponsive to forskolin treatment suggesting that axonal sorting materialises independently of intracellular signalling pathways associated with *Adgrg6* and could in fact be reliant on an intact extracellular NTF (Monk *et al.*, 2009, 2011; Geng *et al.*, 2013; Petersen *et al.*, 2015).

Interestingly, mutations in mouse genes encoding Lam211 receptors (Feltri *et al.*, 2002; Berti *et al.*, 2011; Pellegatta *et al.*, 2013), laminin genes (Chen and Strickland, 2003; Wallquist *et al.*, 2005; Yang *et al.*, 2005) and *Col4a1* (Labelle-Dumais *et al.*, 2019) are associated with radial sorting defects similar to those observed in *Adgrg6* knock-out mice. Petersen *et al.* (2015) show that wild type Schwann cells myelinate co-cultured dorsal root ganglia (DRG) neurons to a higher degree when cultured with a higher concentration of Lam211 and that this response was completely abolished in premature stop codon *Adgrg6* mutant Schwann cells with near absence of *Adgrg6*-NTF mRNA. Although Lam211 is known to bind with β 1-integrin receptors and regulate radial sorting through the focal adhesion kinase (FAK) signalling pathway (Feltri *et al.*, 2002; Berti *et al.*, 2011; Pellegatta *et al.*, 2013), the findings of Monk *et al.* (2011) and Petersen *et al.* (2015) implicate a mechanosensitive role of the *Adgrg6*-NTF in the sorting process, through interaction with Lam211. Moreover, the observation of radial sorting defects in *Col4a1* mouse mutants (Labelle-Dumais *et al.*, 2019) and recognition of Col4 as an *Adgrg6*-NTF ligand (Paavola *et al.*, 2014) provides further evidence for this and highlights the key role of Schwann cell secreted basal lamina in radial sorting. Schematic in figure 1.2 illustrates roles of key proteins in radial sorting and myelination.

1.2.1c Regeneration

In mammals, *Adgrg6* is expressed in mature Schwann cells following myelination and although it appears not to have a role in myelin maintenance, it does appear to have a key role in regeneration of the myelin sheath following nerve injury. Mogha *et al.* (2016) characterise a Schwann cell-specific tamoxifen-inducible *Adgrg6* conditional knockout mouse. Expression of *Mbp* is unaffected in tamoxifen-injected mice under normal conditions; however, examination of sciatic nerve axons following nerve crush injury reveals impaired remyelination and presence of myelin debris that is attributed to a failure in the ability of Schwann cells to recruit macrophages to the damage site (Mogha *et al.*, 2016). Fewer axons are myelinated and of those axons that are, the myelin sheath is significantly

thinner. Axon regeneration is also impaired in tamoxifen-injected mice (Mogha *et al.*, 2016). This may be attributed to non-myelinating terminal Schwann cells (tSCs), which have roles in guidance of regenerative axons and reinnervation of neuromuscular junctions (Jablonka-Shariff *et al.*, 2019).

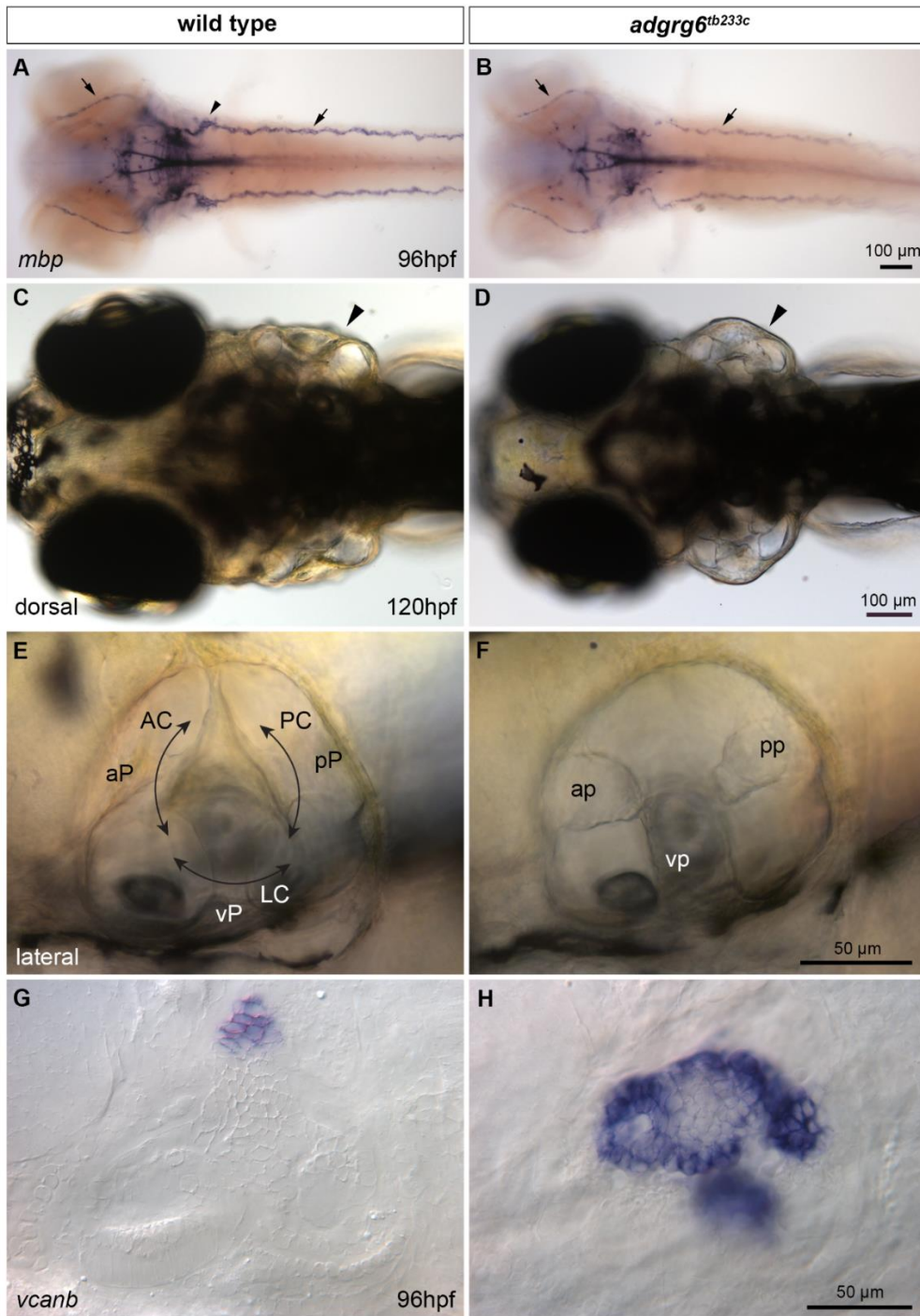


Figure 1.1 Peripheral myelination and inner ear phenotypes in *adgrg6^{tb233c}* zebrafish mutants.

(A-B) mRNA expression of *mbp* is downregulated along the posterior lateral line (arrows, nerve; arrowhead, ganglion) in *adgrg6^{tb233c}* mutants (B) in comparison to wild-type (A) larvae, shown at 96 hpf (dorsal view). **(C-F)** live images of 120 hpf larvae, illustrating formed semicircular canals in wild-type larvae (C, E) and the otic phenotype observed in *adgrg6* zebrafish mutants (D, F). Otic vesicles are swollen (arrowhead, D) and projections are unfused (F) in *adgrg6* mutants. Double-headed arrows indicate presence of individual semicircular canals in wild-type larvae. **(G-H)** *vcanb* mRNA is temporally expressed during canal morphogenesis and is downregulated in wild-type larvae by 96 hpf whereas persistent overexpression is observed in *adgrg6* mutants. Abbreviations: AC, anterior canal; aP, anterior pillar; ap, anterior projection; LC, lateral canal; PC, posterior canal; pP, posterior pillar; pp, posterior projection; vP, ventral pillar; vp, ventral projection.

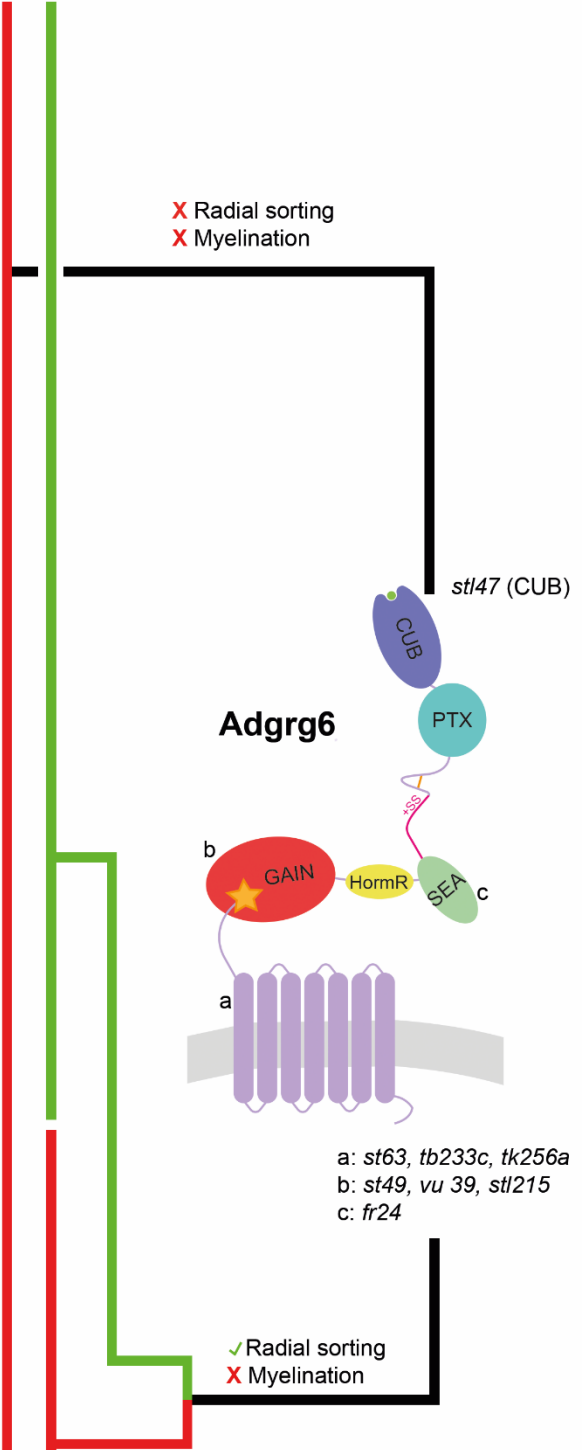
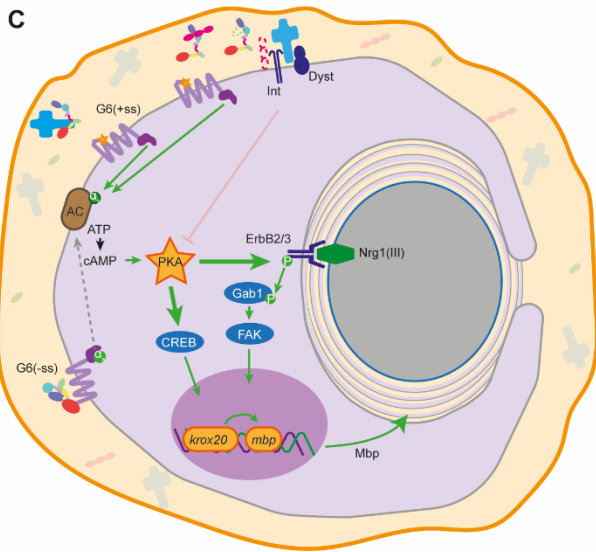
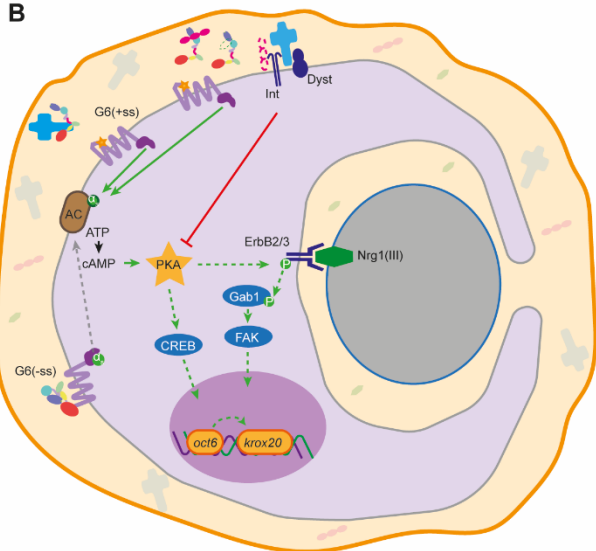
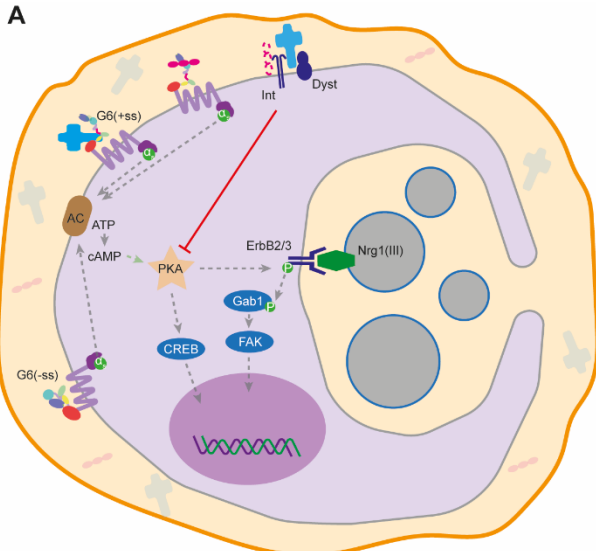


Figure 1.2 Schematic illustration of intracellular signalling pathways involved in the coordination of radial sorting and myelination of the PNS.

(A) basal activity of intracellular signalling networks in immature Schwann cells (iSCs, magenta cell) that radially sort neuronal axons (grey cell). Activation of protein kinase A (PKA) is inhibited by lam211 (cyan molecule in the ECM, amber) at this stage. **(B)** following axonal sorting, lam211 and other *Adgrg6* ligands are proposed to mediate activation of *Adgrg6* that leads to activation of adenylyl cyclase and accumulation of cAMP. This effector molecule is known to activate PKA, which in-turn activates transcription factor CREB in addition to the signalling pathway associated with ErbB receptors. Collectively, activation of CREB and FAK mediate transcription of myelination genes, including *oct6* and *krox20*. At this early stage some inhibitory influence of lam211 on PKA may remain to control the initiation of myelination. **(C)** in promyelinating Schwann cells, the inhibitory effects of lam211 are thought to subside, enabling stronger activation of myelination signalling pathways that result in ensheathment of axons with multiple layers of myelin. The right hand panel illustrates processes that are active (green) or disrupted (red) in various *adgrg6* zebrafish mutants. Category **a** mutations reside in the transmembrane domain, **b** in the GAIN domain (including *stachel* sequence and GPS site) and **c** in the recently identified SEA domain (Leon *et al.*, 2020). The receptor and its domain information can be found in figure 1.4. In the left panel faded arrows indicate basal activity; dashed grey arrows indicate direction of signalling cascade; dashed green arrows indicate moderate activation; absolute green arrows indicate strong activation; absolute black arrow indicates molecule conversion; red blunt arrow indicates inhibition. Abbreviations: AC, adenylyl cyclase; CREB, cAMP response element-binding protein; Dyst, dystroglycan receptor; ECM, extracellular matrix; FAK, focal adhesion kinase; G6, *Adgrg6*; Gab1, GRB2 Associated Binding Protein 1; Int, integrin receptor; iSCs, immature Schwann cells; PKA, protein kinase A; +ss/-ss, *Adgrg6* isoforms (see sections 1.3.2 and 1.3.3b).

1.2.2 The vertebrate inner ear

The vertebrate inner ear contains sensory end-organs with auditory and vestibular function that respond to sound, gravitational and movement stimuli (reviewed in Whitfield, 2015). Defective development of the inner ear or its functional impairment are heavily associated with deafness and abnormalities in balance, including dizziness (Whitfield *et al.*, 2002; Dallan *et al.*, 2008). Approximately 1.79 in a thousand new-borns are affected by hearing impairment (Watkin and Baldwin, 2012), whilst vestibular symptoms are reported by a third of the general population and are often misinterpreted as other neural conditions (Agrup, Gleeson and Rudge, 2007).

Multiple studies have illustrated the expression of *adgrg6* in the zebrafish inner ear and highlighted deformities of the developing semicircular canals in zebrafish *adgrg6* mutant larvae (Monk *et al.*, 2009; Geng *et al.*, 2013; Liebscher *et al.*, 2014; Leon *et al.*, 2020). Although equivalent phenotypes have not yet been observed in *Adgrg6* mouse mutants or in association with human pathogenic mutations, the zebrafish inner ear offers a system in which to further investigate signalling pathways associated with *Adgrg6*. Zebrafish homozygous *adgrg6* mutants are adult viable whereas mutations in mice (Monk *et al.*, 2011) and humans (Ravenscroft *et al.*, 2015) are lethal, leading to early death from myelination and cardiovascular defects (Monk *et al.*, 2011) that could mask any potential ear defects.

1.2.2a The zebrafish vestibular system

The inner ear contains three semicircular canals, anterior, posterior and lateral, which perform a vestibular function by detecting linear and angular acceleration in three-dimensional space (Fritsch *et al.*, 2007; Geng *et al.*, 2013). Each individual canal is composed of a fluid filled duct that ends in an ampulla, harbouring a sensory patch of mechanosensing hair cells known as crista (Whitfield, 2015). In zebrafish, the superficially located lateral line sensory system spanning the body complements the inner ear. The zebrafish lateral line system is comprised of neuromasts positioned around the head (anterior, ALL) and across the trunk (posterior, PLL) (Raible and Kruse, 2000). Neuromasts can be visualised as rosettes of support cells and mechanosensitive hair cells that sense changes in surrounding water pressure and movement, and transmit this information to the CNS via bipolar afferent neurons whose cell bodies form the ALL ganglion (ALLg), innervating neuromasts around the head, and PLLg, innervating those along the trunk (Raible and Kruse, 2000). These lateral line neurons are supported and myelinated by Schwann cells (Brösamle and Halpern, 2002). Given that *mbp* expression in Schwann cells along the PLLn is reduced in *adgrg6* mutant zebrafish larvae (see section 1.2.1a and figure 1.1A), transmission of mechanosensory information along these nerves may also be impaired. Adult *adgrg6* zebrafish mutants exhibit defects in coordinating their balance in water and are 'jumpy' if their tanks are knocked (subjective observation not published, Whitfield lab). Interestingly, this phenotype appears more apparent in *adgrg6*^{fr24} mutant adults in which peripheral

mbp expression is absent during earlier development stages (4dpf, Geng et al., 2013). It is likely that the 'jumpy' phenotype is attributed to semicircular canal deformities and compromised vestibular function, however, the enhanced severity in *fr24* allelic mutants highlights a potential effect of impaired myelination of the lateral line.

1.2.2b A role for *Adgrg6* in morphogenesis of the zebrafish semicircular canals system

The otic vesicle, which develops from pre-placodal ectoderm, undergoes topological shape changes to give rise to a complex labyrinth of three semicircular canal ducts positioned orthogonally to each other (Waterman and Bell, 1984; Whitfield, 2015). Waterman and Bell (1984) give a thorough account of this process by tracking topological changes in the developing zebrafish embryo, with support of light and electron microscopy imaging techniques. Alternatively, the expression of *versican* genes, *vcana* and *vcanb*, which encode chondroitin sulphate proteoglycan core proteins, has been shown to mark key events throughout canal formation (Geng et al., 2013). Invaginations of otic tissue gives rise to four projections, the anterior, posterior and ventral, all of which converge towards a lateral projection (Waterman and Bell, 1984). Three bulges of the lateral projection come into contact with individual converging projections before a fusion event, giving rise to the anterior, posterior and ventral pillars (Waterman and Bell, 1984; Geng et al., 2013). Pillar formation allows compartmentalisation of the otic vesicle into three fluid filled semicircular canals – the anterior, posterior and lateral (figure 1.1E). *vcana* is robustly expressed in the projection epithelia at 56 hpf; however, expression is significantly downregulated by 84 hpf following the fusion events that give rise to pillars and remains only weakly expressed in cells of the dorsolateral septum by 4 dpf (Geng et al., 2013). Contrastingly, in *adgrg6* zebrafish mutants the anterior, posterior and ventral projections grow past bulges of the lateral projection and the overall ear appears swollen (figure 1.1D, F) in comparison to wild-type embryos (Whitfield et al., 1996; Geng et al., 2013). Not only are the projections overgrown, but robust expression of *versican* genes persists beyond 84 hpf, by which point in wild-type embryos the pillars have formed and *versican* is downregulated (figure 1.1G-H) (Waterman and Bell, 1984; Geng et al., 2013). The expression of numerous other genes that encode ECM components including enzymes exhibit unusually high levels of expression in *adgrg6* mutant larvae at 4dpf (Geng et al., 2013). These observations indicate a role for *Adgrg6* in regulating the contact and fusion events that lead to formation of pillars, and possibly in repression of genes encoding ECM components.

Expression of *adgrg6* has been observed in cells of the otic projection epithelia (figure 1.3B) and its adhesive properties uncovered from PNS studies on radial sorting (Petersen et al., 2015; Morgan et al., 2019) accentuate *Adgrg6* as a candidate regulator of the contact and fusion events that underlie pillar formation. Nevertheless, forskolin treatment is sufficient to rescue the fusion events in both hypomorphic CTF mutants and NTF nonsense mutants that are known to exhibit overgrown

projections (Geng *et al.*, 2013; Diamantopoulou *et al.*, 2019). This unexpected result indicates that fusion is dependent on intracellular cAMP signalling activity (figure 1.3D-E). Alternatively, the NTF has been observed to act independently to the CTF during heart trabeculation in a paracrine manner (Patra *et al.*, 2013) and may do so in the inner ear to facilitate contact and fusion between opposing projection cells (figure 1.3C). *Adgrg6* is expressed in a range of cells across organs exposed to mechanical stimuli (Musa *et al.*, 2019) during development and therefore potential adhesive roles in the ear may require further investigation.

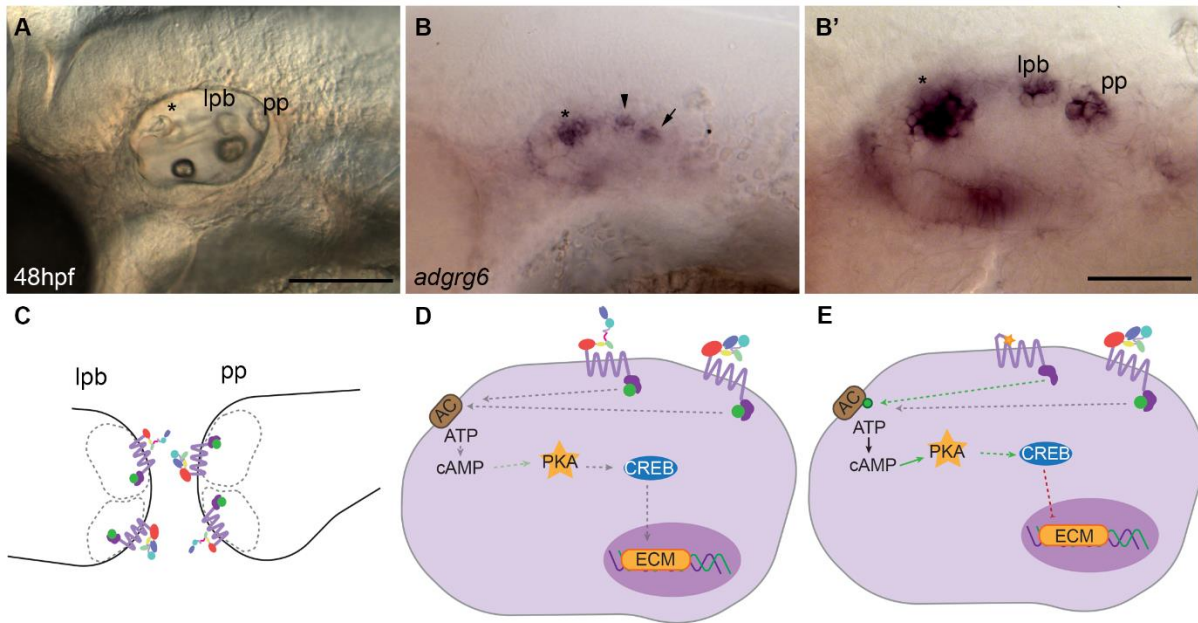


Figure 1.3 Otic expression of *adgrg6* in the developing embryo and proposed roles of its encoded protein, in semicircular canal morphogenesis.

(A) live image of the otic vesicle at 48 hpf illustrating positions of the developing epithelial projections. Anterior and lateral projection (anterior bulge) (asterisk) are in contact, posterior projection (pp) and posterior bulge of the lateral projection (lpb) are also shown. (B) expression of *adgrg6* mRNA in the regions highlighted in (A) (arrowhead, lpb; arrow, pp); (B') magnified view of image in B. (C) schematic representation of potential *Adgrg6* expression in projection epithelia. (D-E) schematic illustration of proposed intracellular signalling pathways associated with *Adgrg6* in projection epithelial cell (magenta); (D) basal conditions; (E) activation of *Adgrg6* or treatment with compounds that mediate cAMP accumulation are thought to result in down-regulated expression of various ECM genes, including *versican*. Faded arrows, basal levels of activity; dashed grey arrows, direction of signalling cascade; dashed green arrows, moderate activation; absolute green arrows, strong activation; absolute black arrow, molecule conversion; red blunt arrow, inhibition. Abbreviations: AC, adenylyl cyclase; CREB, cAMP response element-binding protein; ECM, extracellular matrix; PKA, protein kinase A.

1.3 Adhesion G protein-coupled receptor G6

1.3.1 G protein-coupled receptors (GPCRs)

1.3.1a Classes of GPCRs

The G protein-coupled receptor (GPCR) superfamily is the largest family of transmembrane receptors in the human genome that regulate a diverse range of developmental and physiological processes through conserved signalling pathways (Manglik and Kruse, 2017). These receptors transduce signals across the cell membrane upon binding of an extracellular ligand, initiating conserved intracellular G protein signalling pathways. The superfamily is comprised of six classes of receptors including rhodopsin-like (A), secretin family (B), metabotropic glutamate (C), fungal mating pheromone (D), cAMP (E), and frizzled and smoothed (F) (Langenhan, Aust and Hamann, 2013; Basith *et al.*, 2018). All GPCRs share a conserved core structure that includes a 7-pass transmembrane domain (7TM) connected by extracellular and intracellular loops. However, GPCRs differ in their sequence identity that underlies differences in ligand-binding sites, activation mechanisms and association with intracellular signalling pathways.

Adhesion GPCRs (aGPCRs) are the second largest group of GPCRs (family B2) comprising 33 homologues in the human genome, encoded by considerably large genes (Fredriksson *et al.*, 2003; Hamann *et al.*, 2015; Langenhan, 2019). They are characterised by a long NTF and are most closely related to secretin family receptors (Langenhan, Aust and Hamann, 2013). aGPCRs are becoming a growing target for anti-cancer therapies; their mis-regulation or respective gene mutations can be causative of immune defects and are often detected in cancers (Shashidhar *et al.*, 2005; Boyden *et al.*, 2016).

1.3.1b G protein signalling pathways

GPCRs signal by means of conserved pathways to transduce an external cue into an internal cell response governed by heterotrimeric G proteins that are composed of three subunits α , β and γ . The β and γ subunits interact tightly whereas the α subunit is able to dissociate following ligand-induced activation of GPCRs (Syrovatkina *et al.*, 2016). This transition acts as a binary switch to activate various intracellular signalling pathways associated with an individual $G\alpha$ subunit family. There are four families of G proteins, identified by their $G\alpha$ subunit, including $G\alpha_s$, $G\alpha_i$, $G\alpha_{q/11}$ and $G\alpha_{12/13}$ (Syrovatkina *et al.*, 2016; Lizano, Hayes and Willard, 2020). Each family is comprised of multiple members that share a high degree of amino acid sequence identity and function; however, their expression can vary in different cell types (Syrovatkina *et al.*, 2016). $G\alpha_s$ and $G\alpha_i$ proteins are well known to modulate adenylyl cyclase; $G\alpha_s$ stimulates adenylyl cyclase to generate cAMP from ATP whereas $G\alpha_i$ inhibits adenylyl cyclase, thereby limiting cAMP levels (Syrovatkina *et al.*, 2016; Langenhan, 2019; Baxendale

et al., 2021). Alternatively, $G\alpha_{q/11}$ and $G\alpha_{12/13}$ are known to interact with various targets including phospholipase C, for $G\alpha_{q/11}$ and multiple RhoGEFs, for $G\alpha_{12/13}$ (Syrovatkina *et al.*, 2016; Lizano, Hayes and Willard, 2020). Therefore, activation of GPCRs can lead to a range of intracellular responses, dependent on the G protein they couple with.

1.3.2 The *adgrg6* gene

The zebrafish *adgrg6* gene (figure 1.4A, mutant alleles included in Table 1.1) has a 1:1 correspondence with the orthologous human gene (Ensembl) and the protein shares approximately 50% identity with the human protein. The highest identity is in the transmembrane region, which also exhibits homology to secretin-like GPCRs (Patra, Monk and Engel, 2014). Alternative splicing in the N-terminus has been found in other aGPCRs (Salzman *et al.*, 2016; Xu *et al.*, 2019), and is thought to enhance receptor versatility and offers a regulatory mechanism for their activity (Bjarnadóttir *et al.*, 2006). The human and zebrafish *ADGRG6* genes are known to have four main alternative splice forms (Patra *et al.*, 2013), which include alternative splicing (+ss, -ss) of a short exon 6, coding for 23 amino acids in zebrafish (28 in human), in the linker between the SEA and PTX domains (figure 1.4) (Moriguchi *et al.*, 2004; Patra *et al.*, 2013; Leon *et al.*, 2020). Presence or absence of the penultimate exon alters the C-terminal coding sequence, which has the potential to alter down-stream signalling events (Moriguchi *et al.*, 2004). Expression of multiple *Adgrg6* isoforms may influence mechanical interactions with its binding partners and/or G protein coupling, enhancing versatility of the receptor.

1.3.3 aGPCR Structure, *Adgrg6*

1.3.3a Structural domains

aGPCRs are characterised by a long extracellular region (ECR) associated with a 7-pass transmembrane domain (7TM) and a short cytoplasmic C-terminal tail (figure 1.4) (Stacey *et al.*, 2000; Bjarnadóttir *et al.*, 2004, 2006). The ECR of *Adgrg6* is composed of conserved structural domains including the Complement C1r/C1s, Uegf, Bmp1 (CUB), Pentraxin (PTX), Hormone Receptor (HormR) (Moriguchi *et al.*, 2004), and GPCR autoproteolysis-inducing (GAIN) domains (Araç *et al.*, 2012), and a newly identified Sperm protein, Enterokinase and Agrin (SEA) domain, which contains a furin cleavage site in the human protein (Leon *et al.*, 2020). Autoproteolytic cleavage at the GPCR Proteolysis Site (GPS) within the GAIN domain separates the protein into N- and C-terminal fragments (NTF, CTF), which nevertheless can remain non-covalently associated at the membrane, with the tethered agonist *stachel* sequence of the CTF embedded within beta sheets of the NTF GAIN domain (Araç *et al.*, 2012; Langenhan, Aust and Hamann, 2013; Liebscher *et al.*, 2014; Petersen *et al.*, 2015). The human protein undergoes similar events to separate at the furin cleavage site that may offer alternative modes of activation, not conserved in zebrafish (Leon *et al.*, 2020).

Structural domains comprising the NTF are shared across GPCR subfamilies (Langenhan, Aust and Hamann, 2013), facilitating a diverse array of functions upon interaction with ECM components (reviewed in Purcell and Hall, 2018). The CUB domain has been shown to bind protein targets with collagen-like regions (Blanc *et al.*, 2007; Paavola *et al.*, 2014), a property that makes it a key interactive component of numerous proteins including those with roles in developmental patterning and cell signalling (Gaboriaud *et al.*, 2011). A CUB domain subtype has been identified that contains a Ca²⁺-binding site comprised of a glutamine and two aspartate residues conserved among several receptors including Adgrg6 (Gregory *et al.*, 2003; Blanc *et al.*, 2007; Leon *et al.*, 2020). The presence of this site has been shown to facilitate conformational changes and protein-ligand interaction that may play key roles in receptor function (Gaboriaud *et al.*, 2011). The PTX, HormR and SEA domain may also be targeted by ECM ligands, offering multiple activation routes that could facilitate dynamic physiological application of Adgrg6 (Araç *et al.*, 2012).

1.3.3b Structural conformation of the Adgrg6 ECR

X-ray crystallography of ECR regions has been valuable in resolving their domain organisation and structural conformations in four aGPCRs (Vakonakis *et al.*, 2008; Salzman *et al.*, 2016; Leon *et al.*, 2020; Ping *et al.*, 2021). Crystallisation of the zebrafish Adgrg6 ECR -ss form lacking exon 6 has revealed that this isoform adopts a closed conformation, in which the CUB domain interacts with the HormR domain (Leon *et al.*, 2020). This closed configuration, also confirmed for the -ss ECR in solution by negative stain electron microscopy and small angle X-ray scattering, is dependent on the presence of a Ca²⁺-binding site within the CUB domain, together with a disulphide-stabilised loop between the SEA and PTX domains. This loop inserts between the CUB and HormR domains, stabilising their interaction (Leon *et al.*, 2020).

The 23aa linker in the +ss form appears to disrupt the stability of the CUB-HormR interaction as the ECR is imaged in a variety of conformations, indicating an ability to switch between an open and closed state (Leon *et al.*, 2020). This mobility translates to an increase in cellular Adgrg6 signalling, measured in an *in vitro* cAMP assay, in comparison with basal activity associated with the closed isoform (Leon *et al.*, 2020).

In contrast, an intact Ca²⁺-binding site remains necessary for optimal receptor function. Disruption of the Ca²⁺-binding site, by CRISPR/Cas9 site-directed mutagenesis in zebrafish *adgrg6*^{st1464} mutant larvae, induces ear and myelination defects similar to those observed in strong loss-of-function *adgrg6* zebrafish mutants (Monk *et al.*, 2009; Geng *et al.*, 2013; Leon *et al.*, 2020). Although the mutated ECR appears to switch between open and closed configurations, the +ss Adgrg6 isoform is unable to mediate an increase in cAMP accumulation above basal levels (Leon *et al.*, 2020). These findings

propose a complex mechanism by which the ECR may regulate Adgrg6; however, an intact Ca²⁺-binding site and 23aa linker are necessary to trigger a boost in basal Adgrg6 signalling. The Ca²⁺-coordinating residues are conserved in the Adgrg6 CUB domain across a range of species, including humans (Leon *et al.*, 2020), highlighting the broad significance of these mechanistic insights from the zebrafish protein. However, it is important to consider that these structural discoveries, including similar research on the ECR of ADGRG1, are elucidated from crystallisation of the ECR alone and do not provide conclusive evidence of the full length receptor conformations *in vivo* (Salzman *et al.*, 2016; Leon *et al.*, 2020).

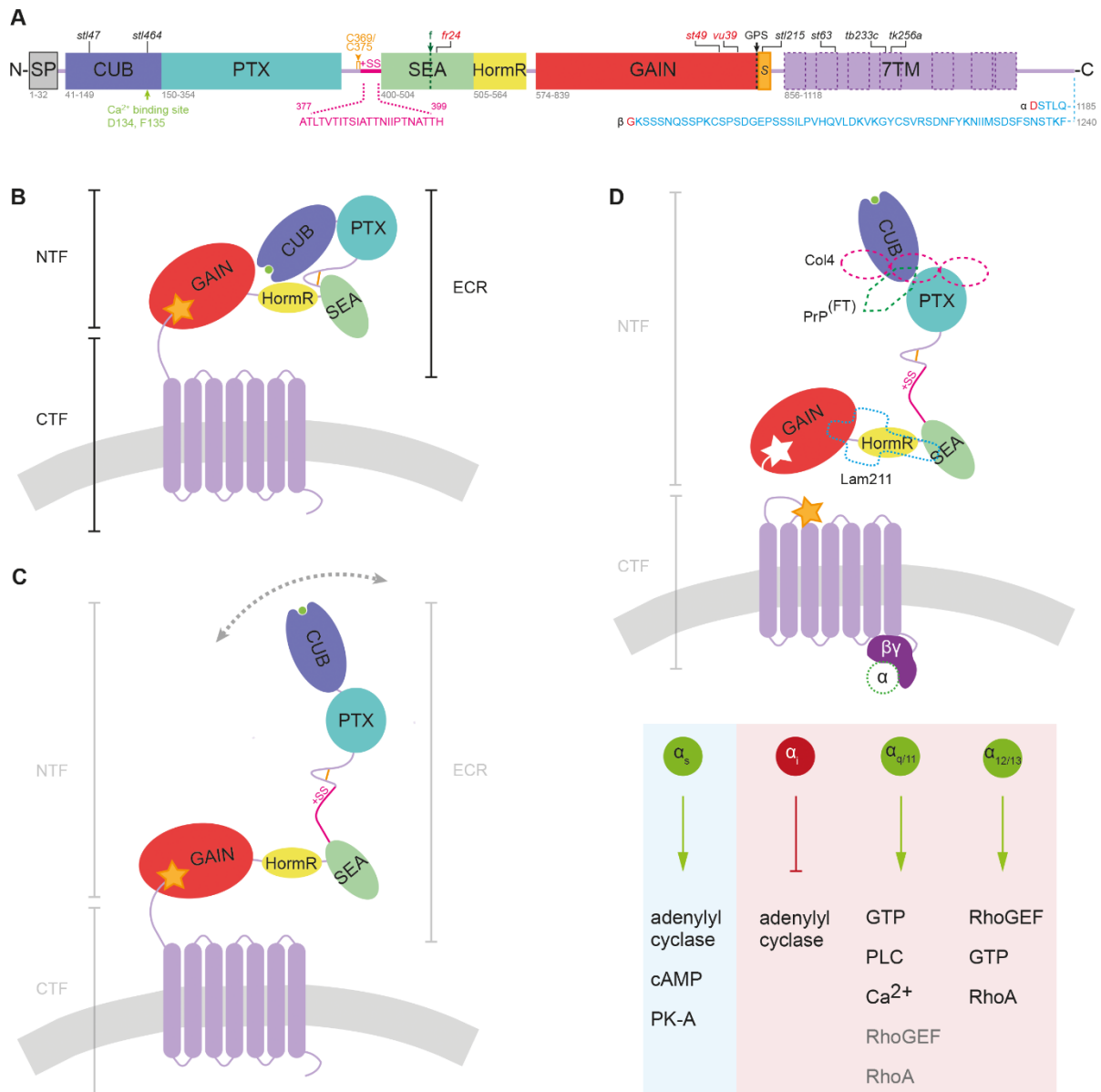


Figure 1.4 Schematic models of zebrafish Adgrg6 protein structure and mechanism of activation.

(A) zebrafish Adgrg6 protein sequence and domain organization, drawn to scale: signal peptide (SP), Complement C1r/C1s, Uegf, BMP1 (CUB), Pentraxin (PTX), Sperm protein, Enterokinase and Agrin (SEA), hormone receptor (HormR), GPCR autoproteolysis-inducing (GAIN), *stachel* sequence (S) and 7-pass transmembrane (7TM, magenta) domains. The sequence of Adgrg6 splice isoforms is shown below the diagram: S1, including exon 6 (+SS, pink), and the short (α) and long (β) isoforms resulting from inclusion or exclusion, respectively, of exon 25 (amino acid sequence in blue; splice site in red). The two cysteine residues (C369, C375) that form a bond in the linker between PTX and SEA domain are shown in amber. Cleavage sites are highlighted by dotted lines: GPCR autoproteolytic site (GPS, black), and position of furin cleavage site in mammalian ADGRG6 (f, green). Positions of widely studied zebrafish mutations are shown above the diagram: truncating (nonsense) mutations in red; missense mutations in black. **(B)** structure of Adgrg6 S2 isoform in closed conformation (not to scale). Domains correspond to those illustrated in (A); Ca²⁺ – binding site (green) within CUB domain, cell membrane (grey). **(C)** structure of Adgrg6 S1 isoform in open conformation. **(D)** overview of potential Adgrg6 *stachel* activation mechanism (not to scale). Tethered *stachel* sequence (amber star) self-activates Adgrg6 following removal of NTF. The NTF is also thought to signal in trans (not shown). Known Adgrg6

NTF ligands (dashed shapes) include Collagen IV (pink, Col4), prion protein flexible tail (PrP^{FT}, green), and Laminin-211 (Lam211, turquoise). Signalling is transduced by various G protein α subunits activating intracellular pathways, elucidated from zebrafish *Adgrg6* studies (light blue) and mouse or human ADGRG6 studies (light red). This figure is taken from Baxendale et al. (2021) and summarizes findings of (Moriguchi *et al.*, 2004; Geng *et al.*, 2013; Patra *et al.*, 2013; Liebscher *et al.*, 2014; Paavola *et al.*, 2014; Petersen *et al.*, 2015; Küffer *et al.*, 2016; Leon *et al.*, 2020; Lizano, Hayes and Willard, 2020).

Table 1.1 List of key zebrafish *adgrg6* mutants (Baxendale *et al.*, 2021)

Mutation	Amino Acid	Domain	Phenotype	Reference
<i>stl47</i>	Δ 5+3, N68K, fs*28	CUB	ear, radial sorting, PNS myelination	(Petersen <i>et al.</i> , 2015; Morgan <i>et al.</i> , 2019)
<i>stl464</i>	<i>D134A, F135A</i>	CUB	ear & PNS myelination	(Leon <i>et al.</i> , 2020)
<i>fr24</i>	L463*	SEA	ear & PNS myelination	(Geng <i>et al.</i> , 2013)
<i>st49</i>	Y782*	GAIN	ear & PNS myelination	(Pogoda <i>et al.</i> , 2006; Monk <i>et al.</i> , 2009)
<i>vu39</i>	W804*	GPS	ear & PNS myelination	(Geng <i>et al.</i> , 2013)
<i>stl215</i>	Δ <i>G831, I832</i>	<i>Stachel</i>	ear & PNS myelination	(Liebscher <i>et al.</i> , 2014)
<i>st63</i>	<i>C917Y</i>	TM2	PNS myelination	(Pogoda <i>et al.</i> , 2006; Monk <i>et al.</i> , 2009)
<i>tb233c</i>	<i>I963N</i>	TM4	ear & PNS myelination	(Geng <i>et al.</i> , 2013)
<i>tk256a</i>	<i>P969L</i>	TM4	ear & PNS myelination	(Geng <i>et al.</i> , 2013)

Note: amino acid sequence and numbering are based on the reference sequence NM_001163291.2, with the exception of W804, which was reported as C804 in the reference sequence (see discussion in Geng *et al.*, 2013). N68 was reported as Q68 in Petersen *et al.* 2015. Italic text indicates amino acid identity or similarity with the human protein. Abbreviations: Δ , deletion; fs, frame shift; see figure 1.4 for domain name abbreviations.

1.3.4 Adgrg6 activation mechanism and intracellular signalling pathway

1.3.4a Overview

Although GPCRs are incorporated into the cell membrane, they are somewhat structurally plastic and undergo conformational changes upon ligand binding. Such molecules can alter the stabilised state of GPCRs from active to inactive, particularly for constitutively active receptors, or inactive to active, which in turn modulates intracellular binding or dissociation of G protein subunits (Manglik and Kruse, 2017). Amino acids can similarly elicit stabilising effects by forming salt-bridges, disulphide bridges or hydrogen bonds that are also fundamental to conformational changes in proteins. GPCRs including the adhesion subtype can regulate expression of numerous gene targets by coupling to multiple G protein subunits, driving a complex network of cellular activity. While intracellular G protein signalling pathways are largely conserved in aGPCRs, the mechanisms by which aGPCRs are activated can differ due to the sizeable NTF.

1.3.4b Adgrg6 coupling to G proteins

Studies in zebrafish have shown that myelination defects in *adgrg6* mutants can be rescued by treatment with compounds that increase cAMP levels including forskolin and 3-isobutyl-1-methylxanthine (IBMX), a phosphodiesterase inhibitor that prevents cAMP degradation (Monk *et al.*, 2009; Diamantopoulou *et al.*, 2019; Baxendale *et al.*, 2021). The swollen ear phenotype in *adgrg6^{tb233c}* hypomorphic mutants can also be ameliorated by treatment with these compounds suggesting that Adgrg6 couples to a $G\alpha_s$ signalling pathway in both Schwann cells and in the ear (Geng *et al.*, 2013; Diamantopoulou *et al.*, 2019). Coupling to $G\alpha_s$ has been confirmed by several groups by detecting changes in intracellular cAMP levels following expression of ADGRG6 (Liebscher *et al.*, 2014; Paavola *et al.*, 2014; Petersen *et al.*, 2015). Nevertheless, this may not represent the full picture as GPCRs can couple to multiple G protein subunits (reviewed in Langenhan, 2019). For instance, application of a novel enterokinase-activated tethered ligand system of human ADGRG6 has revealed downstream increases in serum response factor (SRF) and element (SRE), partially sensitive to the $G\alpha_{q/11}$ inhibitor YM-254890, indicating activation of both $G\alpha_{12/13}$ and $G\alpha_{q/11}$ pathways (Lizano, Hayes and Willard, 2020). However, a study utilising chimeric G proteins concluded that the human receptor can couple to $G\alpha_s$ and $G\alpha_i$, but not $G\alpha_{q/11}$ (Mogha *et al.*, 2013). Given the evidence, a complex interplay of multiple signalling pathways is likely to be associated with the Adgrg6 receptor *in vivo*.

1.3.4c Adgrg6 NTF binding partners and intracellular signalling

Early aGPCR studies highlighted that the NTF-CTF interaction at the cell membrane provides an inhibitory control mechanism to limit receptor signalling through G proteins (Okajima, Kudo and Yokota, 2010; Paavola *et al.*, 2011). Paavola *et al.* (2011) reported that an increase in active

downstream signalling effector RhoA observed in ADGRG1-expressing cells is elevated 2-fold in cells expressing NTF truncated ADGRG1. This finding highlights that ADGRG1 can signal intracellularly without its NTF whilst also illustrating the constitutive activity of NTF truncated aGPCRs, which has been confirmed for multiple such receptors (Liebscher *et al.*, 2014; Stoveken *et al.*, 2015).

The Adgrg6 NTF has been found to interact with ECM components; direct binding between the NTF and Lam211 has been shown by co-immunoprecipitation (Petersen *et al.*, 2015) whereas binding with Col4 was illustrated by a biotinylated pulldown approach (Paavola *et al.*, 2014). The approximate binding sites of these molecules along the Adgrg6-NTF were elucidated by testing against truncated fragments of the NTF; Col4 binds across the CUB and PTX domains (Paavola *et al.*, 2014) whereas Lam211 appears to bind somewhere across the SEA, HormR and GAIN domains (Petersen *et al.*, 2015; Leon *et al.*, 2020).

Col4 and the PrP flexible tail residues 23-50 (PrP_{FT23-50}) share a region with high similarity that has been shown to directly mediate an increase cAMP accumulation in Adgrg6 expressing cells (Paavola *et al.*, 2014; Küffer *et al.*, 2016). Taken together with the earlier work by Paavola *et al.* (2011) this suggests that such ligands release the inhibitory effects imposed by the NTF. Interestingly, Lam211 treatment does not mediate a similar response at first sight (Petersen *et al.*, 2015). In fact, cellular cAMP accumulation decreases following Lam211 treatment. In this instance Adgrg6 activation requires the application of force in the form of sample vibration, thought to somewhat mimic the *in vivo* environment at the cell membrane, highlighting the dynamic behaviour of such ligands (Petersen *et al.*, 2015). The application of a mechanical force may be necessary to pull the NTF away from the CTF. Although these observations are yet to be confirmed by different groups, they highlight diverse mechanisms through which NTF-ligands mediate activation of the Adgrg6 intracellular signalling pathway. It also remains unclear how interactions between the Adgrg6-NTF and its binding partners are regulated; however, the dynamic ability of the NTF to switch between open and closed states could have a role in exposing and/or smothering its ligand binding sites (Leon *et al.*, 2020).

1.3.4d Adgrg6: stachel mediated activation

Liebscher *et al.* (2014) utilised cell based cAMP assays to confirm coupling of ADGRG6 to the G α_s pathway. Utilising such assays as a measure of ADGRG6 activity, the group uncovered a tethered peptide agonist, embedded in beta sheets of the GAIN domain (Araç *et al.*, 2012), terming it the 'stachel' peptide that self-activates receptor signalling. The group initially generated several ECR truncated forms of human ADGRG6; however, deletion of the C-terminal GPS region close to abolished cAMP accumulation in COS-7 cells. Treatment of these cells with peptides derived from the C-terminal GPS region were able to rescue cAMP accumulation but none more so than the 16 amino acid *stachel*

sequence (Liebscher *et al.*, 2014). A similar experimental approach by Stoveken *et al.* (2015), measuring GTP γ S binding kinetics, was used to elucidate the *stachel* sequence for ADGRG1. Although direct binding between receptor and *stachel* peptide has not yet been visualised, *in vivo* treatment of hypomorphic *adgrg6^{st63}* zebrafish larvae with the human ADGRG6 *stachel* peptide has been shown to mediate moderate restoration of Schwann cell *myelin basic protein (mbp)* mRNA expression, which encodes a major component of the myelin sheath, in the PNS (Liebscher *et al.*, 2014). *Stachel* sequence peptides have since been identified in multiple aGPCRs (Demberg *et al.*, 2015; Stoveken *et al.*, 2015; Wilde *et al.*, 2016), but the mechanism of their release from the NTF to self-activate receptors appears somewhat unclear.

Although early studies suggested that removal of the aGPCR NTF enables *stachel*-mediated activation (Liebscher *et al.*, 2014; Stoveken *et al.*, 2015), differential basal activity has been detected in full length wild-type *Adgrg6*-expressing cells (Leon *et al.*, 2020) whereas *stachel*-independent pathway activity has been observed for multiple other aGPCRs (Kishore *et al.*, 2016; Salzman *et al.*, 2017). Kishore *et al.* (2016) detected differential accumulation of multiple intracellular signalling molecules, including serum response factor (SRF), in cells expressing engineered ADGRG1 or ADGRB1 receptors, lacking their respective *stachel* peptides, in comparison with cells expressing vehicle or full-length controls. Furthermore, cells expressing a mutant isoform of ADGRG1 (H381S), defective in GPS auto-proteolysis, exhibit an increase in signalling following exposure to monobody ligands, a response that is unaffected by disruption of the *stachel* sequence (Salzman *et al.*, 2017). Molecular dynamic simulations of aGPCRs, including ADGRG1, illustrate a further dimension in which the *stachel* sequence is transiently exposed through structural flaps within the GAIN domain (Beliu *et al.*, 2021). Although these mechanisms are not yet confirmed for *Adgrg6*, they highlight further modes of activation among aGPCRs that are not mutually exclusive to the NTF dissociation model (Kishore *et al.*, 2016; Salzman *et al.*, 2017; Beliu *et al.*, 2021). Exploiting equivalent techniques to study *Adgrg6* may reveal further evidence of this among aGPCRs.

1.4 *Adgrg6* and drug discovery

1.4.1 Identification of *ADGRG6* as disease gene

aGPCRs have a diverse role in development and physiological processes; mutations residing in aGPCR genes are associated with a wide range of human diseases including cytoskeletal (Xu *et al.*, 2019), nervous system (Piao *et al.*, 2004; Ravenscroft *et al.*, 2015; Libé-Philippot *et al.*, 2017; Purcell *et al.*, 2017; Folts *et al.*, 2019), cancer (Shashidhar *et al.*, 2005; Boyden *et al.*, 2016) and others (reviewed in Langenhan and Schöneberg, 2016; Langenhan, Piao and Monk, 2016; Cazorla-Vázquez and Engel, 2018; Baxendale *et al.*, 2021). As mentioned in earlier sections, ADGRG6 has been identified as a conserved

developmental modulator of myelination by Schwann cells in the PNS of vertebrates (Monk *et al.*, 2009; Ravenscroft *et al.*, 2015; D’Rozario, Monk and Petersen, 2017), whilst also holding key roles in ear (Geng *et al.*, 2013) and cardiac development (reviewed in Patra, Monk and Engel, 2014). In particular, key pathogenic mutations are found in patients with LCCS9, a rare and lethal form of Arthrogryposis Multiplex Congenita (AMC), characterised by the formation of joint contractures and underlying defects in myelination (Ravenscroft *et al.*, 2015).

Alternatively, there is growing evidence from genome-wide association studies (GWAS) that implicates noncoding *ADGRG6* variants with adolescent idiopathic scoliosis (AIS) (Kou *et al.*, 2013, 2018), affecting 3% of children in the UK (Lenssinck, M., & Frijlink, 2005; Baxendale *et al.*, 2021). AIS is characterised by atypical curvature of the spine that arises during pubertal growth (Kou *et al.*, 2013; Liu *et al.*, 2021). Studies in mice have shown that *Adgrg6* is expressed regions of the intervertebral disc that supports lateral and rotational spine flexibility. Moreover, mice *Adgrg6* mutants have been shown to model features of AIS; spine Cobb angles were detected in excess of the 10° (coronal plane) scoliosis threshold (Liu *et al.*, 2021). Numerous single nucleotide polymorphisms (SNPs) in *ADGRG6* have also been linked with other disease conditions (Table 1.2) and its dynamic expression during development and in adult tissues (Waller-Evans *et al.*, 2010; Kou *et al.*, 2013, 2018; Patra *et al.*, 2013; Musa *et al.*, 2019) raises the likelihood of potential roles in human disease.

Table 1.2 List of key *ADGRG6* variants associated with human disease conditions (Baxendale *et al.*, 2021)

Disease/condition	Amino Acid	Domain	Mutation (SNP reference)	Reference
LCCS9	<i>R7*</i>	SP	nonsense homozygous	(Ravenscroft <i>et al.</i> , 2015)
LCCS9	Q716T, fs*16	GAIN	duplication c2144dup homozygous	(Ravenscroft <i>et al.</i> , 2015)
LCCS9	V769E	GAIN	missense homozygous	(Ravenscroft <i>et al.</i> , 2015)
Intellectual Disability	<i>W1088C</i>	TM6–7 extracellular loop	missense homozygous	(Hosseini <i>et al.</i> , 2019)
Periodontitis	<i>R1057Q</i>	TM5–6 intracellular loop	Missense (rs536714306)	(Kitagaki <i>et al.</i> , 2016)
COPD	<i>S123G</i> , K230Q	CUB, PTX	Missense (rs17280293)	(Terzikhan <i>et al.</i> , 2018)
Hypobaric adaptation	<i>S123G</i>	CUB	Missense (rs17280293)	(Eichstaedt <i>et al.</i> , 2017)
Pulmonary function	K230Q	PTX	Missense (rs11155242)	(Hancock <i>et al.</i> , 2010)

Note: amino acid sequence and numbering are based on the reference sequence NM_198569.3. Italic text indicates amino acid identity or similarity with the zebrafish protein. Abbreviations: COPD, chronic obstructive pulmonary disease; fs, frame shift. See figure 1.4 for domain name abbreviations.

1.4.2 GPCRs as druggable targets: Adgrg6

Compounds targeting GPCRs constitute a major class in the global market share of therapeutic drugs, reflecting the diverse roles of these receptors in cellular physiology, accessibility at the cell surface, and the presence of binding pockets within their structure (Manglik and Kruse, 2017). Adhesion class GPCRs, however, are less well represented as targets for licenced drugs, but offer similar potential. Drug discovery for aGPCRs presents many challenges, in part due to the expression of such receptors across different tissues and the likelihood of drug polypharmacology due to structural similarities between aGPCRs. In particular, the gedunin class of partial agonists can act on multiple aGPCRs including ADGRG1 (Stoveken *et al.*, 2018) and has been shown to downregulate *vcanb* and restore *mbp* expression in *adgrg6* mutant zebrafish larvae (Diamantopoulou *et al.*, 2019).

The recent structural characterisation of the Adgrg6 ECR (Leon *et al.*, 2020) should facilitate drug design; however, the structure of the CTF, and in particular of the pocket where the *stachel* peptide binds, are still uncharacterised. The Adgrg6 ECR has structural similarities with the extendable ECR of the epidermal growth factor receptor (EGFR) (Leon *et al.*, 2020). Cetuximab, an anti-cancer monoclonal antibody drug, targets the ECR of EGFR, preventing its extension to the active isoform (Li *et al.*, 2005). Leon *et al.* (2020) speculate that the dynamic Adgrg6 S1 ECR may be druggable through an equivalent approach to modulate mechanosensory and/or signal transducing functions. Although there are challenges for targeting ADGRG6, small molecule modulators have potential for therapeutic use against many ADGRG6-disease linked conditions or to mediate remyelination by Schwann cells following nerve injury or segmental demyelination associated with peripheral myelin diseases (see section 1.1.2).

Biologics such as the PrP, known to modulate Adgrg6 signalling through $G\alpha_s$ and restore *mbp* expression in *adgrg6* zebrafish mutants (Küffer *et al.*, 2016), offer an another route for therapeutics. The PrP_{FT}, which shares a region of similarity with the Adgrg6-NTF ligand collagen IV, triggers an increase in cAMP accumulation in the SW10 Schwann cell line as well as HEK cells expressing ADGRG6 (Küffer *et al.*, 2016). However, recent work by Henzi *et al.* (2020) targeting Adgrg6 activation with a PrP_{FT} fusion protein to treat peripheral nerve demyelination in the sciatic nerves of PrP knockout mice, was unsuccessful in illustrating therapeutic effects of the biological molecule on myelination. Transcriptomic data from the treated neuropathic mouse model did not highlight signs of active promyelinating signalling pathways. The data revealed activation of cytoskeletal pathways, a known alternate target of PrP, and therefore any agonism for Adgrg6 could be rendered ineffective in PrP knockout mice (Huang *et al.*, 2007; Henzi *et al.*, 2020). Notably, Henzi *et al.* (2020) suggest that such biologics may present challenges for crossing the blood-nerve barrier and therefore small molecules may offer better success.

1.4.3 Small molecule ligands of GPCRs as biological tools

In addition to therapeutics, chemical ligands that bind directly with the *Adrg6* protein could provide valuable tools to stabilise the receptor in an active or inactive conformation. aGPCRs undergo complex integration at cell the membrane, interacting with ECM components and potential cell-cell adhesions, which have thus far made thermostable isolation of such receptors challenging. A chemical ligand for *Adrg6* could facilitate isolation of the receptor in its *in vivo* conformation to subsequently determine its crystal structure that, other than the ECR alone (Leon *et al.*, 2020), remains uncharacterised.

In addition, chemical ligands of *Adrg6* could be utilised to manipulate its signalling pathway activity. Although small molecules such as forskolin and IBMX have been utilised to manipulate the *Adrg6* pathway, such compounds target downstream components, which can have widespread nonspecific effects throughout cells and across tissues in the zebrafish larvae. Agonist and antagonist compounds are widely utilised as pharmacological tools to modulate the activity of key developmental signalling pathways, including those of the Hedgehog (Hh) and Wnt proteins, which signal via Smoothened and Frizzled family GPCRs, respectively (reviewed in Agostino and Pohl, 2020). A precedent for the translation of small molecules originally identified through developmental biological research to the clinic is the Smoothened inhibitor vismodegib, now a treatment for basal cell carcinoma (Ingham, 2018).

1.4.4 Small molecule zebrafish screens for *Adrg6* modulators

Zebrafish present an excellent whole-animal model for precision medicine (reviewed in Baxendale, van Eeden and Wilkinson, 2017). The multimodal, mechanosensitive nature of aGPCRs and the potential for polypharmacology present problems for traditional *in vitro* drug discovery pipelines. aGPCR function is very likely to be context-dependent; as mentioned in previous sections, mechanosensitive interactions between *Adrg6* and components of the ECM are integral in coordinating radial sorting and myelination. *In vivo* screening naturally provides these physiological contexts, which are less likely to be recapitulated in an *in vitro* cell line-based screening platform. The use of zebrafish drug screening approaches also has the advantage of eliminating compounds with toxic or off target effects in the primary screen.

Hypomorphic allelic mutant organisms – those with weak phenotypes – are increasingly utilised in phenotypic drug screens, including two screens conducted on *adrg6* zebrafish mutants (Bradley *et al.*, 2019; Diamantopoulou *et al.*, 2019; Iyer *et al.*, 2019; Di Nardo *et al.*, 2020). Hypomorphic mutants are particularly advantageous as they are amenable to modulation, by small molecules, in two directions: rescue of the phenotype or its further exacerbation. They may also exhibit a higher sensitivity to small molecule centred therapeutic approaches as a weaker phenotype is more liable to

rescue than a severe phenotype due to a lesser phenotypic discrepancy to recover. Therefore, screening on hypomorphs is also more likely to pull out weak or partial ligands of a target protein that may not exceed a set threshold for hits when screening compounds on severe phenotypic mutants, resulting in the possibility of such compounds being overlooked.

A second specific advantage of *adgrg6* zebrafish mutants is the viability of homozygous mutant adults, allowing batches of 100% mutant embryos to be produced for screening assays. Two different screens taken advantage of zebrafish *adgrg6* hypomorphic mutants and the clear and consistent mRNA or transgene expression changes associated with them, to develop robust and reliable screening assays (Bradley *et al.*, 2019; Diamantopoulou *et al.*, 2019). Moreover, comparison of both hypomorphic and strong alleles in secondary screening assays has allowed the differentiation of different classes of hit compounds.

Diamantopoulou *et al.* (2019) screened the Tocriscreen Total and Spectrum Collection libraries, utilising the expression of *versican* mRNA in the mutant ear as a phenotypic readout of Adgrg6 pathway activity in the primary screen. Several classes of small molecules were identified that could rescue the otic phenotype in *adgrg6^{tb233c}* hypomorphic mutants, some of which also rescued the myelination defect. The hit compounds included colforsin (a water-soluble forskolin derivative that raises cAMP), a group of dihydropyridines, and a cluster of gedunin derivatives (Diamantopoulou *et al.*, 2019), some of which were independently identified as modulators of multiple other aGPCRs including ADGRG1 (Stoveken *et al.*, 2018). Whereas colforsin was able to rescue both hypomorphic (*tb233c*) and strong (*fr24*, containing a premature stop codon) alleles, validating association of Adgrg6 to G α_s , other hit compounds, including gedunin derivatives, were ineffective at rescuing the *fr24* allele (Diamantopoulou *et al.*, 2019). This latter class of compounds are of particular interest, as they may act directly at the level of the receptor, assuming the Adgrg6-CTF, predicted to be absent in *fr24* mutants, as the prospective target for such compounds. Further work will be needed to test these compounds in cell-based cAMP or Ca²⁺ immobilisation assays to determine direct agonism for Adgrg6 (Liebscher *et al.*, 2014; Lizano, Hayes and Willard, 2020).

Bradley *et al.* (2019) monitored changes in *mbp*-driven transgene expression in Schwann cells of *adgrg6^{st63}* hypomorphic mutants, for their compound screen of the Pharmakon 1600 library. They identified apomorphine, a dopamine agonist, for its ability to induce upregulation of *mbp*-driven GFP in *adgrg6* mutants and to mediate an increase in cAMP levels in Adgrg6-expressing cells (Bradley *et al.*, 2019). These observations are suggestive of apomorphine as an Adgrg6 agonist; however, the increase in cAMP is detected at high concentrations that may be associated with cellular cytotoxic

effects (Scarselli *et al.*, 1999; Vaglini *et al.*, 2008). *In silico* approaches may reveal compounds of similar nature with lesser toxic effects.

Differences in the hit molecules identified between the Bradley *et al.* (2019) and Diamantopoulou *et al.* (2019) screens are likely to reflect the different commercially-available compound collections that were used, together with differences in the zebrafish alleles used for screening and experimental conditions of the screening assays, including compound concentration and exposure time. For example, the apomorphine compound did not exceed the hit compound threshold of the primary screen performed by Diamantopoulou *et al.* (2019); it may need to be administered under alternative assay conditions to rescue the ear phenotype that forms the basis of the primary screen in this study.

Compounds from the Diamantopoulou *et al.* (2019) screen that downregulate *versican* alone should not be discounted as they may require a higher concentration or alternative assay conditions to restore *mbp* expression. Alternatively, such compounds may target a specific *Adgrg6* isoform or its signalling pathway components localised to the zebrafish larval ear alone. Furthermore, compounds within this subset that directly act to downregulate *versican* expression could have ulterior therapeutic applications against inflammation and cancer progression as overexpressed Versican is a recognised marker of both (Kim *et al.*, 2009; Baxendale *et al.*, 2021). Although the majority of literature surrounding *Adgrg6* highlights its roles in myelination, aGPCRs are multimodal in nature and *Adgrg6* may hold potential for therapeutic applications against cancers.

Taken together, the research findings illustrate a space for multifaceted drug screening approaches that combine zebrafish phenotypic strategies with *in vitro* cell-based assays to overcome the individual limitations of each in identifying aGPCR modulators. The two methodologies above have been successful in identifying a shortlist of small molecule hits from screening chosen compound libraries. The availability of tailored technologies such as the automated VAST-SDCM imaging system for zebrafish larva is improving the throughput of zebrafish small molecule screens (Early *et al.*, 2018; Bradley *et al.*, 2019). However, the lower-cost semi-quantitative *in situ* hybridisation approach also remains effective (Diamantopoulou *et al.*, 2019).

1.5 Key Aims and Hypotheses

Given the key roles of *Adgrg6* in myelination of the PNS by Schwann cells and morphogenesis of the semicircular canals in zebrafish larvae, this project exploits homozygous *adgrg6* mutant larvae for an *in vivo* phenotypic screen of small molecules. Specifically, the project aims to identify candidate small molecule modulators of *Adgrg6* or its signalling pathway by screening a library of compounds to identify those that can downregulate *versican* expression in the inner ear and rescue myelination defects in hypomorphic *adgrg6^{tb233c}* mutant larvae. This approach is largely similar to that adopted in Diamantopoulou et al. (2019, previous work by Whitfield lab) to maintain consistency in the screening of compounds. Although small molecule screening is to be performed against developmental phenotypes, there is evidence supporting a role of *Adgrg6* in regeneration of the myelin sheath following nerve crush (Mogha *et al.*, 2016) and therefore candidate modulators could have significant clinical potential in various other diseases and conditions in which the myelin sheath deteriorates.

Expression of *adgrg6* and multiple key Schwann cell myelination markers was characterised in wild-type and *adgrg6^{tb233c}* mutant larvae to determine their phenotypic differences before selecting *myelin basic protein (mbp)* as the most suitable marker for a counter-screening assay. In the first instance, library compounds were screened on a primary *versican* assay before hits from this assay were tested on the counter-screening *mbp* assay, conditions for which were optimised in the current project. Furthermore, positive hits from the *mbp* assay were tested on multiple other *adgrg6* allelic mutant larvae in addition to *in vitro* tests in Human Embryonic Kidney cells to determine agonism for *Adgrg6*. Preliminary work was also performed on known ADGRG1 antagonist compounds to determine potential antagonism towards *Adgrg6*.

Key Objectives:

1. Examine expression of multiple Schwann cell myelination markers by whole-mount *in situ* hybridisation in wild-type and *adgrg6^{tb233c}* mutant larvae. Hypothesis: expression of such markers will be reduced in *adgrg6* zebrafish mutants in comparison to wild-type larvae.
2. Screen Sigma's LOPAC library compounds on a primary *versican* assay. Hypothesis: overlapping library compounds that have been recognised as hits in previous small molecule screens on *adgrg6* zebrafish mutants (Bradley *et al.*, 2019; Diamantopoulou *et al.*, 2019) will be positive hits in the current project.
3. Optimise conditions for a counter-screening *mbp* assay and test hits identified in the primary screen. Hypothesis: a subset of *versican* screening assay hits will also rescue *mbp* expression in *adgrg6* zebrafish mutants, possibly through modulating *Adgrg6* or components of its signalling pathway. Under optimised *mbp* assay conditions, novel hit compounds are likely to

be identified that may have been missed in previously screened libraries (Diamantopoulou *et al.*, 2019).

4. Test *mbp* assay hits in a *versican* assay on *adgrg6^{fr24}* mutants in which the mutation predicts an early-truncated Adgrg6 protein, which completely lacks the CTF. Hypothesis: a subset of *mbp* assay hits will not downregulate *versican* in *adgrg6^{fr24}* mutants, possibly because these compounds interact with the protein to mediate rescue of the mutant phenotype.
5. Express various alleles of human and zebrafish *ADGRG6* in HEK293 cells and determine activity of signalling pathway. Hypothesis: known mutations of human and zebrafish *ADGRG6* will limit the functional capacity of the receptor, reducing downstream cAMP accumulation *in vitro*.
6. Test *mbp* assay hits, including candidate Adgrg6 modulators, in cAMP assays on HEK293 cells. Hypothesis: a subset of *mbp* assay hits will modulate Adgrg6 pathway activity *in vitro*; candidate receptor modulators will mediate a response specifically in Adgrg6-expressing cells.

Chapter 2.

Materials & Methods

2.1 Molecular work

2.1.1 RNA extraction

Larval RNA was extracted to be used as a template in cDNA synthesis, ultimately to transcribe DIG-labelled RNA probes. 20 – 30 embryos were flash frozen on dry ice and stored overnight at -80 °C. For RNA extraction, embryos were thawed on ice before adding 250 µL of TRIzol reagent (Life Technologies) that mediates breakdown of cell membranes whilst protecting RNA integrity during the homogenisation step. Embryos were homogenised with a pellet pestles cordless motor homogeniser (Sigma) for approximately 30 seconds (until no zebrafish remains were visible to the naked eye). Following an incubation at room temperature (RT) for 5 minutes, 50 µL of chloroform was added and mixed by inverting tubes for 15 seconds before placing at RT for 3 minutes, allowing the chloroform to separate molecules with respect to solubility. Tubes were centrifuged at 13000 g for 15 minutes at 4 °C; 100 – 150 µL of the upper aqueous layer was transferred to a fresh tube containing 83% of its volume in Isopropanol (83 µL for 100 µL), mixed and left at RT for 8 minutes to precipitate RNA. Tubes were subsequently centrifuged at 13000 g for 15 minutes at 4 °C to pellet the RNA. The supernatant was carefully removed and discarded before adding 250 µL of 75% RNase-free cold ethanol and centrifuging at 13000 g for 10 minutes at 4 °C. Ethanol was discarded and the pellets pulse-centrifuged to 8000 g before removing any remaining ethanol. The RNA pellet was air-dried for ~5 minutes before re-suspending in 20 µL of MilliQ water . RNA purity was determined by nano-drop before storage at -80 or -20 °C.

2.1.2 cDNA synthesis

cDNA was synthesised from RNA to be used as a template for PCR. Synthesis was performed using the SuperScript III First-Strand Synthesis System kit (Life Technologies), following the protocol provided.

1-5 ng of template RNA was added to 50 ng of random hexamers (primers) and 10 ng of dNTPs, reaching a final volume of 10 µL with the addition of MilliQ water. This was incubated at 65 °C for 5 minutes before being placed on ice for a further minute. During the incubation, the cDNA synthesis mix was prepared comprising 2 µL of 10X RT buffer, 4 µL of 25 mM MgCl₂, 2 µL of 0.1 M DTT, 1 µL of RNaseOUT (40 U/µL) and 1 µL of SuperScript III RT (200 U/µL). The cDNA synthesis mix was added to the RNA and primers, mixed gently before the following incubation protocol: 10 minutes at 25 °C, 50

minutes at 50 °C and termination with 5 minutes at 85 °C before chilling on ice. Template RNA was degraded by adding 1 µL of RNase H and incubating the samples for 20 minutes at 37 °C. cDNA purity was determined by nano-drop before storage at -20 °C.

2.1.3 Primers

Table 2.3 Primers for PCR and sequencing

Gene/plasmid	Primer sequence	Length	Purpose
<i>adgrg6</i>	FP1: GTGGGTAATGTCGTTGACT	19	Sequencing
	FP2: CGGACCCTCACTGACC	16	
	FP3: TCTGGACGGCTGGTTAG	17	
<i>ADGRG6</i>	FP1: GAATGTAGTCGACTGGC	17	Sequencing
	FP2: TGAATATTACAACCTCGGAA	19	
	FP3: ATGGACTTTGCATTGCTGTT	20	
pHEP- <i>adgrg6</i> (pcDNA3.1(+))	Nhe1-FP: CACACAGCTAGC- ATGATTTTCGTTTCATCAG	29	Subcloning of PCR template
	Not1-RP: CACACAGCGGCCGC- TTGCAGGGTACTATCTGC	32	
pHEP- <i>ADGRG6</i> (pcDNA3.1(+))	Nhe1-FP: CACACAGCTAGC- ATGATGTTTCGCTCAGAT	30	Subcloning of PCR template
	Not1-RP: CACACAGCGGCCGC- AAACTTTGTGCTGTGGCT	32	
pHEP-GFP plasmid (pcDNA3.1(+))	FP: GTAGGCGTGACGGTGGGAGGTC	23	Sequencing
	RP: GTCAGCTTGCCGTAGGTGGCATC	23	
<i>cldnk</i>	FOP: CAGGAGCACAAAACAAGAACCTAG	24	RNA probe synthesis from
	ROP: ATAAGTGGACATTAGAGGTGGCAA	24	
	FIP: GCCCAGTCTGTACCATTCTTTAT	24	PCR template
	RIPT7: TAATACGACTCACTATAGGG- ACAATGGGAAACTCTAACAGGGAA	44	
	FOP: TTAGCTGTTCTCTAAGACCTCCCA	24	
<i>pou3f1/oct6</i>	ROP: AGACAGTGTTCATGTTGCCATT	24	RNA probe synthesis from
	FIP: CTTGTCAGTTTTCTAAGTCGGAGC	24	
	RIPT7: TAATACGACTCACTATAGGG- CGAACTCTCCCAAACCTTTCTGTC	44	PCR template

- Note: highlighted region indicates enzyme binding site

Table 4.2 Zebrafish *adgrg6* primers for site-directed mutagenesis

Primer sequence	Allele	Length
FP: CAGGGGGCTGGAATAGCGACGGCTGCAAGGTC	C804W	32
RP: GACCTTGCAGCCGTCGCTATTCCAGCCCCCTG		
FP: AGTTTTGCAACGTGGGATGGGGTGTCCCTGCTGCAATTGTT	<i>tb233c</i>	41
RP: AACAATTGCAGCAGGGACACCCCATCCACGTTGCAAAACT		
FP: GGGGTGTCCCTGCTGCAATTGTTGGAATTGTGTTGGCTGTG	<i>tk256a</i>	41
RP: CACAGCCAACACAATTCCAACAATTGCAGCAGGGACACCCCA		
FP: ACAGCTATGTGGTGGCCAGCAGTGTGGCAACTTCAC	V756E	37
RP: GTGAAGTTGCCAACACTGCTGGCCACCACATAGCTGT		
FP: CGTCTGCTTGTGTAATCGCCTCACACTTTGGCA	H826R	35
RP: TGCCAAAGTGTGTGAGGCGATTACACAAGCAGACG		

Table 2.3 Human ADGRG6 primers for site-directed mutagenesis

Primer sequence	Allele	Length
FP: TTGGAGGATGCAACACGTCAGGATGTGTTGCACACAGAG RP: CTCTGTGTGCAACACATCCTGACGTGTTGCATCCTCCAA	W817C	39
FP: AATTCTGCAACATTGGCTGGGGTTTGCTGCCTTAGTGGTG RP: CACCACTAAGGCAGGCAAACCCCAGCCAATGTTGCAGAATT	<i>tb233c</i>	41
FP: GGGGTTTGCTTGCTTAGTGGTGTGTCAGTTGTTCTAGCGAGC RP: GCTCGCTAGAACAACTGACACCACTAAGGCAAGCAAACCCC	<i>tk256a</i>	41
FP: TGAGTTATGTGATGGCGTGCAGTATTGGAAACATTACTATCC RP: GGATAGTAATGTTTCCAATACTGCACGCCATCACATAACTCA	V769E	42
FP: TGTAACCGCTTACACACTTTGGAGTTCTGATGGA RP: TCCATCAGAACTCCAAAGTGTGTGAAGCGGTTACA	H839R	35

2.1.4 Polymerase Chain Reaction

2.1.4a PCR overview

PCR was performed with tailored primers to amplify zebrafish gene cDNA for DIG-labelled probe synthesis or to generate *adgrg6* mutant DNA constructs (site-directed mutagenesis, section 2.1.4c). PCR was performed with varying reaction volumes; however, the ratio of reactants remained the same throughout. Primers were purchased from IDT and re-suspended in MilliQ water to a final concentration of 100 μ M on arrival. These were further diluted to give a working concentration of 10 μ M and all aliquots stored at -20 °C. A 20 μ L reaction contained 1 μ L of template DNA (10 – 20 ng), 4 μ L of 3X Taq Reddymix polymerase (Thermo Fisher Scientific), 0.5 μ L of forward primer (FP), 0.5 μ L of reverse primer (RP) and the remainder MilliQ water. The protocol for PCR is included below; primer annealing temperatures were set to ~5 °C below their melting temperature (T_m).

Table 2.4 PCR thermocycler protocol

Step	Temperature (°C)	Time (s)	Notes
Initial denaturation	98	30	(5 min for colony PCR)
Denaturation	98	20	
Primer annealing	58 – 65	30	Step 2 – 4 ~30 cycles
Extension	72	30 – 60/kb	Based on enzyme efficiency
Final extension	72	600	
Sample storage	10	∞	Stored at -20 °C upon completion

- Note: extension step set to 5 – 10 minutes for site-directed mutagenesis

2.1.4b Nested PCR

A nested PCR was performed to improve sensitivity and specificity, mediating amplification of target cDNA sequence to a high enough level for RNA probe synthesis (described later). An initial PCR is performed with primers that anneal to the cDNA sequence outside a second internal set of primers (figure 2.1). The first PCR product is utilised as the template DNA in a second PCR with the internal set

of primers. The inner reverse primer contains an RNA polymerase binding site at the 5' end, necessary for subsequent RNA probe synthesis from the purified product (Qiagen PCR purification kit).

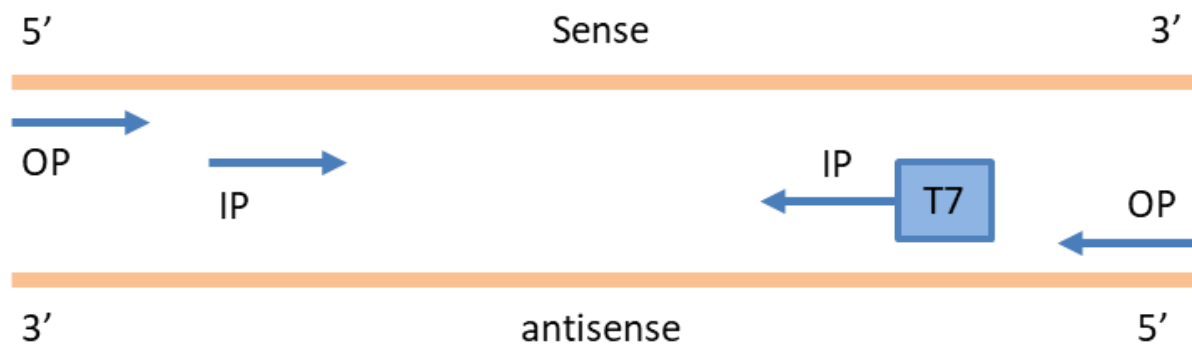


Figure 2.1 Nested PCR primer setup.

The cDNA sequence of a specific gene is amplified through two PCR reactions, first with the outer primer (OP) set followed by the inner primer (IP) set using the product from the first PCR. T7: T7 RNA polymerase binding site at the 5' end of the inner reverse primer.

2.1.4c Site-directed mutagenesis of human and zebrafish *ADGRG6*

Allelic variants of human and zebrafish *ADGRG6* were generated by using PCR to introduce point mutations. Specifically designed primer sets contained individual point mutations positioned in between complementary DNA sequence (table 2.2 and 2.3). A wild-type construct for the human (ref: NM_198569.3) and zebrafish (ref: NM_001163291.2) gene, externally ordered and sequenced by Sosei Heptares, was utilised as the template for generating mutant alleles. PCR was performed with a Phusion polymerase kit, using similar thermocycler settings to above but a prolonged extension step of 5-10 minutes. Final products were amplified by cloning (see section 2.1.7) before sequencing samples from GENEWIZ to confirm incorporation of point mutations.

2.1.5 Plasmid digestion

Various plasmid constructs were utilised throughout this study, either as templates for RNA probe synthesis or to overexpress *adgrg6* in HEK293 cells. Constructs were linearised by incubating 1 µg at 37 °C for >3 hours with 2.5 µL of appropriate restriction enzyme, 10 µL of buffer and MilliQ water to a final volume of 100 µL. Following digestion, DNA was purified with a PCR purification kit (Qiagen).

2.1.6 Ligation

Human and zebrafish *ADGRG6* alleles were cloned into the pHEP-GFP plasmids (based on pcDNA3.1(+)) by first digesting the insert sequence before ligating into a pre-linearised pHEP-GFP plasmid. Ligation was performed at 16 °C overnight using a 3:1 molar ratio of insert:vector (50 ng) with 1 µL of T4 ligase, 2 µL buffer and MilliQ water to a final volume of 20 µL.

2.1.7 Transformation of competent cells

Plasmid constructs were amplified by transformation of competent *E.coli* DH5 α cells before culturing a single transformed colony overnight. Competent cell stocks stored at -80 °C were thawed on ice before 10 – 20 ng of plasmid DNA was mixed with ≤ 50 μ L of competent cells, maintaining sterility throughout, and left on ice for approximately 30 minutes. The samples were heat shocked at 42 °C for 45 seconds before placing back on ice for a further 10 minutes. Cells were grown in 200 – 300 μ L of super optimal broth (SOC, lacking antibiotic) for approximately 20 minutes (shaking incubator 200rpm, 37 °C) before spreading on pre-warmed LB agar plates containing antibiotic for selection of competent cells (majority of plasmids contained ampicillin resistance). Plates were incubated in a 37 °C incubator overnight to allow competent cell colonies to grow. A single colony was cultured overnight in ≤ 100 mL of LB broth (with antibiotic) on a shaking incubator (200 rpm) at 37 °C. The competent cells were pelleted by centrifuging at 4500 rpm for 15 minutes; supernatant was discarded and plasmid DNA purified from the competent cells using a Mini/Midi-prep kit (Qiagen), following the manufacturer's protocol.

2.1.8 Synthesis of DIG-labelled RNA probes

1 – 2 μ g of linearised DNA (PCR product or linearised plasmid DNA) was used as the template to synthesise RNA probes, to be used in whole-mount *in situ* hybridisation. A 20 μ L reaction was prepared containing 1 μ L of DIG-labelled RNA mix, 2 μ L of 5X transcription buffer, 1 μ L of RNase inhibitor, 2 μ L of appropriate antisense-strand RNA polymerase and 14 μ L of template DNA amounting to 1 – 2 μ g. This was incubated at 37 °C for ≥ 2 hours before running 2 μ L of the product (mixed with 1 μ L of loading dye and 2 μ L of MilliQ water) on a 1% agarose gel (80V, 20 minutes) to confirm synthesis of RNA by visualisation of a second band migrating faster than the template DNA. After confirmation, 1 μ L of DNase I was added to the remaining 18 μ L and incubated at 37 °C for a further 20 minutes to degrade the template DNA. The RNA was precipitated by mixing with 10 μ L of 7.5 M ammonium acetate and 75 μ L of 100% RNase-free ethanol before pelleting by centrifugation at 13000 g for 20 minutes at 4 °C. The supernatant was carefully removed and 800 μ L of 75% RNase-free ethanol was added before a second centrifugation step at 13000 g for 5 minutes at 4 °C. The supernatant was carefully removed and RNA pellet air-dried for 5 minutes at RT before re-suspension in 20 – 30 μ L of MilliQ water, based on the size of the pellet (smaller volume for smaller pellet). RNA purity was determined by nano-drop before storage at -20 °C.

Table 2.5 List DIG-labelled RNA probes

Gene	Restriction enzyme/RNA polymerase	Template	Reference
<i>adgrg6</i>	Not1/Sp6	Plasmid	(Geng <i>et al.</i> , 2013)
<i>cldnk</i>	/T7	PCR product	self-designed

<i>krox20 (egr2)</i>	Xba1/T3	Plasmid	(Oxtoby and Jowett, 1993)
<i>oct6 (pou3f1)</i>	/T7	PCR product	self-designed
<i>mbp</i>	Sall/Sp6	Plasmid	(Geng <i>et al.</i> , 2013)
<i>sox10</i>	Sall/T7	Plasmid	(Geng <i>et al.</i> , 2013)
<i>vcanb</i>	SacII/Sp6	Plasmid	(Geng <i>et al.</i> , 2013)

2.2 Zebrafish husbandry

All zebrafish strains were raised and maintained in the Bateson Centre aquaria facility at the University of Sheffield, in accordance with the Home Office regulations on the use of animals in research (Animals Scientific Procedures Act 1986).

2.2.1 Zebrafish wild types

The wild-type zebrafish strains utilised in this study include AB (ZDB-GENO-960809-7) and London wild type (LWT). *Nacre (mitfa^{w2/w2})* strain (ZDB-GENO-990423-18) embryos lacking melanophores (Lister *et al.*, 1999) were employed as wild type controls in drug screening experiments, for the ease of distinguishing them from mutant embryos in a 96-well plate format.

2.2.2 Zebrafish transgenic and mutant lines

Table 2.6 Zebrafish transgenic line

Line	Source
Tg(<i>mbp:EGFP-CAAX</i>)	(Almeida <i>et al.</i> , 2011)

Table 2.7 Zebrafish *adgrg6* mutant lines

Allele	Source
<i>tb233c</i> (I963N)	(Whitfield <i>et al.</i> , 1996; Geng <i>et al.</i> , 2013)
<i>tk256a</i> (P969L)	(Whitfield <i>et al.</i> , 1996; Geng <i>et al.</i> , 2013)
<i>fr24</i> (L463X)	(Carney <i>et al.</i> , 2010; Geng <i>et al.</i> , 2013)

2.2.3 Zebrafish care

Adult zebrafish were housed in Tecniplast tanks with circulating water maintained at 28.5 °C with a 14-hour light/10-hour dark cycle.

2.2.4 Zebrafish crosses and harvesting of embryos

Single pair mating: an adult male and female fish were placed into a small breeding tank comprising a solid external tank that contained an internal tank with a perforated bottom. These tanks also contain a removable divider to isolate the fish from each other before mating.

Tank-wide mating: a sieve containing marbles over an embryo collection container were placed into an adult tank and left overnight.

Embryos were harvested into E3 medium (5 mM NaCl, 0.17 mM CaCl₂, 0.33 mM MgSO₄) containing methylene blue. Healthy embryos were sorted into groups of approximately 50 and kept in an incubator at 28.5 °C, staged according to Kimmel et al. (1995).

2.3 *in vivo* drug screening

2.3.1 Sigma LOPAC library preparation

The drug screening assay was performed using the Sigma Library of Pharmacologically Active Compounds (LOPAC), comprising 1280 compounds arrayed across 16 original 96-well plates at a concentration of 10 mM. These were diluted 1:2 by the addition of DMSO to generate master copy plates at 5 mM which in turn were diluted 1:2 with DMSO to generate daughter copy plates at final concentration of 2.5 mM. These were split equally into v-bottom 96-well microtitre plates (Matrix) containing 2.5 µL of compound/well at 2.5 mM, to be used for screening. A select few 1.5 mM plates were generated by mixing 1.5 µL of 2.5 mM compounds with 1 µL of DMSO. All plates, containing 80 library compounds present in columns 2 – 11, were aluminium heat-sealed and stored at -20 °C until required for screening experiments.

2.3.2 Compound plate preparation

On the day of running a drug screening assay, the microtitre plates were thawed at RT and pulse centrifuged at 2000 g for 1 minute to collect all of the compounds at the base of the wells. The mesh-bottomed embryo plate was prepared before continuing compound plate preparation (described below). 2.5 µL of DMSO only and 10 mM IBMX (in DMSO), positive control compound known to restore wild-type levels of *vcanb* and *mbp* expression in *adgrg6^{tb233c}* zebrafish mutants (Diamantopoulou *et al.*, 2019), was added to the first and last columns in the appropriate wells as indicated in the plate layout (figure 2.2). These controls were included in quadruplicate in original screening plates and duplicate in cherry picked retest plates, to enable assessment of plate validity upon completion of the assay.

Using a multi-channel P300 pipette, 247.5 µL of fresh pre-warmed (28.5 °C) E3 with no methylene blue was added to each well (1 column at a time), mixing the contents by pipetting up and down to give a final concentration of 15 – 25 µM for screening. The final 250 µL were transferred to the equivalent empty well in the assay plate.

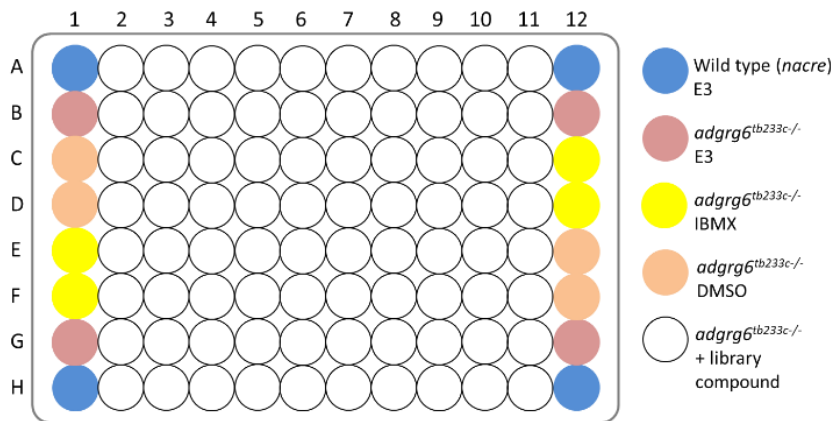


Figure 2.2 Layout of compound screening assay plate.

Control compounds were administered in columns 1 and 12, including 1% DMSO as a negative control, and 50 – 100 μM 3-isobutyl-1-methylxanthine (IBMX) as a positive control. IBMX is a phosphodiesterase inhibitor that has previously been shown to mediate rescue of the *adgrg6*^{tb233c} ear and myelination phenotype (Geng *et al.*, 2013). Columns 2 – 11 contain 80 library compounds at a final concentration of 15 – 25 μM for the screening assay.

2.3.3 Preparation of embryos

Wild-type (*nacre*) and *adgrg6*^{tb233c} mutant embryos were raised to 50 hpf before being dechorionated by hand with forceps and incubated at 20 °C overnight to slow down their development, allowing them to reach 60 hpf the following morning (estimated in accordance with Kimmel *et al.*, 1995). For *mbp* screening experiments the embryos were kept at 28.5 °C after dechorionating to develop at the natural rate until 54 hpf for drug administration. At the appropriate stage of development, embryos were washed into fresh E3 with no methylene blue and aliquoted into Multiscreen 96-well mesh-bottomed plates (100 mm; Millipore) resting in their lid containing a small volume of E3, keeping the embryos healthy. At this point the compound plate was prepared (described above) before blotting off excess E3 onto a paper towel and placing the mesh-bottom plates into the 25 μM compound plate.

Assay plates were enclosed in plastic trays that were incubated at 28.5 °C for 24 – 30 hours depending on the experiment type. A thick layer of paper towels soaked in distilled water was included in the plastic trays to retain humidity and prevent evaporation of zebrafish growth media. Following the incubation, mesh-bottomed plates containing embryos were transferred into 4% (v/v) paraformaldehyde (PFA) and stored at 4 °C overnight before bleaching with 3% H₂O₂/0.5% KOH solution for approximately 20 minutes to remove pigment. Embryos were stored in 100% methanol at -20 °C as described below in the *in situ* hybridisation protocol.

2.4 Testing of candidate Adgrg6 antagonists

Mundulone (Sosei Heptares) and Dihydromunduletone (Sosei Heptares) were recently identified as ADGRG1 antagonists (Stoveken *et al.*, 2016) and were tested as candidate antagonists of Adgrg6 in the zebrafish model system.

2.4.1 Compound administration in media

Wild type zebrafish embryos were raised to 24 – 60 hpf prior to drug administration in E3 media; *adgrg6*^{tb233c} embryos were raised as experimental controls. At the appropriate developmental stage, embryos were dechorionated manually and transferred into fresh E3 with no methylene blue before being placed in a 24-well plate; 10 embryos/well in 400 µL of E3 media. A 100× compound log dilution series was prepared in DMSO before diluting 1:20 in E3 and adding 100 µL of this directly to the plate wells for testing. The plates were given a quick swirl to mix the compounds in the final 500 µL volume of E3 containing embryos; DMSO was kept at 1% (v/v) per well as for previous screening experiments and the highest administered drug concentration was 25 µM due to toxicity of the compounds. Assay plates were stored at 28.5 °C for the appropriate duration before transferring embryos into Eppendorf tubes and fixing overnight in 4% PFA at 4 °C.

2.4.2 Compound microinjection

Needles were pulled using a Flaming/Brown P-97 micropipette puller that pulls a single non-filament capillary into two microinjection needles by applying heat at the centre-most point of the capillary. Needles were filled with the compound at an appropriate concentration in DMSO plus dye (to aid visualisation) using Eppendorf microloader pipette tips. A high DMSO percentage was used to prevent compound crystallisation in the microinjection needle. The microinjection volume was calibrated using a graticule before administering the compound into zebrafish embryos.

Wild type zebrafish were raised to 48 hpf before being dechorionated manually by forceps. Embryos were anaesthetised with 4% (w/v) tricaine (MS222) in E3 media for a couple of minutes before being transferred into a layer of 3% (w/v) methylcellulose on a microscope slide or a 1.5% (w/v) agarose mould for ease of injection. Embryos were oriented with anterior at the top, posterior to the bottom and the left ear in view. The pressure-microinjector was calibrated with a graticule before performing injections free-hand by piercing the left ear with the needle and administering 1 nL of the compound or DMSO (control injection). Following the injection, embryos were carefully transferred back into fresh E3 media and incubated at 28.5 °C for up to 120 hpf, during which time their phenotype could be monitored and they could be imaged in methylcellulose. Embryos were fixed in 4% PFA at the appropriate stage and underwent the WISH protocol if necessary.

2.5 Whole-mount *in situ* hybridisation

2.5.1 Protocol

Whole-mount *in situ* hybridisation (WISH) was performed to visualise mRNA expression of various genes, including expression of *vcanb* and *mbp* following screening assay treatments. The protocol was performed similarly to that described by Thisse and Thisse (2008), with some minor changes. The composition of reagents utilised throughout the protocol are described in table 2.8.

Preparation of embryos

Embryos were fixed overnight at 4 °C or for 30 minutes at room temperature in 4% Paraformaldehyde (PFA) before bleaching with 3% H₂O₂/0.5% KOH solution for approximately 20 minutes (~30 embryos) to remove pigment. Larger samples may require up to 30 minutes for the removal of pigment. The reaction was stopped by a wash with 25% (v/v) methanol in PBS before dehydrating the embryos with increasing concentration of methanol through 5-minute washes in 50%, 75% and 100% (v/v) methanol. After the final wash, embryos were stored in 100% (v/v) methanol at -20 °C until at least overnight before use.

Day 1

Embryos were rehydrated by gradually removing methanol and increasing PBS through a series of 10-minute washes in 75%, 50% and 25% (v/v) methanol. Embryos underwent 4× 5-minute washes in PBST before permeabilisation with 10 µg/mL proteinase K for a duration correspondent to the developmental stage of the embryos: 9-18 somites for 3 minutes, 18 somites – 24hpf for 10 minutes, 36 – 120 hpf for up to 40 minutes (72 hpf 25 minutes, 96 hpf 30minutes). Permeabilisation was stopped by fixation for 20 minutes in 4% PFA at room temperature followed by 4× 5-minute washes in PBST before pre-hybridisation for ≥3 hours at 70 °C in pre-warmed hybridisation mix (HM). Following pre-hybridisation embryos were incubated with appropriate pre-warmed DIG-labelled RNA probe (1:100 – 1:500 dilution in fresh HM) overnight at 70 °C.

Day 2

Note: all HM and SSC steps were performed at 70 °C with solutions pre-warmed before washes.

The RNA probe in HM was retained for future use and embryos were washed with HM- (lacking tRNA or heparin) for 10 minutes. A series of 10-minute washes were performed with decreasing concentration of HM- and increasing concentration of 2X SSC before a wash in 100% 2X SSC. Embryos were twice-washed with 0.2X SSC for 30 minutes at 70 °C before being washed out of SSC and into PBST at RT through a series of 10-minute washes. 4X 10-minute PBST washes were performed before

blocking the embryos for ≥ 3 hours at RT in blocking buffer. This was replaced by an anti-DIG antibody diluted 1:5000 in fresh blocking buffer for an overnight incubation at 4 °C with gentle agitation.

Day 3

Embryos were washed for 15 minutes 6X with PBST to remove residual unbound antibody before 3X 5-minute washes with alkaline Tris buffer at RT. Staining of embryos was performed at RT or ~ 30 °C until the desired staining was visible (1-4 hours, some probes may require overnight staining at 4 °C). Staining was halted by stop solution and embryos were fixed overnight at 4 °C with 4% PFA. On the following day embryos were transferred through a glycerol series, to improve optical transparency, and stored at 4 °C in 75% glycerol ready for mounting and imaging.

2.5.2 Drug treated embryos

The WISH protocol is performed on drug-treated embryos in a 96-well mesh-bottom plate using the Biolane HTV1 16V *in situ* robot (Intavis) (figure 2.3) to increase throughput. Solutions are washed in and out of a wash chamber containing the mesh-bottom plate of embryos, following the same protocol as above. Importantly, any freshly synthesised probes were tested before hand on a few zebrafish samples to ensure a valid signal was detected by *in situ* hybridisation before their use on screening plates. Furthermore, probe solution was topped up by freshly synthesised probes if signals began to drop from repeated use.



Figure 2.3 Biolane HTV1 16V *in situ* robot (Intavis) for automated WISH.

This Biolane robot contains two large chambers with the capacity to hold up to two assay plates each at any one time allowing WISH on up to four screening plates in synchrony. The WISH solutions for each day are prepared and attached as inputs to the chambers before initiating the automated protocol. Note: the overnight probe incubation (day 1), alkaline Tris buffer washes and staining (day 3) steps are performed manually by transferring mesh-bottom plates through a series of small trays containing ~ 30 mL of each solution.

Table 2.8 List of in situ hybridisation reagents

Reagent	Consistency
4% PFA	16 g PFA, 400 mL 1X PBS
PBST	0.1% Tween-20 in PBS
HM	50% formamide, 5X SSC, 0.1% Tween-20, 500 µg/mL tRNA
20X SSC	175 g NaCl, 88g Sodium citrate, 800mL H ₂ O, pH 7.0
Blocking buffer	2% Fetal Bovine Serum, 2 mg/mL Bovine Serum Albumin, 1X PBST
Alkaline Tris buffer	100 mM Tris HCl (pH 9.5), 50 mM MgCl ₂ , 100 mM NaCl, 0.1% Tween-20
Staining solution	225 µL of 50 mg/mL NBT, 175 µL of 50 mg/mL BCIP in 50 mL Alkaline Tris buffer
Stop solution	1X PBS, 1 mM EDTA, 0.1% Tween-20

2.5.3 Scoring of embryos in assay plates

The staining of embryos in screening assay plates was scored to determine the rescuing effect if any of administered compounds. The *vcanb* and *mbp* scoring systems described in Diamantopoulou *et al.*, (2019) (also included in figure 4.2 in section 4.2.3) were used to score the embryos in each well. The scoring was performed subjectively by eye using a bench-top confocal microscope. Experimental outcomes were validated upon confirmation that ear and myelination phenotypes were rescued in IBMX treated *adgrg6^{tb233c}* mutant larvae and no rescue was observed in DMSO treated *adgrg6^{tb233c}* mutant larvae, although some experimental variability in staining were detected.

2.5.4 Brightfield and DIC imaging

For live imaging, zebrafish embryos were anaesthetised with 4% tricaine (MS222) in E3 media for a short period before mounting them in a microscope slide window-chamber containing 3% methylcellulose. The window-chamber was created by placing ≤ 5 square shaped layers (2 cm X 2cm) of electrical insulation tape onto a microscope slide and cutting out a 5 mm X 5 mm square directly in the middle using a scalpel blade. Embryos were oriented anterior to the left and posterior to the right before a coverslip was carefully lowered onto the methylcellulose ensuring no bubbles formed on contact. Images were taken by an Olympus BX-51 microscope, C3030ZOOM/MicroPublisher 6 camera and CELL B/Ocular advanced scientific camera control software and any calibration needed was performed on Fiji or Photoshop. Subsequent to the images being taken, embryos were transferred back into fresh E3 or fixed in 4% PFA overnight.

Images of fixed embryos were taken in 75% glycerol and the yolks were removed by cutting them away from the rest of the body using needle and forceps. Removal of the yolk allows a clearer DIC image to be taken and reduces sample glare. To image at higher magnification (for example to image

the ear), embryos were cut in half along the midline to give a thinner sample, reducing the blurring effect of surrounding tissue and improving sample resolution.

2.6 Immunohistochemistry

2.6.1 Zebrafish antibodies

Table 2.9 List of primary antibodies

Primary antibody	Dilution	Supplier
Mouse acetylated α -tubulin	1:300	Sigma
GFP-Booster Atto488	1:400	Chromotek

Table 2.10 List of secondary antibodies

Secondary antibody	Dilution	Supplier
Alexa fluor 647 goat anti-mouse	1:400	Invitrogen

2.6.2 Antibody Staining

Antibody staining experiments were performed to visualise neuronal anatomy and myelinating Schwann cells in zebrafish larvae. Live embryos for whole-mount immunohistochemistry were maintained in E3/PTU to inhibit skin pigmentation before the appropriate stage for fixation overnight in 4% PFA. No bleaching step was required and embryos were transferred gradually into methanol for overnight storage at -20 °C similarly to the WISH protocol.

Day 1

Embryos were gradually rehydrated from methanol into PBSTr at RT before 3X washes in PBSTr. Subsequently, embryos were incubated for >3 hours in block solution, containing PBSTr and 10% of appropriate serum depending on secondary antibody host. Following the block step, the primary antibody was added (diluted in block solution, 1% DMSO) before incubating overnight at 4 °C with gentle agitation.

Day 2

4X 30 – 60 minute PBSTr washes were performed to remove residual unbound primary antibody. The appropriate secondary antibody was added (1:400 dilution in blocking solution) and embryos were incubated at 4 °C overnight with gentle agitation.

Day 3

Excess secondary antibody was washed out by 4X 30-minute PBSTr washes at RT before gradually transferring embryos into low-melting point agarose for imaging.

2.6.3 Confocal A1 Microscope

Embryos for fluorescent imaging were washed in PBSTr and yolk removed by needle and forceps before mounting them in low-melting point agarose in an imaging dish. For imaging on the A1 confocal (Nikon), an inverted microscope, embryos were oriented anterior to the left, posterior to the right and dorsal down, ensuring that the left side of the embryo was as close as possible to the base of the dish before the agarose gel set. Images were taken by the Nikon A1 confocal using the NIS Elements software and $\leq 5\%$ laser power.

2.7 Human cell culture

2.7.1 Cell lines and culture

HEK293 cell lines were used for cell-based signalling assays and immunocytochemistry, kindly provided by Sosei Heptares and members of the Peden lab group at the University of Sheffield. Cell-based cAMP assays were conducted at the Sosei Heptares Research & Development facility in Cambridge, during a 3-month placement. Preliminary immunocytochemistry experiments were performed at the University of Sheffield, under the guidance of Peden lab members.

HEK293 cells were cultured in Dulbecco's modified Eagle medium (DMEM) and CHO cells in DMEM with F12, all purchased from Sigma, along with phosphate-buffered saline (PBS). Foetal bovine serum (FBS) was diluted 1:10 in the media before its application. Other reagents were purchased from alternative suppliers; TrypLE from Thermo Fisher Scientific, Hank's buffered saline solution (HBSS) from Lonza and 1 M HEPES from Life Technologies.

All cells were routinely cultured in T175 flasks (Greiner) maintained in 99% humidity, 5% (v/v) CO₂ at 37 °C and were passaged at least twice a week into fresh media (Mon & Fri) after reaching ~90% confluency. When cells reached confluency, overlying media was discarded before washing the cells with 10 mL of PBS before adding 5 mL of TrypLE and swirling around the flask to ensure the base was coated. The flask was incubated for 3 – 5 minutes at 37 °C to allow TrypLE to detach cells from the base of the flask. 15 mL of DMEM was added to suspend the cells in a final volume of 20 mL, ensuring an even spread by pipetting the cells gently up and down. Cells were pelleted by centrifuging in a falcon tube at 2000 g for 5 minutes, supernatant discarded before resuspending the cells in 20 mL of fresh media. Cells were counted by loading 600 – 1000 μ L of the sample into a cell counter before passaging appropriately (~1:20) into a new T175 flask with fresh media, based on the estimated population. Cells required for assays were dispensed into assay plates and any remainder discarded.

2.7.2 Cell transfection

2.7.2a Transfection by BacMam

BacMam viral cultures were grown, housing each human or zebrafish *ADGRG6* allelic construct (listed alongside SDM primers in table 2.2 and 2.3) for the transfection of HEK cells. An appropriate dilution or dilution series of BacMam virus in DMEM was dispensed across 384-well plates (Greiner); 10 μ L per well. Following cell count, a dilution of cells in DMEM was prepared with a final population of 0.375×10^6 cells/mL; this was dispensed 20 μ L per well across the 384-well plate containing BacMam. Each well contained a mixture of 7500 cells, BacMam and DMEM in a final volume of 30 μ L and was incubated at 37 °C (99% humidity, 5% (v/v) CO₂) for a 24-hour transfection period, allowing protein levels to reach a maximum.

2.7.2b Transient transfection

Cells were transfected directly with human or zebrafish *ADGRG6* constructs without any carrier vehicle. Prior to the day of transfection, cells were passaged and dispensed into 6-well plates with 220 000 cells/well that were incubated overnight at 37 °C (99% humidity, 5% (v/v) CO₂). On the following morning, transfection mix was prepared for each well containing 5 μ L FuGENE (Promega), 2 μ g of plasmid DNA and 100 μ L of Opti-mem (Invitrogen) made up to a final 2 mL volume in DMEM. After a 15 minute incubation at RT, the media in the 6-well plates was replaced with the appropriate transfection media for each well. Cells were incubated at 37 °C (99% humidity, 5% (v/v) CO₂) for up to 48 hours to allow protein levels to reach a maximum.

2.7.3 Immunocytochemistry

2.7.3a Antibodies

Table 2.11 List of primary antibodies

Primary antibody	Dilution	Supplier
Rabbit GFP	1:600	Abcam
Mouse GM130 (GOLGA2)	1:400	Abcam
Wheat Germ Agglutinin conjugated Alexa fluor 647	1:800 (in media)	Invitrogen

Table 2.12 List of secondary antibodies

Secondary antibody	Dilution	Supplier
Alexa fluor 488 goat anti-rabbit	1:1000	Invitrogen
Alexa fluor 594 goat anti-mouse	1:1000	Invitrogen

2.7.3b Antibody staining

Antibody staining was performed on transfected cells to examine localisation of multiple cellular markers alongside GFP-tagged *Adgrg6*. Incubation of cells with primary antibodies was performed pre-

fixation for Wheat Germ Agglutinin (WGA) and post-fixation for GFP and GM130 (GOLGA2) antibodies. Apart from WGA, which was diluted in cell media, all antibodies were diluted in blocking solution comprised of PBS and 1% bovine serum albumin (BSA).

For staining with WGA, cells were incubated on ice for approximately 30 minutes before fixation with 4% PFA at RT for 15 minutes. Subsequently, cells were incubated in 1mL of 100mM glycine for 5 minutes at RT before blocking (PBS + 1% BSA) for 30 minutes. Next, cells on coverslips were placed onto 50 μ L of diluted primary antibody for 30 minutes before 3X washes in block solution to remove residual antibody. Cells were incubated in 450 μ L of diluted secondary antibody for 30 minutes before 3X washes in PBS to remove residual secondary antibody. Following this protocol, coverslips were mounted on slides with mounting media and imaged under an Olympus Epifluorescence microscope.

2.7.3c ImageJ line analysis

GFP expression and antibody staining along a drawn line across multiple cells, including their membrane, was quantified using the line analysis function in ImageJ. Raw fluorescence intensity values from the analysis, taken at 108 nm intervals, were normalised as a percentage of the highest pixel value in the dataset.

2.7.4 Compound treatment

2.7.4a Forskolin dose-response

A FSK 7-point half-log series-dilution and DMSO was prepared to be administered to a BacMam transfection series cell plate. 50 μ L of 600X FSK (0.6 mM) was added to well A1 in a fresh 384-well plate containing 34 μ L of DMSO in well B1 and 45 μ L of DMSO in wells C – H of the first column. 16 μ L of FSK from A1 was mixed with the DMSO in B1 before performing a series dilution of FSK from A1 across alternate wells to G1, transferring 5 μ L of FSK each time. The same step was performed for FSK in B1 across alternate wells up to F1 (H1 contained DMSO alone as a control). Following completion of this half-log series in DMSO 1 μ L of FSK from the column was transferred into 99 μ L of assay buffer in columns 3 and 4, composed of HBSS, 20 mM HEPES and 0.5 mM IBMX at pH 7.4. Transfection media in cell plates was blotted off before dispensing 25 μ L of assay buffer into each well using a multi-drop (Thermo Fisher Scientific). 5 μ L of the 7-point FSK dilution series and DMSO alone was stamped across the cell plate and incubated at 37 °C for 1 hour.

2.7.4b Drug treatment of HEK293 cells

A 384-well compound source plate was prepared containing a 10-point half-log dilution series of up to 16 compounds in duplicate (figure 2.4) across rows. 50 μ L of 150x compound was added to columns 2 and 14 before activating the Bravo robot, supplied with DMSO, to perform the half-log serial dilution

protocol between columns 2 – 11 and 14 – 23. Following completion of the protocol DMSO and 150x Forskolin (FSK in DMSO) was dispensed across columns 1, 12, 13 and 24 as control compounds. An intermediate plate was generated by stamping 2 μ L of source plate compounds into 48 μ L of assay buffer (HBSS, 20 mM HEPES and 0.5 mM IBMX at pH 7.4). Before administering compounds to transformed cells, transfection media was blotted off and 25 μ L of serum free media was dispensed into each well using a multi-drop (Thermo Fisher Scientific). 5 μ L of compounds from the intermediate plate was stamped onto the cells in media using the Bravo robot before incubating the cells at 37 $^{\circ}$ C for an appropriate time based on experimental objective.

	1	2	3	4	5	6	7	8	9	10	11	12	13	14	15	16	17	18	19	20	21	22	23	24	
A		1												1											
B		2												2											
C		3												3											
D		4												4											
E		5												5											
F		6												6											
G		7												7											
H		8												8											
I		9												9											
J		10												10											
K		11												11											
L		12												12											
M		13												13											
N		14												14											
O		15												15											
P		16												16											

Figure 2.4 Layout of compound source plate.

16 compounds were dispensed into columns 2 and 14 to be diluted by the Bravo robot, giving a 10-point half-log dilution series. Three source plates were generated with compounds in columns 2 and 14 at 2, 10 and 50 mM. Light green wells contain DMSO whereas dark green wells contain 150 μ M FSK; blue wells were originally empty wells to be filled by the Bravo robot.

2.7.5 cAMP assay

The cAMP assay was performed according to the manufacturer's protocol (cisbio, cAMP Gs dynamic kit), on assay plates following incubation with DMSO, FSK or screening compounds. A cAMP standardised dilution series was prepared as a control according to the manufacturer's detail before dispensing the cAMP detection reagents. 20x stock of D2-labelled cAMP and anti-cAMP cryptate antibody was diluted in lysis buffer to give a 1x solution of each. 7.5 μ L of D2-labelled cAMP was dispensed across the 384-well plate before dispensing 7.5 μ L of anti-cAMP cryptate antibody. Assay plates were incubated for 1 hour at RT on a plate shaker to allow mixing of detection reagents and

cells to undergo lysis. Following this incubation, homogeneous time-resolved fluorescence (HTRF) signal of each well was measured on a Pherastar plate reader. The HTRF readings were converted to exact cAMP concentration using the cAMP standard curve.

2.8 Statistics

Quantitative data analysis was performed in Graphpad Prism 8, including application of statistical tests, for zebrafish *mbp* assay optimisation and cell based assays. Expression of *mbp* was quantified in Fiji by setting a colour threshold in the region of interest. This method is described in literature by Diamantopoulou et al. (2019). Datasets were initially subjected to a normal distribution check before selecting the appropriate type of statistical test for data analysis (highlighted in figure legend). Error bars on all graphs illustrate standard deviation unless otherwise stated.

The zebrafish screening and assay optimisation experiments were performed in a 96-well plate format (see earlier section 2.3) and IBMX, a positive control compound, was included as a treatment, however, in this particular study it is unsuitable to validate experimental assay plates by calculating z-primes. The screening style is subjective and the intensity of staining is compared by eye to a crude scoring system that returns z primes <0.5 . The assay window also has a restricted range in line with the current scoring systems. However, repeat treatments were performed to ensure any phenotypic rescue mediated by compound treatment were reproducible. Each compound identified as a hit in screening assays is considered as such following n of 2.

Chapter 3.

Characterisation of Schwann cell development in wild type and *adgrg6^{tb233c}* zebrafish mutants

3.1 Introduction

Adgrg6 is an adhesion class GPCR with key regulatory roles in zebrafish larval development; including morphogenesis of the semicircular canals in the inner ear and myelination of the PNS by Schwann cells (see chapter 1 section 1.2). Previous work has illustrated the expression of *adgrg6* in otic epithelia (Geng *et al.*, 2013) and Schwann cells along the posterior lateral line (PLL) (Monk *et al.*, 2009). Furthermore, expression of Adgrg6 transcriptional readouts has been examined, including *versican* in the ear (Geng *et al.*, 2013) and Schwann cell myelination markers along the PLL of the zebrafish larvae (Monk *et al.*, 2009; Geng *et al.*, 2013). However, expression of *adgrg6* and myelinating Schwann cell markers along anterior nerves remains to be fully characterised. Additionally, almost all of these markers have been examined in zebrafish *adgrg6* mutants utilised by other research groups; their expression in *adgrg6^{tb233c}* hypomorphic mutants, utilised in pharmacological screening assays by the Whitfield lab, remains to be assessed. The current chapter aims to illustrate a thorough account of their expression in wild-type and *adgrg6^{tb233c}* mutant zebrafish across multiple larval stages, and in particular highlight key anterior and posterior phenotypic differences in the PNS that can be used as potential readouts of Adgrg6 pathway activity *in vivo*.

In the PNS, radial sorting of peripheral axons by Schwann cells is delayed in NTF *Adgrg6* mice and zebrafish mutants (Monk *et al.*, 2011; Petersen *et al.*, 2015) whilst Schwann cell development in *adgrg6* nonsense zebrafish mutants is arrested at the promyelinating stage (Monk *et al.*, 2009). Developmental arrest at this stage is associated with myelination defects, including a decrease in the number of myelin wraps ensheathing an axon (Monk *et al.*, 2009, 2011). Numerous studies have highlighted a decrease in expression of *myelin basic protein* mRNA and/or expression of its protein, a key structural component of the myelin sheath, in a range of *Adgrg6* mice and zebrafish mutants (Monk *et al.*, 2009; Geng *et al.*, 2013; Mogha *et al.*, 2013; Paavola *et al.*, 2014) in addition to human cases with pathogenic mutations (Ravenscroft *et al.*, 2015). Furthermore, axon-intrinsic clustering of sodium channels is observed, which in wild-type larvae are restricted to the nodes of Ranvier to facilitate saltatory conduction of action potentials (Voas *et al.*, 2009).

Early-onset Schwann cell markers include *sox10* and *erbb* genes, the expression of which is similar between wild-type and *adgrg6* mutant zebrafish lines (Monk *et al.*, 2009), indicating that Schwann cell development at this stage is independent of Adgrg6 activity. However, expression of promyelinating Schwann cell markers, including *oct6* (*pou3f1*), *krox20* (*egr2*) (Monk *et al.*, 2009) and *mbp* (Monk *et al.*, 2009; Geng *et al.*, 2013; Liebscher *et al.*, 2014; Paavola *et al.*, 2014; Petersen *et al.*, 2015), is downregulated in zebrafish *adgrg6* mutant larvae compared to wild types. The former two genes encode transcription factors in a signalling cascade that leads to the transcription of *mbp*. Monk *et al.* (2009) uncovered that functional Adgrg6 activity is necessary for the downstream activation of *oct6* and *krox20* transcription, driven by Adgrg6 activity-induced cAMP signalling that has been reproduced in multiple studies to date (Liebscher *et al.*, 2014; Ghidinelli *et al.*, 2017; Lizano, Hayes and Willard, 2020). Although the expression of *mbp* in *adgrg6^{tb233c}* zebrafish mutants has been illustrated in previous studies (Geng *et al.*, 2013; Diamantopoulou *et al.*, 2019), it has not been fully characterised along the anterior lateral line (ALL). Furthermore, expression of *oct6* and *krox20* remains to be characterised in these mutants.

A further gene of interest, *claudin k*, encodes a tight junction protein expressed in myelinating Schwann cells associated with the zebrafish lateral line (Takada and Appel, 2010). Given the reduced extension of Schwann cells observed in *Adgrg6* mice and zebrafish mutants, the expression of *claudin k* may also display an observable phenotype. The key Schwann cell gene markers examined in this study are included in Table 3.1.

Schwann cell markers (Table 3.1) are also expressed in myelinating oligodendrocytes in the CNS, with the current exception of *adgrg6*. Moreover, their expression patterns are visibly complex, indicative of the intricate anatomy of axons that Schwann cells myelinate in the nervous system. The objective for this chapter is to identify clear differences in expression of Schwann cell markers, between wild-type and *adgrg6^{tb233c}* mutant zebrafish, which have potential to be scored in terms of staining intensity and/or distribution. Otic expression of *vcanb*, 'on' in *adgrg6* mutants and 'off' in wild types, is amenable to scoring in such terms and has provided a valuable phenotypic readout to screen for small molecule modulators of the Adgrg6 pathway (Diamantopoulou *et al.*, 2019). A similarly suitable PNS phenotype could form the basis of a semi-quantitative counter-screening assay to test specificity of primary assay hits. Although our group has previously utilised PNS expression of *mbp* as the foundation for such an assay, the focus has been on expression along the PLL (Diamantopoulou *et al.*, 2019). Schwann cell myelination markers are known to be expressed along the ALL and cranial nerves (Brösamle and Halpern, 2002), which may also exhibit altered phenotypes in *adgrg6* mutants.

Table 3.1 Schwann cell gene markers

Gene	Protein function	Stage of expression	Reference
<i>adgrg6</i>	Signal transduction across membrane	Immature, myelinating, (also in inner ear and other tissue)	(Monk <i>et al.</i> , 2009; Geng <i>et al.</i> , 2013, fig. 7, S4)
<i>cldnk</i>	Tight junction protein	Myelinating	(Takada and Appel, 2010)
<i>krox20 (egr2)</i>	Transcription factor	Promyelinating	(Lyons <i>et al.</i> , 2005)
<i>mbp</i>	Myelin sheath	Myelinating	(Lyons <i>et al.</i> , 2005)
<i>oct6</i>	Transcription factor	Promyelinating	(Jaegle <i>et al.</i> , 2003)
<i>(pou3f1)</i>			
<i>sox10</i>	Transcription factor	Neural crest, myelinating, (also in inner ear)	(Dutton <i>et al.</i> , 2001)

3.2 Results

In order to study the expression pattern of various gene markers, larvae were fixed at developmental stages ranging from 48 – 120 hours post fertilisation (hpf) before performing whole-mount *in situ* hybridisation (WISH) or whole-mount immunohistochemistry. Beyond 24 hpf, larvae were incubated in E3 medium containing phenylthiourea to inhibit pigmentation that may interfere with visualisation of gene or protein expression patterns.

3.2.1 Expression pattern of *adgrg6*

The expression of *adgrg6* mRNA was initially examined to highlight the key tissues and organs where it may have a role in development. Figure 3.1 and 3.2 illustrate the expression of *adgrg6* mRNA between 48 and 96 hpf in zebrafish larvae. As reported previously (Geng *et al.*, 2013), *adgrg6* mRNA is expressed in the heart, nose, ethmoid plate, fins and otic vesicle at 48 hpf (figure 3.1, 3.2). Prolonged staining also highlighted expression along the lateral line. Expression in all these regions is reported for the first time in *adgrg6^{tb233c}* zebrafish mutants. Notably, the expression pattern of *adgrg6* is largely similar between wild types and *adgrg6* mutants at this stage in line with previous observations (Monk *et al.*, 2009; Geng *et al.*, 2013). Expression of *adgrg6* in the inner ear and along the PLL was examined in further detail to determine if published observations were consistent in the wild types and mutants utilised in this study.

3.2.1a Otic expression of *adgrg6*

A closer look at the ear shows strong *adgrg6* expression in the developing epithelia of the otic vesicle including some weak expression in supporting cells of the anterior macula in wild type and *adgrg6^{tb233c}* mutant larvae (figure 3.1E-F). At this stage in wild-type larvae, robust expression is seen in the anterior projection of the otic vesicle that is developing towards the converging anterior bulge of the lateral projection (figure 3.1E), prior to a contact and fusion event that leads to formation of the anterior pillar, imaged at 72 hpf (figure 3.1G). Comparatively, in *adgrg6^{tb233c}* mutants, *adgrg6* is expressed strongly in the anterior projection epithelia at 48 hpf (figure 3.1F). Expression in the posterior projection and posterior bulge and their development looks similar in wild types and mutants at this stage. At 72 hpf, *adgrg6* is moderately expressed in epithelial cells of the fully formed anterior, posterior and ventral pillars (figure 3.1G) whereas *adgrg6^{tb233c}* mutants display expression at the tips of overgrown, unfused projections (figure 3.1H) of the otic vesicle that fail to compartmentalise the inner ear into three semicircular canals: anterior, posterior and lateral/horizontal. The expression pattern and phenotype observed in *adgrg6^{tk256a}* and *adgrg6^{fr24}* mutants is similar (Figure 3.3 A, C). Geng *et al.* (2013) have also characterised *adgrg6* expression in the *fr24* allele.

Overall the expression of *adgrg6* during semicircular canal morphogenesis is similar to that of *versican* genes, which persists beyond 96 hpf in *adgrg6* mutants (see Chapter 1 figure 1.1) (Geng *et al.*, 2013). As expression of *adgrg6* mRNA is unaffected in mutants, the inner ear defects likely result from abnormalities in its protein expression or restricted functional capacity of the receptor, highlighting a key role for Adgrg6 and/or its signalling pathway in regulating *versican* expression and the contact and fusion events leading to pillar formation in the zebrafish inner ear.

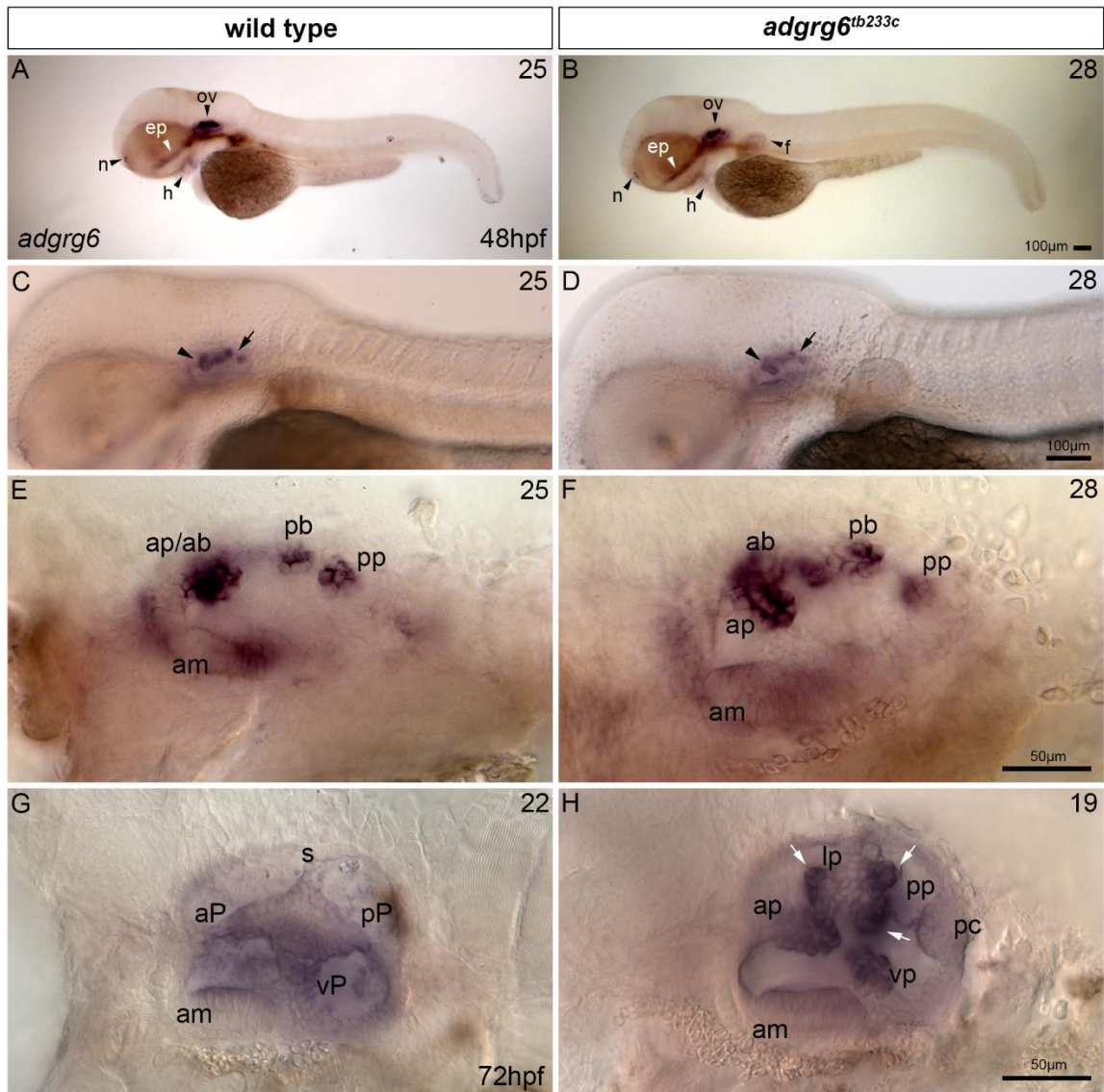


Figure 3.1 *adgrg6* mRNA expression pattern in the inner ear, at 48 and 72 hpf, of wild-type and *adgrg6*^{tb233c} mutant zebrafish.

(A-F) expression of *adgrg6* in wild-type (A, C, E) and *adgrg6*^{tb233c} mutant (B, D, F) embryos at 48 hpf. All images are lateral views, anterior to the left and posterior to the right. (C-F) close up view of *adgrg6* expression in otic vesicle (ov), arrowhead (C, D) marks expression at anterior projection (ap) and anterior bulge (ab) of lateral projection (E, F), arrow (C, D) marks posterior projection (pp) and posterior bulge (pb) of lateral projection (E, F). (G-H) otic expression of *adgrg6* in wild-type (G) and *adgrg6*^{tb233c} mutant (H) larvae at 72 hpf. Arrows (H) mark expression at the anterior, posterior and ventral bulges of lateral projection. Abbreviations: ab, anterior bulge; am, anterior macula; ap, anterior projection; aP, anterior pillar; ep, ethmoid plate; f, fin; h, heart; lp, lateral projection; n, nose; ov, otic vesicle; pb, posterior bulge; pp, posterior projection; pP, posterior pillar; s, septum; vp, ventral projection; vP, ventral pillar.

3.2.1b Expression of *adgrg6* and *sox10* along the posterior lateral line nerve

In the wild-type larval PNS, *adgrg6* is expressed in Schwann cells along the PLL, shown between 48-96 hpf (figure 3.2, 3.4), as previously reported (Monk *et al.*, 2009). This expression is weak in comparison to that in the inner ear and requires a prolonged staining step during the WISH protocol. The overstained ear, fin, heart and nose appear almost black, providing a reference to highlight the level of staining required to observe *adgrg6* expression along the PLL in zebrafish larvae. For the first time, *adgrg6* expression is detected in Schwann cells along the PLL of *adgrg6^{tb233c}*, *adgrg6^{tk256a}* and *adgrg6^{fr24}* allelic mutants (figure 3.2-3.4). The expression pattern is similar to that observed in wild-type larvae, including in *fr24* allelic mutants (figure 3.3) that contain an early stop codon. These observations suggest that the associated mutations do not affect mRNA expression through physiological processes such as nonsense-mediated mRNA decay. A small number of wild-type and mutant larvae displayed no expression of *adgrg6* along the PLL; however, these may have required further staining still for it to be detected. Expression of *adgrg6* is also detected in the ceratobranchials and is similar in wild type and *adgrg6* mutant larvae, shown at 96 hpf (figure 3.2E-F).

Expression of *sox10*, a marker of neural crest-derived glia, was examined as a secondary early-onset marker of Schwann cells. Figure 3.4 illustrates PLL expression of *adgrg6* and *sox10* in wild type and *adgrg6^{tb233c}* zebrafish mutants, at 72 hpf. The hypomorphic mutants were selected specifically for these experiments as they are utilised in the small molecule screening assays in chapter 4. As reported in previous literature (Dutton *et al.*, 2001), *sox10* is expressed in Schwann cells along the PLL nerve (PLLn) and around the PLL ganglion (PLLg) of wild-type larvae (figure 3.4C), similar to the expression pattern of *adgrg6* at this stage. In fact, previous work by Geng *et al.* (2013) proposed that *adgrg6* is not only synexpressed with but also regulated by *sox10*. Expression of *sox10* is reported for the first time in *adgrg6^{tb233c}* mutants (figure 3.4D) and displays a similar pattern of expression to wild types, in line with published observations on other *adgrg6* zebrafish mutants (Monk *et al.*, 2009). Taken together, these observations highlight the presence of Schwann cells along PLL nerves. In the brain, dispersed punctate staining illustrates the distribution of *sox10*-positive cells in both wild-type and *adgrg6* mutant larvae.

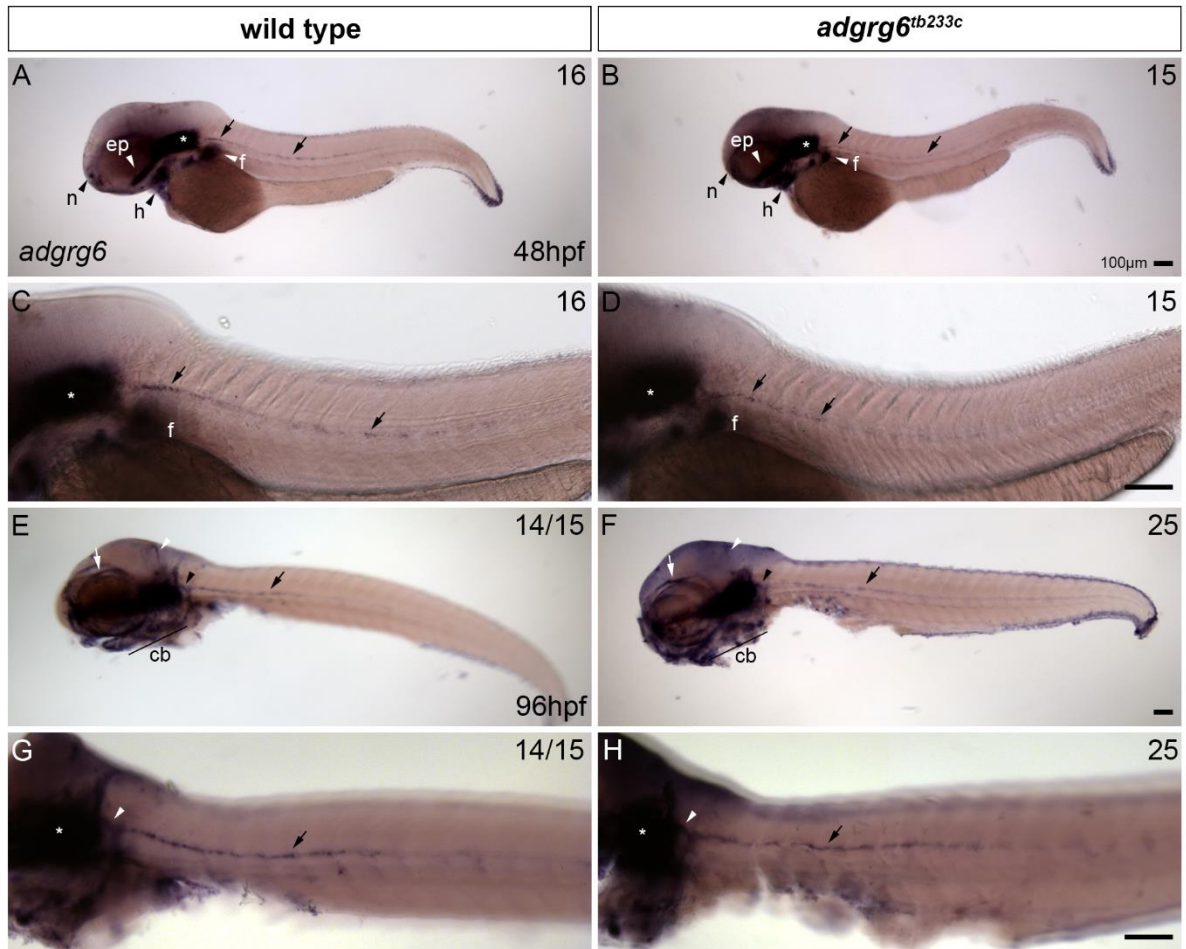


Figure 3.2 *adgrg6* mRNA expression along the lateral line, at 48 and 96 hpf, in wild-type and *adgrg6^{tb233c}* mutant zebrafish.

(A-D) expression of *adgrg6* in wild-type (A, C) and *adgrg6^{tb233c}* mutant (B, D) embryos at 48 hpf. All images are lateral views, anterior to the left and posterior to the right. (C-D) close up view of *adgrg6* expression in Schwann cells along the PLL. (E-H) expression of *adgrg6* in wild-type (E, G) and *adgrg6^{tb233c}* mutant (F, H) larvae at 96 hpf. (G-H) close up view of *adgrg6* expression in Schwann cells along the PLL. Arrows mark expression along PLL (black) and ALL (white) nerve; arrowheads (E-H) mark expression at PLL ganglia (PLLg); asterisk indicates overstained otic vesicle. Abbreviations: cb, ceratobranchials; ep, ethmoid plate; f, fin; h, heart; n, nose.

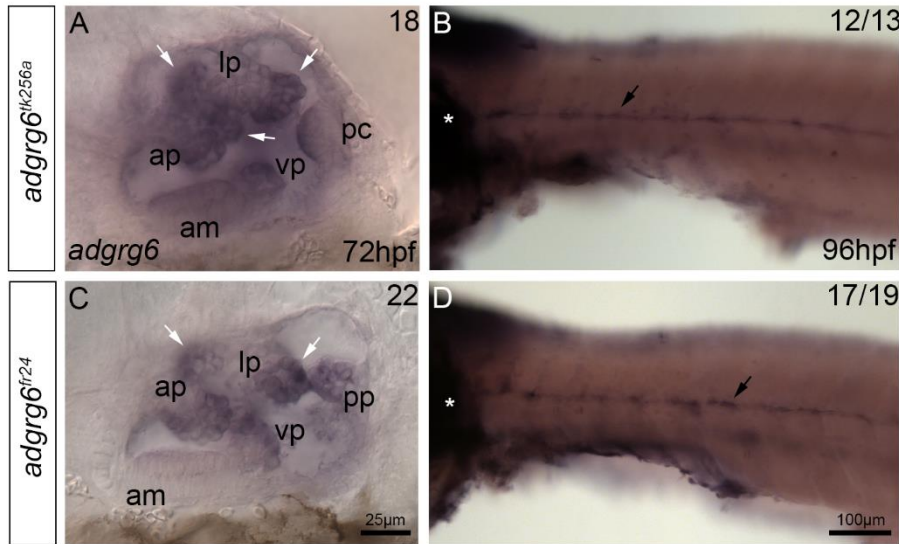


Figure 3.3 *adgrg6* mRNA expression in *adgrg6^{tk256a}* and *adgrg6^{fr24}* mutant larvae.

(A-B) expression of *adgrg6* in the otic vesicle (A), at 72 hpf, and in Schwann cells along the PLL (B), at 96 hpf, in *adgrg6^{tk256a}* mutants. (C-D) expression of *adgrg6* in the otic vesicle (C), at 72 hpf, and in Schwann cells along the PLL (D), at 96 hpf, in *adgrg6^{fr24}* mutants. All images are lateral views, anterior to the left and posterior to the right. White arrows mark expression at the anterior, posterior and ventral bulge of lateral projection; black arrows mark expression along PLL; asterisk indicates overstained ear. Abbreviations: am, anterior macula; ap, anterior projection; lp, lateral projection; vp, ventral projection.

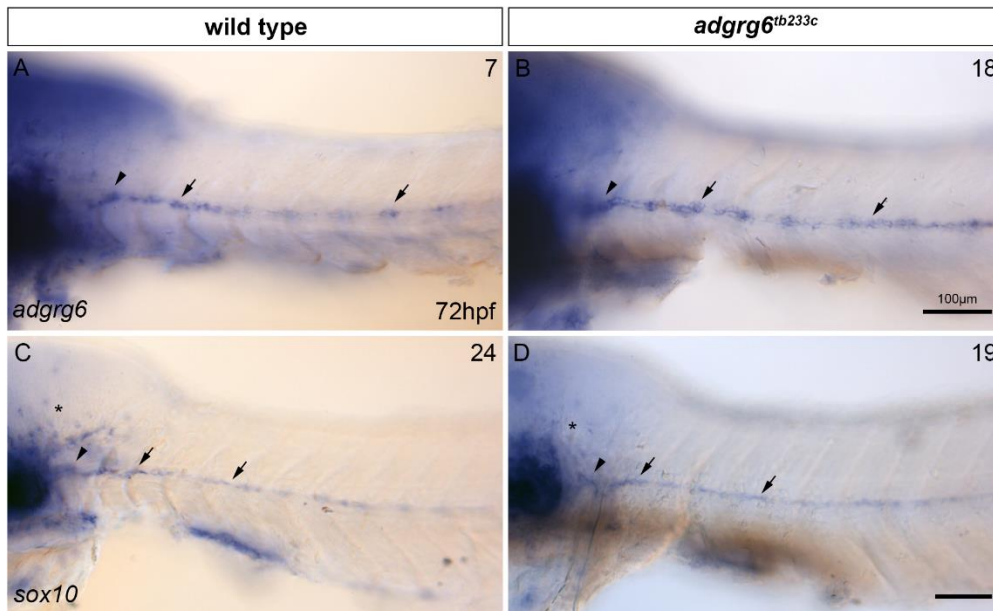


Figure 3.4 *adgrg6* and *sox10* mRNA expression along PLL in wild-type and *adgrg6^{tb233c}* mutant larvae.

(A-B) expression of *adgrg6*, at 72 hpf, in wild-type and *adgrg6^{tb233c}* mutant larvae. (C-D) expression of *sox10*, at 72 hpf, in wild-type and *adgrg6^{tb233c}* mutant larvae. All images are lateral views, anterior to the left and posterior to the right. Arrows mark expression in Schwann cells along PLL; arrowheads mark expression in Schwann cells at the PLLg; asterisk highlights dispersed *sox10* positive cells in the CNS.

3.2.2 Anterior expression of *sox10* and *adgrg6* in wild-type and *adgrg6^{tb233c}* mutant larvae

The expression of *adgrg6* and *sox10* was characterised along ALL and cranial nerves to illustrate localisation of Schwann cells. Figure 3.5 illustrates *sox10* and *adgrg6* expression along nerve branches located in the anterior zebrafish larva, shown from dorsal and ventral viewpoints.

Similar to *adgrg6* expression along the PLL, expression of *sox10* and *adgrg6* mRNA is weak along anteriorly located nerve branches and required a prolonged staining step during the WISH protocol and a series of stringent methanol washes to clear non-specific background staining. In wild-type 72 hpf larvae, *sox10* is weakly expressed in Schwann cells along the supraorbital (dorsal view) and infraorbital (ventral view) branches of the ALL nerve (figure 3.5), as shown in previous literature (Dutton *et al.*, 2001). In the dorsal-most plane, fine punctate expression of *sox10* is apparent in cells dispersed within the brain. Interestingly, expression of *sox10* is observed along a possible third nerve located medially along the dorso-ventral axis that could indicate presence of neural crest-derived glial cells. As expected, the expression pattern of *sox10* in *adgrg6^{tb233c}* zebrafish mutants is similar to that observed in wild types.

The expression pattern of *adgrg6* in Schwann cells, at 72 hpf and 96 hpf (figure 3.5), largely overlaps with that of *sox10*. Expression is detected along the supraorbital and infraorbital nerves, at 72 and 96 hpf, illustrating the presence of Schwann cells. As reported in previous literature (Geng *et al.*, 2013), *adgrg6* is strongly expressed in cells of the olfactory epithelium, shown at 72 and 96 hpf, the basihyal bone, shown at 72 hpf, and the ceratobranchials, shown at 96 hpf. Interestingly, *adgrg6* expression is observed for the first time along a nerve located medially along the dorso-ventral axis, shown at 72 and 96 hpf, where *sox10* expression was also detected. The expression of both markers in this region could indicate more likely presence of Schwann cells as expression of *adgrg6* has not previously been seen in oligodendrocytes. However, expression in other cell types should not be discounted as *adgrg6* and *sox10* expression overlaps in various tissue including heart, mesoderm, head and pectoral fin chondrocytes and otic and olfactory epithelium (Geng *et al.*, 2013). Similar to the expression of *adgrg6* along the PLL, there is no difference in its expression pattern between wild-type and *adgrg6^{tb233c}* mutant larvae.

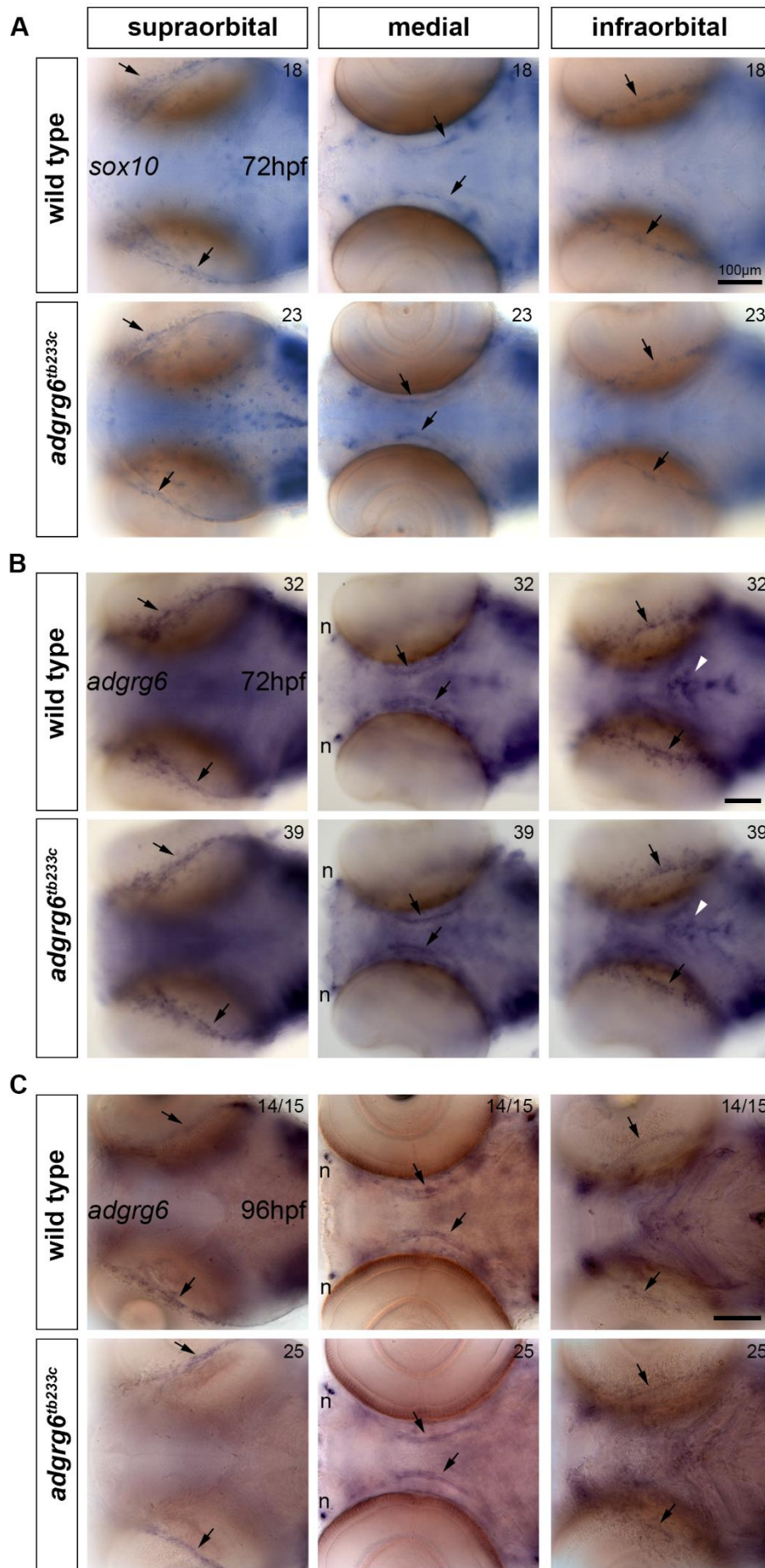


Figure 3.5 *sox10* and *adgrg6* mRNA expression along anterior lateral line and cranial nerves in wild-type and *adgrg6*^{tb233c} mutant larvae.

(A) expression pattern of *sox10* in Schwann cells associated with anterior cranial nerves (arrows), at 72 hpf, is similar between wild-type (top panel) and *adgrg6*^{tb233c} mutant (bottom panel) larvae. Expression of *adgrg6* in Schwann cells, at 72 hpf (B) and 96 hpf (C), is also similar between wild-type (B-C, top panel) and *adgrg6*^{tb233c} mutant (B-C, bottom panel) larvae. Dorsal (supraorbital) and ventral (medial, infraorbital) views shown with anterior to the left, and posterior to the right. Arrows mark expression along nerves whereas arrowheads mark expression at basihyal bone (B, infraorbital panels). Expression of *adgrg6* is also detected in the nose (n, medial panels) at 72 (B) and 96 (C) hpf. Embryos display pigmented background staining as an overnight incubation in staining solution was necessary to detect the weak expression these transcripts in Schwann cells.

3.2.3 Characterisation of *mbp* mRNA and transgenic *mbp*-driven EGFP expression in wild-type and *adgrg6^{tb233c}* mutant zebrafish larvae

Myelin basic protein forms a key structural component of the myelin sheath in myelinating glia, including oligodendrocytes and Schwann cells. We have previously shown that expression of *mbp* mRNA is significantly downregulated in *adgrg6^{tb233c}* mutants, particularly around the PLLg. Moreover, we have utilised this phenotypic difference to counter-screen small molecule hits identified from a primary *versican* screening assay on *adgrg6^{tb233c}* zebrafish mutants (Diamantopoulou *et al.*, 2019). However, in the interest of designing an optimised counter-screening assay, the expression of *mbp* was thoroughly characterised in the current project including its expression along the ALL, which is yet to be fully examined in *adgrg6^{tb233c}* zebrafish mutants. Previous studies have highlighted that *mbp* expression is detected in the PNS at 72 hpf, and therefore larvae were fixed between 72 and 96 hpf to characterise the expression of *mbp*. Figure 3.6 illustrates expression of *mbp* mRNA in wild-type and *adgrg6^{tb233c}* mutant larvae.

3.2.3a Expression of *mbp* mRNA in zebrafish larvae

At 96 hpf, strong expression of *mbp* was detected in the CNS and *mbp*-positive Schwann cells were detected along the PLLn and the supraorbital and infraorbital branch of the ALLn. Expression along the PLLn appears marginally stronger than that along the ALLn (figure 3.6Ai). In all larvae, robust expression was detected around the PLLg and ALLg in addition to three distinct puncta (figure 3.6Ai, ii) of expression near the ear cristae that could indicate presence of Schwann cells along afferent axons to the statoacoustic ganglion (SAG). A fourth, weaker, punctum of staining marks expression along the middle line associated with the MI2 neuromast (Raible and Kruse, 2000); however, this expression was not detected in all wild-type larvae. Furthermore, weak expression is detected along the anteroventral (AV) nerve that fasciculates with the facial (VII) nerve (figure 3.6Ai'); this expression is also not detected in all larvae. Finally, expression of *mbp* was detected along a medial nerve (figure 3.6Aiv), where *adgrg6* and *sox10* expression was previously detected (figure 3.5), probably marking dorsally extending axons of the trochlear nerve (Higashijima, Hotta and Okamoto, 2000). The medial stain is present in the region of the ventromedial hindbrain anterior to the trochlear nerve and therefore could illustrate myelinating glia along the oculomotor nerve (Higashijima, Hotta and Okamoto, 2000). Overall, these observations are consistent with those published previously by Brösamle and Halpern (2002).

As expected, expression of *mbp* was unaffected in the CNS of *adgrg6^{tb233c}* zebrafish mutants (figure 3.6Av). In the PNS, however, expression of *mbp* was largely reduced. A marginal decrease in expression was observed in Schwann cells along the ALL and PLLn whereas expression around the PLLg

appeared significantly reduced (figure 3.6v, vi). Staining at the three puncta near the cristae was reduced, illustrating a decrease in expression along nerves associated with the SAg. Notably, 7/26 (26.9%) embryos displayed no *mbp* expression around the PLLg and near the cristae (figure 3.6D). We have previously published similar phenotypic observations in Diamantopoulou et al. (2019). Further inspection of mutants reveals that expression along the middle line is missing (figure 3.6vi); a fourth punctum of staining is not observed as in some wild-type larvae. Moreover, weak expression detected along the AV and VII bundle in wild-type larvae was missing in *adgrg6^{tb233c}* mutants. However, most surprising was the complete absence of *mbp* expression along the assumed oculomotor and trochlear nerves. This loss of expression was observed for the first time in *adgrg6* zebrafish mutants and could indicate that these axons are myelinated by Schwann cells, as *adgrg6* has not been shown to be expressed in oligodendrocytes or regulate their development.

At 96 hpf, the expression pattern of *mbp* is complex and illustrates the intricate anatomy of nerves in the CNS and PNS. At earlier developmental stages however, including 72 and 78 hpf (figure 3.6B), the expression pattern of *mbp* appears less complex. Expression in the CNS is moderate at 72 hpf and strong at 78 hpf but marginally weaker than that at 96 hpf. In the PNS, expression is detected in Schwann cells along the PLL nerve and around the ganglion at both stages. Weak expression along the supraorbital line is also detected in some larvae; however, expression is stronger at the ALLg and posterior to the ALL fork. At similar stages in *adgrg6^{tb233c}* mutant larvae *mbp* expression along the PLLn and around the ALLg is weak whereas expression around the PLLg is completely missing (figure 3.6Biii, iv). The complete absence of expression around the PLLg is a consistent and recognisable phenotype at this stage of development in *adgrg6^{tb233c}* mutants. This phenotypic difference between wild type and mutant larvae is one that can be scored with ease, similar to *mbp* expression around the same region at later stages, which we utilised in our previous counter-screening assay (Diamantopoulou et al., 2019). Expression of *mbp* in the CNS remains similar between wild-type and mutant larvae at the earlier stages, similar to at 96 hpf.

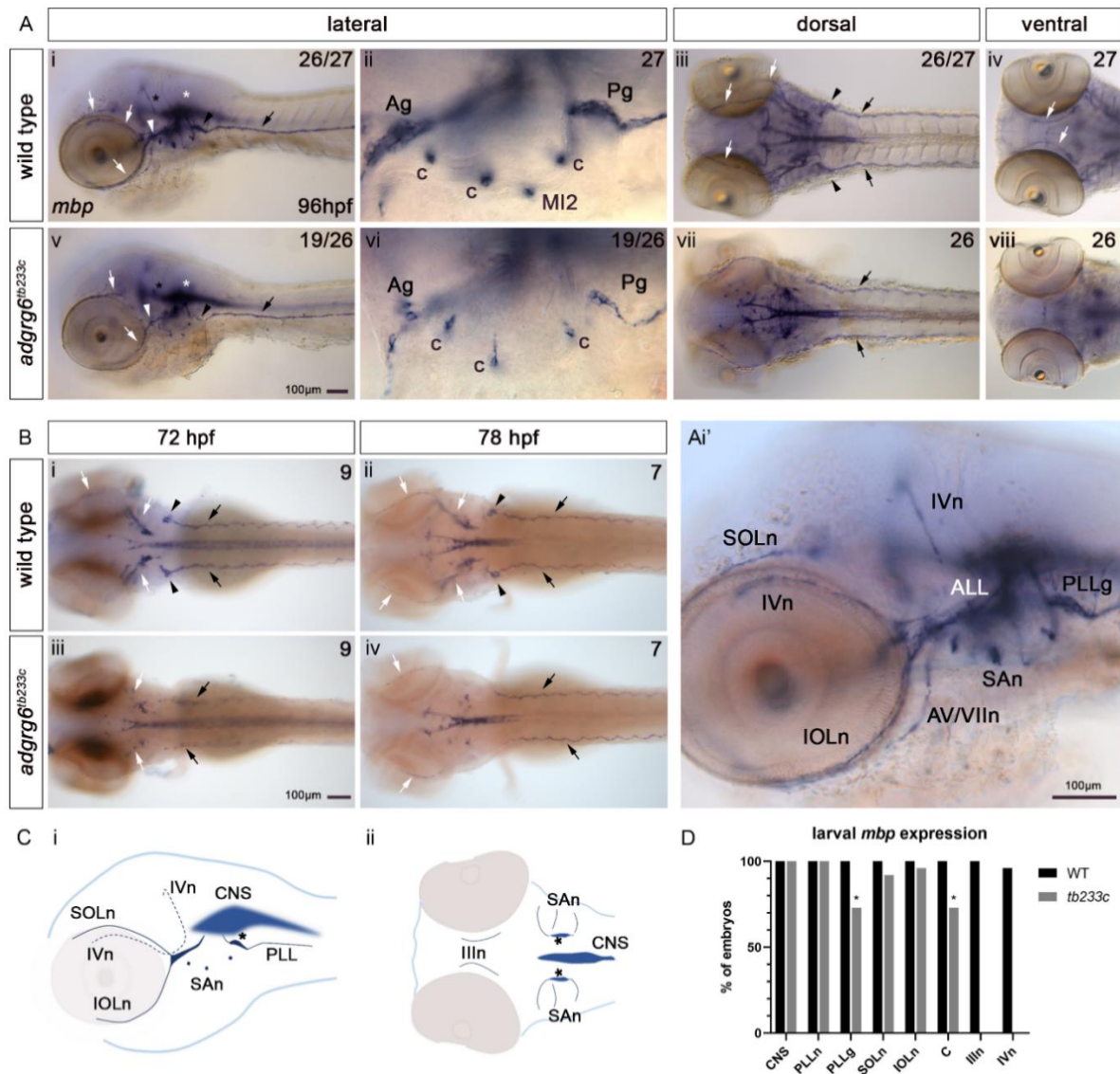


Figure 3.6 *mbp* mRNA expression in Schwann cells along the lateral line and cranial nerves, between 72 and 96 hpf, in wild-type and *adgrg6^{tb233c}* mutant larvae.

(A) Schwann cell expression of *mbp*, at 96 hpf, is down-regulated in *adgrg6^{tb233c}* mutants (v-vi, lateral; vii, dorsal; viii, ventral) in comparison to wild-type (i-ii, lateral; iii, dorsal; iv, ventral) larvae. CNS expression (white asterisk) is similar in wild type and *adgrg6^{tb233c}* mutants. (A ii, vi) close up of expression around the ALL ganglia (Ag), PLL ganglia (Pg), middle line MI2 neuromast and statoacoustic nerves near the cristae (c). (Ai') blow up of wild-type lateral view (in Ai) illustrating expression of *mbp* in Schwann cells along ALL and cranial nerves. Abbreviations: ALL, anterior lateral line; AVn, anteroventral nerve; IIIIn, oculomotor nerve; IOLn, infraorbital nerve; IVn, trochlear nerve; PLLg, posterior lateral line ganglion; SAn, statoacoustic nerves; SOLn, supraorbital nerve; VIIn, facial nerve. **(B)** Schwann cell expression of *mbp* is also downregulated at 72 hpf and 78 hpf in *adgrg6^{tb233c}* mutants (Biii, iv) in comparison to wild-type larvae (Bi, ii), dorsal brightfield images. **(C)** schematic representation of *mbp* expression in the CNS and PNS, shown laterally (Ci) and ventrally (Cii). **(D)** quantification of *mbp* expression, in terms of percentage embryos, detected in the CNS and PNS of wild-type and *adgrg6^{tb233c}* mutant larvae at 96 hpf. Asterisk (in D) indicates regions that exhibit significant downregulated *mbp* expression in *adgrg6* mutants. Arrows mark expression along ALL (white), cranial (white) and PLL (black) nerves; arrowhead marks expression around ALL (white, Ag) and PLL (black, Pg) ganglia; white asterisk marks CNS expression; black asterisk marks dorsal extending axon of IV nerve. Anterior to the left and posterior to the right in all images.

3.2.3b Transgenic *mbp*-driven EGFP expression along the lateral line and cranial nerves

Next, the expression of an *mbp*-driven transgene was examined in zebrafish larvae to determine if EGFP expression was consistent with that of *mbp* mRNA in wild-type and *adgrg6^{tb233c}* mutant larvae. This work was performed on the Tg(*mbp*:EGFP-CAAX) zebrafish line fixed at 120 hpf, at which stage background fluorescence is significantly reduced. In this transgenic reporter line, *mbp* regulatory elements drive membrane expression of enhanced green fluorescence protein (EGFP) to mark myelinating glia, including oligodendrocytes in the CNS and Schwann cells in the PNS. Following fixation, larvae were subjected to whole-mount immunohistochemistry with a GFP-boost antibody, to augment the EGFP signal, and an anti-acetylated α -tubulin antibody, to mark neuronal axons. Combined immunofluorescence staining with these antibodies also illustrates the localisation of Schwann cells in relation to the anatomy of cranial nerves in zebrafish larvae. Figure 3.7 and 3.8 illustrate intensity projections of anti-acetylated α -tubulin and EGFP staining in Tg(*mbp*:EGFP-CAAX) larvae and F2 generation *adgrg6^{tb233c}* mutants crossed with this line. Intensity projections in figure 3.7 are taken from z-stacks split into two groups across the lateral axis – superficial and deep – whereas 3.8 illustrates intensities from the collective z-stack.

Anti-acetylated α -tubulin staining highlights the anatomy of cranial nerves and sensory afferents associated with the lateral line and its neuromasts including the anterior and posterior regions. In the anterior, the superficially located ALLg is juxtaposed with the trigeminal ganglia (figure 3.7 superficial stacks). Two anterior branches arise from the ALLg, including the supraorbital and infraorbital nerves. The transgene expression illustrates the presence of myelinating Schwann cells along these nerves and around the ALLg. Similar to the ALL, EGFP is expressed along the PLL nerve and around its ganglia (figure 3.8iii, iii’).

The anti-acetylated α -tubulin stain illustrates the organisation of oculomotor (III), trochlear (IV), trigeminal (V), facial (VII), octaval (VIII) and vagal (X) nerves (figure 3.7-3.8). The fluorescent staining and cranial nerve organisation shown is consistent with that published in the literature using equivalent markers (Higashijima, Hotta and Okamoto, 2000; Raible and Kruse, 2000). Transgenic EGFP fluorescence is detected along these cranial nerves, indicating the presence of myelinating Schwann cells, although no staining is detected around the trigeminal ganglion. Most interesting is the expression along the oculomotor and trochlear nerves that innervate the eye muscles (figure 3.7 deep stacks and 3.8i’-iii’). Staining along these nerves is consistent with the expression of *mbp* mRNA in the same region at 96 hpf and expression of *sox10* and *adgrg6* specifically in the region of the oculomotor nerve. It is likely that mRNA expression of these genes marks Schwann cells associated with the oculomotor and trochlear nerves.

The anatomy of cranial nerves and lateral line afferents, highlighted by the anti-acetylated α -tubulin stain, is similar between wild-type and *adgrg6^{tb233c}* mutants. Notably, however, expression of *mbp*-driven EGFP in PNS regions is downregulated in *adgrg6* mutants. Expression in mutants is comparable to wild types along a few nerves, including the PLL and the supraorbital branch of the ALL. Expression around the ALLg also appears comparable whereas expression around the PLLg is significantly downregulated. Furthermore, only weak expression is detected along the infraorbital line, trochlear, facial and vagal nerves. Almost no expression is detected along the oculomotor nerve, similar to *mbp* mRNA expression along the same region. Considering these observations, it appears that a lack of myelinating Schwann cells does not have a consequential effect on neuron anatomy. Overall these observations are consistent with the expression pattern of *mbp* mRNA in wild-type and *adgrg6* mutant larvae, illustrating that reduced expression of mRNA is likely to result in reduced protein expression. This would need to be confirmed with an antibody stain to the Mbp protein.

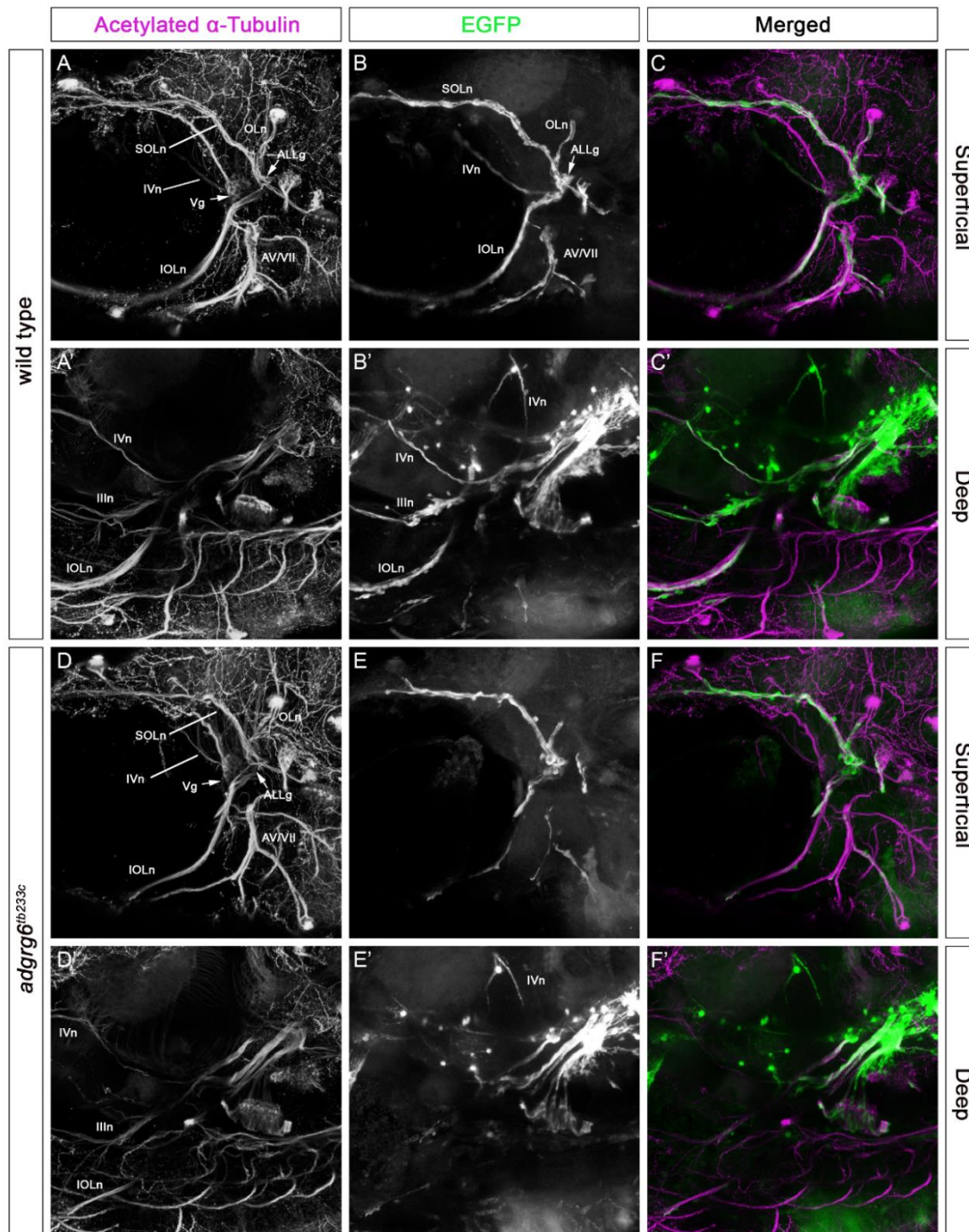


Figure 3.7 Expression pattern of acetylated α -tubulin in 96 hpf *tg(mbp:EGFP-CAAX)* larvae in the wild type and *adgrg6^{tb233c}* background.

(A-C) antibody staining of acetylated α -tubulin (A) and *mbp*-driven EGFP expression (B) in 96 hpf wild-type larvae. **(D-F)** in *adgrg6^{tb233c}* mutant larvae antibody staining of acetylated α -tubulin (D) is similar to wild-type larvae whereas *mbp*-driven EGFP expression (E) is down-regulated in Schwann cells. Merged images of wild-type (C, C') and *adgrg6^{tb233c}* mutant (F, F') larvae are shown. GFP-boost antibody applied to elevate fluorescent signal. Images are standard deviation intensity projections from z-slices grouped into superficial (A-C, D-F) and deep (A'-C', D'-F') localisation in the zebrafish larva. All images are lateral views, with anterior to the left and posterior to the right. Abbreviations: ALLg, anterior lateral line ganglion; AV, anteroventral nerve; Illn, oculomotor nerve; IOLn, infraorbital nerve; IVn, trochlear nerve; OLn, ; otic line nerve; Vg, trigeminal ganglion; SOLn, supraorbital nerve; VII, facial nerve.

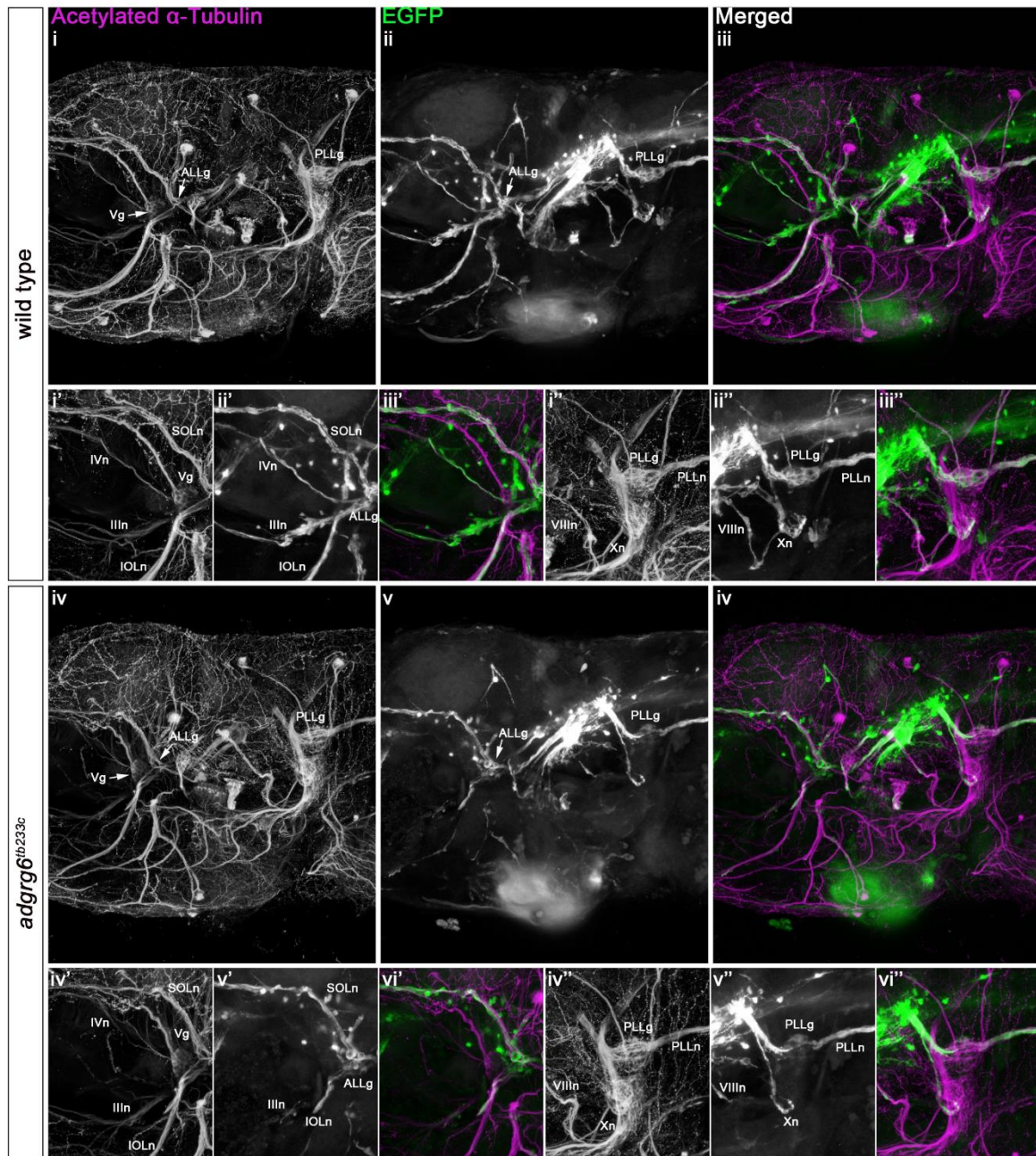


Figure 3.8 Expression pattern of acetylated α -tubulin in 96 hpf $tg(mbp:EGFP-CAAX)$ larvae in the wild type and $adgrg6^{tb233c}$ background.

(i-iii) antibody staining of acetylated α -tubulin (i) and *mbp*-driven EGFP expression (ii) in 96 hpf wild-type larvae. (iv-vi) in $adgrg6^{tb233c}$ mutant larvae antibody staining of acetylated α -tubulin (iv) is similar to wild-type larvae whereas *mbp*-driven EGFP expression (v) is down-regulated in Schwann cells. Close ups of ALL (i'-vi') and PLL (i''-vi'') in wild-type (ALL, i'-iii'; PLL, i''-iii'') and $adgrg6^{tb233c}$ mutant (ALL, iv'-vi'; PLL, iv''-vi'') larvae are included. Merged images of wild-type (iii) and $adgrg6^{tb233c}$ mutant (vi) larvae are shown. GFP-boost antibody applied to elevate fluorescent signal. Images are standard deviation intensity projections from superficial and deep z-slices grouped from previous figure (3.7). All images are lateral views, with anterior to the left and posterior to the right. Abbreviations: ALLg, anterior lateral line ganglion; AV, anteroventral nerve; IIIIn, oculomotor nerve; IOLn, infraorbital nerve; IVn, trochlear nerve; OLn, ; otic line nerve; PLLg, posterior lateral line ganglion; Vg, trigeminal ganglion; SOLn, supraorbital nerve; VIIIIn, facial nerve; VIIIIn, octaval nerve; Xn, vagus nerve.

3.2.4 Characterisation of additional Schwann cell myelination markers

The mRNA expression of additional Schwann cell myelination markers including *oct6*, *krox20* and *cldnk* was characterised to determine if they exhibit phenotypic differences in *adgrg6^{tb233c}* mutant larvae, similar to those observed for *mbp* that have been utilised as a readout for small molecule screening purposes. However, such phenotypes must be clear and consistent whilst also being amenable to evaluation in terms of staining area and/or intensity, allowing for a window of intermediate levels of expression to be recognised.

3.2.4a Expression of *oct6* in wild-type and *adgrg6^{tb233c}* mutant zebrafish larvae

The expression of *oct6* was characterised first as it is the earliest known gene marker that shows defective expression in *adgrg6* zebrafish mutants (Monk *et al.*, 2009). Its expression pattern was examined in larvae fixed at 48 and 96 hpf. The staining of embryos during WISH was extended overnight at 4°C before expression was detected in the PNS. Figure 3.9 illustrates the expression of *oct6* mRNA in wild-type and *adgrg6^{tb233c}* mutant larvae.

At 48 and 96 hpf in wild-type larvae, *oct6* is robustly expressed in the brain (figure 3.9A, C), as previously reported (Lister *et al.*, 2006; Monk *et al.*, 2009). This expression is unaffected in *adgrg6^{tb233c}* zebrafish mutants (figure 3.9B, D), similar to other *adgrg6* allelic zebrafish mutants (Monk *et al.*, 2009). Expression of *oct6* along ALL and anterior cranial nerves, if any, was difficult to detect because of strong ubiquitous expression in the brain.

Notably in wild-type larvae, *oct6* is weakly expressed around the PLLg and sporadically along the PLLn, at 48 hpf. This expression appears to increase during development as stronger, uniform expression is seen along the PLLn, at 96 hpf compared with 48 hpf (figure 3.9A, C). In contrast, no expression of *oct6* is observed along the PLL of *adgrg6^{tb233c}* mutant larvae at 48 hpf and only marginal expression is detected at 96 hpf, around the PLLg and sporadic segments of the PLLn (figure 3.9B, D). Three robust puncta of expression (figure 3.9C', D') are detected for the first time near the cristae of the ear that may illustrate Schwann cells myelinating statoacoustic nerves (Liu *et al.*, 2011). Characterisation of *adgrg6* and *sox10* revealed strong expression of their transcripts in the ear that could mask their expression in Schwann cells residing in this region. Although PNS expression of *oct6* displays a detectable phenotypic difference between wild-type and *adgrg6^{tb233c}* mutant embryos, expression in wild types is moderate at best and does not exhibit a significant window that would allow accurate evaluation of intermediate levels, as is possible for *mbp* expression around the PLLg. Furthermore, detection of *oct6* mRNA localised to the PNS required overnight staining, which was also inconsistent.

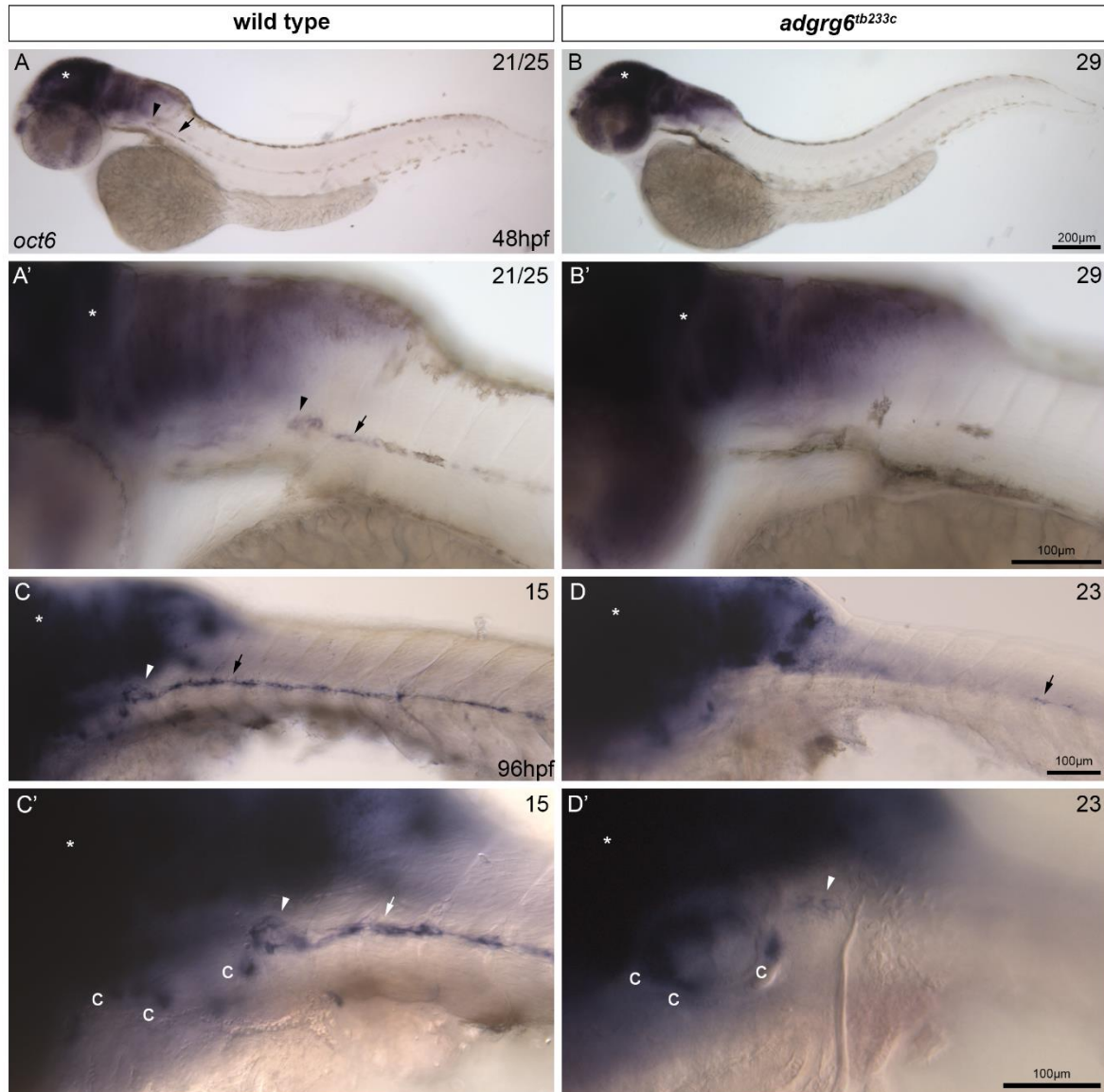


Figure 3.9 *oct6* mRNA expression, at 48 and 96 hpf, in wild-type and *adgrg6^{tb233c}* mutant larvae.

(A-D) Schwann cell expression of *oct6*, at 48 hpf (A-B) and 96 hpf (C-D), is down-regulated along the lateral line in *adgrg6^{tb233c}* mutants (B, 48 hpf; D, 96 hpf) in comparison to wild-type (A, 48 hpf; C, 96 hpf) larvae. Overstained CNS expression (white asterisk) is similar in wild type and *adgrg6^{tb233c}* mutants. (A'-D') close up of expression in Schwann cells along the PLL (arrow, nerve; arrowhead, ganglion) and statoacoustic nerves near the cristae (c). All lateral views, with anterior to the left and posterior to the right.

3.2.4b Expression of *krox20* in wild-type and *adgrg6^{tb233c}* mutant zebrafish larvae

A second marker of myelinating Schwann cells is the expression of *krox20*, regulated by Oct6. Zebrafish larvae were fixed at 72 hpf as *krox20* is known to be expressed at this developmental stage in wild-type zebrafish larvae. Figure 3.10 shows the expression pattern of *krox20* in wild-type and *adgrg6^{tb233c}* mutant larvae, at 72 hpf.

As previously reported, *krox20* is strongly expressed in the hindbrain of wild-type larvae (figure 3.10). Moreover, similar to *oct6*, this expression in the brain is unaffected in *adgrg6^{tb233c}* mutant larvae as in other *adgrg6* zebrafish mutants (Monk *et al.*, 2009). In the wild-type PNS, *krox20* is weakly expressed in Schwann cells along the PLL and the ALL nerves (figure 3.10A, C) whereas moderate expression is detected around the ganglia. Similar levels of expression are also detected along a region of the ALLn residing between the ganglion and the anterior entry zone to the CNS (figure 3.10A white arrow). Interestingly, weak expression is also detected along the presumed oculomotor nerve (figure 3.10C’).

Comparatively in *adgrg6^{tb233c}* mutants, *krox20* expression is completely absent along the ALL and around the PLLg, whilst extremely low and sporadic expression can be detected along the PLLn. Expression along the oculomotor nerve is only detected in 4/21 (19.0%) larvae. The expression of *krox20* appears stronger and more uniform than that of *oct6* along the PLL; however, it also does not present a significant window to allow accurate evaluation of intermediate levels of expression with ease.

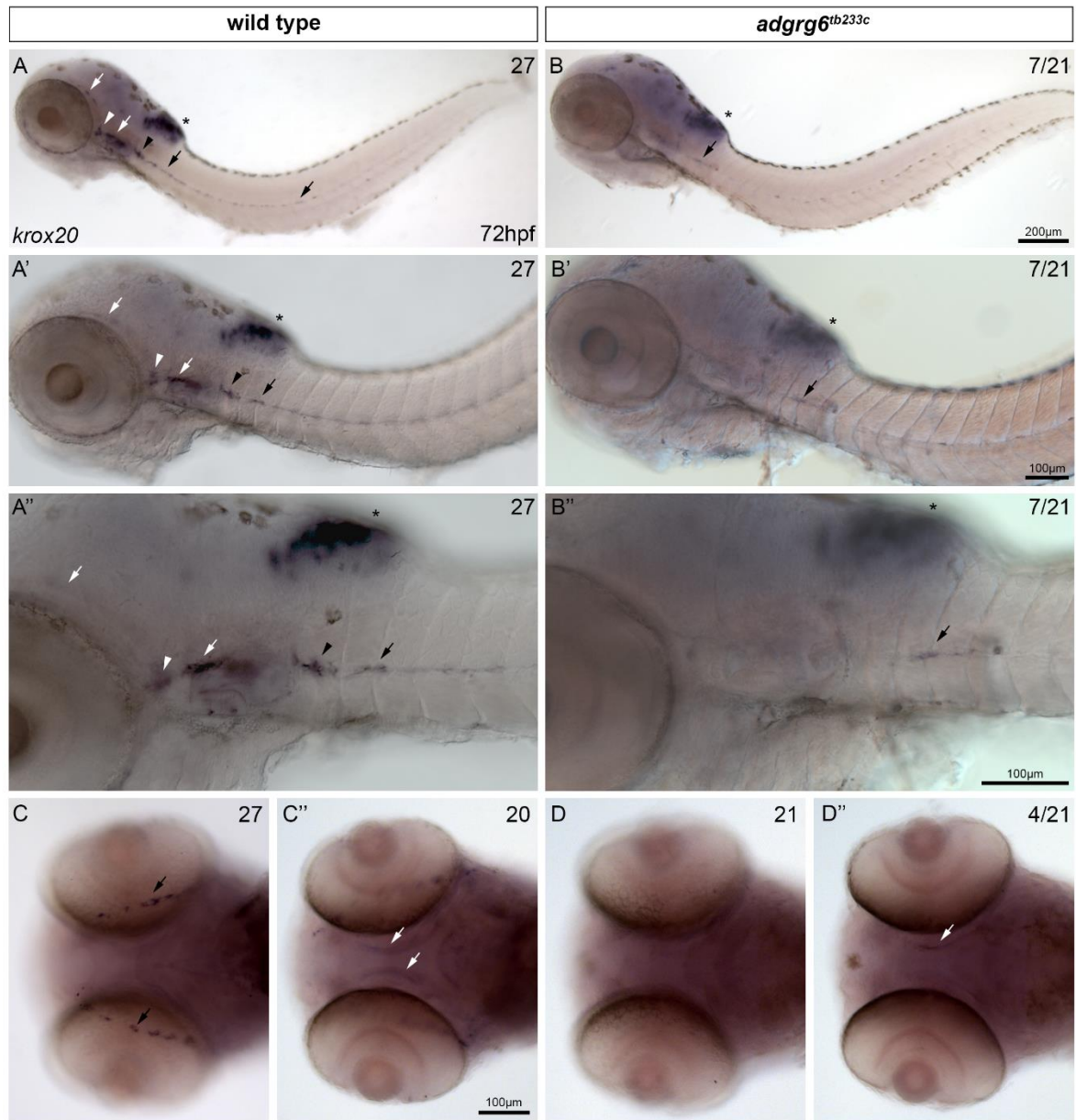


Figure 3.10 *krox20* mRNA expression, at 72 hpf, in wild-type and *adgrg6^{tb233c}* mutant larvae.

(A-D) Schwann cell expression of *krox20*, at 72 hpf (A-D), is down-regulated along the lateral line and cranial nerves in *adgrg6^{tb233c}* mutants (B, lateral; D, dorsal) in comparison to wild-type (A, lateral; C, ventral) larvae. CNS expression (asterisk) is similar in wild type and *adgrg6^{tb233c}* mutants. (A'-B', A''-B'') close up of expression in Schwann cells along the ALL and PLL. (A-B) all lateral views with anterior to the left and posterior to the right (white arrow, SOLn; black arrow, PLLn; white arrowhead, ALLg; black arrowhead, PLLg). (C-D, superficial; C'-D', deep) all ventral views with anterior to the left and posterior to the right (black arrow, IOLn; white arrow, IIIln). Abbreviations: ALLg, anterior lateral line ganglion; IIIln, oculomotor nerve; IOLn, infraorbital nerve; PLLg, posterior lateral line ganglion; PLLn, posterior lateral line nerve; SOLn, supraorbital nerve.

3.2.4c Expression of claudin k in wild-type and *adgrg6*^{tb233c} mutant zebrafish larvae

The myelin-associated Claudin K protein is a known marker of autotypic tight junctions of oligodendrocytes and myelinating Schwann cells (Münzel *et al.*, 2012). In zebrafish larvae, *cldnk* expression starts at 48 hpf in the hindbrain and has been shown to be expressed in Schwann cells along the PLL at 72 hpf (Münzel *et al.*, 2012), but has not previously been characterised in *adgrg6*^{tb233c} mutant larvae. Therefore, to characterise its expression in this project, wild-type and *adgrg6*^{tb233c} mutant larvae were fixed at 72 and 96 hpf. Figure 3.11 shows the expression pattern of *cldnk* at these stages in wild types and *adgrg6* mutants.

In line with published literature, *cldnk* is expressed in hindbrain oligodendrocytes of wild-type larvae, moderately at 72 hpf and strongly at 96 hpf (figure 3.11A, C). As expected, expression of *cldnk* in hindbrain oligodendrocytes of *adgrg6*^{tb233c} mutants is unaffected (figure 3.11B, D). Similar to previous observations by Münzel *et al.* (2012), *cldnk* is expressed in Schwann cells along the ALL and PLL. At 72 hpf, weak expression is detected around the PLLg whereas sporadic expression is detected along the PLLn and supraorbital branch of the ALLn. Similar to the expression in oligodendrocytes, this expression in Schwann cells is stronger at 96 hpf in wild-type larvae, reaching moderate levels around the PLLg and showing uniform expression along the PLLn (figure 3.11C). Strong expression is also observed in individual cells associated with the supraorbital branch (figure 3.11C') of the ALLn whereas expression is uniform along the infraorbital branch (figure 3.11E). Notably, expression is also detected along the presumed oculomotor nerve (figure 3.11E').

In contrast, *adgrg6*^{tb233c} mutants display reduced expression of *cldnk* in Schwann cells. At 72 hpf, no expression of *cldnk* is detected along the ALL and PLL, whereas at 96 hpf weak and sporadic expression is detected along the PLLn (figure 3.11B, D). Individual cells associated with the supraorbital branch of the ALL exhibit moderate expression; however, fewer cells are detected along this nerve in comparison with wild-type larvae. Expression along the infraorbital and oculomotor nerve was also reduced and detected in 16/49 (32.7%) and 29/49 (59.2%) larvae respectively (figure 3.11F''). Although expression of *cldnk* around the PLLg and PLLn was consistent in wild-type and mutant larvae, similar to that of *krox20*, levels were moderate at best and therefore do not offer a significant window that allows evaluation of intermediate levels with accuracy.

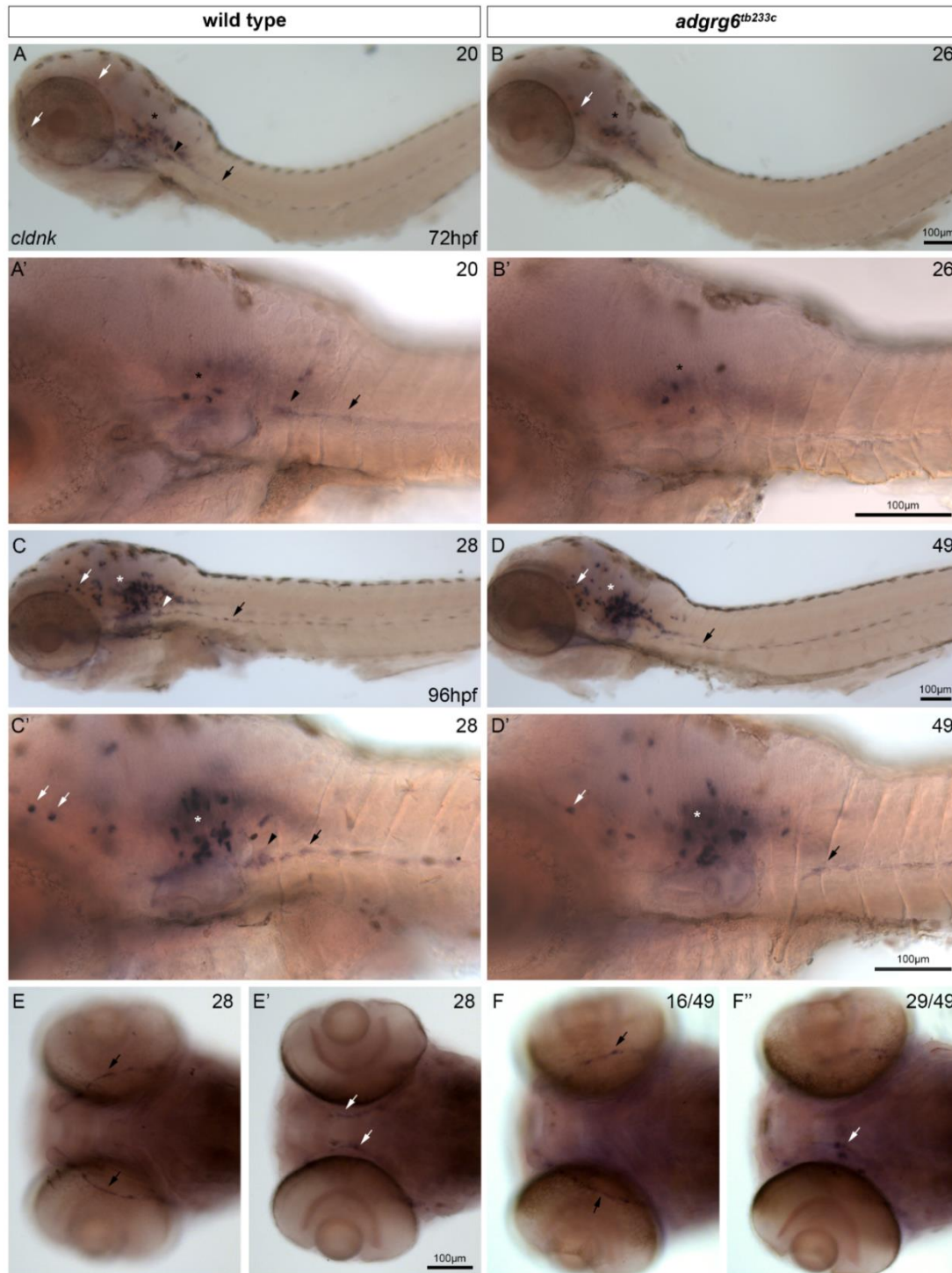


Figure 3.11 *cldnk* mRNA expression, at 72 and 96 hpf, in wild-type and *adgrg6^{tb233c}* mutant larvae.

(A-F) Schwann cell expression of *cldnk*, at 72 (A-B) and 96 hpf (C-F), is down-regulated along the lateral line and cranial nerves in *adgrg6^{tb233c}* mutants (B, D, lateral; F, dorsal) in comparison to wild-type (A, C, lateral; E, ventral) larvae. CNS expression (asterisk) is similar in wild type and *adgrg6^{tb233c}* mutants. (A'-D') close up of expression in Schwann cells along the ALL and PLL. (A-D) all lateral views with anterior to the left and posterior to the right (white arrow, ALLn; black arrow, PLLn; white arrowhead, ALLg; black arrowhead, PLLg). (E-F, superficial; E'-F', deep) all ventral views with anterior to the left and posterior to the right (black arrow, IOLn; white arrow, III n). Abbreviations: ALLg, anterior lateral line ganglion; ALLn, anterior lateral line nerve; III n, oculomotor nerve; IOLn, infraorbital nerve; PLLg, posterior lateral line ganglion; PLLn, posterior lateral line nerve.

3.3 Discussion

In this chapter, larval expression of *adgrg6* was thoroughly characterised in wild-type larvae and for the first time in *adgrg6^{tb233c}* hypomorphic mutants that exhibit developmental defects in the inner ear and PNS. Expression of *adgrg6* and *sox10* was also shown for the first time along peripheral nerve branches localised in the anterior zebrafish larvae, including expression along anterior lateral line nerves and the likely oculomotor nerve illustrated by an acetylated α -tubulin stain. Characterisation of *mbp* mRNA and *mbp*-driven EGFP expression in wild-type and mutant larvae provided evidence for Schwann cell myelination of the oculomotor and trochlear nerves, although expression of *adgrg6* or *sox10* was not detected along the latter. Finally, mRNA expression patterns of myelination markers, including *cldnk* for the first time, largely revealed down-regulated expression around peripheral nerves and ganglia of *adgrg6^{tb233c}* mutants in comparison to wild types.

The *adgrg6* expression pattern was largely consistent with previous observations on alternative *adgrg6* allelic mutants including its expression in otic tissue (Geng *et al.*, 2013) and Schwann cells associated with the posterior lateral line nerve (Monk *et al.*, 2009), indicating that mutations could manifest in phenotypes similar to those observed in alternative *adgrg6* zebrafish mutants. Notably, *adgrg6* expression in otic tissue was significantly stronger than that in Schwann cells associated with the lateral line, which could be taken as an indication of a more significant role in inner ear development. In line with previous literature, staining in otic tissue was concentrated at the projection tips signifying that *adgrg6* expression has an important role in the contact and fusion events that underlie pillar formation, which likely manifests in activity of the Adgrg6 G α s pathway as forskolin and IBMX treatment restore pillar formation in *adgrg6^{tb233c}* mutants (Geng *et al.*, 2013; Diamantopoulou *et al.*, 2019). However, the adhesive NTF of Adgrg6 could also have a role in the process that is yet to be identified.

Although *adgrg6* is weakly expressed along the lateral line and cranial nerves, peripheral myelination appears to be heavily reliant on the activity of its encoded receptor as expression of various myelination gene markers was down-regulated in *adgrg6^{tb233c}* mutants. Furthermore, a complete lack of *mbp* expression has previously been observed in the PNS of *adgrg6^{f24}* allelic mutants that are predicted to express an NTF truncated protein (Geng *et al.*, 2013); similar phenotypes have also been observed in other alleles (Monk *et al.*, 2009; Geng *et al.*, 2013; Paavola *et al.*, 2014; Leon *et al.*, 2020). However, it is important to note that there are additional key regulators of peripheral nerve myelination by Schwann cells including ECM ligands for Adgrg6 (Paavola *et al.*, 2014; Petersen *et al.*, 2015; Küffer *et al.*, 2016; Ghidinelli *et al.*, 2017) and neuregulin signalling (Shin *et al.*, 2014; Ghidinelli *et al.*, 2017). *Nrg1III*-deficient neurons fail to be myelinated by Schwann cells highlighting the necessity

of trans-neuregulin signalling in this process (Ghidinelli *et al.*, 2017) whereas laminin-211 has been shown to regulate myelination *in vitro* (Petersen *et al.*, 2015). Ghidinelli *et al.* (2017) propose that the transition from axonal sorting to PNS myelination is intricately coordinated by the activity of these components but activation of Schwann cell myelination pathways is co-dependent on *Adgrg6* and neuregulin signalling. Expression of each appears independent from that of the other (Monk *et al.*, 2009); however, examining phosphorylation of intracellular effector molecules that are regulated by both pathways, such as Gab1 (Ghidinelli *et al.*, 2017), in *adgrg6* mutant Schwann cells may reveal further insights surrounding the pathway dynamics.

The expression of a selection of Schwann cell markers illustrated localisation of Schwann cells along the oculomotor and trochlear nerve in addition to along the lateral line nerves that has been shown previously (Brösamle and Halpern, 2002; Monk *et al.*, 2009). Although the acetylated α -tubulin stain provided a reference for Schwann cell localisation along cranial nerves, electron microscopy imaging of the zebrafish larva would provide more conclusive evidence of the association of Schwann cells with these nerves. Myelination markers were differentially downregulated in *adgrg6^{tb233c}* mutants, highlighting regions with greater phenotypic sensitivity to mutations in *adgrg6*. For example, expression of all markers, including *mbp*, *oct6*, *krox20* and *cldnk*, around the posterior lateral line ganglia was consistently downregulated whereas weak expression of *mbp* and *cldnk* was detected along the posterior lateral line nerve in *adgrg6^{tb233c}* mutants. It is not clear why certain regions are more sensitive to *adgrg6* mutations than others; however, it could result from different rates at which they develop or a greater reliance on *Adgrg6* activity-induced myelination in comparison to neuregulin-dependent myelination pathways (Shin *et al.*, 2014; Ghidinelli *et al.*, 2017).

Notably, the differential expression of myelination markers offers multiple readouts of *Adgrg6* activity, which can form the foundation of small molecule screening assays on *adgrg6^{tb233c}* mutants. Although expression of myelination markers was largely downregulated, their expression around the posterior lateral line ganglia in particular was clear and consistent throughout. Our group has utilised expression of *mbp* around the PLL ganglia as a readout for a small molecule counter-screening assay aiming to identify modulators of the *Adgrg6* pathway (Diamantopoulou *et al.*, 2019). Expression of *mbp* along the oculomotor nerve could offer similar benefits, although the superficial location of the PLL ganglia provides ease of scoring under a standard benchtop dissection microscope. The oculomotor nerve has a deeper medial location in between larval eyes, which can be difficult to visualise clearly under such microscopes. Moreover, this expression is in a thin line in comparison with that around the ganglia, which exhibits a dense area of staining with higher intensity. Although other myelination markers examined in this chapter also displayed decreased expression in *adgrg6^{tb233c}* larvae, their overall expression in wild types was too weak, requiring inconsistent and longer periods of staining for

sufficient visualisation. Therefore, *mbp* expression around the posterior lateral line ganglia remains the optimal readout. However, its less complex expression pattern at 72 and 78 hpf appears more suitable for use in a screening assay than the expression at 90 hpf used previously (Diamantopoulou *et al.*, 2019). Therefore, earlier developmental stages were preferred for optimisation of a counter-screening *mbp* assay, in the next chapter, that will be utilised to assess the specificity of hits identified from an initial screen against the *vcanb* phenotype in *adgrg6^{tb233c}* zebrafish mutants.

Chapter 4.

Phenotypic screening in zebrafish larvae reveals candidate modulators of the adhesion GPCR Adgrg6

4.1 Introduction

In zebrafish, *Adgrg6* has been identified as a key developmental regulator in the peripheral nervous system and the inner ear along with multiple other tissues. A selection of mutations in the human *ADGRG6* gene are associated with a severe form of Arthrogyryposis Multiplex Congenita and multiple variants have been linked to other conditions, including intellectual disability (Hosseini *et al.*, 2019) and idiopathic scoliosis (Karner *et al.*, 2015; Xu *et al.*, 2019). Therefore, targeting this receptor with small molecules could serve a therapeutic potential. Compounds targeting GPCRs constitute a major class of approved drugs, owing to their pharmacological tractability in terms of accessibility at the cell membrane and presence of binding pockets within their structure (Hauser *et al.*, 2017; Baxendale *et al.*, 2021). However, adhesion GPCRs are yet to be fully exploited; largely due to their multimodal nature, including functions in different tissues and mechanosensing mechanisms of activation, which presents numerous challenges in designing pharmacological assays to screen for compounds that modulate their activity. The current chapter aims to identify candidate small molecule modulators of *Adgrg6* through screening assays performed on multiple *adgrg6* allelic mutant zebrafish larvae.

The zebrafish larva offers a valuable *in vivo* system in which compounds can be screened with added physiological context, taking into consideration the mechanosensing *Adgrg6*-NTF and its interactions with ECM components, including laminin-211 (Petersen *et al.*, 2015), collagen IV (Paavola *et al.*, 2014) and the prion protein (Küffer *et al.*, 2016). The previous chapter along with past publications by our group have highlighted clear and consistent peripheral myelination and inner ear phenotypes in *adgrg6* mutants (Geng *et al.*, 2013; Diamantopoulou *et al.*, 2019), including downregulated expression of *mbp* at the PLLg and persistent expression of otic *vcanb* in the inner ear. Our group has exploited expression of both genes, *vcanb* in a primary screen and *mbp* in a counter-screen, to assay for hits that can rescue the phenotypes associated with *adgrg6*^{tb233c} mutants (Diamantopoulou *et al.*, 2019). This combined approach has the added advantage of identifying false-positive compounds that may downregulate expression of both genes.

Although a shortlist of small molecule Adgrg6 modulators were identified in our past screen of the Tocris Total and Spectrum Collection compound libraries, further screening is necessary to identify novel candidate modulators of Adgrg6 along with gathering more evidence to support previously shortlisted compounds. Our work to date has revealed the tetranortriterpenoids as a significant cluster of structurally similar candidate modulators of Adgrg6 (Diamantopoulou *et al.*, 2019). A comprehensive list of candidate Adgrg6 modulators is likely to reveal key structural motifs and characteristics that are required in a therapeutic modulator, and could be utilised *in silico* to screen for further compounds that may be of interest. This approach could also highlight compounds that are overlooked as a result of toxic effects imposed on zebrafish larvae. Furthermore, a wide-ranging and substantial selection of candidate modulators may reveal groupings of structurally similar compounds likely to interact with the Adgrg6 NTF or CTF.

A key aim of the current chapter is to optimise assay conditions for the counter-screening *mbp* assay. The conditions we have utilised previously – treatment between 60-90 hpf at 25µM (Diamantopoulou *et al.*, 2019) – were tailored for rescuing the inner ear phenotype and therefore may not be optimal for rescuing the myelination phenotype in *adgrg6^{tb233c}* mutants. Expression of *mbp* mRNA in zebrafish larvae has been observed as early as 48 hpf along the posterior lateral line (Brösamle and Halpern, 2002) and Bradley *et al.* (2019) have assayed for Adgrg6 pathway hits by administering compounds at 48 hpf in an Mbp screening assay on *adgrg6^{st63}* zebrafish hypomorphs (see Chapter 1 figure 1.4 and Table 1.1). Compounds administered at this earlier developmental stage may better target the initial onset of *mbp* expression which in-turn could have an improved prognosis. Following optimisation, a primary screen of small molecules will be performed against the *vcanb* phenotype in *adgrg6^{tb233c}* zebrafish mutants, before utilising the optimised *mbp* assay as a counter-screening approach to identify hits likely acting as Adgrg6 pathway modulators. This approach was implemented to maintain consistency with previous screening work by the Whitfield lab (Diamantopoulou *et al.*, 2019) as part of the ongoing screening project on *adgrg6^{tb233c}* zebrafish mutants.

Due to the vast network of components involved in signalling pathways, phenotypic screening approaches can be limited in highlighting a single target protein that is modulated by a therapeutic hit compound. This can be somewhat overcome, by comparing both hypomorphic and strong alleles in secondary screens to differentiate different classes of hit compounds. The Whitfield lab (Diamantopoulou *et al.*, 2019) and Bradley *et al.* (2019) have adopted this approach to shortlist candidate Adgrg6 modulators, identifying compounds that rescue phenotypes in hypomorphic mutants but fail to do so in strong alleles that express N-terminal truncated forms of the receptor. In the current study, compounds will be similarly tested on various *adgrg6* mutants including the

hypomorphic (missense) *tb233c* allele, a stronger missense *tk256a* allele and the *fr24* truncating mutant allele.

Key chapter aims & hypotheses:

1. Optimise a counter-screening *mbp* assay to improve detection of hit compounds
2. Identify compounds that mediate a decrease in *vcanb* mRNA expression in *adgrg6^{tb233c}* zebrafish mutants
3. Identify candidate modulators of the Adgrg6 pathway, which restore wild-type *vcanb* and *mbp* expression levels in *adgrg6^{tb233c}* zebrafish mutants. Hypothesis: a portion of *vcanb* assay hits, including previously identified dihydropyridine compounds, will also restore wild-type levels of *mbp* expression in *adgrg6^{tb233c}* zebrafish mutants
4. Identify candidate Adgrg6 modulators by testing assay hits on the stronger allele, *adgrg6^{fr24}*, where the mutation predicts an early-truncated Adgrg6 protein, which completely lacks the CTF. Hypothesis: hits identified through the hypomorph screen known to target intracellular GPCR pathway components, including adenylyl cyclase, should decrease *vcanb* expression in *adgrg6^{fr24}* zebrafish mutants, but those interacting directly with the receptor should not have any rescuing effect.

4.2 Results

4.2.1 Optimisation of the *mbp* counter-screening assay

In order to test small molecules of interest on a counter-screening *mbp* assay, the experimental conditions were first optimised to improve the efficiency of phenotypic rescue by known hit compounds and therefore increase the likelihood of further hit compound identification in small molecule screening experiments. Various assay conditions were trialled (Table 4.1, 4.2), including a range of treatment windows and small molecule concentrations, with a focus on targeting the onset of peripheral *mbp* expression in zebrafish larvae. To test these variables, our screening positive control compound, IBMX, a phosphodiesterase inhibitor that prevents breakdown of cAMP leading to rescue of the *mbp* phenotype, was utilised along with multiple dihydropyridines that formed a significant cluster of previously identified hit compounds from screening of the Tocris and Spectrum library on *adgrg6^{tb233c}* mutants (Diamantopoulou *et al.*, 2019). Of the dihydropyridines, cilnidipine was selected as it was recognised as a strong hit from this cluster whereas nilvadipine was selected on the basis of being an externally ordered compound which was structurally similar and induced similar rescue of the *mbp* phenotype in *adgrg6^{tb233c}* mutants.

Assay optimisation steps were performed on *adgrg6^{tb233c}* hypomorphic zebrafish mutants, as this is the primary mutant line utilised in the screening assays. As illustrated in the previous chapter, expression of *mbp* mRNA is downregulated throughout the PNS of *adgrg6^{tb233c}* mutants; however, expression in Schwann cells localised to the posterior lateral line ganglion (PLLg) was selected specifically as the readout to evaluate assay conditions. Although *mbp* expression along the oculomotor nerve is also consistently reduced, it is difficult to evaluate with ease due to its deep and linear expression pattern. Zebrafish larvae were mounted dorsally and imaged under brightfield conditions, following *in situ* hybridisation, to simply capture the staining without cellular resolution of larval morphology that could interfere with quantification. A region of interest (ROI) spanning 150 pixels (W) by 100 pixels (H) was drawn to capture the PLLg stain that is evaluated as a percentage of total area in the ROI, similar to the quantification pipeline highlighted by Diamantopoulou *et al.* (2019).

A range of assay conditions were trialled, including some that highlighted toxicity of the trial compounds and others that were more suited to illustrate their therapeutic effects. Toxicity was recorded in terms of observations made on embryo health and included phenotypes ranging from dead embryos to truncated growth and/or oedema (Table 4.1, 4.2). Three trials suited for phenotypic rescue are highlighted in figure 4.1A and B; these include previously utilised conditions (60-90 hpf, 25 μ M), conditions implemented by Bradley *et al.* (2019) (48-72 hpf, 10 μ M) and the optimal trial conditions (54-78 hpf, 15 μ M). In the 10 μ M 48-72 hpf trial, *mbp* expression was increased by drug

treatment; however, expression was not restored to wild type levels. The 25 μ M 60-90 hpf trial displayed a better phenotypic rescue as IBMX and nilvadipine both appear to restore *mbp* expression to wild-type levels with no significant difference observed in terms of staining area between drug-treated mutants and wild-type DMSO-treated controls. However, cilnidipine treatment displayed only partial rescue of the phenotype. Notably, *mbp* expression in wild-type DMSO-treated control larvae displayed high variability in comparison to that observed in the other trials, which could affect validity of results. This was the only trial in which the speed of embryo development was manipulated by adjusting incubation temperature prior to compound treatment and therefore the irregularity in staining could reflect variations in embryo development during this phase.

Although all compounds mediated an increase in *mbp* expression at the PLLg in *adgrg6^{tb233c}* mutants in comparison to the DMSO control, significance for all three was only apparent in the 54-78 hpf trial. Importantly under these conditions, expression levels of *mbp* were similar to those seen in wild-type larvae; no significant difference in the area of staining was observed between drug-treated mutants and wild-type DMSO-treated controls. Overall, the 54-78 hpf assay window with compounds administered at 15 μ M (control IBMX, 50 μ M) displayed the highest efficacy. Further optimisation steps could yet be performed, however, in the interest of time the above conditions were carried forward for secondary screening assay purposes.

Table 4.5 Experimental conditions trialled with IBMX for optimisation of a counter-screening *mbp* assay

Conc.	Day 1		Day 2		Day 3			Day 4		Treatment observations	
	0	24	30	48	54	60	72	78	90		96h
50µM		Dark Red	Dark Red	Dark Red	Dark Red	Dark Red	Dark Red				Dead
100µM		Dark Red	Dark Red	Dark Red	Dark Red	Dark Red	Dark Red				Dead
50µM			Dark Red	Dark Red	Dark Red	Dark Red	Dark Red				Dead
100µM			Dark Red	Dark Red	Dark Red	Dark Red	Dark Red				Dead
50µM				Light Green	Light Green	Light Green	Light Green	Dark Green	Dark Green	Dark Green	2 oedema
100µM				Light Pink	Light Pink	Light Pink	Light Pink	Dark Pink	Dark Pink	Dark Pink	Truncated growth, oedema, 2 dead
50µM				Light Pink	Light Pink	Light Pink	Light Pink				Truncated growth, oedema
100µM				Light Pink	Light Pink	Light Pink	Light Pink				Truncated growth, oedema, 3 dead
50µM				Dark Red	Dark Red	Dark Red	Dark Red	Dark Red			Dead
100µM				Dark Red	Dark Red	Dark Red	Dark Red	Dark Red			Dead
50µM					Dark Green	Dark Green	Dark Green	Dark Green			Healthy
100µM					Light Pink	Light Pink	Light Pink	Light Pink			4 oedema
100µM						Dark Green	Dark Green	Dark Green	Dark Green		Healthy

Table 4.6 Experimental conditions trialled with dihydropyridines for optimisation of a counter-screening *mbp* assay

Conc.	Day 1		Day 2		Day 3			Day 4		Treatment observations	
	0	24	30	48	54	60	72	78	90		96h
10µM		Light Pink	Light Pink	Light Pink	Light Pink	Light Pink	Light Pink				Truncated growth, oedema, some dead
25µM		Dark Red	Dark Red	Dark Red	Dark Red	Dark Red	Dark Red				Dead
10µM			Light Pink	Light Pink	Light Pink	Light Pink	Light Pink				Truncated growth, oedema, some dead
25µM			Dark Red	Dark Red	Dark Red	Dark Red	Dark Red				Dead
10µM				Light Green	Light Green	Light Green	Light Green	Dark Green	Dark Green	Dark Green	Mostly healthy, some with oedema
20µM				Light Pink	Light Pink	Light Pink	Light Pink				Truncated growth, oedema
25µM				Dark Red	Dark Red	Dark Red	Dark Red				Dead
25µM				Dark Red			Dead				
15µM					Dark Green	Dark Green	Dark Green	Dark Green			Healthy
20µM					Light Pink	Light Pink	Light Pink	Light Pink			Oedema
25µM						Light Green	Light Green	Light Green	Light Green		Mostly healthy, oedema arising (Nilvadipine)

- Note: conditions under which rescue of phenotype was observed are highlighted in green, optimal conditions in dark green. Unsuccessful trials in red, high toxicity in dark red.

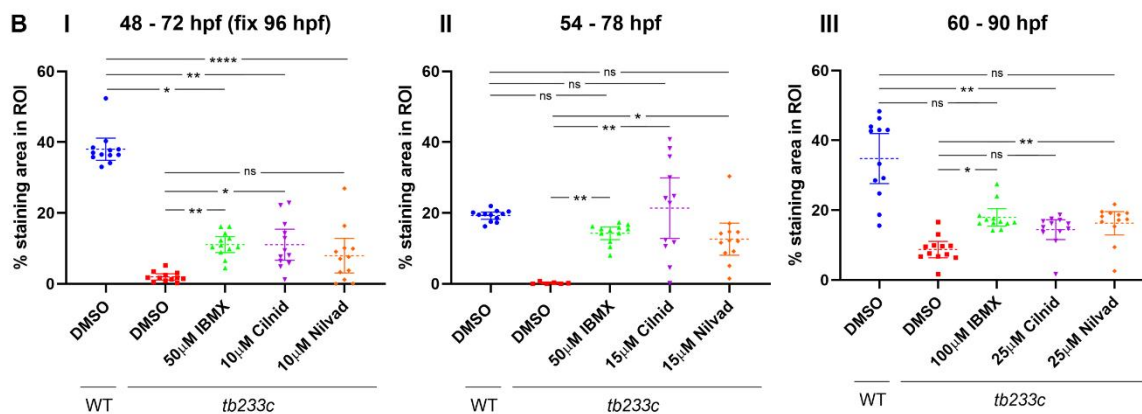
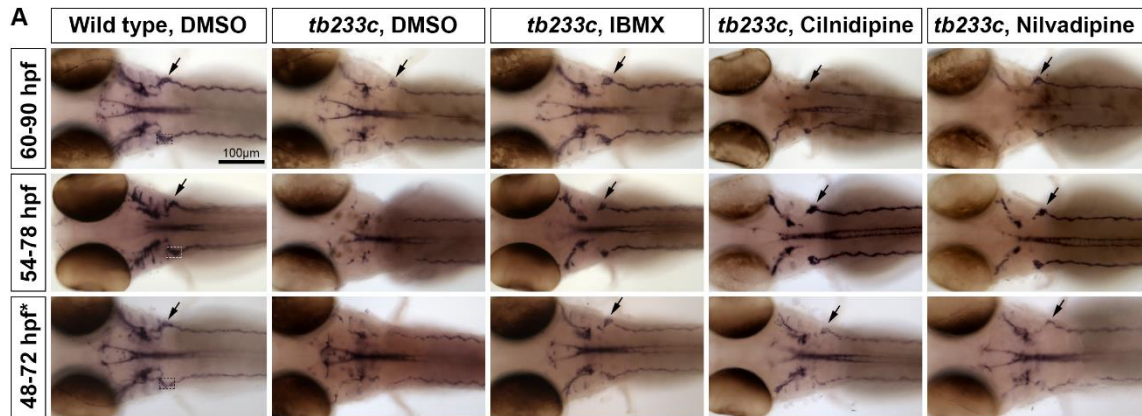


Figure 4.1 Optimisation of a counter-screening *mbp* assay.

(A) dorsal bright-field images of *mbp* transcript expression in larvae following compound incubation under assay conditions that displayed some or complete rescue of the *adgrg6^{tb233c}* mutant phenotype, included in Table 4.1 and 4.2 (green). Dotted rectangle (150 pixels x 100 pixels) enclosing left PLL ganglion of wild-type larvae illustrates region of interest (ROI) quantified in (B). Arrows indicate *mbp* expression in Schwann cells around the PLL; asterisk in 48-72 panel indicates fixation of embryos at 96 hpf following 24-hour incubation in E3 growth media. **(B)** quantified area of *mbp* expression as a percentage of total ROI illustrated in (A). Method of quantification was similar to that utilised by Diamantopoulou et al. (2019). Each point represents staining around a single PLLg of a zebrafish larva. Error bars, confidence interval 95%; ns, $p \geq 0.05$; *, p 0.01-0.05; **, p 0.001-0.01; ***, p 0.0001-0.001; ****, p < 0.0001. Statistical test: one-way Anova.

4.2.2 Pharmacological screening

In this chapter, Sigma's commercially available library of pharmacologically active compounds (LOPAC1280) was screened for small molecules that can downregulate otic *vcanb* expression and, of the hits, those that may upregulate *mbp* expression in *adgrg6^{tb233c}* hypomorphic mutants. This compound library was selected because it covers a vast range of structural space and includes CNS active compounds that may also exhibit better delivery to Schwann cells in the PNS. Importantly, the LOPAC library contains 685 structurally unique compounds of which 275 are structurally diverse from any compounds we have previously tested on *adgrg6^{tb233c}* mutant larvae, and therefore offers potential for the identification of novel hit compounds for the Adgrg6 signalling pathway. Overlap in compounds with the Tocris and/or Spectrum libraries allows for blind retesting of compounds to determine if previous assay results are reproducible. This method of testing may also reveal key information on compound efficacy, as compound formulation can vary across libraries. Moreover, clinically approved compounds are present within the LOPAC library for which pharmacokinetics and safety will have previously been assessed, enabling compounds to be tested for repurposing and reducing potential development costs if they are found to be therapeutic.

4.2.3 Primary screening assay

As part of the primary screen, library compounds were tested on a *vcanb* assay described in Diamantopoulou et al. (2019), with hit compounds identified as those that could significantly downregulate otic *vcanb* mRNA expression. This assay has multiple advantages for the primary screen; expression of *vcanb* is robust and highly localised to the otic vesicle, and the staining intensity is reproducible and offers ease of scoring under a bench top dissection microscope to evaluate efficacy of tested compounds on *adgrg6^{tb233c}* mutants. The *vcanb* assay was performed on *adgrg6^{tb233c}* hypomorphic mutants because these are likely to exhibit higher sensitivity to small-molecule-centered therapeutic approaches, as weaker phenotypes can sometimes be rescued more easily in comparison to a strong phenotype. Furthermore, any compounds that interact directly with Adgrg6 would be overlooked if screening on the *fr24* allelic mutants that are predicted to express an early truncated protein. Homozygous *adgrg6^{tb233c}* zebrafish mutants are adult viable therefore 100% homozygous embryos were obtained from adult pairs for these experiments.

4.2.3a First round of screening

Conditions for the *vcanb* screening assay have been previously optimised to capture rescue of the *adgrg6^{tb233c}* mutant phenotype. Embryos were raised up to 60 hpf before being subject to 30 hours of compound treatment in growth media, administered at 25 μ M similar (figure 4.2A, adapted from Diamantopoulou et al., 2019). The positive control compound, IBMX, was administered at its optimal

concentration of 100 μ M. These conditions were consistent with screening of the Spectrum and Tocris libraries on *adgrg6*^{tb233c} zebrafish mutants. Treatments were performed on three larvae per well in a 96-well plate with controls included in columns 1 and 12 and 80 test compounds in columns 2 through to 11. Following treatment, larvae were fixed at 90 hpf before being subjected to semi-automated *in situ* hybridisation for evaluation of *vcanb* expression as a readout of Adgrg6 pathway activity. The final staining was evaluated in accordance with the *vcanb* 0-3 scoring system highlighted in Diamantopoulou et al. (2019) (figure 4.2B), with 0 indicating a reduction in expression to the levels seen in wild-type larvae (full rescue), and 3 indicating no loss of expression (no rescue).

The hit threshold score was set to <6 (summing the individual scores of three larvae) to account for variabilities in staining during the *in situ* hybridisation protocol. Compounds that mediated a significant reduction in *vcanb* expression in *adgrg6*^{tb233c} mutants scoring <6 were recognised as initial hits and represented approximately 5% of (64/1270) library compounds (fig. 4.3B). The majority of compounds, 91% (1161/1270), had no rescuing effect on *vcanb* expression in *dgrg6*^{tb233c} mutant larvae at the administered concentration. The remaining 4% (45/1270) of compounds were identified as toxic, following observation of dead embryos or embryo absence. However, these outcomes can result from death of an unhealthy embryo that affects remaining healthy embryos, bacterial or fungal growth, or toxic/corrosive effects of compounds. The compound frequency decreases with respect to decreasing *vcanb* score; the hit to non-hit ratio is largely similar to those for the Spectrum and Tocris libraries. Notably, hit percentage was marginally higher in previous screening due to a weaker hit threshold; compounds scoring 6-7.5 were recognised as borderline hits (Diamantopoulou *et al.*, 2019).

The LOPAC library compounds were clustered based on fingerprint similarity using Ward's method of hierarchical agglomerative clustering (work by Antonio de la Vega de León). As the LOPAC library covers all major drug target classes (<https://www.sigmaaldrich.com/life-science/cell-biology/bioactive-small-molecules/lopac1280-navigator.html>) containing a diverse range of scaffolds, ordering compounds based on structural similarity reveals a spread of hits and few structurally similar hits (figure 4.3A). The hits identified from the primary screen included a cluster of structurally similar compounds belonging to the dihydropyridine class, also identified from the Spectrum and Tocris screens (Diamantopoulou *et al.*, 2019). Not all compounds from within this class were identified as hits (figure 4.3A, magenta points), which could reflect limited efficacy at the 25 μ M administered concentration.

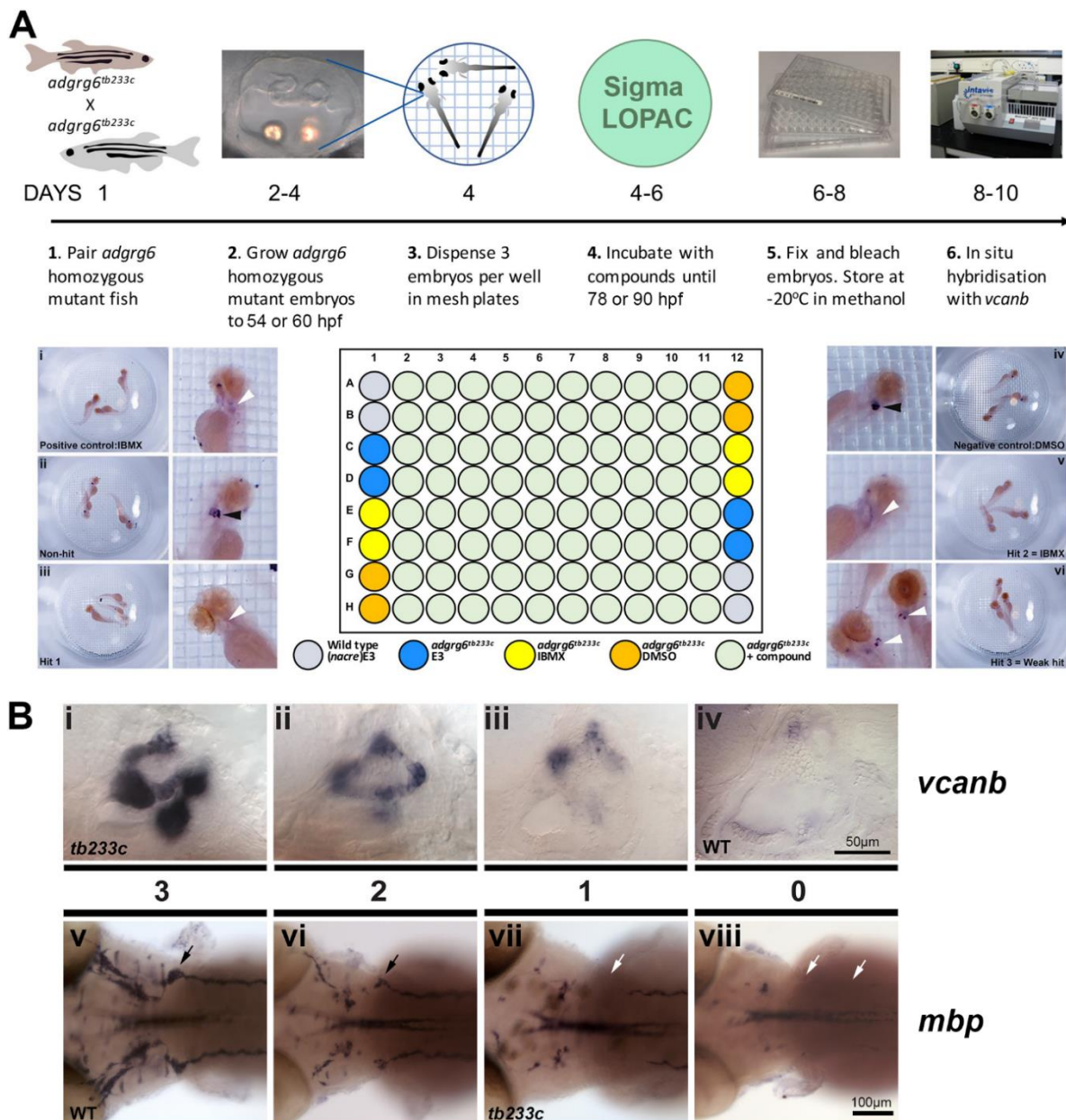


Figure 4.2 Overview of the screening assay protocol and scoring systems utilised to assess *vcanb* and *mbp* expression following compound treatment.

(A) schematic illustration of screening assays (from Diamantopoulou *et al.*, 2019). 100% *adgrg6*^{tb233c} homozygous mutant embryos collected from adult pairs; raised to 54 hpf (*mbp* assay) or 60 hpf (*vcanb* assay); three healthy embryos manually liquoted into mesh bottom plates; mesh plates transferred to 15µM (*mbp* assay) or 25µM (*vcanb* assay) compound plate; assay plates incubated for appropriate duration before fixing embryos in 4% PFA overnight at 4°C. (i-iii) images of *vcanb* stained larvae treated with positive control, hit or non-hit compounds. (Bi-iv) scoring system (from Diamantopoulou *et al.*, 2019) used to assess *vcanb* mRNA expression levels in the inner ear, lateral view, of *adgrg6*^{tb233c} mutant larvae after treatment. 0 (full rescue), reduction in expression to wild-type levels (may include weak expression in dorsolateral septum); 3 (no rescue), no loss of expression. 1 and 2 (intermediate rescue), partially reduced expression. (Bv-viii) scoring system used to assess *mbp* mRNA expression levels at the PLLg (arrow), dorsal view, of *adgrg6*^{tb233c} mutant larvae after treatment. 3 (full rescue), increase in expression to wild-type levels; 1 (no rescue), no change in expression; 2 (intermediate rescue); 0, down-regulated expression of *mbp* (PNS overall, right arrow). Anterior, left; posterior, right.

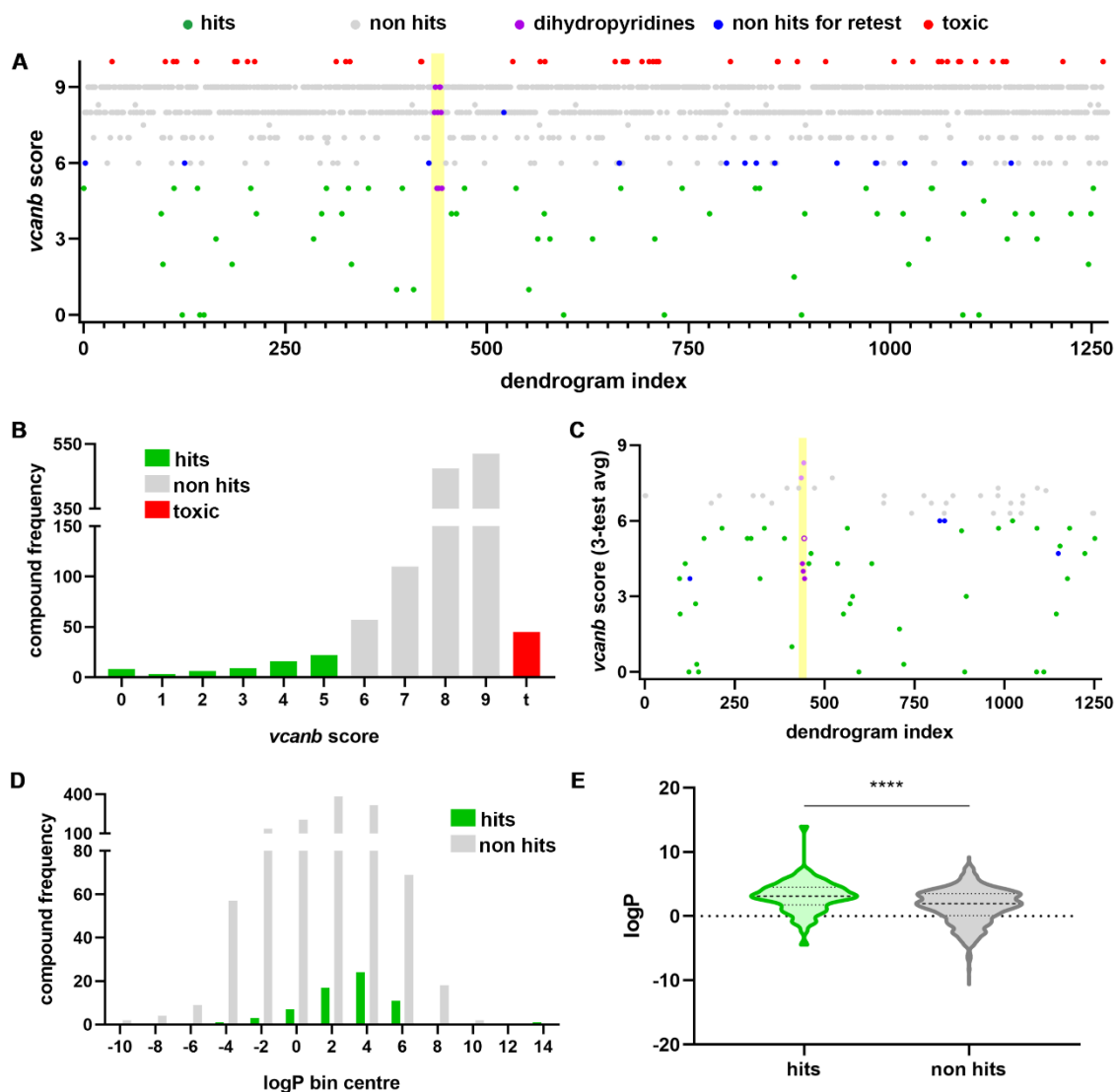


Figure 4.3 A primary drug screen reveals 48 hit compounds that consistently downregulate *vcanb* in *adgrg^{tb233c}* mutant larvae.

(A) scatter plot displaying total *vcanb* staining scores (of 3 larvae) from the primary screen. Library compounds are ordered along the x-axis based on similarities in their chemical structure and presented as individual points. Red points, toxic/corrosive; grey points, no effect on *vcanb* expression (non-hits); green points, reduce *vcanb* expression (hits); blue points, selected for retest based on structural similarity with hits; magenta points, dihydropyridines (comprised of hits and non-hits). Dihydropyridine dendrogram index range highlighted in amber. (B) frequency of *vcanb* staining scores in primary screening assay. Green, hit score; grey, non-hit score; red, toxic/corrosive compounds. (C) retesting 82 compounds revealed 48 (green, magenta and blue) that consistently downregulate *vcanb* after two retests. Scatter plot as in A; grey points, non-hits; faded magenta points, dihydropyridine non-hits (2 compounds); empty magenta point, felodipine. Dihydropyridine dendrogram index range highlighted in amber. (D) frequency distribution of log(P) values for primary screen hit (green) and non-hit (grey) compounds. Bin width: 2 (+/-1 of centre value). (E) log(P) population of hit (green) and non-hit (grey) primary screen compounds. **** $p < 0.0001$, student's T-test.

4.2.3b Retesting compounds of interest

Library compounds were also clustered based on structural similarity alongside the Spectrum and Tocris library compounds to reveal networks of structurally similar compounds (work of by Antonio de la Vega de León, figure 4.4). Following results of the primary screening assay, this form of data visualisation can reveal whether compounds with similar structure are likely to act as hits or non-hits. Network clustering revealed a collection of compounds from the LOPAC library that, although identified as non-hits, could be of further interest due to structural similarity with identified hits. Furthermore, a small group of such compounds gave a *vcanb* score on the margins of the hit threshold score and on this basis were selected for a retest. Overall, 18 compounds of interest were selected, including 3 dihydropyridines and 15 other compounds that formed at least one structure-based connection with an identified hit from across all three libraries and returned a *vcanb* score between 6-8 in the primary screen. In total, 82 compounds were retested twice on the *vcanb* assay to identify compounds that were consistently mediating down-regulation of *vcanb* in *adgrg6^{tb233c}* mutants. At this stage of the screening pipeline, the hit threshold score was adjusted to include compounds consistently scoring ≤ 6 as a three-test average. Of the original hits, 67% (43/64) were consistently identified as hit compounds, which is similar to the hit identification rate for the Tocris library following retests. In comparison, only 28% (5/18) of the additional compounds selected for retests were identified as hits, scoring between 3.7-6. There is a strong positive correlation between the two retest scores along with an r^2 value of 0.7 instilling confidence in the reproducibility of our assay output (figure 4.6 (supplement) B). Overall, the data indicates that low scoring compounds from the primary screen are more likely to be consistently identified as hit compounds.

Interestingly, 9 dihydropyridines were present in the LOPAC library, of which 3 were identified as hits after the primary screen, including the previously identified hits cilnidipine and nimodipine (Diamantopoulou *et al.*, 2019). However, retesting felodipine, an initial non-hit, revealed that it too was able to down-regulate *vcanb* expression in *adgrg6^{tb233c}* mutant larvae, although it appears less efficacious than the original hits. Taken together these results indicate, as with any assay, that experimental conditions are not optimal to recognise all hit compounds. However, in this instance computational approaches like network clustering can reveal compounds that may be of further interest and should not be overlooked. An additional dihydropyridine, lercanidipine hydrochloride hemihydrate, was also retested but remained a non-hit; however, at double the assay concentration it was also able to mediate downregulation of *vcanb* in *adgrg6^{tb233c}* mutant larvae (data included as co-author contribution in Diamantopoulou *et al.*, 2019).

Aqueous solubility and lipophilicity of compounds is integral for their absorption into cells by membrane penetration. Log(P) of a compound provides an experimental readout of these properties

for a compound dissolved in an immiscible biphasic system of water and octanol, a lipid-simulating organic compound (Wang and Hou, 2011). Log(P) analysis (figure 4.3D, E) of LOPAC library compounds reveals that the majority of compounds favour a lipophilic state; however, hit compounds are more lipophilic than non-hit compounds (figure 4.3D-E). It is not surprising that the majority of LOPAC library compounds exhibit a log(P) between 0 and 5 as this is the accepted standard for drug-like compounds and is a key requirement of the Lipinski rules (Wang and Hou, 2011), which evaluate the overall drug-likeness of compounds.

At this stage, it is important to consider that compounds recognised as hits may also include false positives that downregulate gene expression non-specifically throughout zebrafish larvae, and therefore all hits should be treated with caution. The counter-screening *mbp* assay holds an advantage as in this assay hits are recognised as those that can up-regulate gene expression; any generic transcription down-regulators can be eliminated from further study.

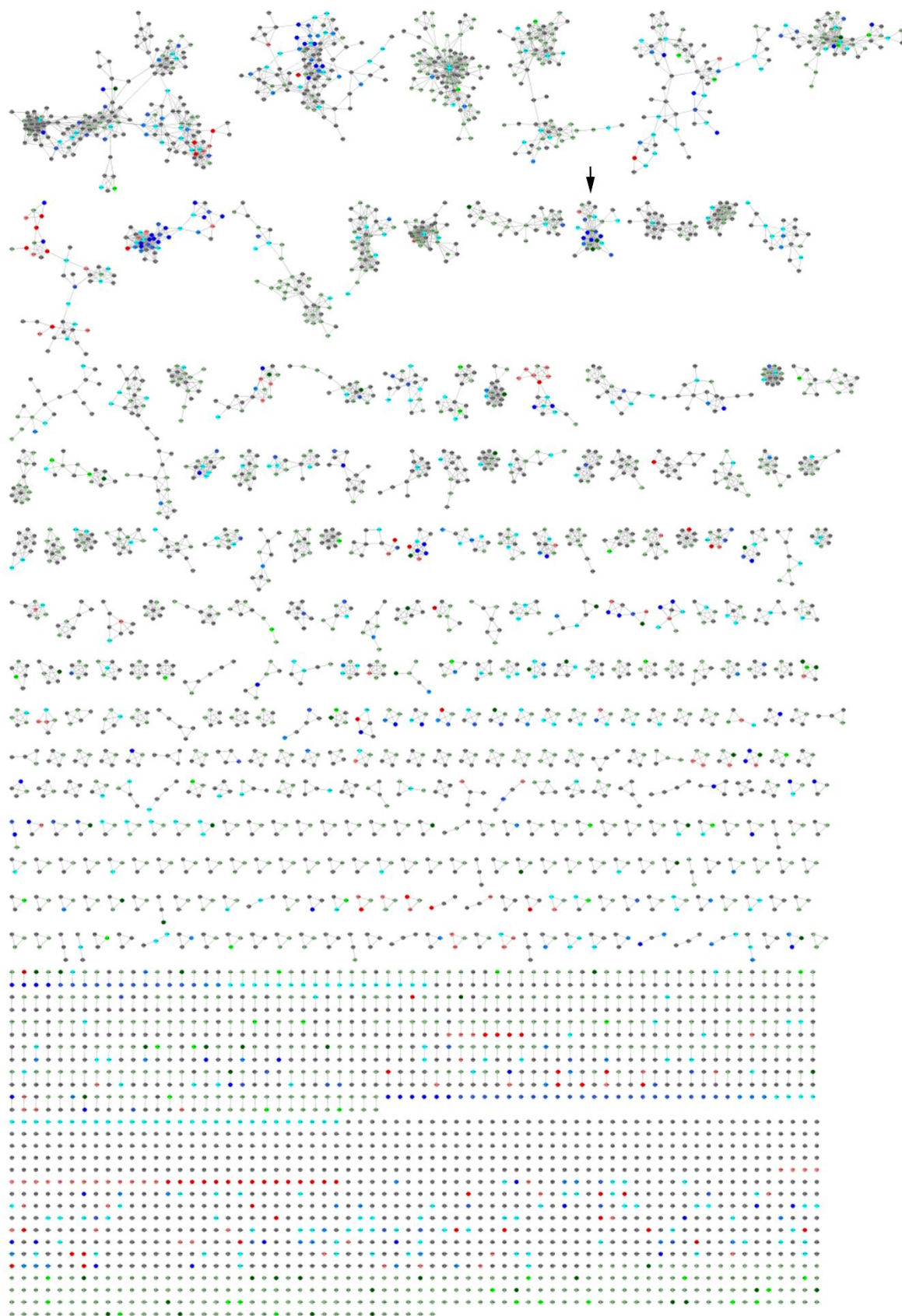


Figure 4.4 Network analysis of LOPAC, Spectrum and Tocris library compounds.

Structural analysis of library compounds reveals networks of structurally similar compounds present across three compound libraries screened on *adgrg6* zebrafish mutants by the Whitfield lab. This work

was performed by Antonio de la Vega de León (Chemoinformatics, University of Sheffield) based on structural similarity (using Tanimoto coefficient). In total 4400 compounds are shown from three libraries; LOPAC, Spectrum and Tocirs. Individual points represent single compounds; those that are structurally similar (above the similarity threshold) form links based on their similarity whereas structurally unique compounds form no connections. LOPAC library primary screen *vcanb* scores: pale green, non-hit; dark green, hit; bright green, scored 6 in *vcanb* assay. Spectrum and Tocris scoring categories illustrated in Diamantopoulou et al. (2019). Arrow indicates network of dihydropyridines compounds.

4.2.3c Compounds overlapping across screened libraries

Comparison of *vcanb* scores for compounds that overlap across the LOPAC, Spectrum and Tocris libraries (figure 4.5) reveals high reproducibility of the assay output. Approximately 80% (77/96) of compounds that overlap across all libraries exhibit a *vcanb* score within a range of 0-2. Moreover, comparison of compounds that overlap between the LOPAC and Spectrum or LOPAC and Tocris libraries reveals that over 90% (293/326, 283/316 respectively) of compounds fall within a *vcanb* score range of 0-2. Very few compounds fall outside this range and any inconsistencies could result from slight differences in compound formulation, compound inactivation or variations in staining during *in situ* hybridisation.

Although variation in *vcanb* scores for overlapping compounds is low, a difference of even 1 point can result in identification of a compound as a hit or non-hit. The classification of compounds, following retests, was examined to further explore compound efficacy and reproducibility of the screening assay. Over 85% of compounds overlapping across all libraries were classified the same whereas over 92% of compounds overlapping between the LOPAC and Spectrum (309/326) or LOPAC and Tocris (293/316) libraries fell in the same category (figure 4.5B). Although a small number of compounds fell into the unmatched category, i.e. hit in one library and not the other, a subgroup of these were not followed up after retests as they displayed weaker efficacy to other compounds and stronger hits were of greater interest. Taking this into consideration, under 8% of compounds overlapping across all libraries and under 5% of compounds overlapping between LOPAC and Spectrum or LOPAC and Tocris displayed inconsistency in their classification as a hit of interest, i.e. one that was followed up in further testing.

A closer look at compounds overlapping across all libraries with inconsistent classification (figure 4.5C) reveals that 4 were identified as hits of interest from the LOPAC screen whereas 1 and 2 fell into the same category from the Spectrum and Tocris libraries respectively. Interestingly, dihydropyridines accounted for 2 out of these 7 compounds, including nifedipine and nitrendipine. The former was identified as a hit from the Tocris screen whereas the latter was identified from the Spectrum screen. Both compounds were identified as either a non-hit or unfollowed hit in two of the remaining libraries, which suggests that either their efficacy is limited at the administered concentration or their formulation varies across libraries. The 4 LOPAC compounds scored between 3-5.67, highlighting that they were not the strongest hit compounds in the *vcanb* assay. The additional Tocris compound, methiothepin mesylate, displayed a *vcanb* assay score of 1 that is indicative of a strong hit; however, this compound also appeared toxic in the later *mbp* counter-screening assay and therefore does not appear to be a significant compound of interest (unpublished thesis work by Elvira Diamantopoulou).

Comparison of overlapping compounds identified as toxic (figure 4.5D) in at least one library reveals that 2 compounds are universally toxic. Head-to-head comparison of LOPAC library compounds with the Spectrum or Tocris reveals 5 and 7 respective compounds that are consistently toxic. A further 10 and 11 respective compounds are toxic in one and a non-hit in the other. Interestingly, 2 compounds identified as toxic in the Tocris screen were identified as hits in the LOPAC screen. These findings can be taken as indications that compound potency could vary in different libraries as a result of differences in formulation, and therefore toxic effects of certain molecules may be more apparent in libraries containing a form with higher potency. However, compounds could also be misclassified as toxic if unhealthy embryos are present within the screening sample, which in turn may release toxins that affect the health of remaining embryos.

4.2.3d Structurally novel compounds in the LOPAC library

The LOPAC library also contained numerous compounds with a novel structure, not present in the previously screened Spectrum or Tocris libraries. This gave the advantage of screening compounds with the aim of identifying novel hits that could downregulate *vcanb* mRNA expression. Approximately 3.5% (24/685) of structurally novel compounds mediated a significant decrease in *vcanb* expression (figure 4.5E). Although these compounds varied in structure from those screened before, they included isomers of previously screened compounds, for example cilnidipine, which has previously been recognised as a strong hit compound from the Tocris screen (Diamantopoulou *et al.*, 2019). Network clustering of all screened libraries highlighted the true novel compounds as those that formed no connections with compound clusters containing molecules from the Spectrum or Tocris libraries (figure 4.4), i.e. structurally diverse from those screened previously. These included LOPAC compounds that formed either no structural similarity connections or those which formed connections with other internal library compounds alone. In total, 275 such compounds were identified of which 3.6% (10/275) (table 4.3) mediated a significant downregulation of *vcanb* expression in *adgrg6^{tb233c}* mutant larvae. Compounds within this subgroup that can also upregulate *mbp* expression in the counter-screening assay will be of interest as novel hits for the Adgrg6 signalling pathway.

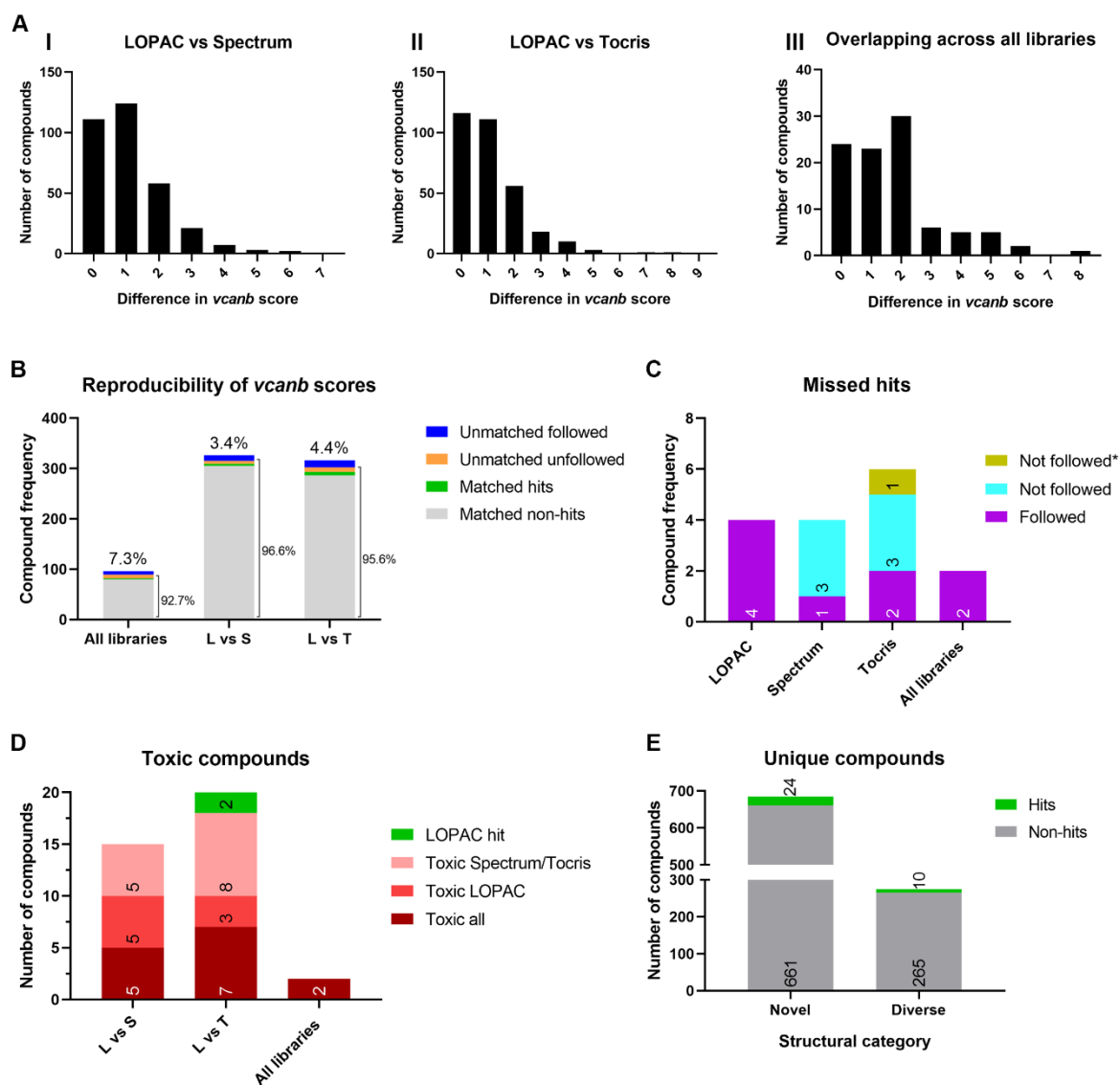


Figure 4.5 Primary screen performance of compounds that were common between multiple libraries.

(A) *vcanb* scores of compounds common to LOPAC and Spectrum libraries (I); LOPAC and Tocris libraries (II); all libraries. **(B)** categorisation of compounds that were common to multiple libraries. Unmatched compounds include those that were not recognised as hits in all libraries compared. This included two classes of compounds; those that were classes as hits in at least on library and were followed up in further work and those that were classed as hits but were not followed up in further work. This is likely due to weaker efficacy, partial toxicity, or miss-selection. **(C)** unmatched compounds that overlap across all libraries (blue and amber in B). 4 common compounds were identified as hits in the LOPAC screen alone, similarly 4 in the Spectrum screen and 6 in the Tocris screen (one not followed up as a result of miss-selection during hits cherry pick). 2 were identified as hits in all library screens. **(D)** classification of toxic compounds that overlapped across multiple libraries. **(E)** number of structurally novel compounds in the LOPAC library i were structurally diverse from any compounds tested previously by the Whitfield lab. All data was elucidated from comparison of compounds SMILES (simplified molecular-input line-entry system).

Table 4.7 List of structurally novel hit compounds from the *vcanb* assay

Drug	CATNUM	<i>vcanb</i> score (3 test avg of 3 larvae)
7-Chloro-4-hydroxy-2-phenyl-1,8-naphthyridine	C 5982	0.00
CHM-1 hydrate	C1244	0.00
Auranofin	A 6733	0.33
Thapsigargin	T 9033	2.67
5HPP-33	H 9415	3.00
Ebastine	E9531	3.67
Nemadipine-A	N4163	3.67
PD-166866	PZ0114	4.71
S-Methylisothiourea hemisulfate	M 3127	5.33
Avridine	PZ0123	5.67

- see figure 4.5E

4.2.4 Counter-screen

4.2.4a Testing primary screen hits on the optimised *mbp* assay

In the counter screen, 48 hit compounds from the *vcanb* screening assay were tested on their ability to increase *mbp* expression around the PLLg in *adgrg6^{tb233c}* mutant larvae, under optimised assay conditions. Expression of *mbp* at the PLLg of *adgrg6^{tb233c}* mutant larvae was scored 0 – 3 in each of three larvae per well (figure 4.2B): 1 for no change in expression, 3 for complete restoration (wild-type levels), 2 for intermediate restoration and 0 for down-regulated expression of *mbp* (PNS overall). 35% (17/48) of compounds were identified as assay hits (2-test average ≥ 4.5), all of which also down-regulated *vcanb* expression (figure 4.6). The *mbp* assay hits form a collection of compounds most likely to modulate the Adgrg6 pathway as they mediate a noticeable rescuing effect on both transcriptional readouts of the pathway. Critically, application of the *mbp* assay allowed identification of 6 compounds (15%) acting as non-specific transcription downregulators rather than pathway hits (examples, figure 4.8C). These compounds were eliminated from further work. The remaining 52% (25/48) of compounds comprised those that mediated no effect on *mbp* expression at the administered concentration (examples, figure 4.8B). These are regarded as *vcanb*-specific hits as they may target signalling pathways specifically in the inner ear. However, this list may also contain compounds that have the potential to rescue the *mbp* phenotype but fail to do so as a higher treatment concentration is necessary to mediate a therapeutic effect.

The cluster of dihydropyridine hits from the *vcanb* assay were identified as *mbp* assay hits. It is important to note that although this cluster appears to contain 4 compounds, nemadipine-A (DI, 444) falls below the network clustering threshold and therefore should be regarded as a structurally diverse dihydropyridine when compared to the other three compounds, including nimodipine, felodipine and cilnidipine. The remaining *mbp* hits cover a vast structural space (figure 4.6A). Similarly, the *vcanb*-specific hits also cover a vast structural space and only 2 compounds, IC 261 (DI, 1090) and SU 5416 (DI, 1091), form a direct connection within a network cluster of structurally similar compounds (figure 4.4).

There does not appear to be a strong correlation between compound performance between the *vcanb* and *mbp* assays (figure 4.6 (supplement) D), and therefore compounds that mediate strong down-regulation of *vcanb* do not necessarily strongly up-regulate *mbp* expression. This is highlighted especially from the recognition of transcriptional downregulators that completely abolish *vcanb* expression but also mediate a reduction in *mbp* expression in *adgrg6^{tb233c}* mutant larvae; nocodazole is the strongest of such compounds. Compounds falling into this category could be considered toxic

to the zebrafish larvae because of their systemic effects on gene expression that are likely to affect the health of larvae.

Forskolin and mevastatin were recognised as the strongest hit compounds that were able to mediate restoration of both genes to wild-type expression levels in *adgrg6^{tb233c}* mutant larvae (figure 4.6F, 4.7C); in the case of forskolin, *mbp* expression appears upregulated to higher levels than that seen in wild-type larvae (figure 4.7C). Both compounds have been recognised as hits in previous *vcanb* assay screens, but are also known to be toxic to larvae at 25 μ M (unpublished work by Elvira Diamantopoulou). Therefore, application of these compounds at lower concentrations may help to reduce toxicity. These compounds are categorised as known hits that fall outside of the dihydropyridine group and include other compounds such as ivermectin. Overall, of the 17 *mbp* assay hits, 11 compounds were novel hits (table 4.4), including two dihydropyridines, felodipine and nemadipine-A (co-author contributions in Diamantopoulou et al., 2019), whereas 6 compounds were previously known hits, including nimodipine and cilnidipine. Within the subgroup of novel hits, 4 were structurally diverse from any compounds previously screened, including ebastine, nemadipine-A, S-methylisothiourrea hemisulfate (SMT) and thapsigargin; these hits accounted for 1.45% (4/275) of the structurally novel compounds present in the LOPAC library.

Comparison of *mbp* assay compounds overlapping across libraries reveals that danazol, identified as an *mbp* assay hit from the Spectrum library, registers as a *vcanb*-specific hit under the optimised assay conditions. However, three additional compounds were identified as assay hits that registered as either *vcanb* specific or displayed toxic side effects in the previous study; mevastatin, cyproterone acetate and FPL 64176. Collectively these findings indicate that therapeutic effects of tested compounds are more likely to be showcased under optimised *mbp* assay conditions.

As mentioned previously, hits were identified based on *mbp* expression at the PLLg; however, various compounds also mediated an increase in *mbp* expression along other nerves and ganglia (figure 4.7). In particular, all dihydropyridines along with mevastatin, forskolin, pimozide and SMT mediated an increase in expression along anterior lateral line (ALL) regions, in particular around the ALLg. These compounds, barring mevastatin, also elevated *mbp* expression along nerve branches that reside close to the cristae and appear to be associated with the statoacoustic ganglion. Although hits may exhibit similar *mbp* assay scores, their efficacy can be differentiated further by examining changes in *mbp* expression elsewhere within the PNS.

Compounds that were identified as *mbp* assay hits are known to target various proteins, including those conserved in GPCR signalling pathways such as adenylyl cyclase and phosphodiesterases. GPCR pathway components formed the joint largest target group alongside Ca²⁺ channel modulators,

collectively accounting for almost two thirds of hit compounds (figure 4.6E). These targets are not surprising as *Adgrg6* is itself a GPCR, whilst Ca^{2+} channel modulators have been identified as hits in previous work (Diamantopoulou *et al.*, 2019). The remaining compounds are known to target a selection of receptors or enzymes, which may indicate their potential interaction with the *Adgrg6* signalling pathway. However, these hits could also bind directly to the *Adgrg6* receptor and modulate its activity directly to rescue the phenotypes associated with *adgrg6*^{tb233c} mutant larvae.

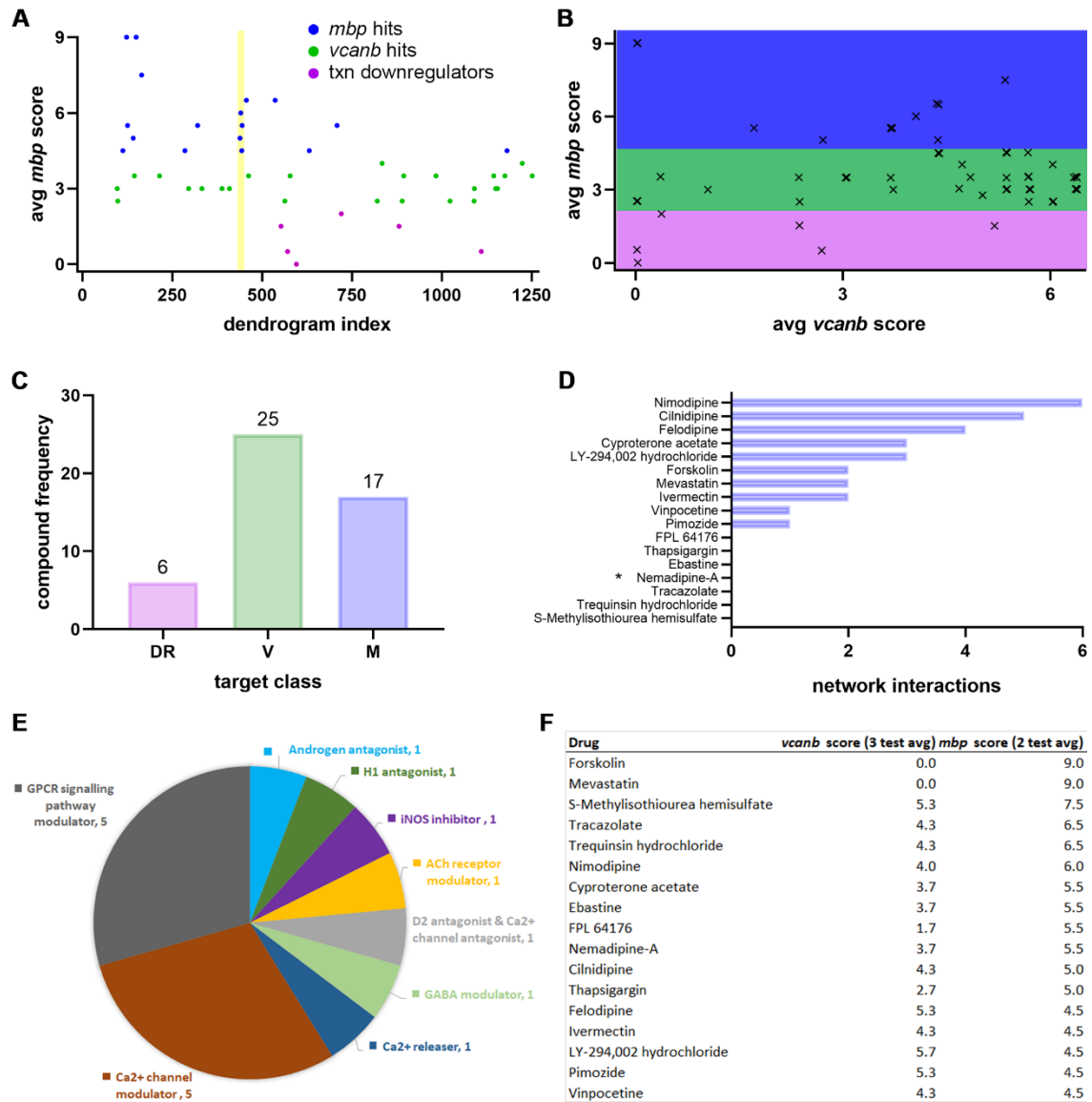


Figure 4.6 Screening 48 selected hits on an optimised *mbp* counter-screening assay reveals 24 *vcanb* specific hits and 17 hits that can also restore *mbp* expression in *adgrg6^{tb233c}* mutant larvae.

(A) scatter plot displaying (2-test) average total *mbp* staining scores (of 3 larvae) of 48 primary screen hits tested in a counter-screening *mbp* assay. Library compounds are ordered along the x-axis based on similarities in their chemical structure and presented as individual points as in figure 4.3. green points, no effect on *mbp* expression (*vcanb*, V, specific hits); blue points, increase *mbp* expression (*Adgrg6* pathway hits, M); magenta points, down-regulate (DR) *mbp* expression in the PNS. Dihydropyridine dendrogram index range highlighted in amber. (B) scatter plot of *vcanb* and *mbp* assay scores for 48 primary screen hits. Jitter (noise) introduced to improve visualisation. Colour categorisation consistent with that in A. (C) compound frequency of down-regulators (DR), *vcanb* specific hits (V) and *Adgrg6* pathway hits (M). (D) number of structural similarity connections with other compounds in figure 4.4. (E) known target classes of 17 *mbp* counter screen hit compounds. (F) table of *vcanb* (3-test avg, 9 embryos screened) and *mbp* (2-test avg, 6 embryos screened) assay scores for 17 *mbp* counter-screen hit compounds.

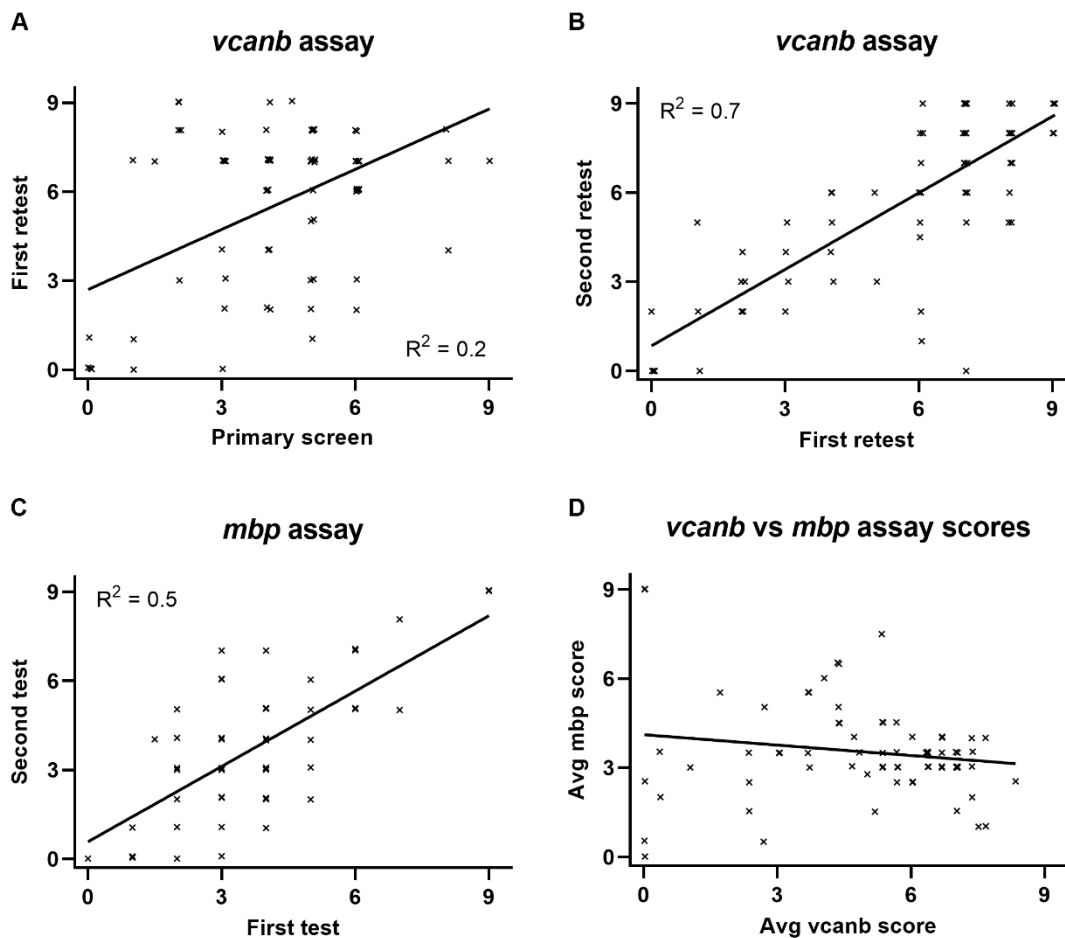


Figure 4.6 (supplement) Comparison of hit compound assay scores (48).

(A-B) *vcanb* scores display positive correlation between primary screen and first retest (A) and both rounds of retest (B). Strong positive correlation, in *vcanb* scores, is observed between the first and second retest (B). **(C)** *mbp* scores display strong positive correlation between first and second rounds of testing. **(D)** comparison of *vcanb* and *mbp* scores reveals no correlation in terms of assay performance.

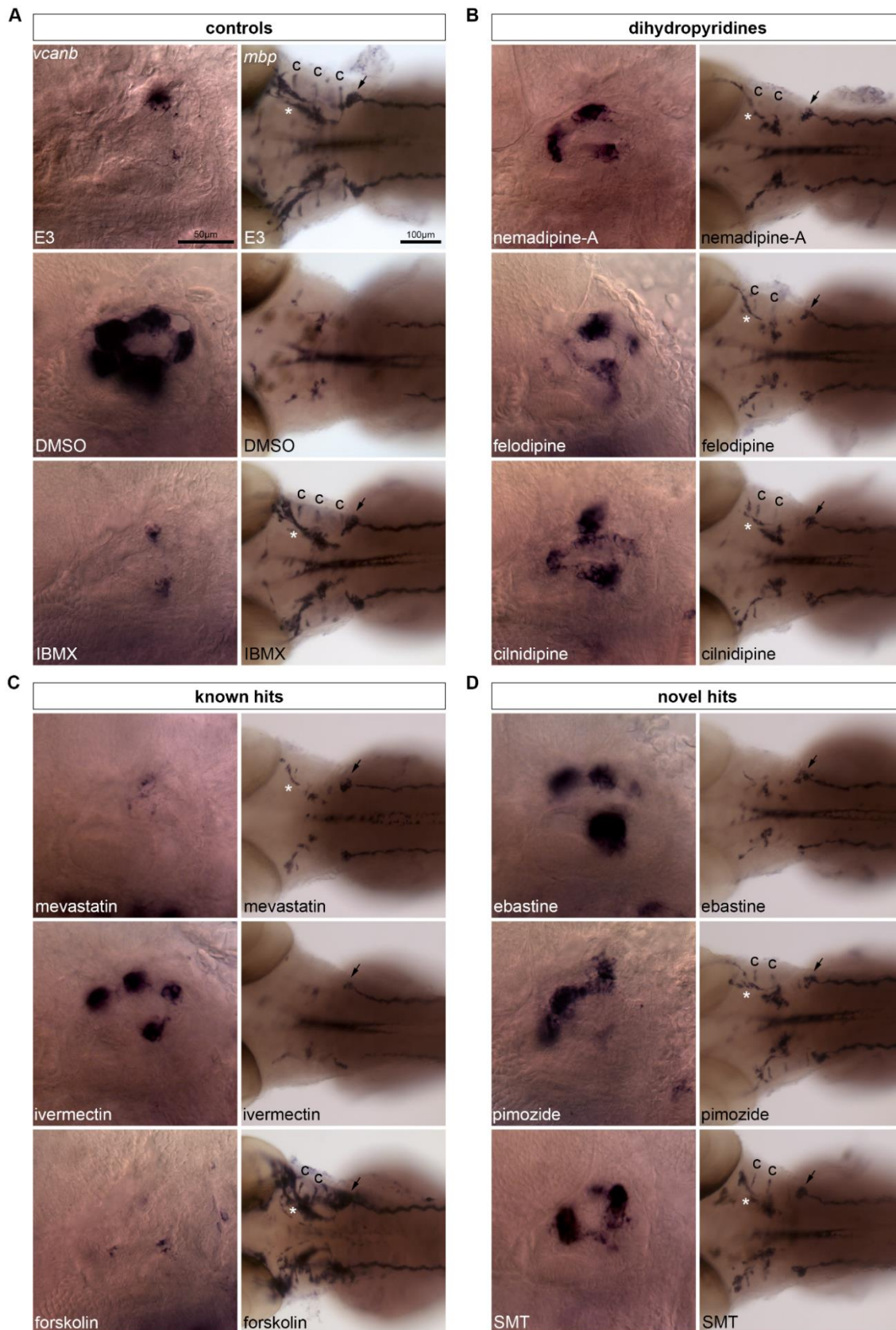


Figure 4.7 Hits that are likely Adgrg6 pathway specific.

Lateral images of the inner ear at 90 hpf stained for *vcnb* and dorsal images of the nervous system at 78 hpf stained with *mbp*. Anterior, left; posterior, right in all images. **(A)** images of control group larvae, including wild types incubated in E3 growth media and *adgrg6^{tb233c}* mutants incubated in DMSO or

IBMX (positive control compound). IBMX is shown to restore wild-type levels of *vcanb* (inner ear) and *mbp* (PLLg) expression in *adgrg6* mutant larvae. **(B-D)** images of *adgrg6* mutants treated with dihydropyridine hit compounds (B), previously known hit compounds from the Spectrum and Tocris screen (C) or novel hit compounds from the LOPAC screen (D). Hits mediate partial or full restoration of *vcanb* expression, in the inner ear, and *mbp* expression, at the PLLg. Overexpression of *mbp* is observed in the PNS of forskolin treated larvae. Compounds were tested at 25 and 15 μ M in *vcanb* and *mbp* assays, respectively. IBMX control was tested at 100 and 50 μ M in *vcanb* and *mbp* assays, respectively. Arrow, *mbp* expression restored at the PLLg; asterisk, expression restored along ALL; c, expression restored along nerves near cristae.

Table 4.4 Novel *mbp* assay hits

Drug	<i>vcanb</i> score (3 test avg)	<i>mbp</i> score (2 test avg)
S-Methylisothiourea hemisulfate	5.33	7.5
Trequinsin hydrochloride	4.33	6.5
FPL 64176	1.67	5.5
Cyproterone acetate	3.67	5.5
Ebastine	3.67	5.5
Nemadipine-A	3.67	5.5
Thapsigargin	2.67	5
Vinpocetine	4.33	4.5
Felodipine	5.33	4.5
Pimozide	5.33	4.5
LY-294,002 hydrochloride	5.67	4.5

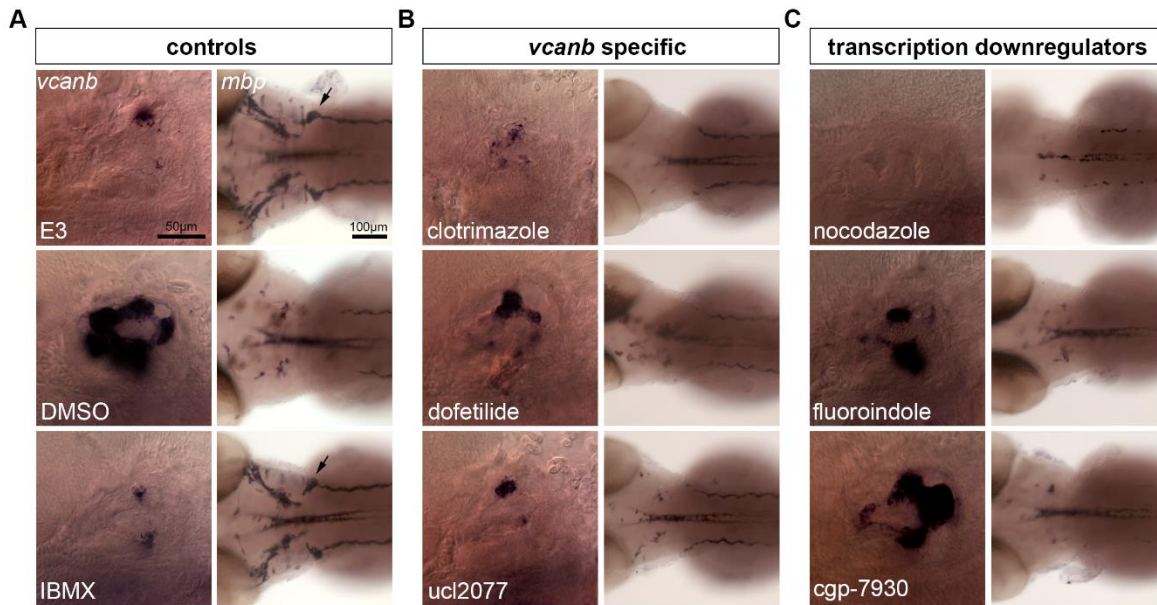


Figure 4.8 Compounds identified as *vcanb* specific or transcriptional downregulators.

Lateral images of the inner ear at 90 hpf stained for *vcanb* and dorsal images of the nervous system at 78 hpf stained with *mbp*. Anterior, left; posterior, right in all images. **(A)** images of control group larvae, including wild types incubated in E3 growth media and *adgrg6*^{tb233c} mutants incubated in DMSO or IBMX (positive control compound). IBMX is shown to restore wild-type levels of *vcanb* (inner ear) and *mbp* (PLLg) expression in *adgrg6* mutant larvae. **(B-C)** images of *adgrg6* mutant larvae that exhibit reduced inner ear *vcanb* expression, but *mbp* expression in the PNS is either unaffected (B) or is downregulated (C) following compound treatment.

4.2.4b Testing hit compounds in dose-response assays

A selection of *mbp* assay hits were tested in dose-response assays to determine their therapeutic window and assess which concentrations can be tolerated by zebrafish larvae. Three compounds including 2 previously known hits, mevastatin and ivermectin, and a novel hit, ebastine, were tested in a concentration series with dilution factor 1.5 ranging from 2.96 μ M to 50.6 μ M. All three compounds mediated a dose-dependent decrease in *vcanb* mRNA expression (figure 4.9A). However, ebastine and mevastatin were toxic at concentrations higher than that used in the screening assay. Mevastatin appears to be the most potent downregulator of *vcanb* expression as complete rescue was detected in all larvae treated at 15 and 22.5 μ M along with 1 larva at 2.96 μ M. Ivermectin was most efficacious at 50.6 μ M as all embryos displayed some reduction in *vcanb* expression. Ebastine, however, appears to have a restricted therapeutic window of 6.67-22.5 μ M, as little or no rescue was observed outside of these concentrations. Furthermore, not all embryos within this concentration range displayed signs of phenotypic rescue, which could result from compound toxicity affecting larval development.

In contrast, rescue of the *mbp* phenotype did not appear to be completely dose-dependent as *mbp* scores fluctuated across the serial dilution range (figure 4.9B). Similar to the *vcanb* assay, ebastine and mevastatin are toxic at concentrations that are above those utilised in the screening assay. Ivermectin mediates complete rescue of *mbp* expression in a selection of larvae at multiple concentrations $\geq 10\mu$ M, but below 10 μ M it mediates no rescue. Alternatively, an increase in *mbp* expression is detected in embryos treated with ebastine or mevastatin at as low as 2.96 μ M. However, complete restoration to wild-type levels were not observed at any concentration, which could indicate some compound toxicity affecting larval development.

A selection of dihydropyridines were also tested in dose-response assays, to determine if their phenotypic rescuing ability was conserved (figure 4.9C). This experimental analysis included nimodipine and nitrendipine, both of which were present in the LOPAC library, in addition to nilvadipine, an external compound that was found to cluster within the dihydropyridine network comprised of LOPAC, Spectrum and Tocris compounds. All compounds mediated dose-dependent restoration of *vcanb* and *mbp* expression in *adgrg6^{tb233c}* mutant larvae. Compounds were generally effective at $\geq 6.67\mu$ M and $\geq 15\mu$ M at restoring respective *vcanb* and *mbp* expression, respectively. Larvae tolerated high concentrations of compounds; however, oedema was observed in a small number treated with compounds at 33.8-50.6 μ M.

A further three compounds, not present in the LOPAC library, were tested in *mbp* dose-response assays, including 2 from the tetranortriterpenoid network cluster, which were identified as strong modulators of Adgrg6 from the Spectrum library (Diamantopoulou *et al.*, 2019), in addition to colforsin,

which is a water-soluble form of forskolin with reduced toxicity (figure 4.9D). These compounds had not yet been tested under the optimised *mbp* assay conditions and represented key categories of hit molecules; candidate *Adgrg6* modulators in the case of tetranortriterpenoids and downstream activators of GPCR signalling pathways in the case of colforsin. Both tetranortriterpenoids, carapin and deoxygedunin, mediated a dose-dependent increase in *mbp* expression; carapin displayed higher efficacy as it restored wild-type levels of *mbp* expression in almost all larvae treated at 22.5-50.6 μ M, whereas deoxygedunin mediated complete rescue in two-thirds of larvae at 33.8-50.6 μ M. In comparison, colforsin was less efficacious as it did not mediate complete restoration of *mbp* expression even at higher concentrations; partial rescue was observed in larvae treated at \geq 15 μ M. This outcome is surprising as colforsin has previously been shown to mediate strong rescue of *mbp* expression (Diamantopoulou *et al.*, 2019). This discrepancy may be explained from the limited absorption of colforsin suspended in water, whereas previously it has been utilised in DMSO suspension. Alternatively, the difference could also result from better performance under the original assay conditions, in which treatment was performed at 25 μ M between 60-90 hpf.

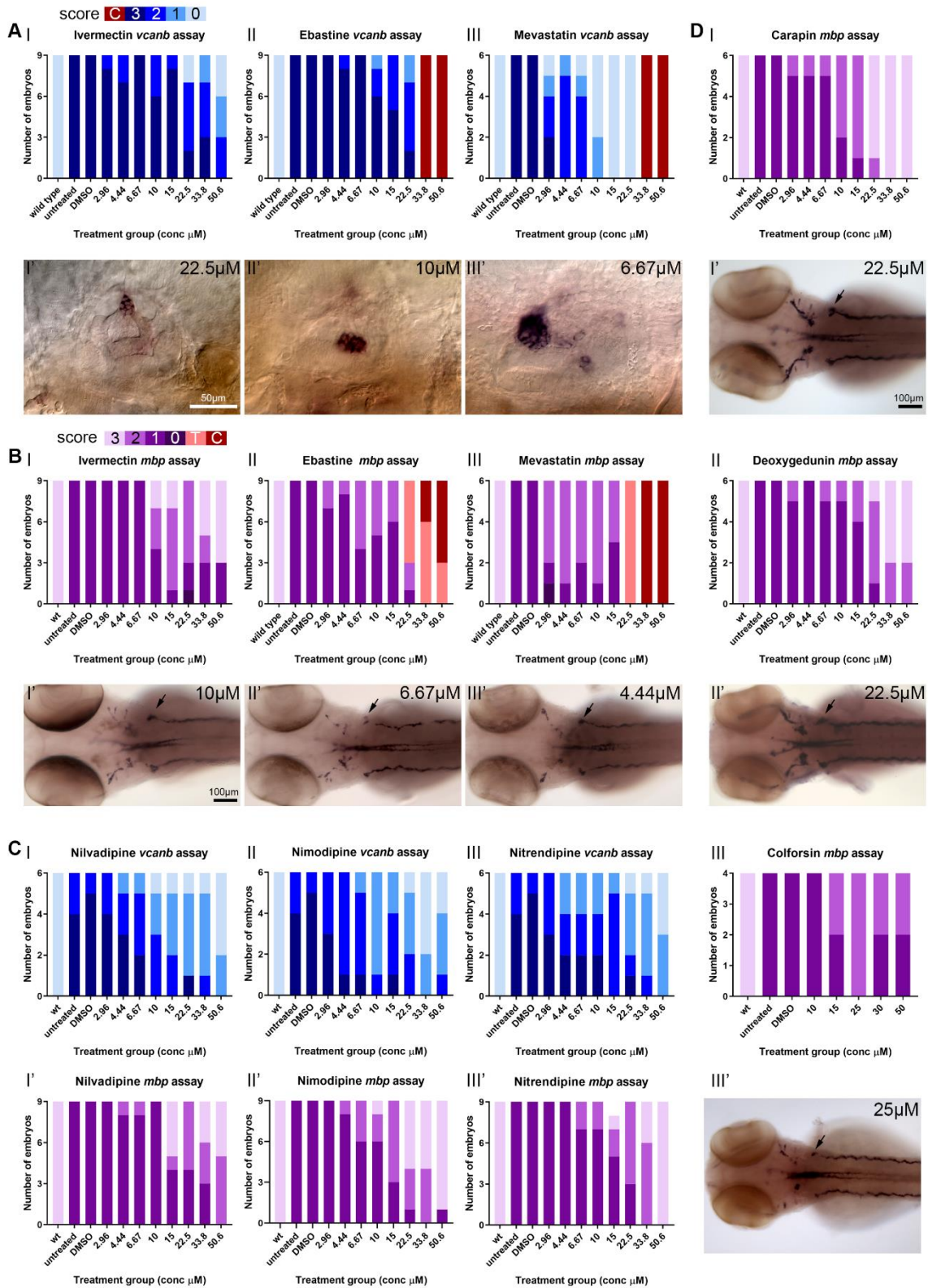


Figure 4.9 Testing *Adgrg6* pathway hits in dose-response assays on *adgrg6*^{tb233c} mutants.

Compounds were tested in a 1.5-fold dilution series on 4-9 *adgrg6*^{tb233c} mutant larvae. Responses recorded in charts showing the number of embryos that scored 0, 1, 2, or 3 in *vcanb* (blue) and *mbp* (magenta) assays; pale intensity indicates full rescue of expression to wild-type levels (*vcanb* score 0 or *mbp* score 3, see figure 4.2) whereas dark intensity indicates no rescue (*vcanb* score 3 or *mbp* score

1, see figure 4.2). Toxic effects are highlighted in red (pale, toxic; dark, no embryos in well). **(A)** larvae treated with ivermectin (I), ebastine (II) or mevastatin (III) in *vcanb* assay, including lateral image of inner ear from an embryo treated with compound concentration specified. Images: ivermectin, score 0; ebastine, score 1; mevastatin, score 1. **(B)** larvae treated with ivermectin (I), ebastine (II) or mevastatin (III) in *mbp* assay, including dorsal image of nervous system from an embryo treated with compound concentration specified. Arrows mark restoration of *mbp* expression at the PLLg. All images are of embryos scored 2 on the *mbp* rescue scale (see figure 4.2), indicating partial restoration of expression at the PLLg. **(C)** larvae treated with dihydropyridines including, nilvadipine (I, I'), nimodipine (II, II') and nitrendipine (III, III') in *vcanb* (I-III) and *mbp* (I'-III') assay. **(D)** larvae, in *mbp* assay, treated with previously identified hits from the Spectrum and Tocris screens (Diamantopoulou *et al.*, 2019) including carapin (I) and deoxygedunin (II) (candidate *Adgrg6* modulators) and colforsin (III) (downstream pathway modulator). (I'-III') dorsal images of embryos treated with compound concentration specified. Images: carapin, score 3; deoxygedunin, score 3; colforsin, score 2. Arrows mark partial or complete restoration of expression at the PLLg. Anterior, left; posterior right in all images.

4.2.5 Testing Adgrg6 pathway hits on other alleles

4.2.5a Strong loss-of-function *adgrg6* mutant allele (*fr24*) in *vcanb* assay

Overall, 17 Adgrg6 pathway modulators have been identified from the LOPAC library. To determine which of these may potentially act directly on the receptor, 15 were tested in a *vcanb* assay on *adgrg6^{fr24}* zebrafish mutants (table 4.5). Forskolin and cilnidipine were not included as these have been tested thoroughly in previous work by the Whitfield lab. The *fr24* allelic mutants were chosen in particular as the mutation introduces a premature stop codon (L463*) within the *adgrg6* coding sequence that predicts a truncated protein lacking everything from the HormR domain to the intracellular C-terminal end (Geng *et al.*, 2013). Therefore, compounds that mediate a decrease in *vcanb* expression in these mutants are likely acting on intracellular signalling pathway components whereas compounds that mediate no rescue are likely to be acting directly on the receptor and are rendered ineffective in its absence in *fr24* allelic mutants.

Interestingly, none of the tested compounds mediated a significant decrease in *vcanb* expression in *fr24* mutants (figure 4.10A) apart from mevastatin, which also appeared toxic (table 4.5). Although these findings suggest that the remaining compounds are likely to act directly on the Adgrg6 receptor, a dose response is necessary to determine if the *vcanb* phenotype can be rescued at higher concentration than 25µM utilised in the assay. A subset of compounds, more likely to act on the receptor, were externally ordered to test in dose-response assays. Compounds with known downstream targets, including those that target GPCR pathway components and Ca²⁺ channels, were not tested at this stage. However, forskolin and tracazolate dose-responses were included as controls as these have been shown to rescue *vcanb* expression in *adgrg6^{fr24}* mutants. In total, 6 compounds were tested, including carapin from the Spectrum library, a key hit that had previously shown no rescue of *vcanb* expression in *adgrg6^{fr24}* mutants tested at 25µM, but had not been tested in a dose-response assay.

In the dose-response assay, forskolin mediated a decrease in *vcanb* expression at tolerated concentrations of ≤6.67µM (figure 4.11A). In comparison, tracazolate failed to mediate a decrease in *vcanb* expression as observed previously; however, toxic side effects were observed in larvae treated at ≥25µM, which could have masked any rescuing effects of the compound (figure 4.11B). Mevastatin was toxic at all concentrations and therefore it is difficult to determine if this compound mediates rescue of the *vcanb* phenotype (data not shown). The remaining 3 compounds mediated no decrease in *vcanb* expression at all the tested concentrations indicating that these are likely to be acting on the Adgrg6 receptor. In future work, these compounds could also be tested in dose-response *mbp* assays on *adgrg6^{fr24}* zebrafish mutants to fully determine the validity of these results.

4.2.5b Missense *tk256a* allelic mutants in optimised *mbp* assay

A subset of the above compounds were also tested in dose-response *mbp* assays on *adgrg6^{tk256a}* mutants to further evaluate their efficacy (figure 4.10B). The *tk256a* allelic mutant, containing a missense mutation in TM4, is predicted to express the full-length protein; however, this mutant shows a strong reduction of *mbp* mRNA expression along the PLLn (Geng *et al.*, 2013). Therefore, any observation of peripheral *mbp* expression would indicate some rescue of the phenotype. Of the 3 compounds tested, all mediated a partial increase in *mbp* expression along the PLL. Although none of the compounds mediated an increase comparable to the IBMX control, carapin appeared the most efficacious as larvae displayed more consistent *mbp* expression along the PLL whereas expression in other samples was sporadic.

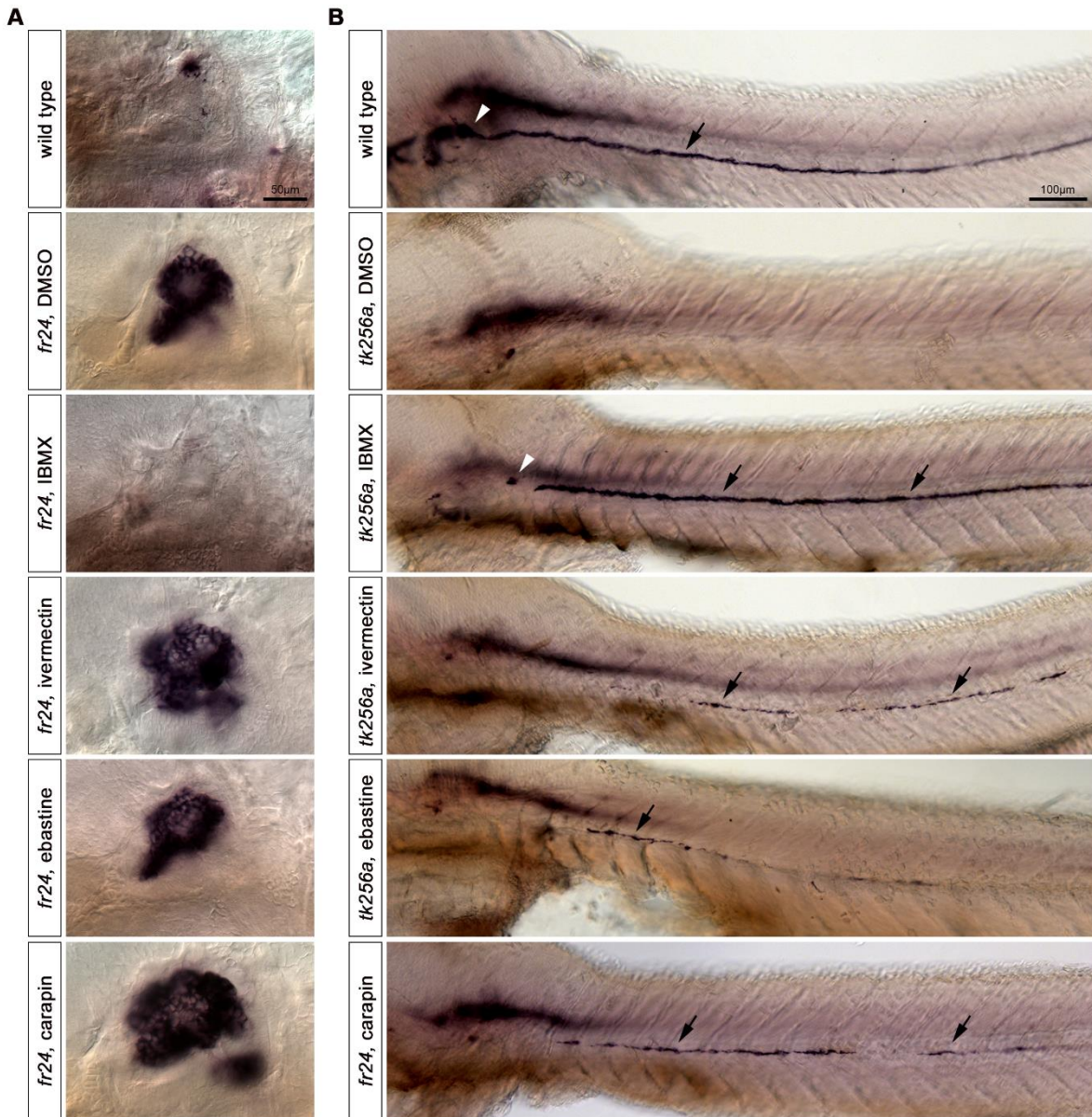


Figure 4.10 Testing Adgrg6 pathway hits on *fr24* and *tk256a* allelic mutants

Compounds were tested under the same conditions as those utilised for the screening assays on *adgrg6^{tb233c}* mutants. All images display lateral view (anterior, left; posterior, right) **(A)** Adgrg6 pathway hits, from screen on *adgrg6^{tb233c}* mutants, fail to restore wild-type levels of *vcanb* expression in *adgrg6^{fr24}* mutants, as is observed for IBMX (positive control). **(B)** all tested compounds mediate partial rescue of *mbp* expression in *adgrg6^{tk256a}* mutants (arrows); carapin displays strongest rescue. No restoration of *mbp* expression is detected at the PLLg, apart from in larvae treated with 50 μ M IBMX control (white arrowhead).

Table 4.5 List of Adgrg6 pathway hits tested on *fr24* allelic mutants

Drug	<i>tb233c vcanb</i> score (3 test avg)	<i>tb233c mbp</i> score (2 test avg)	<i>vcanb</i> score <i>fr24</i> allele (1 test score)
Mevastatin	0.00	9	0
S-Methylisothiurea hemisulfate	5.33	7.5	8.5
FPL 64176	1.67	5.5	8.5
Ebastine	3.67	5.5	8.5
Nemadipine-A	3.67	5.5	8.5
Tracazolate	4.33	6.5	9
Trequinsin hydrochloride	4.33	6.5	9
Nimodipine	4.00	6	9
Cyproterone acetate	3.67	5.5	9
Thapsigargin	2.67	5	9
Ivermectin	4.33	4.5	9
Vinpocetine	4.33	4.5	9
Felodipine	5.33	4.5	9
Pimozide	5.33	4.5	9
LY-294,002 hydrochloride	5.67	4.5	9

- Note: mevastatin displayed some toxic effects on *adgrg6^{fr24}* zebrafish mutants

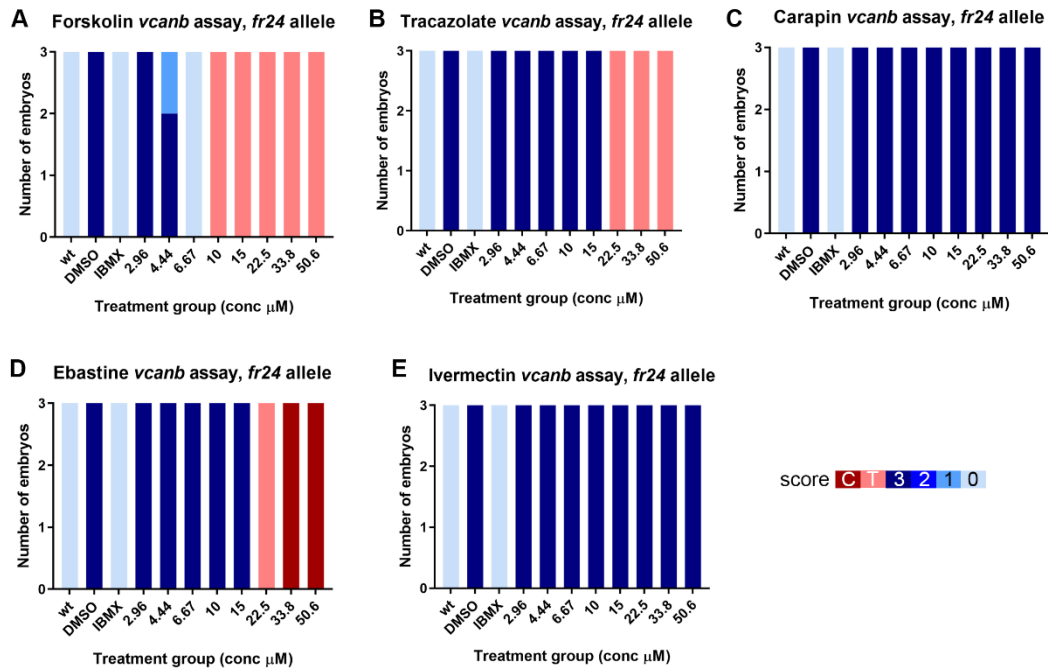


Figure 4.11 Testing *Adgrg6* pathway hits in dose-response *vcanb* assay on *fr24* allelic mutants.

Compounds were tested in a 1.5-fold dilution series on 3 *adgrg6^{fr24}* mutant larvae. Responses recorded in charts showing the number of embryos that scored 0, 1, 2, or 3 in *vcanb* assay; chart key is similar to that in figure 4.9; pale intensity indicates full rescue of expression to wild-type levels (*vcanb* score 0, see figure 4.2) whereas dark intensity indicates no rescue (*vcanb* score 3). Toxic effects are highlighted in red (pale, toxic; dark, no embryos in well). **(A-E)** larvae treated with forskolin (A), tracazolate (B), carapin (C), ebastine (D) and ivermectin (E). Forskolin and tracazolate were included as control compounds that have previously been shown to down-regulate *vcanb* expression in *adgrg6^{fr24}* mutants; however, this effect of tracazolate was not detected in this study.

4.2.6 Retesting apomorphine in phenotypic screening assays

Apomorphine, the most promising candidate modulator for *Adgrg6* identified by Bradley et al. (2019), is present in the LOPAC collection but was not identified as a *vcanb* assay hit in the LOPAC primary screen. Moreover, multiple compounds that clustered within the same structural network also failed to mediate a decrease in *vcanb* expression (figure 4.4). Bradley et al. (2019) initially identified apomorphine by screening for rescue of the *mbp* phenotype in *adgrg6^{st63}* hypomorphic mutant larvae. Therefore, to test the reproducibility of its effects in the current study, it was tested under the same assay conditions alongside the optimised *mbp* assay conditions utilised in the earlier counter screen. *Adgrg6^{tb233c}* mutant larvae were incubated in growth media following compound treatment and fixed at 96 hpf to allow more chance for phenotypic rescue to be detected. Following *in situ* hybridisation, weak *mbp* expression was detected at the PLLg in *adgrg6^{tb233c}* mutant larvae under both assay conditions (figure 4.12A). However, upon quantification, this partial restoration was not significantly different from the DMSO-treated control larvae (figure 4.12B). Moreover, expression was significantly lower than that observed in DMSO-treated wild-type larvae. Compound treatment did not appear toxic, and therefore apomorphine could be administered at higher concentrations to determine if improved rescue can be observed.

To complement this work, apomorphine was retested at higher concentrations in the *vcanb* assay to determine if phenotypic rescue could be observed in *adgrg6^{tb233c}* mutants (figure 4.12C). Larvae treated with 50µM apomorphine displayed a decrease in *vcanb* expression, although complete rescue was not observed. A repeat of the treatment at 25µM concentration revealed no decrease in *vcanb* expression, highlighting that apomorphine is more efficacious at higher concentrations.

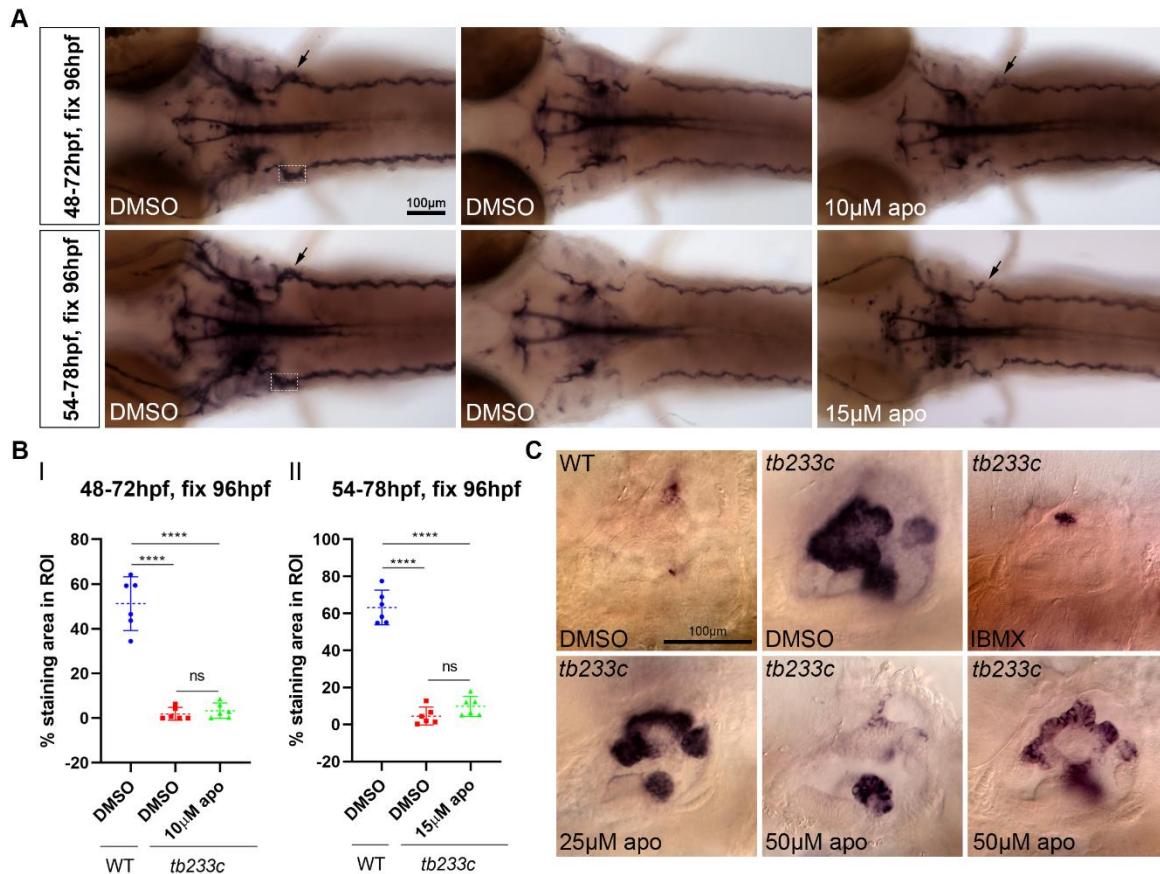


Figure 4.12 Retesting apomorphine in phenotypic screening assays reveals it can mediate partial rescue of the *mbp* and *vcanb* phenotype in *adgrg6^{tb233c}* mutant larvae.

(A) dorsal bright-field images of *mbp* transcript expression in larvae following apomorphine (apo) incubation under assay conditions similar to those utilised by Bradley et al. (2019), top panel, and those utilised in the current project, lower panel. Dotted rectangle (150 pixels x 100 pixels) enclosing left PLLg of wild-type larvae illustrates region of interest (ROI) quantified in (B). Arrows indicate *mbp* expression in Schwann cells around the PLLg; all embryos were fixed at 96 hpf following 24-hour incubation in E3 growth media. **(B)** quantified area of *mbp* expression as a percentage of total ROI illustrated in (A). Although partial rescue was observed in some embryos under both assay conditions, staining area in apomorphine treated larvae was not significantly different to DMSO controls. Method of quantification was similar to that utilised by Diamantopoulou et al. (2019), also in figure 4.1. Each point represents staining around a single PLLg of a zebrafish larva. Error bars, confidence interval 95%; ns, $p \geq 0.05$; ****, $p < 0.0001$. Statistical test: one-way Anova. **(C)** retesting apomorphine in the *vcanb* assay revealed that it fails to down-regulate *vcanb* expression in *adgrg6^{tb233c}* mutants at the 25 μ M screening assay concentration. However, differential levels of downregulation is detected in larvae treated with 50 μ M apomorphine.

4.3 Discussion

In this chapter, expression patterns of *vcanb* and *mbp* mRNA were exploited as transcriptional readouts of *Adgrg6* pathway activity in hypomorphic *adgrg6* zebrafish mutants, to identify potential compound modulators of the *Adgrg6* signalling pathway. A phenotype-based screening platform is described, including a brief summary of the primary *vcanb* assay, optimised by previous members of the Whitfield lab, and a counter-screening *mbp* assay, optimised in this chapter. In total, 1280 compounds from Sigma's library of pharmacologically active compounds (LOPAC), were screened to reveal a range of hits covering a vast structural space. However, the assay concentrations were somewhat arbitrary and therefore non-hits should not be strictly discounted as their limited efficacy could result from suboptimal assay conditions, including administered concentration.

Interestingly, hit compounds displayed a log(P) value that favoured more lipophilic conditions to that of non-hit compounds. A previous study by Long et al. (2019) has highlighted lipophilic favourability in zebrafish active compounds. The group propose that a higher favourability for the lipophilic state could be attributed to the predominant route of absorption in zebrafish, through the lipid-rich yolk sac (Long et al., 2019). Therefore, compounds favouring this route may exhibit higher rescuing efficacy in screening assays.

Reproducibility of screening assays

In total, 48 hit compounds were identified that consistently down-regulated otic *vcanb* expression in *adgrg6^{tb233c}* mutant larvae, 17 of which also restored *mbp* expression at the PLLg in the optimised *mbp* counter-screening assay. The strong positive correlation between *vcanb* retest scores and the largely similar classification of compounds that overlapped across compound libraries illustrated strong reproducibility of the *vcanb* assay output and its overall robustness. The optimised *mbp* counter-screening assay also appears robust due to similar reasons. However, it is important to note that retesting compounds after the primary screen is necessary as approximately 34% of compounds, initially identified as hits, were classified as false-positives following the retests. The high percentage of false-positives can result from natural variation in embryos and slight variation in their staining across numerous assay plates. In comparison, retested compounds are cherry-picked into one individual plate for testing purposes and therefore assay scores are more likely to be comparable as embryos within a single assay plate are treated exactly the same.

Importantly, screening of the LOPAC library enabled blind re-testing of previously identified hits that overlapped with the Spectrum and Tocris libraries. Identification of compounds such as ivermectin and mevastatin along with compounds from the dihydropyridine cluster provides significant evidence

for these compounds as *Adgrg6* pathway hits. These compounds were not only identified as hits across different libraries, but also under different *mbp* assay conditions, which highlights their strong efficacy in mediating up-regulation of *mbp* mRNA expression in *adgrg6^{tb233c}* zebrafish mutants.

Although the screening efforts on *adgrg6* mutants have largely yielded reproducible data, a small number of compounds displayed variable efficacy in the assays, which could result from a range of different reasons. These can include differences in formulation of the compounds across libraries and variability in larval response to treatments, in addition to experimental errors such as unintended plating of unhealthy embryos in assay plates, inconsistent staining of embryos during *in situ* hybridisation and differences in scoring assay plates as this is completed semi-quantitatively by different individuals. The subjectivity in this work can be overcome in future by the use of transgenic lines in which GFP fluorescence can be taken as an unbiased quantitative measure of *vcanb* or *mbp* expression. Moreover, this would capture the assay window better in comparison to the crude scoring system utilised in this study and enable suitable calculation of z primes to validate experimental plates. However, this would also require the use of an automated imaging system to ensure consistency in capturing the appropriate area for quantification. This can be performed by the automated VAST-SDCM imaging system for zebrafish larva, which has been utilised by multiple groups for screening purposes (Early *et al.*, 2018; Bradley *et al.*, 2019). Alternatively, it is important to consider that the subjective and crude approach in the current study has the advantage of evaluating phenotypic rescue with expertise that may not be captured by automation.

Identification of Adgrg6 pathway modulators

In previous work, a counter-screening *mbp* assay was utilised as a second test to identify compounds that may be acting as specific *Adgrg6* pathway modulators in *adgrg6^{tb233c}* mutant larvae, but the conditions for this assay were not fully optimised for the detection of phenotypic rescue (Diamantopoulou *et al.*, 2019). Optimisation of this assay in the current chapter has highlighted improved efficacy of some previously identified hit compounds. Although all previously identified hits have not been tested under the optimised conditions, a small number of overlapping library compounds that were overlooked in previous work have been newly recognised as hit compounds that fall into the category of *Adgrg6* pathway modulators. This outcome indicates that the new conditions are better suited to recognise phenotypic rescue of *mbp* expression in *adgrg6^{tb233c}* mutant larvae.

The counter-screening *mbp* assay was also valuable in identifying *vcanb* hit compounds acting as non-specific down-regulators of transcription that may be detrimental to larval development and overall health. In addition, the remaining compounds were classified as either *vcanb*-specific or as *Adgrg6*

pathway modulators. Although this is not a strict classification, as compounds may mediate rescuing effects at different concentrations, it can highlight compounds that are likely to act specifically in the ear to restore *vcanb* expression and those that act to restore both ear and myelination phenotypes. In doing so, this classification also illustrates potential differences in *Adgrg6* signalling pathways within the ear and those in the PNS. Compounds that are ear-specific may include those that specifically target the epithelial contact and fusion events that lead to formation of the semicircular canal pillars (Geng *et al.*, 2013). However, further work is needed here as the contact and fusion of otic projections in *adgrg6^{tb233c}* mutants has not been assessed in this study. It is also important to consider that *vcanb*-specific compounds may act directly to modulate *vcanb* expression. Such compounds could hold therapeutic potential against cancers as overexpression of versican genes is involved in inflammation and cancer progression (Kim *et al.*, 2009; Andersson-Sjöland *et al.*, 2014).

In future work, hit compounds identified from this study can be assessed from a functional perspective to determine if their ability to mediate restoration of transcriptional targets associated with the *Adgrg6* signalling pathway translates to functional benefits. For example, does restoration of *mbp* at the posterior lateral line ganglion (PLLg) in *adgrg6* mutants translate to improved neuronal function? Recent (unpublished) collaborative work with Francesca De Faveri (Marcottie lab, University of Sheffield) examining afferent neuron firing at the posterior lateral line ganglion revealed that spontaneous firing rates were unaffected in *adgrg6* zebrafish mutant larvae. However, *adgrg6^{fr24}* mutants that lack *mbp* expression altogether along the PLL (Geng *et al.*, 2013) displayed a decrease in peak firing frequency, compared to wild type larvae, in response to mechanical pressure stimulation deflecting the cupula of primary neuromasts along the anteroposterior axis. Furthermore, the first spike latency was increased in these mutants although this did not show statistical significance, likely due to a small sample size in these preliminary experiments. It would be interesting to similarly assess embryos treated with hit compounds, to determine if restoration of *mbp* expression is sufficient to also recover neuronal function. However, the neuronal signalling phenotype is not apparent in hypomorphic *tb233c* mutants, and therefore only compounds that act to restore *mbp* expression in *fr24* mutants, such as forskolin or IBMX (unpublished work by Elvira Diamantopoulou), can be subjected to these tests at this stage. In future, a more tailored experiment that can detect a neuronal phenotype in the hypomorphic allele could hold great value to functionally assess candidate *Adgrg6* modulators. Furthermore, if candidates are found to mediate functional rescue of neuronal signalling this would support the use of such compounds to treat conditions in which the peripheral myelin sheath has deteriorated if myelination processes can be activated similarly to in *adgrg6* zebrafish mutants.

Calcium channel modulators

Compounds from the dihydropyridine cluster have been consistently identified as Adgrg6 pathway modulators throughout the ongoing screening project on *adgrg6*^{tb233c} zebrafish mutants (Diamantopoulou *et al.*, 2019). These compounds are known to act as L-type Ca²⁺ channel blockers that inhibit passive diffusion of cations into the cell and therefore highlight the potential importance of regulating intracellular Ca²⁺ levels for activity of the Adgrg6 signalling pathway and/or myelination itself in Schwann cells. However, a recent study has utilised Ca²⁺ mobilisation assays to illustrate coupling of human ADGRG6 to the G $\alpha_{q/11}$ signalling pathway, which leads to intracellular Ca²⁺ release into the cytoplasm (Lizano, Hayes and Willard, 2020) that could modulate Schwann cell behaviour. Furthermore, identification of screening hits such as FPL 64178, a Ca²⁺ channel activator, and especially thapsigargin, which acts to release intracellular Ca²⁺ into the cytoplasm, highlights a differential role for Ca²⁺ in the Adgrg6 signalling pathway. Based on these findings, it is difficult to assess how exactly Ca²⁺ levels affect activity of the Adgrg6 signalling pathway. It has been documented that ADGRG6 couples to multiple G protein signalling pathways (Monk *et al.*, 2009; Geng *et al.*, 2013; Patra *et al.*, 2013; Liebscher *et al.*, 2014; Lizano, Hayes and Willard, 2020), and therefore Ca²⁺ levels might differentially affect activity of individual G protein signalling pathways associated with Adgrg6; however, they may all act to ultimately favour transcription of myelination genes.

Extracellular Ca²⁺ levels may also have a key role in Adgrg6 signalling. Work on the crystal structure of the receptor by Leon *et al.* (2020) has highlighted the presence of a Ca²⁺ density and a Ca²⁺-binding site within the CUB domain. The Ca²⁺ binding affinity of this region has not yet been elucidated and therefore it is not yet known how variations in Ca²⁺ concentration affect the structural conformation of the NTF, as is known for other proteins that contain a similar Ca²⁺-binding CUB domain (Major *et al.*, 2010; Gaboriaud *et al.*, 2011). However, it has been shown that altering the binding site not only reduces signalling activity, specifically of the +ss isoform, but also leads to ear and myelination phenotypes similar to those associated with other *adgrg6* zebrafish mutants (Leon *et al.*, 2020). Although reduced expression of *mbp* has been observed in Ca²⁺-binding CUB domain mutants, it is not yet clear whether the mutation also affects radial sorting as the Adgrg6-NTF has a key role in this process. Further work is needed to better understand the signalling dynamics of Adgrg6 activity. Application of mini-G proteins that mimic behaviour of heterotrimeric G proteins (Carpenter and Tate, 2016; Nehmé *et al.*, 2017) could be utilised to determine how changes in Ca²⁺ affect G-protein coupling in cells expressing Adgrg6. Moreover, Ca²⁺ channel modulators identified from the phenotypic screen could be tested in such assays to study their mechanism of action.

In previous studies, neuroprotective effects of nimodipine have been shown to promote remyelination by oligodendrocytes (Schampel *et al.*, 2017) and Schwann cells (Tang *et al.*, 2015) in rodents. Mouse models of multiple sclerosis (MS) injected with nimodipine display reduced cell viability of microglia and nitric oxide release, which favours regeneration (Schampel *et al.*, 2017). There is also evidence that illustrates a role for Ca^{2+} signalling in myelinating oligodendrocytes; in zebrafish, high amplitude long duration Ca^{2+} transients prefigure myelin sheath retraction whereas short high frequency transients prefigure its elongation (Baraban, Koudelka and Lyons, 2018). Moreover, conditional deletion of L-type Ca^{2+} channels in oligodendrocyte precursors impairs remyelination in rodent models (Cheli *et al.*, 2016). Although similar evidence has not been gathered for myelinating Schwann cells, these findings illustrate potential mechanisms through which manipulation of calcium levels by dihydropyridines could modulate Schwann cell behaviour, promoting their extension and wrapping around neuronal axons. Ca^{2+} channels are also expressed in neurons and their modulation by dihydropyridines could in fact mediate trans activation of Schwann cells through the neuregulin-ErbB receptor interaction (Ghidinelli *et al.*, 2017).

Intracellular signalling pathway modulators

A selection of compounds that are known to mediate elevation of cAMP were identified as hits, including the adenylyl cyclase agonist forskolin, and the phosphodiesterase inhibitors vinpocetine and trequinsin hydrochloride. These findings provide further evidence of *Adgrg6* signalling through $G\alpha_s$ and potentially $G\alpha_{q/11}$ and $G\alpha_{12/13}$ as these pathways involve cGMP signalling, which is also elevated by the latter class of compounds (Southern *et al.*, 2013; Sriram and Insel, 2018). Furthermore, identification of such compounds provides proof of concept for the screening assays, as the phenotypic rescuing effects of forskolin, on various *adgrg6* zebrafish mutants, have been well documented throughout literature (Monk *et al.*, 2009; Geng *et al.*, 2013), whilst IBMX, another phosphodiesterase inhibitor, is utilised as the positive control within the screening assay (Geng *et al.*, 2013; Diamantopoulou *et al.*, 2019).

Mevastatin, a known inhibitor of Ras and Rho GTPases (Di Bello *et al.*, 2020), was the most potent hit from both screening assays. Its known activity on Ras and Rho enzymes is another indication that the *Adgrg6* pathway is not restricted to signalling through $G\alpha_s$ (Di Bello *et al.*, 2020). Although it is not fully clear how mevastatin potentially manipulates their activity to elevate *mbp* expression, these enzymes are key components in the pathways that underlie cell shape changes, which are fundamental to the growth of otic projections during semicircular canal morphogenesis (Waterman and Bell, 1984; Geng *et al.*, 2013) and the coordination of peripheral myelination (Petersen *et al.*, 2015; Ghidinelli *et al.*, 2017). In the PNS, these signalling pathways may overlap with the neuregulin-ErbB receptor pathways,

which are also important in regulating Schwann cell proliferation and the developmental transition that initiates myelination (Dong *et al.*, 1995; Riethmacher *et al.*, 1997; Jessen and Mirsky, 2005).

Alternatively, mevastatin is also known to modulate cholesterol, a key structural component of the myelin sheath (Fu *et al.*, 1998). Taken together, a potentially complex interplay of different signalling pathways could underlie the restoration of *mbp* expression in *adgrg6^{tb233c}* mutant larvae, by mevastatin. Furthermore, no conclusive evidence was elucidated from testing this compound on the *fr24* allele therefore, it should not be discounted as a direct modulator of Adgrg6.

Candidate Adgrg6 modulators

The strongest candidate modulators of Adgrg6 include ivermectin and ebastine from the LOPAC library and carapin from the previously screened Spectrum library. These compounds could act to rescue the *adgrg6* mutant phenotypes by modulating their known targets, which include $\alpha 7$ acetylcholine receptor (nAChR) for ivermectin and histamine h1 receptor (H1R) for ebastine, whereas the target for carapin is unknown. Activity of nAChRs is known to regulate neuronal growth (Jiang *et al.*, 2013; King and Kabbani, 2016; Fields *et al.*, 2017), which could in-turn affect myelination by Schwann cells *in-trans*. Interestingly, synaptic expression of nAChR is shown to be regulated by the neuregulin signalling pathway (Jiang *et al.*, 2013), which also has a role in coordinating myelination by Schwann cells (Ghidinelli *et al.*, 2017). Although no direct link has yet been shown, published literature suggests that there could be a role for cholinergic signalling in myelination.

The above compounds could also act directly as Adgrg6 modulators as they were ineffective at rescuing *vcanb* expression in *adgrg6^{fr24}* zebrafish mutants. However, they have not yet been tested in the *mbp* assay on *fr24* allelic mutants which may reveal further information regarding their mechanism of action. It is interesting to note that although the target of carapin is unknown, other compounds from the tetranortriterpenoid class, such as gedunin derivatives, have been identified as partial modulators of other adhesion GPCRs, including ADGRG1 (Stoveken *et al.*, 2018). In relation to ebastine, alternative histamine receptor modulators, including GSK247246 (Rangon *et al.*, 2018) and clemastine (Cree *et al.*, 2018) have been shown to mediate off-target effects that increase myelination by oligodendrocytes. An alternate method to elucidate mechanism of action of candidate Adgrg6 modulators is by testing additional compounds known to hit the same signalling pathway such as that associated with H1R. For example, if compounds that target components of the H1R pathway can also rescue phenotypes associated with *adgrg6* zebrafish mutants, it likely indicates cross talk with the Adgrg6 pathway or potentially alternate mechanisms regulating *vcanb* and/or *mbp* expression. This outcome would render potential agonistic modulation of Adgrg6, by ebastine, unlikely. Other LOPAC library compounds, identified as non-hits in the current screen, include those known to target the

histamine pathway, however, their potency to potentially rescue *adgrg6* mutant phenotypes, similarly to ebastine, may be suboptimal under the screening conditions implemented in this study. In future work, a selection of such compounds could be retested in dose-response experiments on *adgrg6* mutants to further interrogate the mechanisms of action that might underlie restoration of mutant phenotypes.

Overall, to determine if the shortlisted candidates can directly modulate Adgrg6 activity, they need to be tested in cell-based signalling assays in which an agonistic relationship can be detected. Various assays are available, including those that can detect changes in cAMP (Liebscher *et al.*, 2014) as a measure of $G\alpha_s$ activity and those that measure coupling of individual mini-G proteins to GPCRs (Carpenter and Tate, 2016; Nehmé *et al.*, 2017) to illustrate compound agonism on expressed receptors.

Conclusions

Phenotypic screens on *adgrg6* zebrafish mutants have yielded a rich resource of material for validation and further study (Bradley *et al.*, 2019; Diamantopoulou *et al.*, 2019; current work). Differences in screening strategies has led to the identification of numerous different hit compounds for the Adgrg6 signalling pathway and as candidate Adgrg6 ligands.

This chapter has illustrated that zebrafish mutant lines can be utilised as a screening tool to uncover a shortlist of candidate Adgrg6 modulators; however, further work is needed to determine potential agonistic effects. Various compounds have been shown to mediate therapeutic effects in *adgrg6* zebrafish mutants, but their effects on general embryo health are yet to be examined thoroughly, including effects on heartbeat, growth and movement of larvae.

A chemical ligand that binds directly with the Adgrg6 could provide a valuable tool to enable isolation of the receptor in its *in vivo* confirmation that could pave the way to uncover further structural and mechanistic insights. Ligands may offer potential for therapeutic use to modulate myelination following injury (Mogha *et al.*, 2016; Bremer, Skinner and Granato, 2017; Gomez-Sanchez *et al.*, 2017; Jablonka-Shariff *et al.*, 2019) or against ADGRG6-linked diseased conditions (Kou *et al.*, 2013, 2018; Karner *et al.*, 2015; Ravenscroft *et al.*, 2015; Hosseini *et al.*, 2019). Additionally, identification of hits with known targets could highlight potential interactions between intracellular signalling pathways to aid our understanding of signalling networks and their effects on cell behaviour. Alternatively, modulators of Adgrg6 pathway components could provide useful biological tools to manipulate intracellular pathways and test novel hypotheses to better understand behaviour of Schwann cells during myelination and/or otic projection epithelia during the contact and fusion events underlying

semicircular canal formation in the inner ear. To determine agonism of shortlisted hit compounds towards Adgr6, they were tested in cell-based cAMP assays in the next chapter.

Chapter 5.

G α_s pathway activity in human and zebrafish

ADGRG6-expressing HEK293 cells

5.1 Introduction

Phenotype-based small molecule screens on zebrafish *adgrg6* mutants (Bradley *et al.*, 2019; Diamantopoulou *et al.*, 2019), including work conducted in the previous chapter, have revealed various candidate receptor modulators. However, direct compound agonism for Adgrg6 is better assessed in simpler biological systems, such as cell-based assays in which a direct relation between compound and receptor can be evaluated. As mentioned in earlier sections, ADGRG6 is well known to signal through conserved GPCR signalling pathways, including pathways associated with various G proteins. Although studies have highlighted ADGRG6 signalling through G $\alpha_q/11$ and G $\alpha_{12/13}$ (Langenhan, 2019; Lizano, Hayes and Willard, 2020), the evidence for G α_s signalling spans multiple biological systems, including the zebrafish larva, whereas evidence for the former G proteins is largely restricted to cell-based systems.

Historically, rescue of *adgrg6* mutant phenotypes in zebrafish has been observed following treatment with compounds that act to elevate intracellular levels of cAMP levels by either increasing its production, in the case of forskolin (Monk *et al.*, 2009), or inhibiting its breakdown, in the case of IBMX (Geng *et al.*, 2013). In light of these observations, cAMP signalling assays have been widely utilised to illustrate *stachel*-peptide-mediated activation of Adgrg6 (Liebscher *et al.*, 2014), in addition to evaluating agonism of biological NTF ligands (Paavola *et al.*, 2014; Petersen *et al.*, 2015; Küffer *et al.*, 2016) and candidate Adgrg6 agonists (Bradley *et al.*, 2019). Alternatively, such assays can be utilised to assess the implications of known human and zebrafish ADGRG6 mutations on activity of the receptor's signalling pathway. Mutations in the human, mouse and zebrafish ADGRG6 gene are associated with altered peripheral myelination (Monk *et al.*, 2009, 2011; Geng *et al.*, 2013; Petersen *et al.*, 2015; Ravenscroft *et al.*, 2015). In zebrafish, they have been shown to differentially affect Schwann cell development, highlighted by variation in the severity of myelination phenotypes. For example, the hypomorphic *adgrg6*^{tb233c} zebrafish mutants display a decrease in peripheral *mbp* mRNA expression whereas expression is missing altogether in *adgrg6*^{tk256a} zebrafish mutants (Geng *et al.*, 2013).

In this chapter, cell-based cAMP accumulation assays will be utilised to examine the effects of *adgrg6* mutations on cellular cAMP accumulation as a measure of Adgrg6 pathway activity and the receptor's functionality. Subsequently, candidate Adgrg6 modulators identified from the zebrafish phenotypic screen will be tested in similar assays to determine if they mediate an agonist-like functional response. However, it is important to consider that Adgrg6 signals through multiple G protein signalling pathways and any responses in terms of cAMP accumulation, or their lack of, may not represent the full picture of cell behaviour.

The focus of the ongoing screening project on *adgrg6* zebrafish mutants has been towards the identification of candidate agonists; however, identification of antagonists may also be of value. Such modulators could reveal the types of compounds that are able to interact with Adgrg6 and reveal structural motifs that may be shared with agonistic compounds. Alternatively, antagonistic compounds could provide useful biological tools for manipulating Adgrg6 activity to uncover further insights surround its signalling pathway or be utilised in isolating the receptor in its inactive state to enhance our understanding of its structure. Although an antagonist screen has not yet been performed for Adgrg6, antagonistic compounds for other adhesion class GPCRs have been identified. These include dihydromunduletone (DHM) and mundulone, which modulate ADGRG1; the former is also found to modulate ADGRG5 (Stoveken *et al.*, 2016). These compounds, DHM in particular, may also modulate Adgrg6 and therefore will be tested in cell-based and zebrafish assays to determine if they can inhibit Adgrg6 activity and mediate phenocopy of *adgrg6* zebrafish mutants in wild-type larvae.

Key chapter aims & hypotheses:

1. Determine functional effects of known human and zebrafish *ADGRG6* mutations. Hypothesis: cells transfected with human or zebrafish *ADGRG6* mutant constructs should display reduced cAMP accumulation in comparison to wild-type transfected cells.
2. Determine agonistic effects, if any, of shortlisted candidate Adgrg6 modulators. Hypothesis: Adgrg6 modulators should elevate cAMP accumulation in cells overexpressing *adgrg6* in comparison to untransfected controls.
3. Determine effects of known ADGRG1 antagonists on cells expressing human or zebrafish *ADGRG6*. Hypothesis: ADGRG1 antagonist compounds are likely to inhibit cAMP accumulation in cells overexpressing human or zebrafish *ADGRG6* in comparison to untransfected controls.

5.2 Results

5.2.1 Effect of human and zebrafish *ADGRG6* mutations on $G\alpha_s$ pathway activity

All cell-based cAMP assays were performed, during a short placement at Sosei Heptares, on the HEK293 cell line that has previously been utilised by multiple other groups for similar work (Paavola *et al.*, 2014; Küffer *et al.*, 2016; Stoveken *et al.*, 2016, 2018). Cells were first transfected with a plasmid containing the human or zebrafish *ADGRG6* gene to overexpress the receptor, including wild-type and mutant isoforms, to determine how mutations affect activity of the $G\alpha_s$ signalling pathway. The core plasmid was obtained from Sosei Heptares and utilises the commercially-available pcDNA3.1(+) backbone. Transduction of HEK293 cells was performed using the baculovirus vector approach to ensure high and consistent expression of the plasmid; virus cultures were generated by the Xavier Ruf from the Biochemistry team at Sosei Heptares. Viral titre was evaluated by qPCR to reveal similar concentrations for all human and zebrafish constructs (data not shown). All transfections were performed overnight for a total period of approximately 20-22 hours; key aspects are highlighted in figure 5.1.

The key mutations that were assessed in cAMP assays included two zebrafish mutations, I963N (*tb233c*) and P969L (*tk256a*) (Geng *et al.*, 2013), along with the pathogenic human mutation, V769E associated with LCCS9 (Ravenscroft *et al.*, 2015). With use of Clustal alignments of the published amino acid and gene reference sequences, zebrafish mutations were mapped onto the human gene and vice versa for the human pathogenic mutation (amino acid sequence in figure 5.2A). All mutant constructs were generated by site-directed mutagenesis, using a wild-type reference sequence construct as the template DNA for gene editing. Following transfection of HEK293 cells with 1 % baculovirus culture of each respective plasmid construct, cells were incubated in assay media containing 500 μ M IBMX for 60 minutes to enable accumulation of cAMP before lysis and detection of cAMP levels. The fold-change in cAMP accumulation, calculated by dividing the response of transfected cells with that of untransfected controls (figure 5.2 (supplement) A and B), is illustrated in figure 5.2.

Transduction with the human or zebrafish wild-type constructs mediated an increase in cAMP accumulation; the human construct mediated a 10-fold increase in cAMP whereas the zebrafish construct mediated an over ≥ 200 -fold increase (figure 5.2B and C). This is taken as an indication of receptor expression contributing to $G\alpha_s$ pathway activity and illustrates that there is constitutive activity in the absence of an applied ligand. Furthermore, a baculovirus dose-dependent increase in cAMP accumulation was observed (figure 5.2 (supplement) C). Examination of cells transfected with mutant allelic constructs reveals that cAMP accumulation is largely elevated in comparison to untransfected controls, except for in cells transfected with the zebrafish *tk256a* allele. This finding

suggests that not all mutations abolish receptor pathway activity. It is surprising however, that transfection with the zebrafish *tk256a* allele does not stimulate cAMP accumulation whereas the same mutation in the human background is associated with elevated cAMP accumulation. Although the affected amino acid residue is conserved in humans, the *tk256a* allelic mutation appears to be more detrimental to receptor expression or signalling in the zebrafish gene in comparison to the human gene.

As expected however, the cAMP fold-change observed in all mutant transfected cells was significantly lower than the wild-type transfected cells. Out of the three alleles tested in both human and zebrafish backgrounds, the mutation associated with the *tk256a* allele appears most severe as it exhibits the lowest fold-change in cAMP accumulation across cells transfected with human or zebrafish gene constructs. Comparatively, the *tb233c* mutation appears least detrimental; however, the fold-change in cAMP accumulation is less than half of that observed in cells transfected with wild type. Severity of zebrafish mutations are also put into perspective alongside the human pathogenic mutation. The human equivalent of the zebrafish *tk256a* allele response is comparable to the pathogenic mutation whereas the response for the human equivalent of the zebrafish *tb233c* allele follows suit in cells transfected with the zebrafish construct. If zebrafish mutants were to be generated with the human pathogenic mutation, they may display similar phenotypes to that observed in *adgrg6^{tb233c}* zebrafish mutants.

To examine the reliance of auto-proteolysis on receptor signalling, a further mutant construct for both the human and zebrafish *ADGRG6* genes was generated that included a histidine to arginine substitution at the GPS site, predicted to abolish auto-proteolysis (insight from Sosei Heptares; Frenster *et al.*, 2021) (figure 5.2D). Although cells transfected with these constructs displayed an increase in cAMP accumulation in comparison to untransfected controls, the cAMP fold-change is significantly lower in comparison to wild-type-expressing cells. The mutation appears to affect zebrafish *adgrg6*-expressing cells more so, as the cAMP fold-change decreases from approximately 200 down to 15, whereas in human *ADGRG6*-expressing cells the fold-change is approximately halved. These observations indicate that zebrafish *Adgrg6* activity is heavily reliant on self-cleavage of the extracellular domain for its signalling activity whereas the human *ADGRG6* is less so. Examination of receptor expression is required to fully confirm this hypothesis.

As mentioned previously, the zebrafish *adgrg6* constructs were generated based on the published reference sequence (NM_001163291.2). However, it was noted in previous work by the Whitfield lab that the naturally occurring zebrafish wild-type sequence contains a conserved tryptophan at position 804 (Geng *et al.*, 2013; Demberg *et al.*, 2017). In the reference sequence, a single base-pair difference

(2412T>G) results in a predicted cysteine residue at this position. It is not confirmed if this difference in the published sequence is an alternate wild-type form present in fish from the Talbot lab, or a sequence error in the published version. Alignment with the human and mouse sequence also reveals a tryptophan at this position (Patra *et al.*, 2013). Therefore, a W804 wild-type *adgrg6* construct was generated to test in cAMP assays and compare cell responses against the tested C804 form. Similarly, a human W817C construct was generated to allow comparison of both forms in the human and zebrafish *ADGRG6* genes. Surprisingly, presence of a tryptophan in the zebrafish construct significantly reduced cAMP accumulation in comparison to the cysteine form (figure 5.2E); the fold-change in cAMP accumulation was similar to that associated with the equivalent human isoform. This observation indicates that the C804 form is overactive in comparison to what appears to be the naturally occurring wild-type form (W804). More surprising yet was the observation that copying the cysteine form in a human background almost abolished cAMP accumulation altogether indicating a pathogenic effect of the amino acid substitution. All zebrafish mutant constructs were generated with a cysteine at position 804 and therefore it is difficult to fully assess the validity of the cAMP response data. These assays should therefore be repeated with the W804 form. The responses of human *ADGRG6* expressing cells may display a more accurate representation of signalling pathway activity.

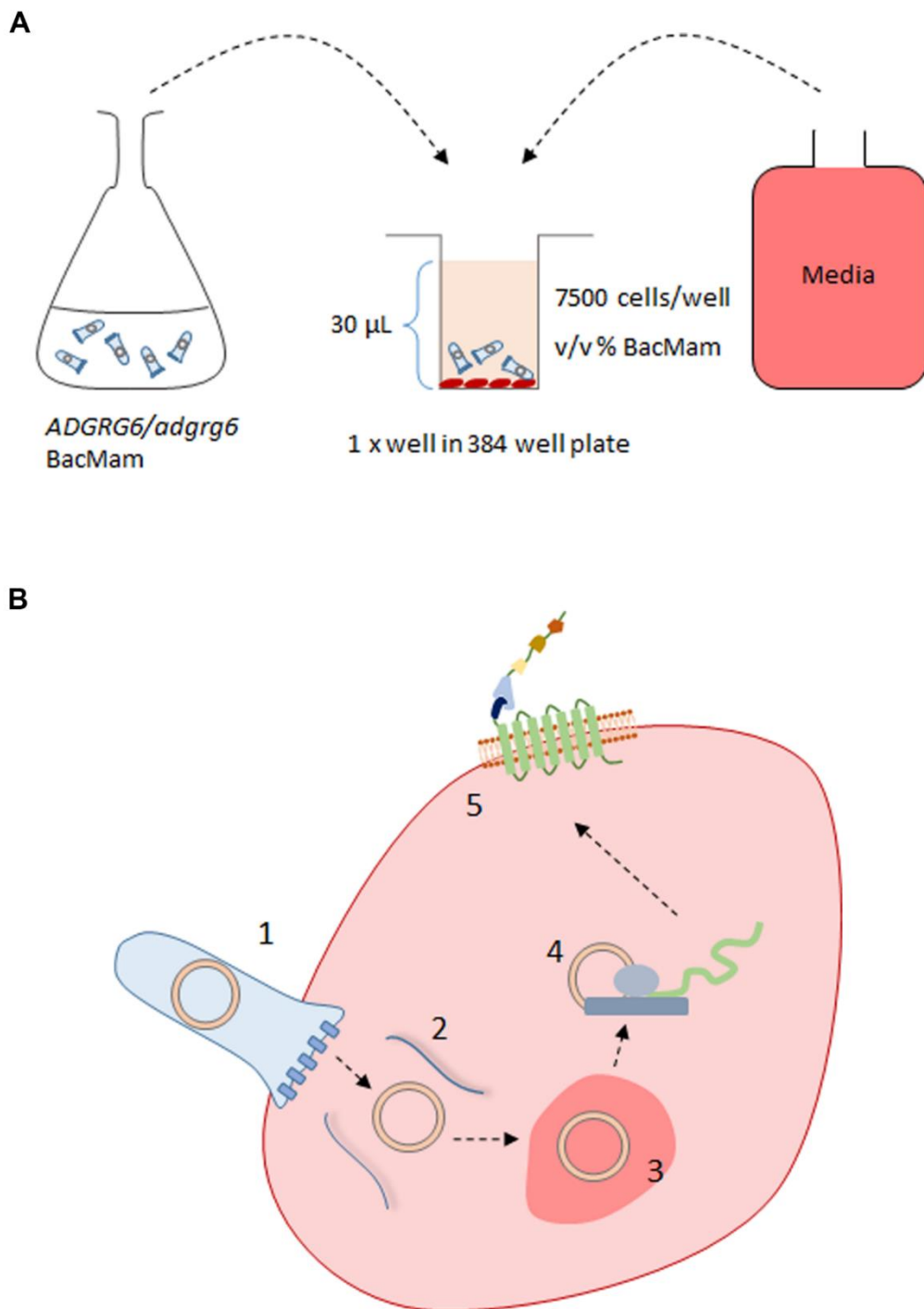


Figure 5.1 Cell baculoviral transduction

(A) HEK293 cells were transduced by a baculovirus vector to facilitate high and consistent expression of the human or zebrafish *ADGRG6*. 7500 cells (layer of four shown in well) were incubated with <5% v/v baculovirus culture overnight. **(B)** schematic to illustrate transduction of HEK293 cells by baculovirus particle. 1, entry by endocytosis; 2, release of plasmid DNA; 3, translocation of DNA to nucleus and its transcription; 4, translation of mRNA; 5, expression of human or zebrafish ADGRG6 protein at the cell membrane.

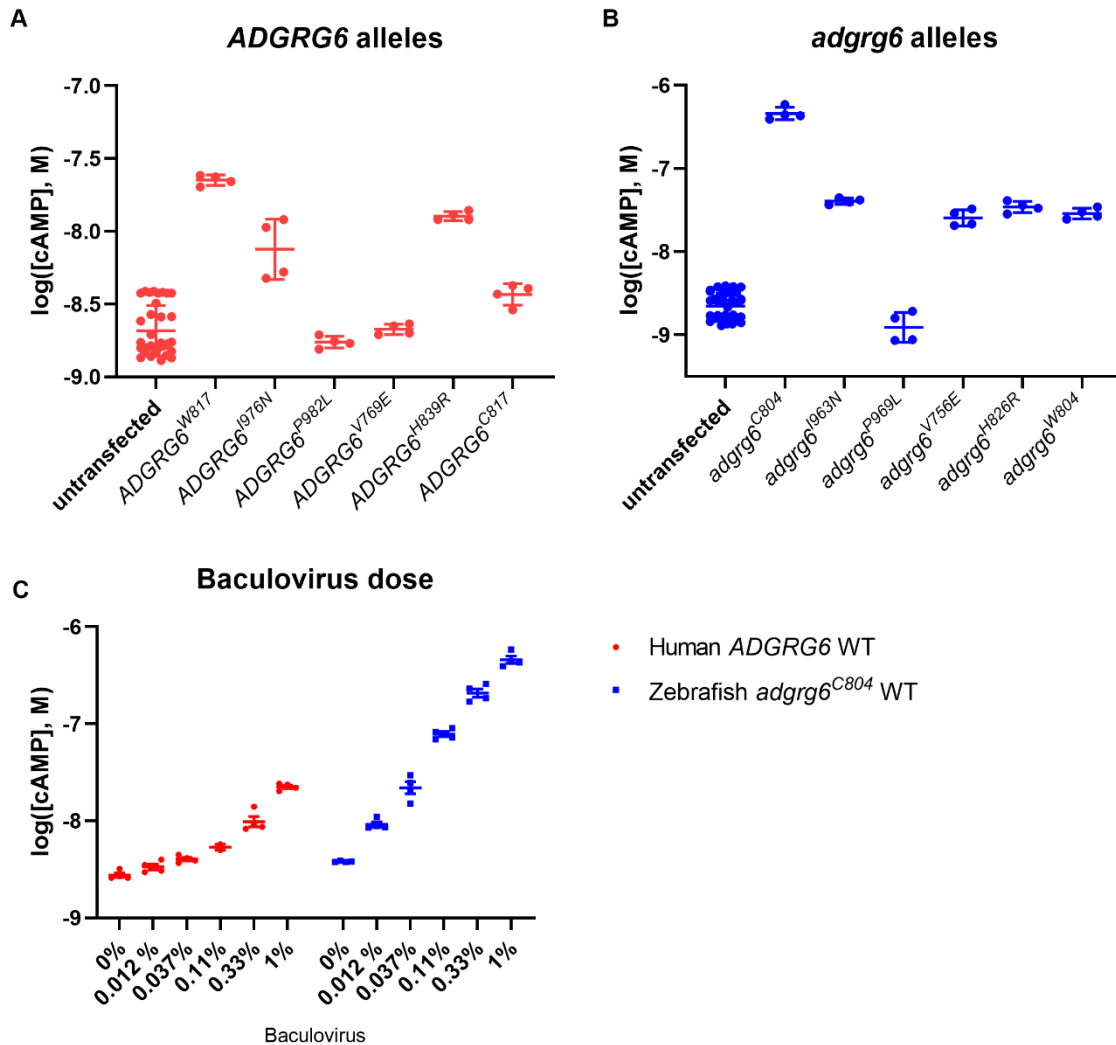


Figure 5.2 (supplement) cAMP levels detected in cells expressing various human and zebrafish *ADGRG6* alleles.

(A-B) cAMP levels detected in HEK293 cells transduced overnight with 1% (v/v) baculovirus (see figure 5.1) for each human (A) or zebrafish (B) *ADGRG6* allele. Increased cAMP is observed in wild type *ADGRG6* transfected cells in comparison to untransfected controls and those transfected with mutant alleles. (C) cAMP levels increase with increasing dose of baculovirus utilised for transduction, highlighting constitutive activity of the receptor. Wild-type isoforms: human *ADGRG6* (red) and zebrafish *adgrg6* (blue).

5.2.2 Expression of human and zebrafish *ADGRG6* constructs

In order to assess expression and localisation of the receptor, C-terminal GFP-tagged constructs for human and zebrafish *ADGRG6* were generated by digesting the gene insert from original plasmids and re-ligating into a plasmid which contains the GFP coding sequence following the *ADGRG6* insertion site. This work was conducted at the University of Sheffield, without facilities for baculovirus transfection, and therefore HEK293 cells were transiently transfected with constructs for approximately 18-20 hours, using FuGENE transfection reagents. Due to limitations on time to conduct such experiments, the wild-type, *tb233c* and LCCS9 constructs were examined in such experiments, although additional constructs were generated to be examined in future work. Following transfection, cells were stained with wheat germ agglutinin (WGA) (pre-fixation) or a GOLGA2 antibody (post-fixation) to illustrate the plasma membrane and Golgi apparatus, respectively. Expression of these markers alongside that of GFP-tagged *ADGRG6* constructs is illustrated in figures 5.3 (human *ADGRG6*) and 5.4 (zebrafish *adgrg6*).

Fluorescent images and line analysis profiles, spanning two *ADGRG6*-transfected cells, illustrate co-localisation of GFP expression with the membrane marker, WGA. Although some GFP fluorescence was widely distributed across the cell, expression was concentrated at tip-like protrusions of the cell membrane. However, cells transfected with human *tb233c* or V769E allelic constructs, display wider expression of GFP throughout the cell that does not specifically localise to the membrane. The *ADGRG6*^{V769E}-expressing cells display extremely low GFP expression at the membrane. These observations suggest that the V769E mutation in *ADGRG6* may affect specific localisation and integration of the receptor at the membrane, which may also underlie the reduced cAMP accumulation responses observed in the earlier section.

To test whether the amino acid at position 804 in the zebrafish sequence affects subcellular localisation of the protein, GFP expression was examined in cells transfected with C804 or W804 form of *adgrg6*. Interestingly, cells transfected with the zebrafish *adgrg6*^{C804} variant, utilised in cAMP assays, display a different expression profile to those transfected with the human wild type. GFP expression from the *adgrg6*^{C804} variant is widely distributed throughout the cell, similar to that observed in cells transfected with human mutant constructs. Cells expressing *adgrg6*^{tb233c} and *adgrg6*^{V756E} displayed a similar GFP profile. Cells expressing *adgrg6*^{W804} exhibit co-localisation of GFP and WGA at cell protrusions, as observed in human wild-type-transfected cells, supporting the interpretation that the zebrafish W804 variant represents the wild-type form. Some GFP expression is widely distributed throughout the cell but less so than in cells expressing *adgrg6*^{C804}. Collectively, these observations suggest that a cysteine at position 804 may limit localisation and integration of the receptor at the membrane as hypothesised for *ADGRG6* allelic mutant isoforms. However, expression of *adgrg6*^{C804}

was associated with high levels of $G\alpha_s$ activity; therefore, weaker GFP expression at the membrane could indicate an inability of transfected cells to tolerate high levels of expression. Assessment of the *ADGRG6*^{W817C} form reveals that GFP expression is detectable across the cell similar to its zebrafish equivalent, but a high degree of co-localisation with WGA is also observed at the cell membrane. This suggests that substitution of tryptophan with cysteine is not as critical in affecting integration of the receptor at the membrane as it appears to be for the zebrafish isoform.

A small number of *adgrg6*^{W804}-expressing cells were identified that displayed widely distributed GFP expression with some strong localisation likely at the Golgi. Therefore, in a separate experiment cells transfected with *adgrg6*^{W804} were stained with a GOLGA2 (GM130) antibody to mark the Golgi and determine if co-localised GFP expression was detected. As expected, although GFP was widely distributed in cells, strong expression did co-localise with GOLGA2 expression at the Golgi. This may indicate presence of Adrg6 in the Golgi for packaging and trafficking to the membrane. Alternatively, as a consequence of overexpressing the GFP-tagged Adrg6 protein, Golgi expression could indicate that cells are unable to correctly fold the amount of protein being expressed, which could also be apparent in cells transfected with mutant constructs. Golgi localisation of GFP remains to be examined in cells transfected with human or zebrafish *ADGRG6* mutant constructs and those expressing the zebrafish *adgrg6*^{C804} wild-type form. Further work may be needed to optimise transfection efficiency as an overview of cells expressing *adgrg6*^{C804} reveals that only a fraction are GFP-positive (figure 5.4 supplement). Therefore, expression profiles observed could illustrate variability in the transfection efficiency. Differences in overall expression between variants and wild-type isoforms also remains to be examined.

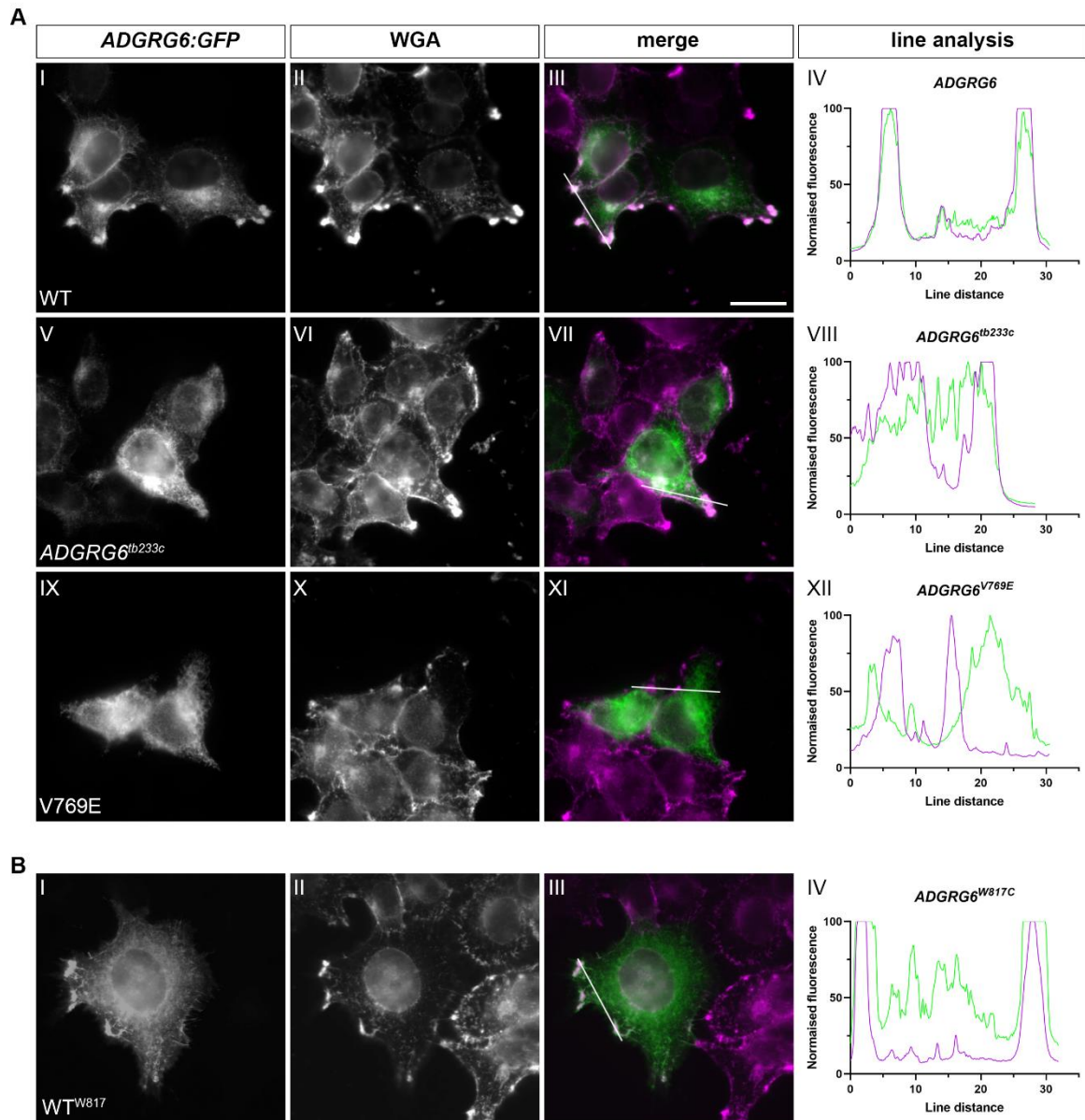


Figure 5.3 Expression of the GFP-tagged human *ADGRG6* gene in HEK293 cells.

(A) GFP fluorescence (first column) and wheat germ agglutinin (WGA) expression (second column) in cells transfected with the human wild type (WT) allele of *ADGRG6* (I-III). Merged images (column three, III) (GFP, green; WGA, magenta) and line analysis profile (IV) illustrate co-localisation of both markers at the cell membrane. GFP fluorescence and WGA expression is similarly shown for cells transfected with the human equivalent of the zebrafish *tb233c* allele (V-VIII) and the human pathogenic mutant allele (IX-XII). **(B)** GFP fluorescence (I) and WGA expression (II) in cells transfected with the human *ADGRG6^{W817C}* variant (equivalent of zebrafish *adgrg6^{C804}*). Line analysis (IV) illustrates some co-localisation of both markers at the cell membrane, although GFP fluorescence is also detected in other regions across the cell. White lines (column three) illustrate section along which fluorescence profiles were examined using the line analysis function in ImageJ, final column. Raw fluorescence intensity values, taken at 108 nm intervals, were normalised as a percentage of the highest pixel value in the line analysis dataset. GFP fluorescent signal strengthened with application of anti-GFP antibody. Scale bar: 20 μ m.

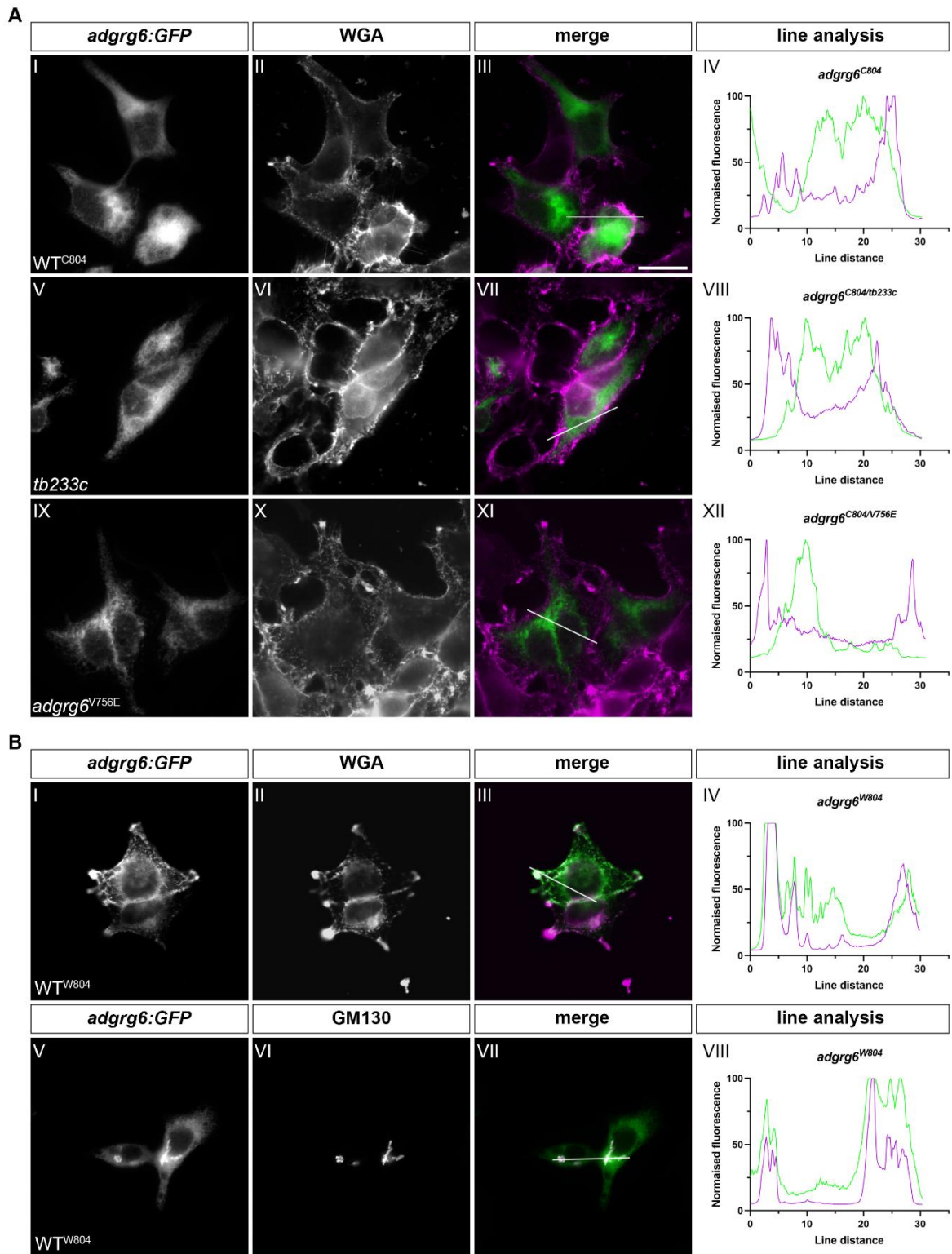


Figure 5.4 Expression of the GFP-tagged zebrafish *adgrg6* gene in HEK293 cells.

(A) GFP fluorescence (first column) and wheat germ agglutinin (WGA) expression (second column) in cells transfected with the zebrafish *adgrg6^{C804}* (*WT^{C804}*) allele (I-III). Merged images (column three, III) (GFP, green; WGA, magenta) and line analysis profile (IV) illustrate that GFP fluorescence does not specifically co-localise with WGA at the cell membrane. GFP fluorescence and WGA expression is similarly shown for cells transfected with the zebrafish *tb233c* allele (V-VIII) and the zebrafish equivalent of human pathogenic mutant allele (V756E) (IX-XII), both in the *adgrg6^{C804}* background. **(B)**

I-IV) GFP fluorescence (I) and WGA expression (II) in cells transfected with the zebrafish *adgrg6*^{W804} wild-type allele. Merged images (III) and line analysis profile (IV) illustrates co-localisation of both markers at the cell membrane, as seen in cells expressing the naturally occurring human wild-type *ADGRG6* allele (see figure 5.4A). **(B V-VIII)** GFP fluorescence (V) and GM130 expression (VI) in cells transfected with the zebrafish *adgrg6*^{W804} wild-type allele. Merged images (VII) and line analysis profile (VIII) illustrates co-localisation of both markers in the Golgi apparatus. White lines (column three) illustrate section along which fluorescence profiles were examined using the line analysis function in ImageJ, final column. Raw fluorescence intensity values, taken at 108 nm intervals, were normalised as a percentage of the highest pixel value in the line analysis dataset. GFP fluorescent signal strengthened with application of anti-GFP antibody. Scale bar: 20 μ m.

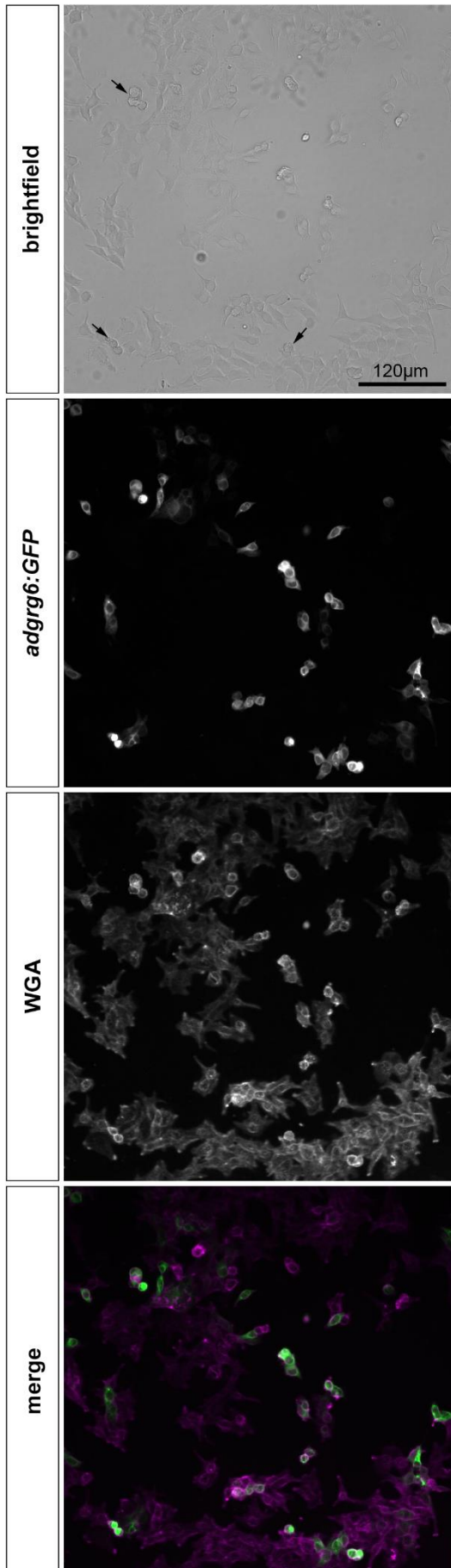


Figure 5.4 (supplement) FuGENE-based transfection efficiency.

Brightfield and fluorescent images of HEK293 illustrate low transfection efficiency as GFP fluorescence was not detected in the majority of cells. Arrows indicate dead cells, some of which were also GFP-positive. GFP, green; WGA stain, magenta. GFP fluorescent signal strengthened with application of anti-GFP antibody.

5.2.3 Optimisation of HEK293 cell baculoviral transfection with human and zebrafish *ADGRG6* constructs for suitability with small molecule treatments

In order to test candidate *Adgrg6* modulators identified from the zebrafish phenotypic screen, the baculovirus cell transfection protocol was first optimised to ensure compatibility with compound treatments. A low concentration of baculovirus was necessary to ensure that overexpression of constructs did not mask the effects of potential agonists. Although cAMP accumulation responses and expression profiles for zebrafish *adgrg6* constructs (see above), together with sequence information from the Whitfield lab (Geng *et al.*, 2013), revealed that *adgrg6*^{W804} is the likely natural wild type, compound treatments were performed on cells transfected with *adgrg6*^{C804}, as this was the published reference sequence. Comparatively, the correct human *ADGRG6*^{W817} wild type construct was utilised alongside.

A known adenylyl cyclase activator, forskoin, was utilised to determine the appropriate concentration of baculovirus required to mediate a minimal increase in cAMP accumulation in transfected cells in comparison to untransfected controls. As before, all transductions were performed overnight for a total period of approximately 20-22 hours before treatment of cells with a half-log dilution series of forskolin for 1 hour followed by detection of cAMP levels. The forskolin dose-response is illustrated in figures 5.5A and B for transfection with human and zebrafish *ADGRG6* respectively.

As expected, treatment with increasing concentrations of forskolin mediated an increase in cellular cAMP accumulation, apparent across transfected and untransfected cells. The cAMP response curve also displayed a baculovirus dose-dependent elevation. This increase is taken as an indication of *Adgrg6* activity in the transfected cells, contributing to an increase in overall cAMP accumulation. As shown previously, transfection with the zebrafish construct is associated with higher cAMP accumulation compared to the human construct (comparison at 1 % baculovirus dose).

The 0.1 % and 0.0033 % baculovirus concentrations for human and zebrafish constructs were selected as most optimal for the transfection of HEK293 cells as these displayed a minimal elevation in the cAMP levels in comparison to untransfected controls. The elevation in cAMP at higher baculovirus doses was deemed too high, as this could mask any effect that agonistic compounds may induce in transfected cells.

In the first instance, colforsin, the water-soluble derivative of forskolin, was tested in the cAMP accumulation assay to determine if it mediated a similar response in HEK293 cells (figure 5.5C). This experiment was performed in particular to determine the validity of using colforsin as a positive control compound in future zebrafish screening assays, as it is known to act as an adenylyl cyclase activator and thus leads to a more direct cAMP response, rather than phosphodiesterase inhibitors,

including IBMX, which inhibit cAMP degradation. Furthermore, zebrafish larvae tolerate colforsin better than forskolin treatment, which can only be applied in short bursts to prevent damage to embryos (Monk *et al.*, 2009; Geng *et al.*, 2013). As expected, a dose-response assay revealed that colforsin mediates a similar dose-dependent increase in cAMP in both transfected and untransfected cells. This finding provides support for the use of colforsin as an additional positive control compound that can be used in the screening assays in place of or in addition to IBMX.

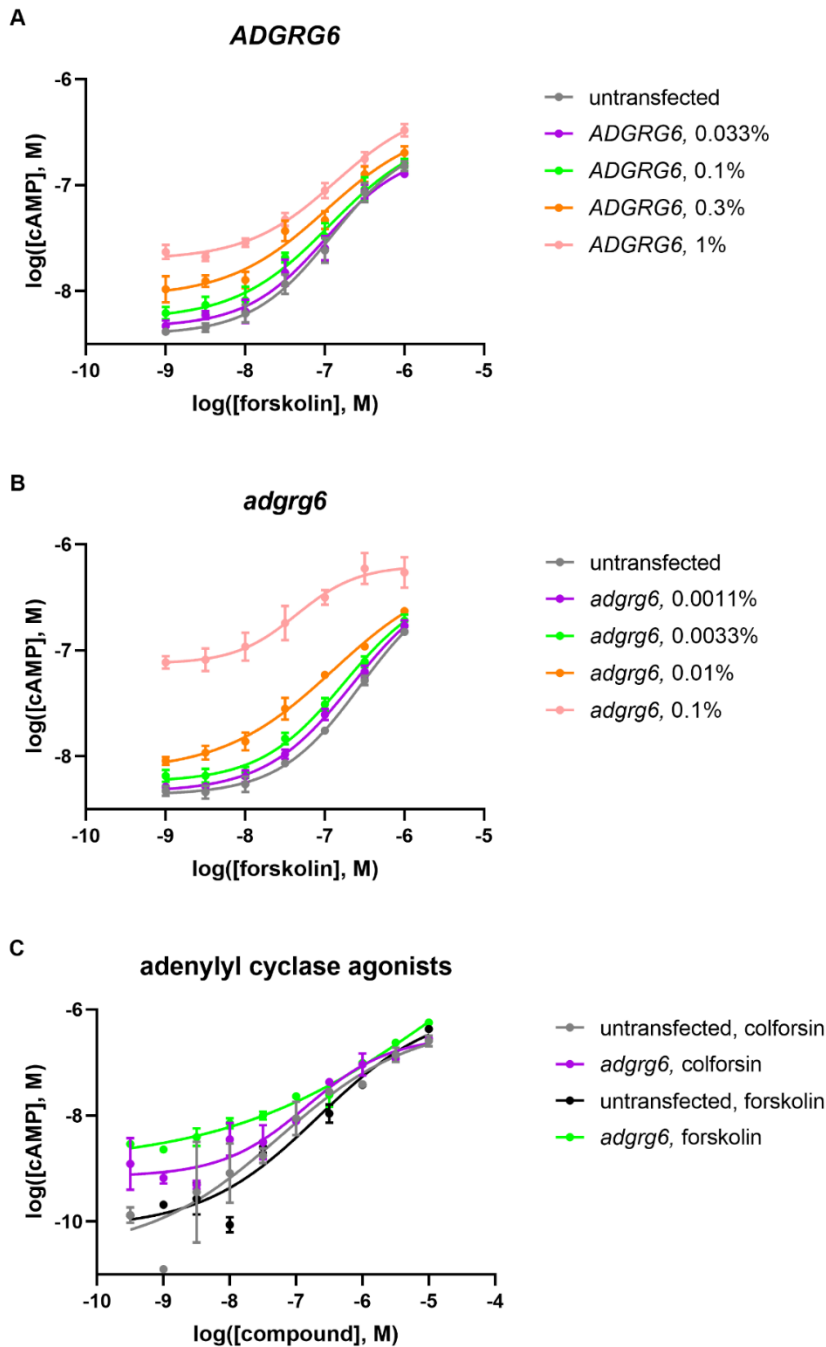


Figure 5.5 Optimisation of baculovirus dose for transduction of HEK293 cells.

(A-B) HEK293 cell cAMP responses to 10-point half-log concentration series of forskolin following overnight transduction with various baculovirus doses of the wild-type human (A) or zebrafish (B, C804 allele) *ADGRG6* gene. The cAMP response curve shifts upwards with increasing doses of baculovirus. Results of two independent assays performed in duplicate **(C)** HEK293 cAMP response to 10-point half-log concentration series of forskolin (black, untransfected; green, transfected) or colforsin (water-soluble form of forskolin) (grey, untransfected; magenta, transfected). Transfection with zebrafish *adgrg6*^{C804} allele only, individual assay performed in duplicate. Both compounds mediate dose-dependent cAMP accumulation in transfected and untransfected cells. Treatments performed for 60 minutes before detection of intracellular cAMP levels. Baculovirus dose: 0.0033%. Error bars: standard deviation.

5.2.4 HEK293 cell responses to candidate *Adgrg6* modulators

Following optimisation of the HEK293 cell transfection protocol, a selection of candidate *Adgrg6* modulators identified from zebrafish screening assays were tested in cAMP accumulation assays to determine if they mediated an agonistic effect on *Adgrg6*. As highlighted by multiple groups (Liebscher *et al.*, 2014; Paavola *et al.*, 2014; Petersen *et al.*, 2015; Küffer *et al.*, 2016; Stoveken *et al.*, 2018; Bradley *et al.*, 2019), an agonist mediates a dose-dependent cAMP increase in cells overexpressing *adgrg6* and no response in untransfected controls, unlike signalling pathway modulators such as forskolin, which mediate a response independent of *adgrg6* expression. The cAMP response of tested compounds is illustrated in figures 5.6 and 5.7.

From the LOPAC screen, hit compounds including ebastine, mevastatin and ivermectin were tested whereas a single dihydropyridine, nilvadipine, was included as an example compound that may mediate a non-specific response. A further two compounds, carapin and apomorphine, were also tested; the former a hit from the Spectrum screen and the latter as a control compound that has previously been shown to mediate *Adgrg6*-dependent elevation of cAMP (Bradley *et al.*, 2019) and partially rescues the ear and myelination phenotypes in *adgrg6*^{tb233c} mutants (see Chapter 4 section 4.2.6). A dose-response for each compound was performed with a half-log dilution series (figure 5.6), similar to forskolin. It is interesting to note that compounds do not appear to mediate a clear dose-dependent increase in cAMP accumulation in transfected or untransfected cells as observed for forskolin. Ivermectin is the only compound from the LOPAC screen that mediates a marginal increase in cAMP accumulation in cells transfected with human *ADGRG6*, specifically at concentrations above $1 \times 10^{-6.18}$ M. Apomorphine also displays a slight dose-dependent increase in transfected cells; however, no clear trends are observed, in contrast to what is seen for forskolin. At high concentrations, ebastine and mevastatin mediate a decrease in cAMP levels in *adgrg6* transfected cells, which could illustrate cell toxicity as observed in zebrafish larvae (see chapter 4, section 4.2.4b). However, this remains to be independently assessed.

As ivermectin and apomorphine were the two compounds that appeared to mediate a slight increase in cAMP accumulation in transfected cells, they were tested further at higher concentrations and under different treatment times to determine if their efficacy could be improved (figure 5.7). Treatments of 30 minutes and 120 minutes were performed to determine if compound effects were either short-lived or required more time for a detectable effect. A 30 minute treatment with ivermectin revealed no clear difference in cAMP response; however, a 120 minute treatment mediated a slight dose-dependent increase in cAMP. This response was not specific to cells overexpressing human or zebrafish *ADGRG6* indicating that a response may result from activation of another receptor or an intracellular signalling pathway component. In comparison, apomorphine did

not show any clear trends and appears to decrease cAMP at higher concentration which could be taken as an indication of toxicity. In previous literature, the increase in Adgrg6-dependent cAMP accumulation following apomorphine treatment was detected in the COS-7 cell line (Bradley *et al.*, 2019), which may be better suited for the detection of its agonistic effects.

Overall, the cAMP responses measured displayed a high degree of variability and therefore any trends should be treated with caution. Given more time, the cAMP assays could be optimised further to enable better detection of compound effects. At this stage, it is also unclear how compound treatments might affect cell integrity and if cell death was apparent in drug-treated samples.

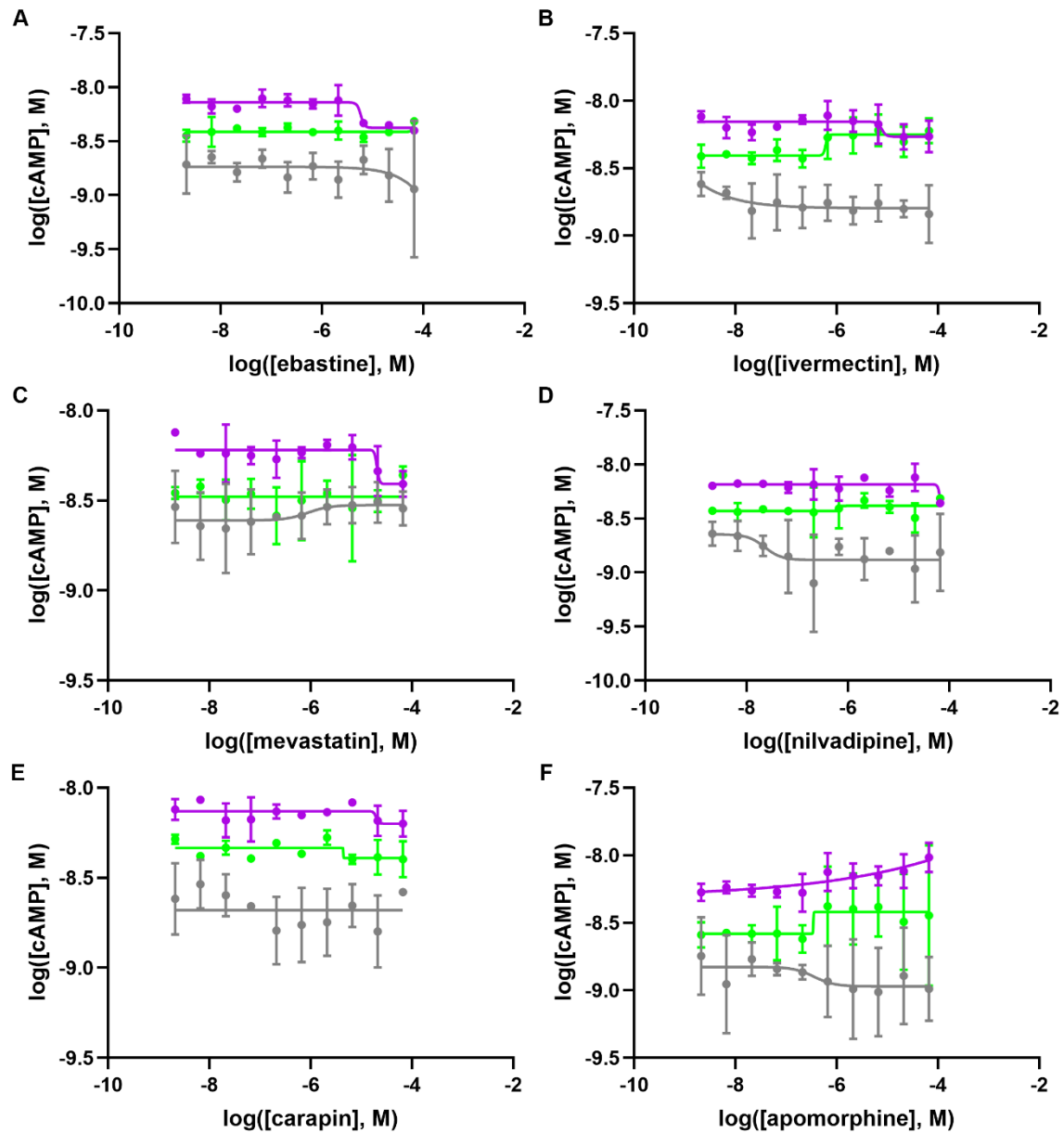


Figure 5.6 HEK293 cell cAMP response curve to treatment with candidate *Adgrgr6* agonists.

(A-F) HEK293 cell cAMP response curve to 10-point half-log compound dilution series of (A) ebastine; (B) ivermectin; (C) mevastatin; (D) nilvadipine; (E) carapin; (F) apomorphine. No clear trends are observed across the dilutions series in untransfected (grey) or transfected (human *ADGRG6*, green; zebrafish *adgrg6*^{C804}, magenta) cells. HEK293 cells were transduced overnight with 0.1% human *ADGRG6* or 0.0033% zebrafish *adgrg6*^{C804} final v/v baculovirus dose. Compound treatments performed for 60 minutes before detection of intracellular cAMP levels. Error bars: standard deviation. Results are from up to two assays performed in duplicate.

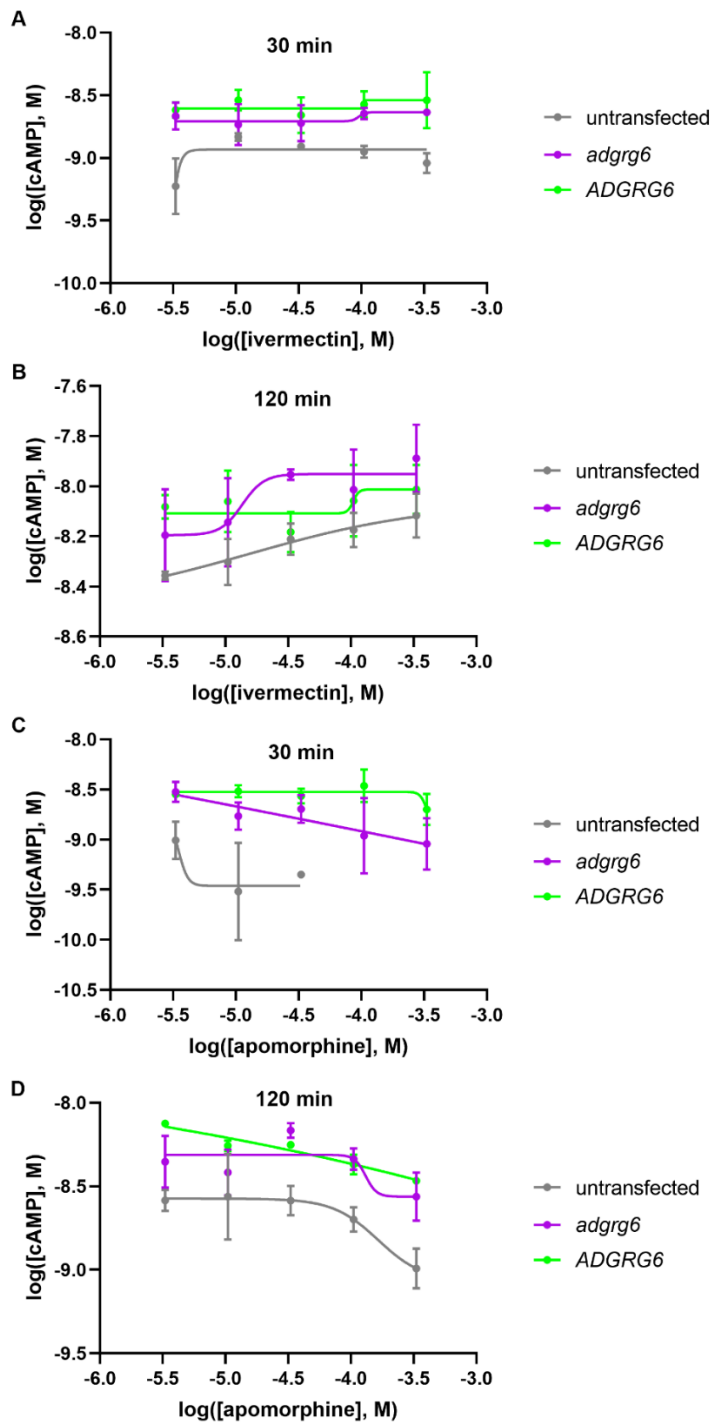


Figure 5.7 HEK293 cell cAMP response curve to 30- or 120-minute treatment with candidate *Adgrgr6* agonists.

(A-D) HEK293 cell cAMP response curve to 5-point half-log compound dilution series of ivermectin (A, 30min; B, 120min); apomorphine (C, 30min; D, 120min). Higher compound concentrations administered to those previously. No clear trends are observed across the dilutions series in untransfected (grey) or transfected (human *ADGRG6*, green; zebrafish *adgrg6*^{C804}, magenta) cells. High variability in the dataset. HEK293 cells were transduced overnight with 0.1% human *ADGRG6* or 0.0033% zebrafish *adgrg6*^{C804} final v/v baculovirus dose. Error bars: standard deviation. Results are from individual assay performed in duplicate.

5.2.5 HEK293 cell responses to known biological Adgrg6 NTF ligands

As no clear responses to compound treatment were observed in terms of cAMP accumulation, known NTF ligands of Adgrg6, including collagen IV (Paavola *et al.*, 2014) and a peptide derived from prion protein (Küffer *et al.*, 2016), were tested in similar assays to determine if conditions were optimal for detecting an agonistic effect. For these experiments, a higher baculovirus dose was also trialled to determine if this was required to detect an elevation in cAMP. Treatments were performed similarly to previous compound treatments for 60 minutes. The cAMP responses to collagen and prion are illustrated in figure 5.8.

Transfection with a higher baculovirus dose elevates cellular cAMP accumulation, as expected. However, no clear agonistic effect of Adgrg6 ligands was detected at either of the two baculovirus doses trialled. This appears to be the case for cells transfected with human or zebrafish *ADGRG6*. Therefore, it can be assumed that conditions for the cAMP assay are not optimal for detecting an agonistic effect in terms of $G\alpha_s$ pathway activity. Numerous factors could contribute to this, including differences in formulation of the ligands that were utilised in the assay along with compatibility of the baculoviral transfection approach with these ligand treatments. However, it is important to consider that the baculoviral transfection approach is effective and widely utilised in experimental research conducted by Sosei Heptares. Furthermore, it was utilised at low doses to minimise any effects on cell viability. Alternatively, there could be differences in cell seeding density and assay buffers utilised for administering treatments. Further work is needed to optimise the conditions for these assays.

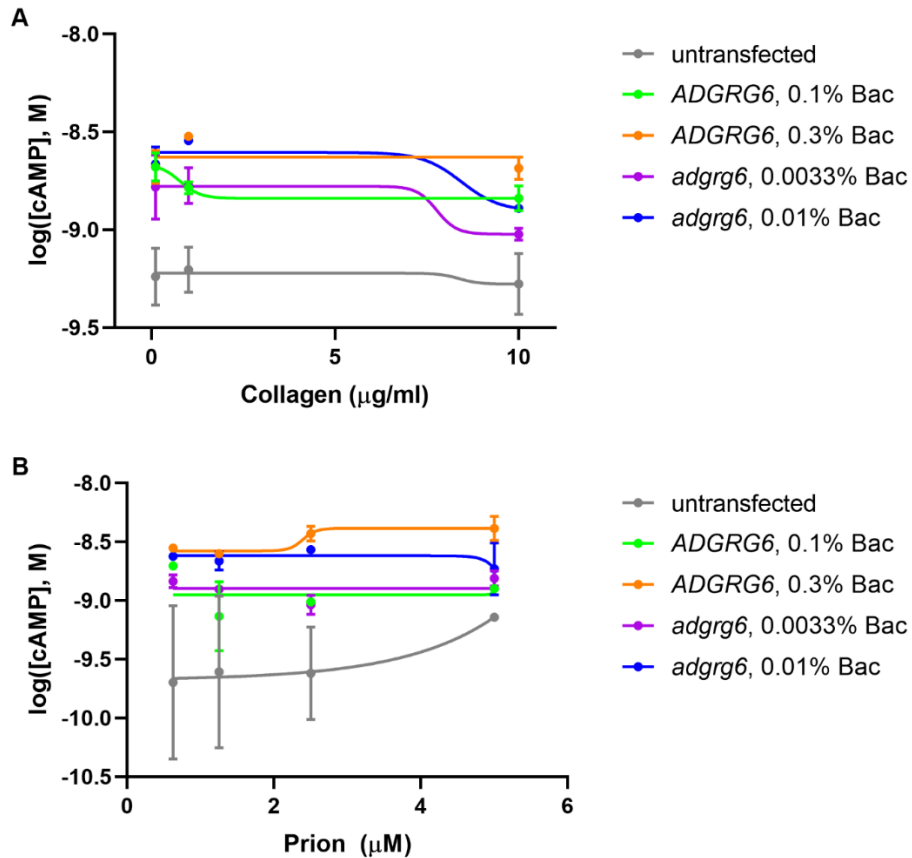


Figure 5.8 HEK293 cell cAMP response curve to known *Adgrgr6* NTF ligands.

(A-B) HEK293 cell cAMP response curve to dilution series of collagen IV (Col4) (A) and Prion protein (PrP) (B). No clear trends are observed across the dilutions series in untransfected (grey) or transfected (human *ADGRG6*, green; zebrafish *adgrg6*^{C804}, magenta) cells. High variability in the dataset. HEK293 cells were transduced overnight with 0.1-0.3% human *ADGRG6* or 0.0033-0.01% zebrafish *adgrg6*^{C804} final v/v baculovirus dose. As expected, higher cAMP levels are detected in cells transduced with a higher baculovirus dose. Error bars: standard deviation. Results are from individual assay performed in duplicate.

5.2.6 Candidate *Adgrg6* antagonists in cAMP assays

Although cAMP responses failed to illustrate ligand-induced agonism towards *Adgrg6*, candidate antagonists were tested under similar assay conditions to determine if $G\alpha_s$ pathway activity could be restricted, specifically in cells expressing human or zebrafish *ADGRG6*. A higher dose of baculovirus was utilised for transfection of HEK293 cells as in this instance compounds were tested in their ability to inhibit cAMP accumulation, which is better judged with a higher starting cAMP concentration. Previously identified *ADGRG1* antagonists, including dihydromunduletone (DHM) and mundulone (MUND) (Stoveken *et al.*, 2016), were tested across a half-log dilution series; their effects on cAMP accumulation are illustrated in figure 5.9 and 5.10.

Interestingly, both DHM and MUND mediate a dose-dependent decrease in cAMP accumulation (figure 5.9), more so in cells transfected with human or zebrafish *ADGRG6* in comparison to untransfected controls. DHM appears more efficacious in comparison to MUND as it appears to mediate a steeper dose-dependent decline in cAMP accumulation, however, its inhibitory effects plateau at high concentrations whereas the inhibitory effect of MUND does not. Furthermore, a steeper dose-dependent decline in cAMP accumulation is observed in cells transfected with zebrafish *adgrg6* in comparison to human *ADGRG6*, indicating that the zebrafish isoform is more sensitive to compound treatment. Specifically, in transfected cells treated with the highest compound dose, cAMP accumulation is significantly lower than that observed in DMSO treated controls (figure 5.10A). Comparatively, no significant difference is observed in untransfected cells treated with compounds or DMSO.

The findings appear to indicate a receptor-dependent effect of candidate antagonists; however, cell responses could also depend on initial cAMP levels. To assess this prospect, cAMP levels of transfected cells were mimicked with the use of forskolin in untransfected cells. Various forskolin concentrations were trialled alongside the antagonist dilution series to identify the most optimal for comparative analysis with transfected cells (data not shown). The most optimal responses are plotted alongside that of transfected cells in figure 5.9. Interestingly, forskolin-treated cells with a similar initial cAMP concentration as *ADGRG6* transfected cells (figure 5.10B), display a similar dose-dependent response with respect to DHM and MUND (figure 5.9A and C). Cellular cAMP levels at the highest administered concentration of DHM and MUND are similar between forskolin-treated cells and *ADGRG6* transfected cells, indicating that the response observed is likely not dependent on the expression of *ADGRG6*, and that the compounds are acting on an alternative receptor or acting on downstream components of the cAMP signalling pathway. By contrast, forskolin-treated cells with a similar initial cAMP concentration as zebrafish *adgrg6*-expressing cells (figure 5.10) also exhibit a somewhat dose-dependent decrease in cAMP with respect to DHM and MUND (figures 5.9 B and D). However, the

decline is not as steep as that observed in transfected cells and plateaus at a higher cAMP concentration to that in transfected cells. Cellular cAMP levels at the highest administered concentration of DHM and MUND are significantly lower in *adgrg6*-transfected cells in comparison to forskolin-treated cells. Collectively, this suggests that the response of *adgrg6*-expressing cells is partially dependent on receptor expression. Interestingly, no significant difference is observed between untransfected DMSO-treated cells and *adgrg6*-expressing cells treated with the highest DHM dose, illustrating that compound treatment masks any effect of *adgrg6* transfection. This can be taken as indication that DHM treatment inhibits all contribution that Adgrg6 signalling may have towards cAMP accumulation.

Comparison of human and zebrafish *ADGRG6*-expressing cells treated with candidate antagonists and cells expressing mutant alleles of *ADGRG6* reveals comparable levels of cAMP accumulation (figure 5.11). In particular, cAMP accumulation is similar between compound-treated cells and those expressing the hypomorphic allele in both the human (I976N) and zebrafish (*tb233c*: I963N) background. However, it is important to consider that these responses were recorded in separate experiments and therefore an accurate comparison requires a repeat of all samples under the same conditions.

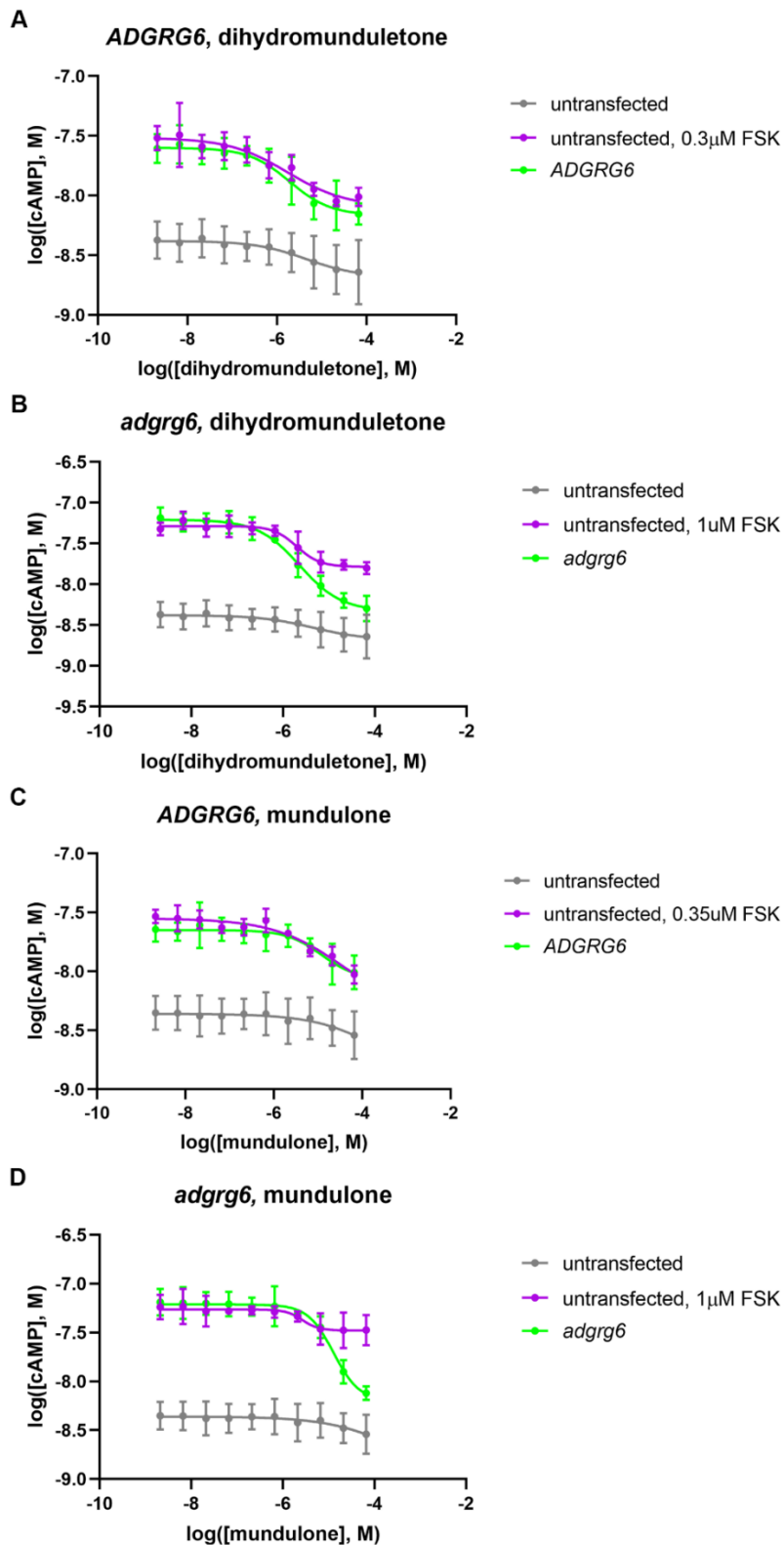


Figure 5.9 HEK293 cell cAMP response curve to treatment with known ADGRG1 antagonists.

(A-D) HEK293 cell cAMP response curve to 10-point half-log compound dilution series of (A-B) dihydromunduletone and (C-D) mundulone. Intracellular cAMP levels of transfected (green) and untransfected (grey) cells decrease with increasing concentration of antagonist compound; however, response is more pronounced in cells transfected with the zebrafish *adgrg6*^{C804} allele (B, D, green

curve). Response of untransfected cells can be shifted up to mimic that of transfected cells by co-treatment with forskolin (0.3-0.35 μ M, mimic *ADGRG6*-transfected cells; 1 μ M, mimic *adgrg6*^{C804}-transfected cells). (A, C) untransfected cells co-treated with 0.3-0.35 μ M forskolin exhibit a decrease in intracellular cAMP levels with increasing concentration of antagonist compound, similar to the response curve of human *ADGRG6*-transfected cells. (B, D) untransfected cells co-treated with 1 μ M forskolin exhibit a decrease in intracellular cAMP levels with increasing concentration of antagonist compound; however, the cAMP response curve plateaus at a higher concentration than that in zebrafish *adgrg6*^{C804}-transfected cells. Therefore, response could be partially dependent on expression of the *adgrg6*^{C804} allele. HEK293 cells were transduced overnight with 3% human *ADGRG6* or 0.3% zebrafish *adgrg6*^{C804} final v/v baculovirus dose. Compound treatments performed for 60 minutes before detection of intracellular cAMP levels. Error bars: standard deviation. Results are from two assays performed in duplicate.

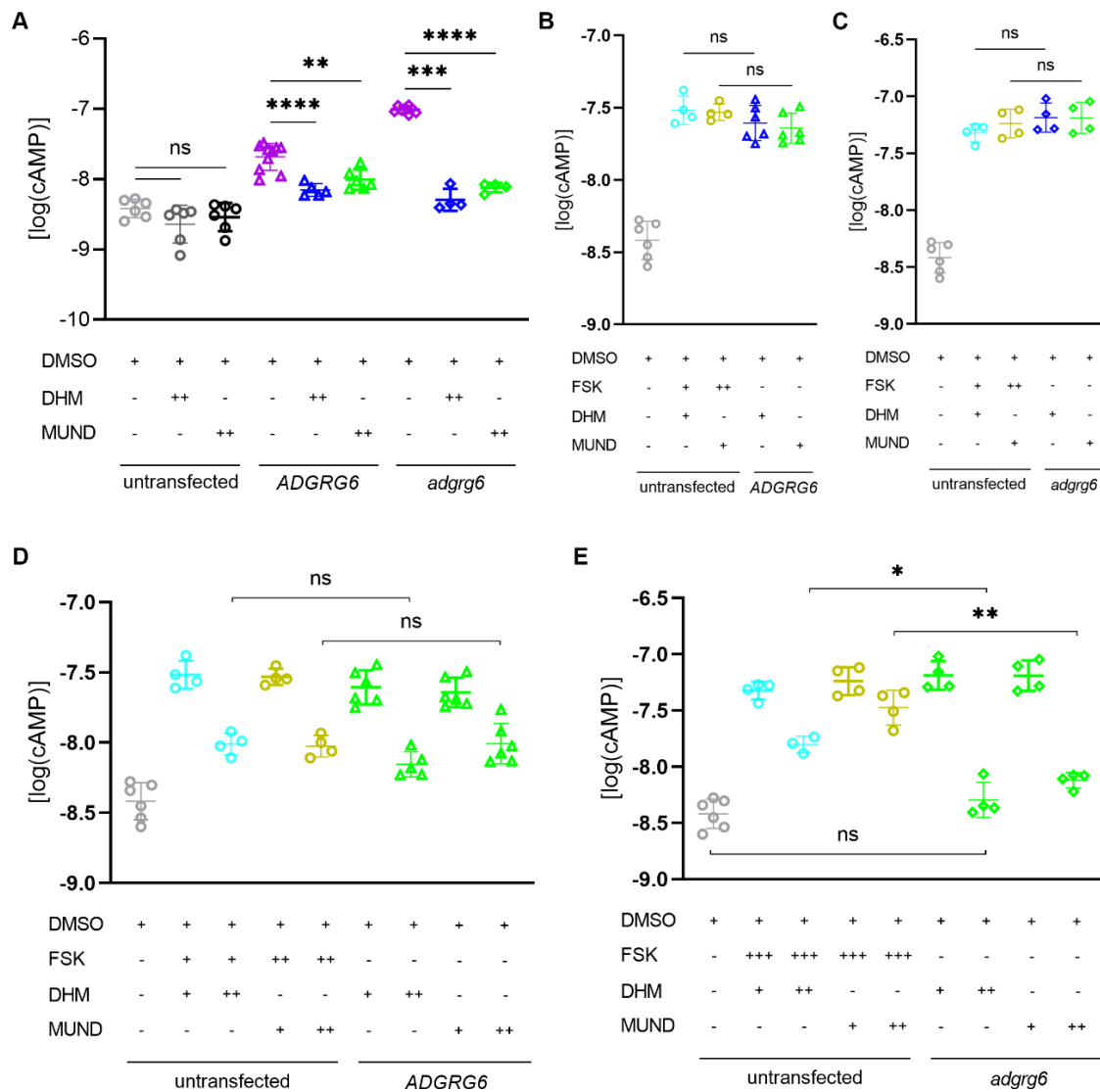


Figure 5.10 HEK293 cell cAMP response to treatment with low and high concentrations of known ADGRG1 antagonists.

Data in this figure largely overlaps with that in figure 5.11, including intracellular cAMP levels of HEK293 cells in response to treatment with the lowest and highest concentrations of ADGRG1 antagonists. Key: DMSO +, 0.1% (v/v); FSK +, 0.3 μ M; FSK ++, 0.35 μ M; FSK +++, 1 μ M; DHM +, $1 \times 10^{-8.68}$ M; DHM ++, $1 \times 10^{-4.18}$ M; MUND +, $1 \times 10^{-8.68}$ M; MUND ++, $1 \times 10^{-4.18}$ M. **(A)** DHM and MUND, administered at $1 \times 10^{-4.18}$ M, mediate a significant decrease in intracellular cAMP levels of HEK293 cells transfected with human or zebrafish *ADGRG6*, no such decrease is apparent in untransfected cells. **(B-C)** at the lowest DHM and MUND concentration tested, untransfected cells can be co-treated with 0.3-0.35 μ M forskolin to mimic cAMP levels in human *ADGRG6*-transfected cells (B) or 1 μ M forskolin to mimic cAMP levels in zebrafish *adgrg6*^{C804}-transfected cells (C). **(D)** at high DHM and MUND concentrations, no significant difference in cAMP levels is observed between cells transfected with human *ADGRG6* and untransfected cells co-treated with 0.3-0.35 μ M forskolin. **(E)** at high DHM and MUND concentrations, cAMP levels in zebrafish *adgrg6*^{C804}-transfected cells is significantly lower than in untransfected cells co-treated with 1 μ M forskolin. Response in DHM-treated *adgrg6*^{C804}-transfected cells is similar to untransfected DMSO-treated controls. Error bars: standard deviation. Statistical test: Brown-Forsythe and Welch ANOVA; ns, $p \geq 0.05$; *, $p 0.01-0.05$; **, $p 0.001-0.01$; ***, $p 0.0001-0.001$; ****, $p < 0.0001$.

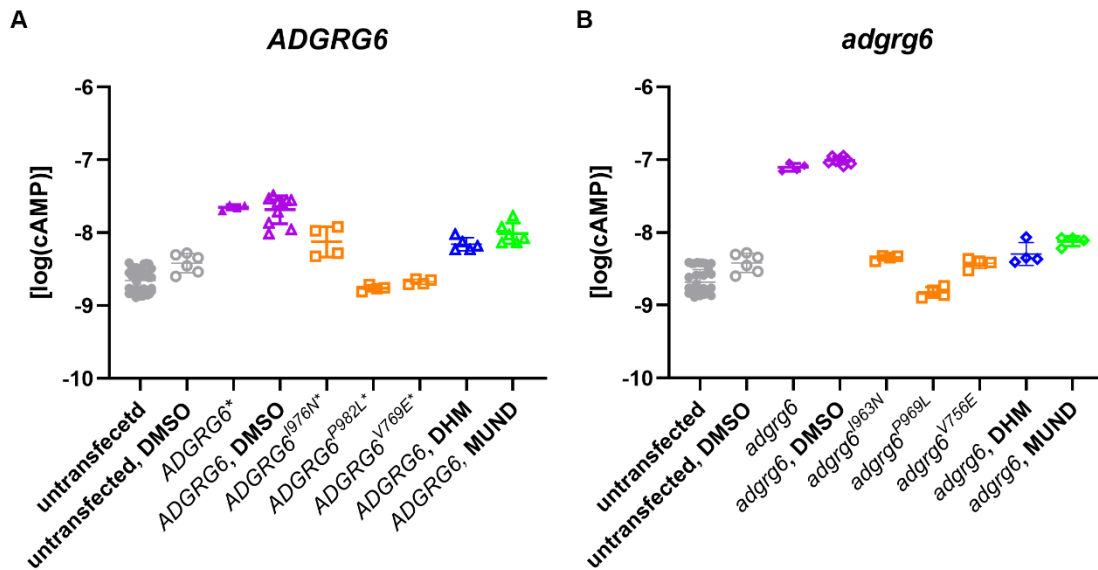


Figure 5.11 Preliminary comparison of cAMP levels in HEK293 cells transfected with various human and zebrafish *ADGRG6* alleles and wild-type-transfected cells treated with candidate receptor antagonists.

(A) cAMP levels detected in human wild-type *ADGRG6*-transfected cells treated with DHM or MUND is similar to those detected in cells transfected with the human equivalent of the zebrafish *tb233c* allele. Asterisk, data corresponds to 1% baculovirus dose for overnight transduction of HEK293 cells. Antagonists tested on cells transduced with 3% baculovirus dose. **(B)** cAMP levels detected in zebrafish *adgrg6*^{C804}-transfected cells treated with DHM or MUND is similar to those detected in cells transfected with the zebrafish *tb233c* allele and the zebrafish equivalent of the human pathogenic mutant allele. Baculovirus dose is consistent for this set (0.3%); however, assays were performed independently. Error bars: standard deviation.

5.2.7 Zebrafish treatment with dihydromunduletone

Cell responses to DHM and MUND treatment indicated that they could be acting as *Adgrg6* antagonists. As DHM displayed higher efficacy, it was tested in wild-type zebrafish larvae to determine if phenocopy of *adgrg6* mutants could be induced. Following compound treatment, inner ear and Schwann cell development was assessed to evaluate antagonistic effects, if any, of DHM. Observations are illustrated in figure 5.12.

A range of treatment conditions were trialled, including various doses of DHM and treatment times, which revealed largely no effect on otic *vcanb* expression. However, a single trial, in which DHM was administered at 3 μ M between 40-70 hpf, expression of *vcanb* was elevated in comparison to DMSO treated controls (figure 5.12A). This indicated that DHM could be interfering with morphogenesis of the semicircular canals, which is known to be regulated by *Adgrg6* (Geng *et al.*, 2013). Assessment of live embryos revealed that otic epithelial projections had not completely fused to form the pillars that compartmentalise the inner ear into three canals, as observed in DMSO-treated controls (figure 5.12B). However, ear and projection size was noticeably smaller than that of DMSO-treated *adgrg6* mutants, suggesting that DHM may interfere with overall development rather than key processes regulated particularly by *Adgrg6*. Developmental delay would also explain the elevated *vcanb* expression that was detected, as *versican* genes are known to be expressed during morphogenesis of the semicircular canals (Geng *et al.*, 2013). Any interference with development could result from DHM's known modulation of *ADGRG1* and *ADGRG5* that are expressed in various cell types (reviewed in Langenhan and Schöneberg, 2016). Examination of peripheral *mbp* expression following similar treatments revealed that expression of *mbp* was reduced in comparison to DMSO-treated wild type controls however, expression appeared stronger than that observed in *adgrg6* mutants. Furthermore, larvae appeared smaller than both DMSO-treated control larvae indicating that compound treatment had truncated overall growth.

The toxic effects of DHM are well documented throughout the literature (Stoveken *et al.*, 2016). Therefore, in the next set of experiments it was injected directly into the ear to avoid the likelihood of non-specific effects on larval development. Injections were trialled at various developmental stages: injections at 48 hpf were most suitable as it proved challenging to pierce the ear at later stages, without causing damage to larvae. Following injections with DMSO or DHM into the lumen of the left ear, larvae were incubated in growth media until 96 or 120 hpf for assessment of the ear phenotype (figure 5.12C). Injection with 2 nl of 3 mM DHM mediated an *adgrg6*-mutant-like phenotype in a subset of wild-type larvae; at least one otic projection failed to fuse with the lateral projection. Larvae that were fixed at 96 hpf for *in situ* hybridisation displayed *vcanb* expression in unfused projections. Comparatively, no impaired developmental phenotypes were observed in DMSO-injected larvae,

indicating that the injection procedure was not the cause of any phenotypes observed in DHM-treated larvae. The dorsal view also illustrated a slight swelling of the DHM-injected ear in comparison to DMSO-injected ears (figure 5.12C). However, this requires quantification of ear size and greater numbers for thorough and accurate assessment. This work is largely preliminary and requires further repeats to determine the consistency and reproducibility of the observations. Nahal Shahidan, a recent PhD student to join the Whitfield lab will be continuing this work forward.

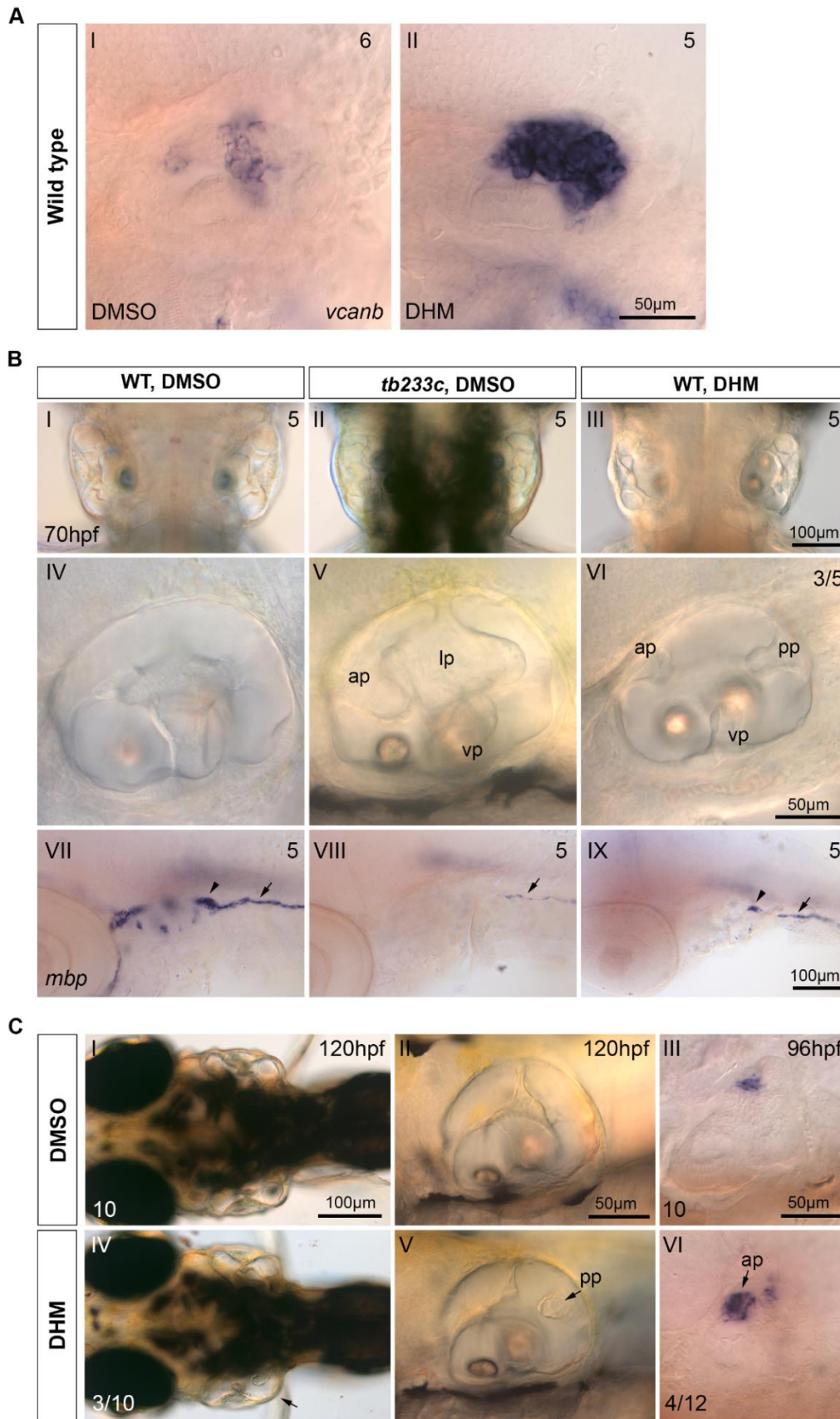


Figure 5.12 Zebrafish phenotypes associated with dihydromunduletone treatment.

(A) 3 µM DHM treatment of wild-type larvae in growth media between 40-70 hpf leads to elevated otic *vcanb* expression in comparison to DMSO-treated controls. Lateral images: anterior, left; posterior,

right. **(B)** 3 μ M DHM-treated wild-type larvae display unfused epithelial projections (VI); however, projection size is smaller than in *adgrg6^{tb233c}* mutants (V). Ear size of DHM-treated larvae (dorsal, III; lateral, VI) appears smaller than in DMSO-treated wild-type and *adgrg6^{tb233c}* mutant larvae, suggesting developmental delay. Dorsal images: anterior, top; posterior bottom. Expression of *mbp* mRNA (lateral view) in the peripheral nervous system (PNS) is downregulated in DHM-treated wild-type larvae, but appears stronger than in DMSO-treated *adgrg6^{tb233c}* mutants. Larval size visibility smaller. Abbreviations: ap, anterior projection; lp, lateral projection; pp, posterior projection; vp, ventral projection. Arrows mark *mbp* expression along posterior lateral line nerve (PLLn), arrowheads mark *mbp* expression around the PLL ganglion (PLLg). **(C)** injection with 2 nl of 3 mM DHM direct into the left ear at 48 hpf leads to unfused projections in three larvae at 120 hpf (dorsal, IV; lateral, V) whereas DMSO-injected controls develop normally (dorsal, I; lateral, II). DHM-injected ear is slightly swollen (arrow). Expression of *vcanb* is detected in unfused projections at 96 hpf. Images: anterior, left; posterior, right unless otherwise stated.

5.3 Discussion

In this chapter, cell-based cAMP assays were utilised to evaluate $G\alpha_s$ signalling pathway activity associated with various isoforms of human and zebrafish ADGRG6, in addition to that associated with candidate Adgrg6 modulators. Multiple cell transfection protocols are described, including baculoviral- and FuGENE-based methodologies, which can be utilised to express different isoforms of Adgrg6 and assess their localisation in the cell or to examine agonistic or antagonistic effects of candidate receptor modulators. Although transfection reagents were largely utilised at low concentrations that are unlikely to affect cell health, cell viability and development should be assessed in future work. Various trends in cAMP accumulation were detected with respect to human and zebrafish ADGRG6 isoforms and candidate antagonist treatments; however, compounds identified through the zebrafish phenotypic screen did not appear to mediate any agonistic effects on the receptor or its signalling pathway. The cAMP signalling assays did not appear to be optimised, as the agonistic effects of known Adgrg6 NTF ligands were also undetectable, and therefore any candidate agonists should not be overlooked based on the findings of this work.

Cellular cAMP levels revealed that mutations in both human and zebrafish ADGRG6 mediate a decrease in $G\alpha_s$ pathway activity. However, all zebrafish mutant constructs were examined with a cysteine at position 804, whereas the wild-type sequence contains a tryptophan at this position (Geng *et al.*, 2013; Demberg *et al.*, 2017). Therefore, it is difficult to make accurate conclusions based on the cell responses detected. In light of this finding, it is also interesting to note that a single base-pair change can generate isoforms that are associated with elevated $G\alpha_s$ pathway activity, as was the case in *adgrg6*^{C804}-expressing cells. Cysteine residues are known to form disulphide bridges (Moriguchi *et al.*, 2004; Marques *et al.*, 2010), and thus presence of a cysteine in the Adgrg6^{C804} isoform could alter protein structure. Multiple cysteines are present within the GAIN domain, including three between position 809 and the GPS cleavage site at 827, which could interact with the additional residue at 804 and induce altered folding of the Adgrg6 NTF. This in turn may influence non-covalent interaction between the N- and C-terminal fragments of Adgrg6 and increase exposure (Beliu *et al.*, 2021) or release (Araç *et al.*, 2012; Liebscher *et al.*, 2014) of the *stachel* sequence, which may underlie elevated receptor activation that was detected in terms of cAMP accumulation. Alternatively, flexibility of the NTF, which has recently been shown to adopt an open and closed conformation (Leon *et al.*, 2020) could also be affected and influence signalling. However, these hypotheses should be treated with caution as the equivalent human receptor isoform appears to behave differently and any responses could result from differences in how well the cells tolerate each construct or receptor isoform.

Although some of the above propositions could account for elevated cAMP accumulation detected in *adgrg6*^{C804} expressing cells, receptor localisation could also influence signalling activity. Expression of the C-terminal GFP-tagged receptor revealed widespread localisation throughout HEK293 cells and little at the cell membrane whereas both human and zebrafish tryptophan isoforms localised strongly at the membrane. Taken together with cAMP accumulation, this observation suggests that Adgrg6 can activate the G α_s pathway without complete integration at the cell membrane. Alternatively, it can be proposed that even weak localisation at the membrane is sufficient to drastically elevate cAMP accumulation in cells expressing *adgrg6*^{C804}, as a result of the amino acid substitution. If so, weak expression at the membrane can be taken as an indication that transfected cells are unable to tolerate high levels of receptor expression due to its constitutive activity. It is therefore difficult to assess whether the trends in cAMP accumulation observed are a consequence of altered function or localisation of the receptor.

In order to make accurate conclusions, cAMP assays should be repeated with cells expressing GFP-tagged constructs to confirm that the GFP tag does not influence receptor signalling. Alternatively, an Adgrg6 antibody could be utilised for a more accurate illustration of receptor expression in cells transfected with untagged *adgrg6* constructs. Importantly, expression and activity of all zebrafish Adgrg6 isoforms should be examined with the wild-type DNA template that codes for a tryptophan at position 804. Following this work, evaluation of overall receptor expression by Western Blot or flow cytometry is necessary to determine if trends in G α_s pathway activity, associated with each receptor isoform, are explained by the quantity of receptor expressed or its signalling capacity.

Examination of candidate Adgrg6 modulators in cAMP assays revealed that DHM and MUND mediate a decrease in G α_s pathway activity in both human and zebrafish *ADGRG6*-expressing cells. This response is similar to that observed against *ADGRG1*-expressing cells (Stoveken *et al.*, 2016). However, the response only appeared receptor-specific in zebrafish *adgrg6*-expressing cells as mimicking cellular cAMP levels of *ADGRG6*-expressing cells with forskolin revealed a similar response to compound treatments, indicating that activity was likely dependent on another receptor or an intracellular G α_s pathway component. Furthermore, preliminary work in zebrafish revealed that direct injections of DHM into the wild type larval ear was sufficient to mediate partial phenocopy of *adgrg6* zebrafish mutants. However, it is important to consider that, although the response in *adgrg6*-expressing cells appears receptor-specific, cells were expressing the C804 allelic form, which appears to behave differently to the wild-type W804 form. DHM may therefore mediate effects independent of receptor expression and in the case of zebrafish injections, act non-specifically to inhibit the intracellular G α_s pathway. Use of *adgrg6*^{C804} may also explain why no agonistic effects of known Adgrg6 ligands and candidate Adgrg6 agonists were detected. To determine validity of results, assays need to

be repeated with cells expressing the Adgrg6^{W804} isoform. Furthermore, it is necessary to confirm that any trends in cellular cAMP responses do not result from compound toxicity. Cell confluency can be taken as a simple measure of cell health for these purposes.

In addition, effectiveness of cell-based cAMP assays could be improved further as an agonistic-like response was not detected in the presence of proposed Adgrg6 modulators such as collagen IV and prion. Although this outcome raises concerns over such molecules as potential Adgrg6 agonists, it is important to consider that the cell-based system may be sub-optimal in capturing the multimodal nature of Adgrg6 activity. Evidence suggests that the mechanosensitive Adgrg6 NTF is integral in regulating receptor activity through interactions with ECM ligands (Paavola *et al.*, 2014; Petersen *et al.*, 2015) that are thought to facilitate release of the *stachel* peptide, which self-activates Adgrg6 (Araç *et al.*, 2012; Liebscher *et al.*, 2014). However, such complex interactive environments are difficult to replicate in *in vitro* cultures. Petersen *et al.* (2015) have highlighted previously that agonistic effects of laminin-211 are not detectable under standard incubation conditions, but in fact require the application of mechanical force in form of sample vibration. A similar approach could be utilised to test candidate agonist compounds in combination with NTF ligands; however, the cAMP assay requires optimisation to first illustrate individual agonist effects of NTF ligands. The above limitations could also be regarded as limitations of the HEK293 cell system, which may not replicate Schwann cell behaviour. To improve the relevance and translatability of such assays in future, they could be performed on cultured Schwann cells.

Alternatively, the assay could be simplified somewhat by testing candidate agonists against a modified receptor form comprising of the CTF alone. This in theory would remove the inhibitory effect of the NTF on Adgrg6 signalling and may in turn enable better detection of agonist-like responses in the presence of shortlisted compounds such as ebastine. Although, any compound that interact directly with the NTF would be rendered ineffective in this system.

It is also important to consider that Adgrg6 activity may not be restricted to the G α_s signalling pathway. Lizano *et al.* (2020) have provided evidence for G $\alpha_{q/11}$ or G $\alpha_{12/13}$ activity in association with the human ADGRG6. Any potential agonistic effects, of shortlisted compounds, on these particular G protein pathways have not been captured in the current study and therefore the compounds should not be overlooked. Interestingly, Lizano *et al.* (2020) utilised a synthetic ADGRG6 isoform containing an enterokinase substrate in place of the adhesive NTF domains. Therefore, no mechanical stimuli was required to induce release of the *stachel* peptide agonist, but instead the simple addition of enterokinase to cleave the NTF. They performed cAMP and Ca²⁺ mobilisation assays in the presence and absence of G $\alpha_{q/11}$ inhibitor to evaluate activity of various G protein pathways. This approach could

be valuable in assessing the effects of candidate Adgrg6 modulators identified in the current study. Alternatively, assays are available in which direct coupling of mini-G proteins, which mimic behaviour of heterotrimeric G proteins, can be assessed for a more direct functional readout (Carpenter and Tate, 2016; Nehmé *et al.*, 2017).

Chapter 6.

Synopsis

6.1 Summary of results

Adgrg6 is a key developmental regulator of semicircular canal morphogenesis in zebrafish and myelination of the PNS by Schwann cells in various species including humans and zebrafish. These roles have largely been elucidated from the study of Adgrg6 zebrafish and mouse mutants (Monk *et al.*, 2009, 2011; Geng *et al.*, 2013), in addition to clinical cases of pathogenic mutation in humans that have presented with lethal developmental phenotypes (Ravenscroft *et al.*, 2015). Although phenotypes associated with *adgrg6* zebrafish mutants have been illustrated in previous work, this thesis presents a further examination of Schwann cell development in *adgrg6^{tb233c}* mutants (chapter 3) and illustrates an effective small-molecule screening platform through which candidate receptor modulators can be identified (chapter 4). Furthermore, insight surrounding receptor expression and its signalling activity is provided, which can be utilised to evaluate severity of mutations and assess the direct effects, if any, of candidate modulators (chapter 5).

In chapter 3, study of *adgrg6* mRNA expression in the wild type and multiple *adgrg6* mutants, including the truncating *fr24* allele, revealed otic expression and, for the first time, Schwann cell localised expression along the posterior lateral line in *fr24*, illustrating that the transcript is not degraded by nonsense-mediated mRNA decay in this mutant. These observations were similar to those published previously for alternative *adgrg6* mutants (Monk and Talbot, 2009; Geng *et al.*, 2013). Expression patterns of myelination genes, including *oct6*, *krox20*, *cldnk* and *mbp*, were assessed to reveal that all were down-regulated in hypomorphic mutants. Such phenotypes likely result from reduced Gα_s pathway activity associated with human and zebrafish *ADGRG6* mutations (chapter 5). Although expression of all myelination genes was detected in Schwann cells along the lateral line in wild type larvae, expression was differentially reduced in mutants illustrating variability in cell development. The reduction in mRNA expression of *mbp* and other myelination genes had no effect on gross neuronal anatomy in *adgrg6* mutants, illustrating that the framework to sense and respond to stimuli remains in place. However, the reduced myelination could manifest in a reduction in efficiency of signal transmission across neurons. This is the case in *adgrg6^{fr24}* mutants (work by Francesca De Faveri, Marcotti lab, University of Sheffield); however, further work is needed to determine if any such phenotypes manifest in hypomorphic mutants. Thorough phenotypic characterisation of the *tb233c* hypomorphic allele highlighted that although expression of various

genes was reduced, the most consistent and robust pattern of all was that of *mbp*, which could be utilised to screen for small molecule *Adgrg6* modulators.

Trialling various pharmacological assay conditions against the *mbp* phenotype in *adgrg6* hypomorphic mutants revealed that compound efficacy, of known *Adgrg6* pathway hits, could be improved beyond that observed under previously utilised conditions (chapter 4). The *mbp* expression assay was optimised to target developmental onset of *mbp* expression, which may underlie the overall increase in its effectiveness. In fact, a selection of compounds, including mevastatin, cyproterone acetate and FPL 64176, which previously had no effect on *mbp* expression in mutants, were able to mediate an increase in expression at the PLLg under optimal assay conditions.

LOPAC library compounds were initially screened against the otic *vcanb* phenotype in *adgrg6* mutants before hits were tested in the counter-screening *mbp* assay to reveal *Adgrg6* pathway-specific hits (chapter 4). Comparison of otic *vcanb* scores for compounds that overlapped with the Spectrum or Tocris libraries, screened by the Whitfield lab, revealed that compound performance was largely similar as over 90% of scores either matched or showed a difference of only 1-2 points. Overall, 48 hits mediated a decrease in *vcanb* expression, of which 17 also induced an increase in *mbp* expression in *adgrg6* hypomorphic mutants. The latter class included 12 novel compounds, including those that had shown no effects on *mbp* expression in previous screens or those tested for the first time. A review of their known targets illustrate potential proteins that may interact with the *Adgrg6* signalling pathway, including key GPCR pathway components such as phosphodiesterase and kinase enzymes. Calcium channel modulators, from the dihydropyridine cluster, were consistently identified as *Adgrg6* pathway hits illustrating a potentially key role of calcium signalling in the *Adgrg6* pathway, which has also been proposed following the detection of $G\alpha_{q/11}$ and $G\alpha_{12/13}$ activity in association with synthetic ADGRG6 signalling (Lizano, Hayes and Willard, 2020).

Testing compounds on multiple allelic mutants such as the nonsense *fr24* mutants, predicted to express an NTF-truncated *Adgrg6*, can reveal compounds likely to interact with the receptor as those that are unable to rescue the ear or myelination phenotypes (Diamantopoulou *et al.*, 2019). However, in this study no compounds other than forskolin mediated a rescue of the *vcanb* phenotype indicating that the majority were potential agonists, which is highly unlikely. Various compounds likely to mediate phenotypic rescue through other mechanisms, including calcium channel modulators and GPCR pathway modulators, were therefore overlooked at this stage to examine a shortlist of likely agonists. This included ebastine, ivermectin and carapin, which all mediated partial rescue of *mbp* expression in the stronger missense (*tk256a*) allelic mutants. However, testing these compounds in

cell-based assays (chapter 5) failed to illustrate an *Adgrg6* agonistic response. This may result from suboptimal assay conditions, as agonistic effects of known ligands was also not detected.

On the other hand, candidate antagonists were shown to mediate a decrease in cAMP accumulation, similar to that observed in cells expressing human or zebrafish *ADGRG6* mutant constructs (chapter 5). Preliminary work in zebrafish revealed potential manipulation of the *Adgrg6* pathway as drug injection of DHM in particular disrupted fusion of individual otic epithelial projections during semicircular canal morphogenesis in wild-type larvae. However, it is unclear if this response is receptor-specific or dependent on *Adgrg6* pathway components that may be common to other GPCR signalling pathways, as somewhat similar responses were detected in untransfected cells. Cells expressing zebrafish *adgrg6* displayed a partially receptor-dependent response, however, the particular transcript expressed contained a single DNA base change from the naturally occurring wild type (Geng *et al.*, 2013). This alteration results in an amino acid substitution, W804C, which affected receptor expression and significantly elevated signalling activity. Therefore, validation of results requires repeats with the naturally occurring wild-type form in future work.

6.2 Combined zebrafish and cell approach

This study adopted a combined approach to small molecule screening, which included initially testing compounds against zebrafish *adgrg6* mutant phenotypes followed by testing the specificity of hits in cell-based assays. Individually, both approaches have their own limitations. Traditionally, phenotypic strategies can fail to conclusively illustrate whether a compound induces the desired restorative effect by modulating a particular disease-associated protein target. Alternatively, cell-based assays can illustrate direct compound modulation of a single protein; however, they fail to capture pharmacokinetic properties that determine if a compound will be therapeutic *in vivo*. In the case of adhesion GPCRs, target-based *in vitro* approaches present further difficulties as the adhesive ECM environment *in vivo* is challenging to replicate. Therefore, as highlighted in this study and multiple others (Liebscher *et al.*, 2014; Bradley *et al.*, 2019; Diamantopoulou *et al.*, 2019), zebrafish present a valuable system in which compounds or biological ligands can be tested against aGPCRs in their natural physiological context. Moreover, testing compounds across multiple zebrafish alleles can reveal those that likely act as receptor agonists, an approach that is growing in popularity (Bradley *et al.*, 2019; Diamantopoulou *et al.*, 2019).

The above strategy has proved successful following the recent identification of apomorphine as a potential *Adgrg6* agonist (Bradley *et al.*, 2019). Initial screening on multiple zebrafish allelic mutants revealed that apomorphine mediated an increase in peripheral GFP-tagged Mbp expression in *adgrg6* hypomorphs that was independent of *stachel* activation. Subsequently, it was shown to elevate cAMP

specifically in cells expressing the receptor. Work in the current study has shown apomorphine to mediate partial rescue of both ear and myelination phenotypes in *adgrg6*^{tb233c} mutants (chapter 4), similar to more efficacious compounds, including ebastine and ivermectin, that may also act as Adgrg6 agonists. Cell-based assays failed to conclusively highlight compound agonism for Adgrg6, although this was likely due to suboptimal experimental conditions as agonistic effects of known ligands was also not detected.

A further advantage of phenotypic screening, highlighted in this study, is that identification of hits with known targets can reveal alternative signalling pathways and molecules that may be associated with the protein of interest, in this case Adgrg6. Consistent identification of calcium channel modulators from the dihydropyridine cluster, corroborating previous work (Diamantopoulou *et al.*, 2019), illustrated an underlying importance of calcium signalling in Adgrg6 pathway activity, in agreement with the findings of Lizano *et al.* (2020), who illustrated association of ADGRG6 activity with the $G\alpha_{q/11}$ and $G\alpha_{12/13}$ pathways.

6.3 Relevance and future directions

Although no direct compound agonism or antagonism for Adgrg6 has conclusively been shown, candidate receptor modulators have been shortlisted that may hold such potential. This includes compounds that have been identified previously such as ivermectin, carapin (Diamantopoulou *et al.*, 2019) and DHM (Stoveken *et al.*, 2016), in addition to novel hits such as ebastine that could have significant research and therapeutic benefits. The crystal structure of the Adgrg6 ECR has been elucidated (Leon *et al.*, 2020) but, the crystal structure of its transmembrane domain and intracellular region (ICR) is not yet known. Shortlisted compounds may provide useful tools to stabilise and purify the receptor, in its *in vivo* active or inactive state, and enable accurate characterisation of its crystal structure. Alternatively, such compounds may hold therapeutic potential to be used as treatments against diseases that are associated with *ADGRG6* gene variants or in regenerative medicine, for example remyelination following nerve injury or to treat peripheral demyelinating diseases such as Charcot Marie Tooth disease. Translational work is underway in collaboration with the Marcotti lab (University of Sheffield) to determine if Adgrg6 pathway hits such as IBMX and forskolin, which increase peripheral *mbp* expression in *adgrg6* mutants, can restore neuronal signalling efficiency in *adgrg6*^{fr24} mutants.

A novel approach that could provide further support for the action of ebastine or other candidate compounds as Adgrg6 agonists is to determine coupling of mini-G proteins to Adgrg6 following treatment (Carpenter and Tate, 2016; Nehmé *et al.*, 2017; Baxendale *et al.*, 2021). Such experiments would provide a direct measure of Adgrg6 activity following small molecule treatments, as opposed

to the detection of downstream effector molecules, such as cAMP, that can be modulated by activity of adenylyl cyclase or phosphodiesterases (Baxendale *et al.*, 2021). It is also important to consider that adhesion GPCRs are mechanosensitive in nature and therefore may require application of mechanical stimuli, in the experimental setup, to mimic the *in vivo* environment and receptor behaviour. Various groups are beginning to cross-collaborate with physics and engineering experts to design equipment better suited to recapture these conditions *in vitro*.

Importantly, the list of candidate Adgrg6 modulators has been expanded by the work conducted in this study. Further examination of compound structures may reveal key motifs that are shared among likely ligands and provide insight to test further compounds with similar structures. This work is already underway as Nahal Shahidan (Whitfield lab, PhD) is using computational strategies to rank compounds from additional libraries based on structural similarity with candidate Adgrg6 modulators that have been identified to date.

For the first time, *in vitro* examination of $G\alpha_s$ pathway activity associated with expression of various human and zebrafish *ADGRG6* alleles revealed variants that associated with reduced and elevated cAMP levels. In particular, the zebrafish C804 wild type isoform appeared overactive in comparison to the naturally occurring wild type. A zebrafish variant line expressing this particular isoform may reveal potential phenotypes that result from Adgrg6 over activation and could potentially be utilised in antagonist screening assays.

Generation of an Adgrg6 stabilised receptor (StaR), in collaboration with Sosei Heptares, offers an alternative approach to tackle Adgrg6 drug discovery. Thermostabilising mutations can be induced that increase protein expression and its conformational stability to enable improved purification of the receptor for determination of its remaining crystal structure. This target-based strategy would support structure based drug discovery by revealing potential binding pockets that can be subject to virtual screening approaches before testing candidate compounds in cell or zebrafish assays to determine potential agonism for Adgrg6 as performed in the current study.

6.4 Concluding remarks

This study illustrates the value of zebrafish as a model system to screen small molecule libraries in medium to high throughput. The small size of embryos and their ability to absorb compounds in growth media is amenable for conducting experiments in a 96-well assay plate. Homozygous *adgrg6* mutants are adult viable therefore 100% homozygous mutant embryos can be obtained for screening purposes. Furthermore, zebrafish hold value in screening for aGPCR modulators *in vivo* as mimicking mechanosensing behaviour of aGPCRs remains a challenge *in vitro*.

The transcripts examined in this study, including *vcanb* and *mbp*, exhibit contrasting expression in *adgrg6* mutants, with the former showing persistent expression whereas the latter is downregulated. Their collective assessment is valuable in revealing Adgrg6 pathway specific modulators and those acting as nonspecific hits that act to downregulate gene expression. Although further work is needed to confirm whether the former class directly interact with Adgrg6, a subset were shown to elevate *mbp* expression in weak and strong missense mutant alleles whilst having no effect on *vcanb* in early truncating *fr24* allelic mutants suggesting that they are the most efficacious candidate receptor modulators. In future, testing such compounds in optimised cell-based signalling assays tailored to detect aGPCR signalling could reveal potential agonism for Adgrg6.

In this study, expression and signalling activity associated with various different human and zebrafish ADGRG6 isoforms was highlighted, revealing that mutations can not only affect Gα_s pathway activity but also receptor localisation at the cell membrane. The next step is to confirm whether similar patterns of expression are observed *in vivo* across various *adgrg6* allelic mutants.

Although direct compound modulation of human or zebrafish ADGRG6 was not shown in this study, our screening pipeline offers a powerful approach to identify promising candidates for further investigation and as starting points in virtual screening and *in silico* approaches. Such compounds may hold potential to treat ADGRG6-related diseases or reveal other structurally similar compounds with higher therapeutic potential. Moreover, such compounds may offer value as biological tools to manipulate the receptor's intracellular signalling pathway, similar to cyclopamine for the Hh pathway or SU5402 for the Fgf pathway (Baxendale and Whitfield, 2016), to further study the fundamental roles of Adgrg6 activity in developmental and physiological processes without blocking its expression altogether.

Bibliography

- Agostino, M. and Pohl, S. Ö. G. (2020) 'The structural biology of canonical Wnt signalling', *Biochemical Society Transactions*, 48(4), pp. 1765–1780. doi: 10.1042/BST20200243.
- Agrup, C., Gleeson, M. and Rudge, P. (2007) 'The inner ear and the neurologist', *Journal of Neurology, Neurosurgery & Psychiatry*, 78(2), pp. 114–122. doi: 10.1136/jnnp.2006.092064.
- Almeida, R. G. *et al.* (2011) 'Individual axons regulate the myelinating potential of single oligodendrocytes in vivo', *Development*, 138(20), pp. 4443–4450. doi: 10.1242/dev.071001.
- Almeida, R. G. *et al.* (2018) 'Myelination of Neuronal Cell Bodies when Myelin Supply Exceeds Axonal Demand', *Current Biology*. Elsevier Ltd., 28(8), pp. 1296–1305.e5. doi: 10.1016/j.cub.2018.02.068.
- Andersson-Sjöland, A. *et al.* (2014) 'Versican in inflammation and tissue remodeling: The impact on lung disorders', *Glycobiology*, 25(3), pp. 243–251. doi: 10.1093/glycob/cwu120.
- Araç, D. *et al.* (2012) 'A novel evolutionarily conserved domain of cell-adhesion GPCRs mediates autoproteolysis', *EMBO Journal*, 31(6), pp. 1364–1378. doi: 10.1038/emboj.2012.26.
- Arthur-Farraj, P. *et al.* (2011) 'Mouse schwann cells need both NRG1 and cyclic AMP to myelinate', *Glia*, 59(5), pp. 720–733. doi: 10.1002/glia.21144.
- Baraban, M., Koudelka, S. and Lyons, D. A. (2018) 'Ca²⁺ activity signatures of myelin sheath formation and growth in vivo', *Nature Neuroscience*, 21(1), pp. 19–25. doi: 10.1038/s41593-017-0040-x.
- Baraban, S. C. *et al.* (2005) 'Pentylentetrazole induced changes in zebrafish behavior, neural activity and c-fos expression', *Neuroscience*, 131(3), pp. 759–768. doi: 10.1016/j.neuroscience.2004.11.031.
- Basith, S. *et al.* (2018) 'Exploring G protein-coupled receptors (GPCRs) ligand space via cheminformatics approaches: Impact on rational drug design', *Frontiers in Pharmacology*, 9(MAR), pp. 1–26. doi: 10.3389/fphar.2018.00128.
- Baxendale, S. *et al.* (2012) 'Identification of compounds with anti-convulsant properties in a zebrafish model of epileptic seizures', *DMM Disease Models and Mechanisms*, 5(6), pp. 773–784. doi: 10.1242/dmm.010090.
- Baxendale, S. *et al.* (2021) 'The adhesion GPCR Adgrg6 (Gpr126): Insights from the zebrafish model', *Genesis*, 6(February), pp. 1–15. doi: 10.1002/dvg.23417.

- Baxendale, S., van Eeden, F. and Wilkinson, R. (2017) 'The Power of Zebrafish in personalised medicine', *Advances in Experimental Medicine and Biology*, 1007, pp. 179–197. doi: 10.1007/978-3-319-60733-7_10.
- Baxendale, S. and Whitfield, T. T. (2016) 'Methods to study the development, anatomy, and function of the zebrafish inner ear across the life course', in *The Zebrafish: Cellular and Developmental Biology Part B 4th Edition*, pp. 165–209. doi: 10.1016/bs.mcb.2016.02.007.
- Beliu, G. *et al.* (2021) 'Article Tethered agonist exposure in intact adhesion / class B2 GPCRs through intrinsic structural flexibility of the GAIN domain Article Tethered agonist exposure in intact adhesion / class B2 GPCRs through intrinsic structural flexibility of the GAIN do', pp. 1–17. doi: 10.1016/j.molcel.2020.12.042.
- Di Bello, E. *et al.* (2020) 'The Innovative Potential of Statins in Cancer: New Targets for New Therapies', *Frontiers in Chemistry*, 8(June), pp. 1–9. doi: 10.3389/fchem.2020.00516.
- Berghmans, S. *et al.* (2008) 'Zebrafish based assays for the assessment of cardiac, visual and gut function - potential safety screens for early drug discovery', *Journal of Pharmacological and Toxicological Methods*, 58(1), pp. 59–68. doi: 10.1016/j.vascn.2008.05.130.
- Berti, C. *et al.* (2011) 'Non-redundant function of dystroglycan and β 1 integrins in radial sorting of axons', *Development*, 138(18), pp. 4025–4037. doi: 10.1242/dev.065490.
- Bjarnadóttir, T. K. *et al.* (2004) 'The human and mouse repertoire of the adhesion family of G-protein-coupled receptors', *Genomics*, 84(1), pp. 23–33. doi: 10.1016/j.ygeno.2003.12.004.
- Bjarnadóttir, T. K. *et al.* (2006) 'Identification of novel splice variants of Adhesion G protein-coupled receptors', *Gene*, 387(1–2), pp. 38–48. doi: 10.1016/j.gene.2006.07.039.
- Blanc, G. *et al.* (2007) 'Insights into how CUB domains can exert specific functions while sharing a common fold: Conserved and specific features of the CUB1 domain contribute to the molecular basis of procollagen C-proteinase enhancer-1 activity', *Journal of Biological Chemistry*. © 2007 ASBMB. Currently published by Elsevier Inc; originally published by American Society for Biochemistry and Molecular Biology., 282(23), pp. 16924–16933. doi: 10.1074/jbc.M701610200.
- Bourrachot, S., Simon, O. and Gilbin, R. (2008) 'The effects of waterborne uranium on the hatching success, development, and survival of early life stages of zebrafish (*Danio rerio*)', *Aquatic Toxicology*, 90(1), pp. 29–36. doi: 10.1016/j.aquatox.2008.07.013.
- Boyden, S. E. *et al.* (2016) 'Vibratory Urticaria Associated with a Missense Variant in ADGRE2', *New England Journal of Medicine*, 374(7), pp. 656–663. doi: 10.1056/nejmoa1500611.

- Bradley, E. C. *et al.* (2019) 'In vivo identification of small molecules mediating gpr126/adgrg6 signaling during schwann cell development', *Annals of the New York Academy of Sciences*, 1456(1), pp. 44–63. doi: 10.1111/nyas.14233.
- Bremer, J., Skinner, J. and Granato, M. (2017) 'A small molecule screen identifies in vivo modulators of peripheral nerve regeneration in zebrafish', *PLoS ONE*, 12(6), pp. 1–17. doi: 10.1371/journal.pone.0178854.
- Brösamle, C. and Halpern, M. E. (2002) 'Characterization of myelination in the developing zebrafish', *Glia*, 39(1), pp. 47–57. doi: 10.1002/glia.10088.
- Van den Bulck, K. *et al.* (2011) 'Zebrafish developmental toxicity assay: A fishy solution to reproductive toxicity screening, or just a red herring?', *Reproductive Toxicology*, 32(2), pp. 213–219. doi: 10.1016/j.reprotox.2011.06.119.
- Bunge, M. B. and Bunge, R. P. (1986) 'Linkage between Schwann Cell Extracellular Matrix Production and Ensheathment Function', *Annals of the New York Academy of Sciences*, 486(1 Neurofibromat), pp. 241–247. doi: 10.1111/j.1749-6632.1986.tb48077.x.
- Bunge, R. P., Bunge, M. B. and Eldridge, C. F. (1986) 'Linkage between axonal ensheathment and basal lamina production by Schwann cells', *Annual Review of Neuroscience*, VOL. 9, pp. 305–328. doi: 10.1146/annurev.neuro.9.1.305.
- Carney, T. J. *et al.* (2010) 'Genetic analysis of fin development in zebrafish identifies furin and Hemicentin1 as potential novel fraser syndrome disease genes', *PLoS Genetics*, 6(4). doi: 10.1371/journal.pgen.1000907.
- Carpenter, B. and Tate, C. G. (2016) 'Engineering a minimal G protein to facilitate crystallisation of G protein-coupled receptors in their active conformation', 29(12), pp. 583–593. doi: 10.1093/protein/gzw049.
- Cazorla-Vázquez, S. and Engel, F. B. (2018) 'Adhesion GPCRs in kidney development and disease', *Frontiers in Cell and Developmental Biology*, 6(FEB), pp. 1–18. doi: 10.3389/fcell.2018.00009.
- Cheli, V. T. *et al.* (2016) 'Conditional deletion of the L-type calcium channel cav1.2 in oligodendrocyte progenitor cells affects postnatal myelination in mice', *Journal of Neuroscience*, 36(42), pp. 10853–10869. doi: 10.1523/JNEUROSCI.1770-16.2016.
- Chen, Z. L. and Strickland, S. (2003) 'Laminin γ 1 is critical for Schwann cell differentiation, axon myelination, and regeneration in the peripheral nerve', *Journal of Cell Biology*, 163(4), pp. 889–899. doi: 10.1083/jcb.200307068.

- Chiu, L. L. *et al.* (2008) 'Using the zebrafish lateral line to screen for ototoxicity', *JARO - Journal of the Association for Research in Otolaryngology*, 9(2), pp. 178–190. doi: 10.1007/s10162-008-0118-y.
- Cornet, C., Di Donato, V. and Terriente, J. (2018) 'Combining Zebrafish and CRISPR/Cas9: Toward a more efficient drug discovery pipeline', *Frontiers in Pharmacology*, 9(JUL), pp. 1–11. doi: 10.3389/fphar.2018.00703.
- Cree, B. A. C. *et al.* (2018) 'Clemastine rescues myelination defects and promotes functional recovery in hypoxic brain injury', *Brain*, 141(1), pp. 85–98. doi: 10.1093/brain/awx312.
- D'Rozario, M., Monk, K. R. and Petersen, S. C. (2017) *Analysis of myelinated axon formation in zebrafish*, *Methods in Cell Biology*. Elsevier Ltd. doi: 10.1016/bs.mcb.2016.08.001.
- Dallan, I. *et al.* (2008) 'Bilateral, isolated, lateral semicircular canal malformation without hearing loss', *The Journal of Laryngology & Otology*, 122(08), pp. 858–860. doi: 10.1017/S0022215108002740.
- Demberg, L. M. *et al.* (2015) 'Identification of the tethered peptide agonist of the adhesion G protein-coupled receptor GPR64/ADGRG2', *Biochemical and Biophysical Research Communications*, 464(3), pp. 743–747. doi: 10.1016/j.bbrc.2015.07.020.
- Demberg, L. M. *et al.* (2017) 'Activation of adhesion G protein-coupled receptors: Agonist specificity of Stachel sequence-derived peptides', *Journal of Biological Chemistry*, 292(11), pp. 4383–4394. doi: 10.1074/jbc.M116.763656.
- Detrait, E. *et al.* (1999) 'Expression of integrins by murine MSC80 Schwann cell line: Relationship to cell adhesion and migration', *Neuroscience Letters*, 267(1), pp. 49–52. doi: 10.1016/S0304-3940(99)00331-6.
- Diamantopoulou, E. *et al.* (2019) 'Identification of compounds that rescue otic and myelination defects in the zebrafish *adgrg6* (*gpr126*) mutant', *eLife*, 8. doi: 10.7554/eLife.44889.
- Diekmann, H. and Hill, A. (2013) 'ADMETox in zebrafish', *Drug Discovery Today: Disease Models*. Elsevier Ltd, 10(1), pp. e31–e35. doi: 10.1016/j.ddmod.2012.02.005.
- Doddrell, R. D. S. *et al.* (2012) 'Regulation of Schwann cell differentiation and proliferation by the Pax-3 transcription factor', *Glia*, 60(9), pp. 1269–1278. doi: 10.1002/glia.22346.
- Dong, Z. *et al.* (1995) 'Neu differentiation factor is a neuron-glia signal and regulates survival, proliferation, and maturation of rat schwann cell precursors', *Neuron*, 15(3), pp. 585–596. doi: 10.1016/0896-6273(95)90147-7.

- Dutton, K. A. *et al.* (2001) 'Zebrafish colourless encodes sox10 and specifies non-ectomesenchymal neural crest fates', *Development*, 128(21), pp. 4113–4125. doi: 10.1242/dev.128.21.4113.
- Early, J. J. *et al.* (2018) 'An automated high-resolution in vivo screen in Zebrafish to identify chemical regulators of myelination', *eLife*, 7, pp. 1–31. doi: 10.7554/eLife.35136.
- Eichstaedt, C. A. *et al.* (2017) 'Evidence of Early-Stage Selection on EPAS1 and GPR126 Genes in Andean High Altitude Populations', *Scientific Reports*, 7(1), pp. 1–9. doi: 10.1038/s41598-017-13382-4.
- Feltri, M. L. *et al.* (2002) 'Conditional disruption of β 1 integrin in Schwann cells impedes interactions with axons', *Journal of Cell Biology*, 156(1), pp. 199–209. doi: 10.1083/jcb.200109021.
- Fields, R. D. *et al.* (2017) 'Cholinergic signaling in myelination', *Glia*, 65(5), pp. 687–698. doi: 10.1002/glia.23101.
- Folts, C. J. *et al.* (2019) 'Adhesion G Protein-Coupled Receptors as Drug Targets for Neurological Diseases', *Trends in Pharmacological Sciences*. Elsevier Ltd, 40(4), pp. 278–293. doi: 10.1016/j.tips.2019.02.003.
- Franz, T. (1993) 'The Splotch (Sp1H) and Splotch-delayed (Spd) alleles: differential phenotypic effects on neural crest and limb musculature', *Anatomy and Embryology*, 187(4), pp. 371–377. doi: 10.1007/BF00185895.
- Fredriksson, R. *et al.* (2003) 'There exist at least 30 human G-protein-coupled receptors with long Ser/Thr-rich N-termini', *Biochemical and Biophysical Research Communications*, 301(3), pp. 725–734. doi: 10.1016/S0006-291X(03)00026-3.
- Frenster, J. D. *et al.* (2021) 'Functional impact of intramolecular cleavage and dissociation of adhesion G protein-coupled receptor GPR133 (ADGRD1) on canonical signaling.', *The Journal of biological chemistry*. Elsevier B.V, 296, p. 100798. doi: 10.1016/j.jbc.2021.100798.
- Fritzsche, B. *et al.* (2007) 'Molecular evolution of the vertebrate mechanosensory cell and ear', *International Journal of Developmental Biology*, 51(6–7), pp. 663–678. doi: 10.1387/ijdb.072367bf.
- Fu, Q. *et al.* (1998) 'Control of Cholesterol Biosynthesis in Schwann Cells', *Journal of Neurochemistry*, 71(2), pp. 549–555. doi: 10.1046/j.1471-4159.1998.71020549.x.
- Gaboriaud, C. *et al.* (2011) 'Structure and properties of the Ca²⁺-binding CUB domain, a widespread ligand-recognition unit involved in major biological functions', *Biochemical Journal*, 439(2), pp. 185–193. doi: 10.1042/BJ20111027.

Gamble, H. J. and Breathnach, A. S. (1965) 'An electron-microscope study of human foetal peripheral nerves.', *Journal of anatomy*, 99(Pt 3), pp. 573–84. Available at:

<http://www.ncbi.nlm.nih.gov/pubmed/5857090>.

Geng, F.-S. *et al.* (2013) 'Semicircular canal morphogenesis in the zebrafish inner ear requires the function of *gpr126* (*lauscher*), an adhesion class G protein-coupled receptor gene', *Development*, 140(21), pp. 4362–4374. doi: doi: 10.1242/dev.098061.

Ghidinelli, M. *et al.* (2017) 'Laminin 211 inhibits protein kinase A in Schwann cells to modulate neuregulin 1 type III-driven myelination', *PLoS Biology*, 15(6), pp. 1–26. doi: 10.1371/journal.pbio.2001408.

Gomez-Sanchez, J. A. *et al.* (2017) 'After nerve injury, lineage tracing shows that myelin and Remak Schwann cells elongate extensively and branch to form repair Schwann cells, which shorten radically on re-myelination.', *The Journal of Neuroscience*, 37(37), pp. 1453–17. doi: 10.1523/JNEUROSCI.1453-17.2017.

Gonçalves, N. P. *et al.* (2017) 'Schwann cell interactions with axons and microvessels in diabetic neuropathy', *Nature Reviews Neurology*, 13(3), pp. 135–147. doi: 10.1038/nrneurol.2016.201.

Gregory, L. A. *et al.* (2003) 'X-ray structure of the Ca²⁺-binding interaction domain of C1s. Insights into the assembly of the C1 complex of complement', *Journal of Biological Chemistry*, 278(34), pp. 32157–32164. doi: 10.1074/jbc.M305175200.

Hall, J. G. (1985) 'Genetic Aspects of Arthrogyrosis', *Clin Orthop Relat Res*, 318(44), pp. 44–53.

Hamann, J. *et al.* (2015) 'Adhesion G protein-coupled receptors', *Pharmacological Reviews*, 67(2), pp. 338–367. doi: 10.1124/pr.114.009647.

Hancock, D. B. *et al.* (2010) 'Meta-analyses of genome-wide association studies identify multiple loci associated with pulmonary function', *Nature Genetics*, 42(1), pp. 45–52. doi: 10.1038/ng.500.

Hauser, A. S. *et al.* (2017) 'Trends in GPCR drug discovery: New agents, targets and indications', *Nature Reviews Drug Discovery*. Nature Publishing Group, 16(12), pp. 829–842. doi: 10.1038/nrd.2017.178.

Henzi, A. *et al.* (2020) 'Soluble dimeric prion protein ligand activates *Adrg6* receptor but does not rescue early signs of demyelination in PrP-deficient mice', *PLoS ONE*, 15(11 November), pp. 1–22. doi: 10.1371/journal.pone.0242137.

Higashijima, S., Hotta, Y. and Okamoto, H. (2000) 'Visualization of cranial motor neurons in live

- transgenic zebrafish expressing green fluorescent protein under the control of the islet-1 promoter/enhancer.', *The Journal of neuroscience : the official journal of the Society for Neuroscience*, 20(1), pp. 206–18. doi: 10.3410/f.1000048.351.
- Hill, A. (2011) 'Hepatotoxicity Testing in Larval Zebrafish', *Zebrafish*, pp. 89–102. doi: 10.1002/9781118102138.ch8.
- Hosseini, M. *et al.* (2019) 'GPR126: A novel candidate gene implicated in autosomal recessive intellectual disability', *American Journal of Medical Genetics, Part A*, 179(1), pp. 13–19. doi: 10.1002/ajmg.a.40531.
- Howe, K. *et al.* (2013) 'The zebrafish reference genome sequence and its relationship to the human genome', *Nature*, 496(7446), pp. 498–503. doi: 10.1038/nature12111.The.
- Huang, S. *et al.* (2007) 'Inducible overexpression of wild-type prion protein in the muscles leads to a primary myopathy in transgenic mice', *Proceedings of the National Academy of Sciences of the United States of America*, 104(16), pp. 6800–6805. doi: 10.1073/pnas.0608885104.
- Ingham, P. W. (2018) 'From drosophila segmentation to human cancer therapy', *Development (Cambridge)*, 145(21). doi: 10.1242/dev.168898.
- Iyer, S. *et al.* (2019) 'Repurposing the aldose reductase inhibitor and diabetic neuropathy drug epalrestat for the congenital disorder of glycosylation PMM2-CDG', *DMM Disease Models and Mechanisms*, 12(11). doi: 10.1242/dmm.040584.
- Jablonka-Shariff, A. *et al.* (2019) 'Gpr126/Adgrg6 contributes to the terminal Schwann cell response at the neuromuscular junction following peripheral nerve injury', *Glia*, (December), pp. 1–19. doi: 10.1002/glia.23769.
- Jaegle, M. *et al.* (2003) 'The POU proteins Brn-2 and Oct-6 share important functions in Schwann cell development', *Genes and Development*, 17(11), pp. 1380–1391. doi: 10.1101/gad.258203.
- Jessen, K. R. and Mirsky, R. (1991) 'Schwann cell precursors and their development', *Glia*, 4(2), pp. 185–194. doi: 10.1002/glia.440040210.
- Jessen, K. R. and Mirsky, R. (2005) 'The origin and development of glial cells in peripheral nerves', *Nature Reviews Neuroscience*, 6(9), pp. 671–682. doi: 10.1038/nrn1746.
- Jessen, K. R. and Mirsky, R. (2019a) 'Schwann cell precursors; multipotent glial cells in embryonic nerves', *Frontiers in Molecular Neuroscience*, 12(March), pp. 1–16. doi: 10.3389/fnmol.2019.00069.
- Jessen, K. R. and Mirsky, R. (2019b) 'The success and failure of the schwann cell response to nerve

- injury', *Frontiers in Cellular Neuroscience*, 13(February), pp. 1–14. doi: 10.3389/fncel.2019.00033.
- Jiang, L. *et al.* (2013) 'Type III neuregulin 1 is required for multiple forms of excitatory synaptic plasticity of mouse cortico-amygdala circuits', *Journal of Neuroscience*, 33(23), pp. 9655–9666. doi: 10.1523/JNEUROSCI.2888-12.2013.
- Kamil, K. *et al.* (2019) 'Peripheral Demyelinating Diseases: From Biology to Translational Medicine', *Frontiers in Neurology*, 10(March), pp. 1–12. doi: 10.3389/fneur.2019.00087.
- Karner, C. M. *et al.* (2015) 'Gpr126/Adgrg6 deletion in cartilage models idiopathic scoliosis and pectus excavatum in mice', *Human molecular genetics*, 24(15), pp. 4365–4373. doi: 10.1093/hmg/ddv170.
- Kim, S. *et al.* (2009) 'Carcinoma-produced factors activate myeloid cells through TLR2 to stimulate metastasis', *Nature*, 457(7225), pp. 102–106. doi: 10.1038/nature07623.
- King, J. R. and Kabbani, N. (2016) 'Alpha 7 nicotinic receptor coupling to heterotrimeric G proteins modulates RhoA activation, cytoskeletal motility, and structural growth', *Journal of Neurochemistry*, pp. 532–545. doi: 10.1111/jnc.13660.
- Kishore, A. *et al.* (2016) 'Stalk-dependent and stalk-independent signaling by the adhesion G protein-coupled receptors GPR56 (ADGRG1) and BAI1 (ADGRB1)', *Journal of Biological Chemistry*, 291(7), pp. 3385–3394. doi: 10.1074/jbc.M115.689349.
- Kitagaki, J. *et al.* (2016) 'A putative association of a single nucleotide polymorphism in GPR126 with aggressive periodontitis in a Japanese population', *PLoS ONE*, 11(8), pp. 1–15. doi: 10.1371/journal.pone.0160765.
- Kou, I. *et al.* (2013) 'Genetic variants in GPR126 are associated with adolescent idiopathic scoliosis', *Nature Genetics*. Nature Publishing Group, 45(6), pp. 676–679. doi: 10.1038/ng.2639.
- Kou, I. *et al.* (2018) 'A multi-ethnic meta-analysis confirms the association of rs6570507 with adolescent idiopathic scoliosis', *Scientific Reports*, 8(1), pp. 1–8. doi: 10.1038/s41598-018-29011-7.
- Küffer, A. *et al.* (2016) 'The prion protein is an agonistic ligand of the G protein-coupled receptor Adgrg6', *Nature*, 536(7617), pp. 464–468. doi: 10.1038/nature19312.
- Labelle-Dumais, C. *et al.* (2019) 'COL4A1 Mutations Cause Neuromuscular Disease with Tissue-Specific Mechanistic Heterogeneity', *American Journal of Human Genetics*. ElsevierCompany., 104(5), pp. 847–860. doi: 10.1016/j.ajhg.2019.03.007.
- Langenhan, T. (2019) 'Adhesion G protein-coupled receptors—Candidate metabotropic

- mechanosensors and novel drug targets', *Basic and Clinical Pharmacology and Toxicology*, 1(January), pp. 1–12. doi: 10.1111/bcpt.13223.
- Langenhan, T., Aust, G. and Hamann, J. (2013) 'Sticky signaling - Adhesion class g protein-coupled receptors take the stage', *Science Signaling*, 6(276), pp. 1–22. doi: 10.1126/scisignal.2003825.
- Langenhan, T., Piao, X. and Monk, K. R. (2016) 'Adhesion G protein-coupled receptors in nervous system development and disease', *Nature Reviews Neuroscience*. Nature Publishing Group, 17(9), pp. 550–561. doi: 10.1038/nrn.2016.86.
- Langenhan, T. and Schöneberg, T. (eds) (2016) *Adhesion G Protein-coupled Receptors, Definitions*. Cham: Springer International Publishing (Handbook of Experimental Pharmacology). doi: 10.1007/978-3-319-41523-9.
- Lenssinck, M., & Frijlink, A. (2005) 'Conservative Interventions in the Treatment of Idiopathic Scoliosis in Adolescents : A Systematic Review of', *Physical Therapy*, 85(12), pp. 1329–1339. Available at: <http://physther.org/content/85/12/1329.short>.
- Leon, K. *et al.* (2020) 'Structural basis for adhesion G protein-coupled receptor Gpr126 function', *Nature Communications*. Springer US, 11(1). doi: 10.1038/s41467-019-14040-1.
- Li, S. *et al.* (2005) 'Structural basis for inhibition of the epidermal growth factor receptor by cetuximab', *Cancer Cell*, 7(4), pp. 301–311. doi: 10.1016/j.ccr.2005.03.003.
- Libé-Philippot, B. *et al.* (2017) 'Auditory cortex interneuron development requires cadherins operating hair-cell mechano-electrical transduction', *Proceedings of the National Academy of Sciences of the United States of America*, 114(30), pp. 7765–7774. doi: 10.1073/pnas.1703408114.
- Liebscher, I. *et al.* (2014) 'A Tethered Agonist within the Ectodomain Activates the Adhesion G Protein-Coupled Receptors GPR126 and GPR133', *Cell Reports*, 9(6), pp. 2018–2026. doi: 10.1016/j.celrep.2014.11.036.
- Lister, J. A. *et al.* (1999) 'Nacre Encodes a Zebrafish Microphthalmia-Related Protein That Regulates Neural-Crest-Derived Pigment Cell Fate', *Development*, 126(17), pp. 3757–3767.
- Lister, J. A. *et al.* (2006) 'Zebrafish Foxd3 is required for development of a subset of neural crest derivatives', *Developmental Biology*. Elsevier Inc., 290(1), pp. 92–104. doi: 10.1016/j.ydbio.2005.11.014.
- Liu, Q. *et al.* (2011) 'Cell adhesion molecule cadherin-6 function in zebrafish cranial and lateral line ganglia development', *Developmental Dynamics*, 240(7), pp. 1716–1726. doi: 10.1002/dvdy.22665.

- Liu, Z. *et al.* (2021) 'An adhesion G protein-coupled receptor is required in cartilaginous and dense connective tissues to maintain spine alignment', *eLife*, 10, pp. 1–28. doi: 10.7554/elife.67781.
- Lizano, E., Hayes, J. L. and Willard, F. S. (2020) 'A synthetic method to assay adhesion-family G-protein coupled receptors. Determination of the G-protein coupling profile of ADGRG6(GPR126)', *Biochemical and Biophysical Research Communications*. Elsevier Ltd, 6(xxxx), pp. 0–5. doi: 10.1016/j.bbrc.2020.11.086.
- Long, K. *et al.* (2019) 'Do Zebrafish Obey Lipinski Rules?', *ACS Medicinal Chemistry Letters*, 10(6), pp. 1002–1006. doi: 10.1021/acsmchemlett.9b00063.
- Lyons, D. A. *et al.* (2005) 'erbb3 and erbb2 are essential for Schwann cell migration and myelination in zebrafish', *Current Biology*, 15(6), pp. 513–524. doi: 10.1016/j.cub.2005.02.030.
- MacRae, C. A. and Peterson, R. T. (2015) 'Zebrafish as tools for drug discovery', *Nature Reviews Drug Discovery*. Nature Publishing Group, 14(10), pp. 721–731. doi: 10.1038/nrd4627.
- Major, B. *et al.* (2010) 'Calcium-dependent conformational flexibility of a CUB domain controls activation of the complement serine protease C1r', *Journal of Biological Chemistry*, 285(16), pp. 11863–11869. doi: 10.1074/jbc.M109.098541.
- Manglik, A. and Kruse, A. C. (2017) 'Structural Basis for G Protein-Coupled Receptor Activation', *Biochemistry*, 56(42), pp. 5628–5634. doi: 10.1021/acs.biochem.7b00747.
- Margulis, M. S., Soloviev, V. D. and Shubladze, A. K. (1946) 'Aetiology and pathogenesis of acute sporadic disseminated encephalomyelitis and multiple sclerosis', *Journal of neurology, neurosurgery, and psychiatry*, 9(2), pp. 63–74. doi: 10.1136/jnnp.9.2.63.
- Marques, J. R. F. *et al.* (2010) 'Amino acid patterns around disulfide bonds', *International Journal of Molecular Sciences*, 11(11), pp. 4673–4686. doi: 10.3390/ijms11114673.
- Michailov, G. V. *et al.* (2004) 'Axonal Neuregulin-1 Regulates Myelin Sheath Thickness', *Science*, 304(5671), pp. 700–703. doi: 10.1126/science.1095862.
- Mogha, A. *et al.* (2013) 'Gpr126 Functions in Schwann Cells to Control Differentiation and Myelination via G-Protein Activation', *Journal of Neuroscience*, 33(46), pp. 17976–17985. doi: 10.1523/JNEUROSCI.1809-13.2013.
- Mogha, A. *et al.* (2016) 'Gpr126/Adgrg6 Has Schwann Cell Autonomous and Nonautonomous Functions in Peripheral Nerve Injury and Repair', *The Journal of Neuroscience*, 36(49), pp. 12351–12367. doi: 10.1523/JNEUROSCI.3854-15.2016.

- Monk, K. R. *et al.* (2009) 'A G Protein-Coupled Receptor Is Essential for Schwann Cells to Initiate Myelination', *Science*, 325(5946), pp. 1402–1405. doi: 10.1126/science.1173474.
- Monk, K. R. *et al.* (2011) 'Gpr126 is essential for peripheral nerve development and myelination in mammals', *Development*, 138(13), pp. 2673–2680. doi: 10.1242/dev.062224.
- Monk, K. R. and Talbot, W. S. (2009) 'Genetic dissection of myelinated axons in zebrafish', *Current Opinion in Neurobiology*, 19(5), pp. 486–490. doi: 10.1016/j.conb.2009.08.006.
- Monuki, E. S. *et al.* (1989) 'SCIP: A glial POU domain gene regulated by cyclic AMP', *Neuron*, 3(6), pp. 783–793. doi: 10.1016/0896-6273(89)90247-X.
- Morgan, R. K. *et al.* (2019) 'The expanding functional roles and signaling mechanisms of adhesion g protein-coupled receptors', *Annals of the New York Academy of Sciences*, 1456(1), pp. 5–25. doi: 10.1111/nyas.14094.
- Moriguchi, T. *et al.* (2004) 'DREG, a developmentally regulated G protein-coupled receptor containing two conserved proteolytic cleavage sites', *Genes to Cells*, 9(6), pp. 549–560. doi: 10.1111/j.1356-9597.2004.00743.x.
- Münzel, E. J. *et al.* (2012) 'Claudin k is specifically expressed in cells that form myelin during development of the nervous system and regeneration of the optic nerve in adult zebrafish', *Glia*, 60(2), pp. 253–270. doi: 10.1002/glia.21260.
- Musa, G. *et al.* (2019) 'Gpr126 (Adgrg6) is expressed in cell types known to be exposed to mechanical stimuli', *Annals of the New York Academy of Sciences*, 126, pp. 96–108. doi: 10.1111/nyas.14135.
- Di Nardo, A. *et al.* (2020) 'Phenotypic Screen with TSC-Deficient Neurons Reveals Heat-Shock Machinery as a Druggable Pathway for mTORC1 and Reduced Cilia', *Cell Reports*, 31(12), p. 107780. doi: 10.1016/j.celrep.2020.107780.
- Nave, K.-A. and Werner, H. B. (2014) 'Myelination of the Nervous System: Mechanisms and Functions', *Annual Review of Cell and Developmental Biology*, 30(1), pp. 503–533. doi: 10.1146/annurev-cellbio-100913-013101.
- Nehmé, R. *et al.* (2017) 'Mini-G proteins : Novel tools for studying GPCRs in their active conformation', *PLoS ONE*, pp. 1–26.
- North, T. E. *et al.* (2007) 'Prostaglandin E2 regulates vertebrate haematopoietic stem cell homeostasis', *Nature*, 447(7147), pp. 1007–1011. doi: 10.1038/nature05883.
- Okajima, D., Kudo, G. and Yokota, H. (2010) 'Brain-specific angiogenesis inhibitor 2 (BAI2) may be

activated by proteolytic processing', *Journal of Receptors and Signal Transduction*, 30(3), pp. 143–153. doi: 10.3109/10799891003671139.

Oxtoby, E. and Jowett, T. (1993) 'Cloning of the zebrafish krox-20 gene (krx-20) and its expression during hindbrain development', *Nucleic Acids Research*, 21(5), pp. 1087–1095. doi: 10.1093/nar/21.5.1087.

Paavola, K. J. *et al.* (2011) 'The N terminus of the adhesion G protein-coupled receptor GPR56 controls receptor signaling activity', *Journal of Biological Chemistry*, 286(33), pp. 28914–28921. doi: 10.1074/jbc.M111.247973.

Paavola, K. J. *et al.* (2014) 'Type IV collagen is an activating ligand for the adhesion G protein-coupled receptor GPR126', *Science Signaling*, 7(338), pp. ra76–ra76. doi: 10.1126/scisignal.2005347.

Parng, C. *et al.* (2002) 'Zebrafish: A Preclinical Model for Drug Screening', *ASSAY and Drug Development Technologies*, 1(1), pp. 41–48. doi: 10.1089/154065802761001293.

Patra, C. *et al.* (2013) 'Organ-specific function of adhesion G protein-coupled receptor GPR126 is domain-dependent', *Proceedings of the National Academy of Sciences*, 110(42), pp. 16898–16903. doi: 10.1073/pnas.1304837110.

Patra, C., Monk, K. R. and Engel, F. B. (2014) 'The multiple signaling modalities of adhesion G protein-coupled receptor GPR126 in development', *Receptors & Clinical Investigation*, 42(1), pp. 115–125. doi: 10.14800/rci.79.

Patton, E. E., Zon, L. I. and Langenau, D. M. (2021) 'Zebrafish disease models in drug discovery: from preclinical modelling to clinical trials', *Nature Reviews Drug Discovery*. Springer US, 20(8), pp. 611–628. doi: 10.1038/s41573-021-00210-8.

Pellegatta, M. *et al.* (2013) 'α6β1 and α7β1 integrins are required in Schwann cells to sort axons', *Journal of Neuroscience*, 33(46), pp. 17995–18007. doi: 10.1523/JNEUROSCI.3179-13.2013.

Petersen, S. C. *et al.* (2015) 'The adhesion GPCR GPR126 has distinct, domain-dependent functions in Schwann cell development mediated by interaction with Laminin-211', 85(4), pp. 755–769. doi: 10.1016/j.neuron.2014.12.057.The.

Piao, X. *et al.* (2004) 'G protein-coupled receptor-dependent development of human frontal cortex.', *Science (New York, N.Y.)*, 303(5666), pp. 2033–6. doi: 10.1126/science.1092780.

Ping, Y. Q. *et al.* (2021) *Structures of the glucocorticoid-bound adhesion receptor GPR97–Go complex*, *Nature*. Springer US. doi: 10.1038/s41586-020-03083-w.

- Pogoda, H.-M. *et al.* (2006) 'A genetic screen identifies genes essential for development of myelinated axons in zebrafish.', *Developmental biology*, 298(1), pp. 118–131. doi: 10.1016/j.ydbio.2006.06.021.
- Preston, M. A. *et al.* (2019) 'A novel myelin protein zero transgenic zebrafish designed for rapid readout of in vivo myelination', *Glia*, 67(4), pp. 650–667. doi: 10.1002/glia.23559.
- Purcell, R. H. *et al.* (2017) 'A disease-associated mutation in the adhesion GPCR BAI2 (ADGRB2) increases receptor signaling activity', *Human Mutation*, 38(12), pp. 1751–1760. doi: 10.1002/humu.23336.
- Purcell, R. H. and Hall, R. A. (2018) 'Adhesion G Protein–Coupled Receptors as Drug Targets', *Annual Review of Pharmacology and Toxicology*, 58(1), pp. 429–449. doi: 10.1146/annurev-pharmtox-010617-052933.
- Raff, M. C., Hornby-Smith, A. and Brockes, J. P. (1978) 'Cyclic AMP as a mitogenic signal for cultured rat Schwann cells', *Nature*, 273(5664), pp. 672–673. doi: 10.1038/273672a0.
- Raible, D. W. and Kruse, G. J. (2000) 'Organization of the Lateral Line System in Embryonic Zebrafish', *Journal of Comparative Neurology*, 198(January), pp. 189–198.
- Rangon, C. M. *et al.* (2018) 'Myelination induction by a histamine H3 receptor antagonist in a mouse model of preterm white matter injury', *Brain, Behavior, and Immunity*. Elsevier, 74(August), pp. 265–276. doi: 10.1016/j.bbi.2018.09.017.
- Raphael, A. R., Lyons, D. A. and Talbot, W. S. (2011) 'ErbB signaling has a role in radial sorting independent of Schwann cell number', *Glia*, 59(7), pp. 1047–1055. doi: 10.1002/glia.21175.
- Ravenscroft, G. *et al.* (2015) 'Mutations of GPR126 Are Responsible for Severe Arthrogyrosis Multiplex Congenita', *American Journal of Human Genetics*, 96(6), pp. 955–961. doi: 10.1016/j.ajhg.2015.04.014.
- Riethmacher, D. *et al.* (1997) 'Severe neuropathies in mice with targeted mutations in the ErbB3 receptor', *Nature*, 389(6652), pp. 725–730. doi: 10.1038/39593.
- Rosenberg, A. F. *et al.* (2014) 'Schwann cells and deleted in colorectal carcinoma direct regenerating motor axons towards their original path', *Journal of Neuroscience*, 34(44), pp. 14668–14681. doi: 10.1523/JNEUROSCI.2007-14.2014.
- Salzman, G. S. *et al.* (2016) 'Structural Basis for Regulation of GPR56/ADGRG1 by Its Alternatively Spliced Extracellular Domains', *Neuron*, 91(6), pp. 1292–1304. doi: 10.1016/j.neuron.2016.08.022.

- Salzman, G. S. *et al.* (2017) 'Stachel-independent modulation of GPR56/ADGRG1 signaling by synthetic ligands directed to its extracellular region', *Proceedings of the National Academy of Sciences of the United States of America*, 114(38), pp. 10095–10100. doi: 10.1073/pnas.1708810114.
- Scarselli, M. *et al.* (1999) 'Apomorphine has a potent antiproliferative effect on Chinese hamster ovary cells', in Poewe, W. and Ransmayr, G. (eds) *Advances in Research on Neurodegeneration*. Vienna: Springer Vienna, pp. 47–55.
- Schaefer, K. and Brösamle, C. (2009) 'Zwilling-A and -B, two related myelin proteins of teleosts, which originate from a single bicistronic transcript', *Molecular Biology and Evolution*, 26(3), pp. 495–499. doi: 10.1093/molbev/msn298.
- Schampel, A. *et al.* (2017) 'Nimodipine fosters remyelination in a mouse model of multiple sclerosis and induces microglia-specific apoptosis', *Proceedings of the National Academy of Sciences of the United States of America*, 114(16), pp. E3295–E3304. doi: 10.1073/pnas.1620052114.
- Shashidhar, S. *et al.* (2005) 'GPR56 is a GPCR that is overexpressed in gliomas and functions in tumor cell adhesion', *Oncogene*, 24(10), pp. 1673–1682. doi: 10.1038/sj.onc.1208395.
- Shin, Y. K. *et al.* (2014) 'Grb2-Associated Binder-1 Is Required for Neuregulin-1- Induced Peripheral Nerve Myelination', 34(22), pp. 7657–7662. doi: 10.1523/JNEUROSCI.4947-13.2014.
- Snaidero, N. *et al.* (2014) 'Myelin membrane wrapping of CNS axons by PI(3,4,5)P3-dependent polarized growth at the inner tongue', *Cell*, 156(1–2), pp. 277–290. doi: 10.1016/j.cell.2013.11.044.
- Southern, C. *et al.* (2013) 'Screening β -arrestin recruitment for the identification of natural ligands for orphan G-protein-coupled receptors', *Journal of Biomolecular Screening*, 18(5), pp. 599–609. doi: 10.1177/1087057113475480.
- Sriram, K. and Insel, P. A. (2018) 'G protein-coupled receptors as targets for approved drugs: How many targets and how many drugs?', *Molecular Pharmacology*, 93(4), pp. 251–258. doi: 10.1124/mol.117.111062.
- Stacey, M. *et al.* (2000) 'LNB-TM7, a group of seven-transmembrane proteins related to family-B G-protein-coupled receptors', *Trends in Biochemical Sciences*, 25(6), pp. 284–289. doi: 10.1016/S0968-0004(00)01583-8.
- Stoveken, H. M. *et al.* (2015) 'Adhesion G protein-coupled receptors are activated by exposure of a cryptic tethered agonist', *Proceedings of the National Academy of Sciences*, 112(19), pp. 6194–6199. doi: 10.1073/pnas.1421785112.

- Stoveken, H. M. *et al.* (2016) 'Dihydromunduletone Is a Small-Molecule Selective Adhesion G Protein-Coupled Receptor Antagonist.', *Molecular pharmacology*, 90(3), pp. 214–24. doi: 10.1124/mol.116.104828.
- Stoveken, H. M. *et al.* (2018) 'Gedunin- and Khivorin-Derivatives are Small Molecule Partial Agonists for Adhesion G protein Coupled Receptors GPR56 / ADGRG1 and GPR114 / ADGRG5.', *Molecular Pharmacology*, p. mol.117.111476. doi: 10.1124/mol.117.111476.
- Svaren, J. and Meijer, D. (2008) 'The molecular machinery of myelin gene transcription in Schwann cells', *Glia*, 56(14), pp. 1541–1551. doi: 10.1002/glia.20767.
- Swinney, D. C. and Anthony, J. (2011) 'How were new medicines discovered?', *Nature Reviews Drug Discovery*, 10(7), pp. 507–519. doi: 10.1038/nrd3480.
- Syrovatkina, V. *et al.* (2016) 'Regulation, Signaling, and Physiological Functions of G-Proteins', *Journal of Molecular Biology*. Elsevier Ltd, 428(19), pp. 3850–3868. doi: 10.1016/j.jmb.2016.08.002.
- Takada, N. and Appel, B. (2010) 'Identification of genes expressed by zebrafish oligodendrocytes using a differential microarray screen', *Developmental Dynamics*, 239(7), pp. 2041–2047. doi: 10.1002/dvdy.22338.
- Tang, Y. Da *et al.* (2015) 'Nimodipine-mediated re-myelination after facial nerve crush injury in rats', *Journal of Clinical Neuroscience*. Elsevier Ltd, 22(10), pp. 1661–1668. doi: 10.1016/j.jocn.2015.03.048.
- Terzikhan, N. *et al.* (2018) 'Heritability and genome-wide association study of diffusing capacity of the lung', *European Respiratory Journal*, 52(3). doi: 10.1183/13993003.00647-2018.
- Vaglini, F. *et al.* (2008) 'Neuropharmacology Apomorphine offers new insight into dopaminergic neuron vulnerability in mesencephalic cultures', 55, pp. 737–742. doi: 10.1016/j.neuropharm.2008.06.041.
- Vakonakis, I. *et al.* (2008) 'Solution Structure and Sugar-Binding Mechanism of Mouse Latrophilin-1 RBL: a 7TM Receptor-Attached Lectin-Like Domain', *Structure*, 16(6), pp. 944–953. doi: 10.1016/j.str.2008.02.020.
- Voas, M. G. *et al.* (2009) 'Schwann Cells Inhibit Ectopic Clustering of Axonal Sodium Channels', *Journal of Neuroscience*, 29(46), pp. 14408–14414. doi: 10.1523/JNEUROSCI.0841-09.2009.
- Wahlbuhl, M. *et al.* (2012) 'Transcription factor Sox10 orchestrates activity of a neural crest-specific enhancer in the vicinity of its gene', *Nucleic Acids Research*, 40(1), pp. 88–101. doi:

10.1093/nar/gkr734.

Waller-Evans, H. *et al.* (2010) 'The orphan adhesion-GPCR GPR126 is required for embryonic development in the mouse', *PLoS ONE*, 5(11), pp. 1–10. doi: 10.1371/journal.pone.0014047.

Wallquist, W. *et al.* (2005) 'Impeded interaction between Schwann cells and axons in the absence of laminin $\alpha 4$ ', *Journal of Neuroscience*, 25(14), pp. 3692–3700. doi: 10.1523/JNEUROSCI.5225-04.2005.

Wang, C. *et al.* (2010) 'Rosuvastatin, identified from a zebrafish chemical genetic screen for antiangiogenic compounds, suppresses the growth of prostate cancer', *European Urology*. European Association of Urology, 58(3), pp. 418–426. doi: 10.1016/j.eururo.2010.05.024.

Wang, J. and Hou, T. (2011) 'Recent Advances on Aqueous Solubility Prediction', *Combinatorial Chemistry & High Throughput Screening*, 14(5), pp. 328–338. doi: 10.2174/138620711795508331.

Waterman, R. E. and Bell, D. H. (1984) 'Epithelial Fusion During Early Semicircular Canal Development in the Zebrafish, *Brachydanio-Rerio*', *Anatomical Record*, 205, pp. A210–A210.

Watkin, P. and Baldwin, M. (2012) 'The longitudinal follow up of a universal neonatal hearing screen: The implications for confirming deafness in childhood', *International Journal of Audiology*, 51(7), pp. 519–528. doi: 10.3109/14992027.2012.673237.

Whitfield, T. T. *et al.* (1996) 'Mutations affecting development of the zebrafish inner ear and lateral line', *Development*, 123, pp. 241–254.

Whitfield, T. T. *et al.* (2002) 'Development of the zebrafish inner ear', *Developmental Dynamics*, 223(4), pp. 427–458. doi: 10.1002/dvdy.10073.

Whitfield, T. T. (2015) 'Development of the inner ear', *Current Opinion in Genetics & Development*. Elsevier Ltd, 32, pp. 112–118. doi: 10.1016/j.gde.2015.02.006.

Wilde, C. *et al.* (2016) 'The constitutive activity of the adhesion GPCR GPR114/ADGRG5 is mediated by its tethered agonist', *FASEB Journal*, 30(2), pp. 666–673. doi: 10.1096/fj.15-276220.

Xu, E. *et al.* (2019) 'A Genetic Variant in GPR126 Causing a Decreased Inclusion of Exon 6 Is Associated with Cartilage Development in Adolescent Idiopathic Scoliosis Population', *BioMed Research International*. Hindawi, 2019(February 2018). doi: 10.1155/2019/4678969.

Yang, D. *et al.* (2005) 'Coordinate control of axon defasciculation and myelination by laminin-2 and -8', *Journal of Cell Biology*, 168(4), pp. 655–666. doi: 10.1083/jcb.200411158.

Appendix

Table of compounds selected for retest following the primary screen

Compound Name	CATNUM	Avg <i>vcanb</i> score	<i>vcanb</i> assay toxicity	Avg <i>mbp</i> score	<i>mbp</i> assay toxicity
Nocodazole	M 1404	0.00	Marginally toxic	0.00	Toxic
Diclofenac sodium	D 6899	2.67	Marginally toxic	0.50	Toxic
CHM-1 hydrate	C1244	0.00	Marginally toxic	0.50	Toxic
DAPH	D 3943	7.20	Non toxic	1.00	Non toxic
2-methoxyestradiol	M 6383	7.67	Non toxic	1.00	Non toxic
5-Fluoroindole-2-carboxylic acid	265128	2.33	Non toxic	1.50	Non toxic
CGP-7930	C 0862	5.63	Non toxic	1.50	Non toxic
DL-Buthionine-[S,R]-sulfoximine	B 2640	7.00	Non toxic	1.50	Non toxic
Oxaprozin	O 9637	0.33	Toxic	2.00	Toxic
Sulindac sulfone	S 1438	7.33	Non toxic	2.00	Non toxic
7-Chloro-4-hydroxy-2-phenyl-1,8-naphthyridine	C 5982	0.00	Marginally toxic	2.50	Non toxic
Danazol	D 8399	2.33	Non toxic	2.50	Non toxic
MNS	M 7445	6.00	Non toxic	2.50	Non toxic
Nifedipine	N 7634	8.33	Non toxic	2.50	Non toxic
(-)-Perillic acid	218359	5.67	Non toxic	2.50	Non toxic
IC 261	I 0658	0.00	Non toxic	2.50	Non toxic
Terbutaline hemisulfate	T 2528	6.00	Non toxic	2.50	Non toxic
AA-861	A 3711	6.33	Non toxic	3.00	Non toxic
5-azacytidine	A 2385	7.00	Non toxic	3.00	Non toxic
p-Benzoquinone	B 1266	6.67	Non toxic	3.00	Non toxic
Betaxolol hydrochloride	B 5683	6.67	Non toxic	3.00	Non toxic
6-Fluoronorepinephrine hydrochloride	B-012	6.67	Non toxic	3.00	Non toxic
Bromoacetyl alprenolol menthane	B-015	7.33	Non toxic	3.00	Non toxic
Benoxathian hydrochloride	B-016	5.33	Non toxic	3.00	Non toxic
Dofetilide	PZ0016	1.00	Non toxic	3.00	Non toxic
8-Cyclopentyl-1,3-dimethylxanthine	C-102	6.33	Non toxic	3.00	Non toxic
UCL 2077	U6758	4.67	Non toxic	3.00	Non toxic
Flunarizine dihydrochloride	F 8257	5.33	Non toxic	3.00	Non toxic
Ellipticine	E 3380	5.00	Non toxic	3.00	Non toxic
5-Fluorouracil	F 6627	7.00	Non toxic	3.00	Non toxic
Histamine, R(-)-alpha-methyl-, dihydrochloride	H-128	7.00	Non toxic	3.00	Non toxic

R(+)-IAA-94	I-117	7.00	Non toxic	3.00	Non toxic
L-Methionine sulfoximine	M 5379	7.00	Non toxic	3.00	Non toxic
NAN-190 hydrobromide	N 3529	7.00	Non toxic	3.00	Non toxic
Pirenzepine dihydrochloride	P 7412	7.00	Non toxic	3.00	Non toxic
Stattic	S7947	6.33	Non toxic	3.00	Non toxic
Retinoic acid	R 2625	3.67	Non toxic	3.00	Non toxic
BIA 2-093	B 5435	5.67	Marginally toxic	3.00	Non toxic
SU 5416	S 8442	5.67	Non toxic	3.00	Non toxic
AC-55649	A9480	6.33	Non toxic	3.00	Non toxic
Paroxetine hydrochloride hemihydrate (MW = 374.83)	P 9623	6.67	Non toxic	3.50	Non toxic
Buspirone hydrochloride	B 7148	5.33	Non toxic	3.50	Non toxic
Piperaquine tetraphosphate tetrahydrate	C7874	6.33	Non toxic	3.50	Non toxic
Cyproheptadine hydrochloride	C 6022	3.67	Non toxic	3.50	Non toxic
Clotrimazole	C 6019	2.33	Non toxic	3.50	Non toxic
Guanfacine hydrochloride	G 1043	6.67	Non toxic	3.50	Non toxic
Histamine dihydrochloride	H 7250	5.67	Non toxic	3.50	Non toxic
Lithium Chloride	L 4408	7.00	Non toxic	3.50	Non toxic
JL-18	J-102	6.33	Non toxic	3.50	Non toxic
(-)-Isoproterenol hydrochloride	I 6504	6.33	Non toxic	3.50	Non toxic
Loratadine	L 9664	3.00	Non toxic	3.50	Non toxic
Isoliquiritigenin	I 3766	7.00	Non toxic	3.50	Non toxic
Dihydrocapsaicin	M 1022	7.00	Non toxic	3.50	Non toxic
Pargyline hydrochloride	P 8013	7.33	Non toxic	3.50	Non toxic
Auranofin	A 6733	0.33	Toxic	3.50	Non toxic
SU 4312	S 8567	7.33	Non toxic	3.50	Non toxic
Avridine	PZ0123	5.67	Non toxic	3.50	Non toxic
PD-166866	PZ0114	4.71	Toxic	3.50	Non toxic
5HPP-33	H 9415	3.00	Non toxic	3.50	Non toxic
Lercanidipine hydrochloride hemihydrate	L 6668	7.67	Non toxic	4.00	Non toxic
Dihydroergotamine methanesulfonate	D 2763	6.67	Non toxic	4.00	Non toxic
DCEBIO	D 9190	4.67	Non toxic	4.00	Non toxic
4-Imidazolemethanol hydrochloride	H 1877	7.33	Non toxic	4.00	Non toxic
R(-)-Isoproterenol (+)-bitartrate	I 2760	6.00	Non toxic	4.00	Non toxic
Aurothioglucose	A0606	6.67	Non toxic	4.00	Non toxic
Felodipine	F 9677	5.33	Non toxic	4.50	Non toxic
Ivermectin	I 8898	4.33	Non toxic	4.50	Non toxic
LY-294,002 hydrochloride	L 9908	5.67	Non toxic	4.50	Non toxic
Pimozide	P 1793	5.33	Non toxic	4.50	Non toxic
Vinpocetine	V 6383	4.33	Non toxic	4.50	Non toxic
Cilnidipine	C1493	4.33	Non toxic	5.00	Non toxic

Thapsigargin	T 9033	2.67	Non toxic	5.00	Non toxic
Cyproterone acetate	C 3412	3.67	Non toxic	5.50	Non toxic
Ebastine	E9531	3.67	Non toxic	5.50	Non toxic
FPL 64176	F-131	1.67	Non toxic	5.50	Non toxic
Nemadipine-A	N4163	3.67	Non toxic	5.50	Non toxic
Nimodipine	N-149	4.00	Non toxic	6.00	Non toxic
Tracazolate	T-112	4.33	Non toxic	6.50	Non toxic
Trequinsin hydrochloride	T 2057	4.33	Non toxic	6.50	Non toxic
S-Methylisothiourea hemisulfate	M 3127	5.33	Non toxic	7.50	Non toxic
Forskolin	F 6886	0.00	Toxic	9.00	Toxic
Mevastatin	M 2537	0.00	Marginally toxic	9.00	Non toxic